UNIVERSITÉ DE NEUCHÂTEL

Application of carbon-chlorine isotopic analysis to determine the origin and fate of chlorinated ethenes in groundwater

PhD thesis presented to the faculty of Sciences of the University of Neuchâtel to satisfy the requirement for the degree of Doctor of Philosophy in Science

by

Alice Badin

Thesis defense: 11th September 2015

Public presentation: 11th December 2015

PhD thesis evaluation committee:

Daniel Hunkeler, Professor (thesis director), University of Neuchâtel, Switzerland

Mario Schirmer, Associate professor (co-director), University of Neuchâtel, Switzerland

Mette M. Broholm, Associate professor, Technical University of Denmark

Ramon Aravena, Research professor, University of Waterloo, Canada

UNIVERSITÉ DE NEUCHÂTEL

Faculté des sciences
Secrétariat-décanat de Faculté
Rue Emile-Argand 11
2000 Neuchâtel - Suisse
Tél: + 41 (0)32 718 2100
E-mail: secretariat.sciences@unine.ch

IMPRIMATUR POUR THESE DE DOCTORAT

La Faculté des sciences de l'Université de Neuchâtel autorise l'impression de la présente thèse soutenue par

Madame Alice BADIN

Titre:

"Application of carbon-chlorine isotopic analysis to determine the origin and fate of chlorinated ethenes in groundwater"

sur le rapport des membres du jury composé comme suit:

- Prof. Daniel Hunkeler, Université de Neuchâtel, directeur de thèse
- Prof. ass. Mario Schirmer, Université de Neuchâtel,
- Prof. Ramon Aravena, University of Waterloo, Canada
- Prof. Mette Martino Broholm, Danish Technical University, Denmark

Neuchâtel, le 1er décembre 2015

Le Doyen, Prof. B. Colbois

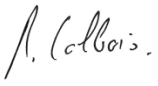

Acknowledgements

As I once heard someone say, « a PhD is a tough journey which doesn't always advance as planned… ». And indeed, the present work would have been tougher to carry out without the precious help and support from colleagues, friends and family whom I would like to sincerely thank.

First of all, I would like to thank my thesis supervisor Daniel Hunkeler for allowing and trusting quite a foreigner to contaminant hydrogeology in his group, and for providing me with a unique environment in which I discovered the exciting world of compound specific isotopes. It was especially an honour to work with such a brilliant scientist who would always give me a hand to get more light on concepts sometimes obscure to me. I am also grateful for his patience and his enthusiasm for my work throughout my project, for allowing me quite some freedom in my work, and for listening to my stubborn and often not ripe project ideas which could then grow thanks to his precious guidance. I also very much appreciated the fact that I could count on him until the very end of my thesis, especially as a last minute person…

I wish to express my sincere gratitude to Christiane Wermeille, my unofficial supervisor from the contaminated sites section of the Federal Office for the Environment (FOEN), for supporting me from the beginning of my thesis project to the end, not only from an administrative aspect (I think we will both very well remember my complicated start in the Advocate project) but also from a moral perspective. It was a great pleasure to be coached during my secondment at FOEN by Christiane who always spent time to explain regulatory basis concepts in the field of contaminated sites and who allowed me the flexibility I needed for my thesis work. I take this opportunity to thank my other colleagues from the contaminated sites section Monika Schwab-Wysser, Rolf Kettler, Reto Tietz, Thomas Lepke, Christoph Reusser, Martine Docourt and Graziella Mazza with whom I had from hilarious moments to interesting philosophical discussions during breaks, and who were always very helpful.

I also owe a lot to Mario Schirmer from the EAWAG, my other unofficial supervisor, thanks to whom this thesis project was set up between the University of Neuchâtel and FOEN. Even though we did not meet often, it was comforting to know that I could count on Mario for any administrative or personal problem. I greatly appreciated his availability and it was very motivating to always receive positive feedback from him.

I think I couldn't have measured much isotopic ratios without the precious help of Jordi Palau, Daniel Bouchard, Simon Jeannottat and Florian Breider to whom I would like to express my sincere gratitude. *c*DCE Cl isotopic ratios from the Rødekro field site have been measured at the University of Waterloo in the group of Orfan Shouakar-Stash, whom I thank. I had also very stimulating discussions with Philipp Wanner, Clara Torrento and Violaine Ponsin who were always kind, supportive and very helpful. In addition to the hydrochemistry team, I thank all my colleagues from the CHYN who also contributed to having a very pleasant atmosphere in the institute. I more particularly thank Yuexia Wu, Jessica Meeks, Christian Möck, Oliver Schilling, Daniel Käser, Sam Bucher, Claire Carlier and Fabio Oriani for long and sometimes philosophical (again!) discussions or for bringing life and "binding" to the institute. Finally, I would like to thank Bibiane Schlunegger, Roberto Costa and Dimitri Boulaz for their help with field work or laboratory analysis. Many thanks also go to Radu Sloboneanu from the institute of mathematics for his help in statistical treatments.

This experience once more proved to me that successful work is best reached through solid collaborations, and I wish to express my gratitude to Christof Holliger, head of the Laboratory for Environmental Biotechnology at the EPFL, and his team who welcomed me in their lab. I more particularly thank Julien Maillard for his precious help as an expert in microbiology, for his general support, his reactivity and his commitment to our project. It was a great pleasure to work in a good spirit with Julien who brought a significant contribution to my work. I also thank his PhD student Géraldine Buttet for her help in setting up the microcosms and the friendly breaks.

Another chance for an equally exceptional collaboration was given to me when we decided to investigate the Danish site Rødekro eight years after its remediation: I would like to thank Mette Broholm, from the Department of Environmental Engineering of DTU, for taking me under her wing in this project, for her reactivity and commitment to our work, as well as for her warm welcome in her home when I visited DTU. I very much enjoyed working over the Rødekro data with Mette who taught me a lot and who considerably contributed to the complex field data treatment. I will also keep great memories of our cozy evenings in those short winter days as well as of our excursions in the region of Copenhagen. These short weeks at the Department of Environmental Engineering of DTU also allowed me to meet a very friendly and helpful team whom I also acknowledge.

I take the opportunity to also thank Niels Just, Jesper Gregersen and Bjarke Foss from the Region of Southern Denmark for providing the possibility to sample Rødekro and for their great help with sampling. Many thanks also to Carsten Jacobsen from GEUS, Denmark, and Phil Dennis from SiREM Lab, Canada, for their valuable collaboration on the molecular biology side of the Rødekro project.

This thesis was carried out in the frame of the European Marie Curie ITN project *Advocate* coordinated by Steve Thornton from the University of Sheffield whom I warmly thank for giving young scientists the opportunity to do research in an exceptional framework. I truly appreciated being part of this exciting project and also sincerely thank all the supervisors and project partners for their coaching and helpful advice during workshops and meetings. I would also like to thank all my project-mates and more particularly Vidhya Chittoor-Viswanathan, Natalia Fernandez, Oksana Voloshchenko-Coban, Alistair Beames, Uwe Schneidewind, Ruth Garcia de la Calle, Naomi Wells and Vivien Hakoun for fruitful discussions, support and fun throughout the whole project.

Because I think it would have been so much harder to carry out the thesis without the priceless support of friends and family, I would like to warmly thank my friends for all sorts of unforgetful times we spent together, from climbing to travelling, playing board games to skyping, cooking to ice-skating…, despite the sometimes long distance. I also thank my family, and especially my parents, who always gave me the freedom to follow my own path and who have always unconditionally been here in difficult times; I will forever be grateful to them for everything they gave me and for their way of introducing me to the world.

Finally, all my gratitude goes to Fabian who supported me, both in the English and French meaning of the word, without ever failing, throughout my whole thesis project. Not only did he directly suffer the depression phases of this roller-coaster ride I seemed to be on and managed to bring my smile back in such phases, but he also tremendously contributed to the work on isotope behaviour modelling. Working together was very fun at first and then sometimes hell but it was a common adventure which added to the many others that make our life together such an exciting journey. I do not know how I could ever express all the gratitude I have for his priceless and unreserved both moral and technical support, but for now, I can say “tusen tusen takk!!”!

This research was completed within the framework of the Marie Curie Initial Training Network ADVOCATE - Advancing sustainable in situ remediation for contaminated land and groundwater, funded by the European Commission, Marie Curie Actions Project No. 265063.

Extended abstract

Chlorinated ethenes are ubiquitous groundwater contaminants posing a threat to one of our main drinking water sources. Despite their spill history dating back to more than 40 years ago, these contaminants are still found in groundwater in numerous industrially developed countries due to their persistence, difficult characterisation in the subsurface and resulting challenging remediation. When adequate redox conditions, microbial communities and/or minerals are present, these compounds are known to undergo natural degradation. Applying natural attenuation as a management strategy is thus being increasingly considered as it constitutes a cost-effective environmental friendly approach. Tools enabling to differentiate degradation pathways, predict the fate of contaminants as well as understand the mechanisms underlying their degradation thus constitute the key to a better management of chlorinated ethenes contaminated sites. Methods allowing for contaminant source tracking are also of interest in a legal context where the contamination precursor is searched for. Among the various tools applied to address such questions, compound specific isotopic analysis (CSIA) – which consists in measuring the ratio between light and heavy stable isotopes of one element (i.e. isotopic composition) of a compound – is being increasingly applied.

This thesis was aimed at exploring the benefits and limits of applying CSIA to substantiate the origin and fate of chlorinated ethenes in groundwater. For this purpose, a first field study aimed at investigating the performance of dual Carbon-Chlorine (C-Cl) isotopic analysis for contaminant source discrimination was carried out. Laboratory experiments were then performed in view of getting more insight in the reaction mechanisms underlying tetrachloroethylene (PCE) reductive dechlorination and to explore the potential of dual C-Cl isotopic analysis to differentiate degradation pathways. A mathematical model was further developed to comprehensively simulate chlorinated ethenes C and Cl isotopic evolution during sequential dechlorination. Simulations were compared to experimental data in order to evaluate this model in its ability to reproduce and thus predict real data. Finally, the contribution of C and Cl isotopic analysis to identify changes in redox processes further affecting chlorinated ethenes in groundwater was challenged when assessing the effect of source thermal remediation by steam injection on a chlorinated ethenes plume.
For regulatory reasons, determining the contamination perpetrator is often of interest. As the isotopic signature of solvents produced from different manufacturers showed a large variability, CSIA was suggested as a method to discriminate the origin of contamination between different suspected sources by comparing their isotopic signatures. Such application however relies on the assumption that isotopic signatures will also differ in the field. Our first goal was thus to determine the source isotopic variability of PCE at a country scale. For this purpose, the C and Cl isotopic composition of PCE found in groundwater underlying 10 contaminated sites located in Switzerland was compared to the so far reported isotopic signatures of PCE produced by different manufacturers. It was shown that such variability was less important between the 10 sites than between PCE from different manufacturers (i.e. -26.0 to -23.7 ‰ for C and -0.5 to 0.6 ‰ for Cl in Switzerland and -37.4 to -23.2 ‰ for C and -4.4 to 1.2 ‰ for Cl in PCE from manufacturers). Additionally, some sites could be differentiated based on their isotopic signatures while others could not. The successful application of CSIA therefore largely depends on cases.

Once chlorinated ethenes have been detected in groundwater, it may be of interest to determine whether they are being naturally degraded or not, as this will influence the site management choice (e.g. application of monitored natural attenuation). Chlorinated ethenes are typically known to undergo sequential biotic reductive dechlorination in strictly anoxic conditions (i.e. PCE → trichloroethylene (TCE) → *cis*-dichloroethylene (*c*DCE) → vinyl chloride (VC) → ethene). However, the exact reaction mechanism underlying each step of reductive dechlorination remains at the stage of hypothesis where three different reaction mechanisms have so far been proposed.

As molecules containing light isotopes are generally degraded faster than molecules containing heavy isotopes due to energetic reasons, the isotopic composition of chlorinated ethenes is bound to vary during their sequential degradation. CSIA has thus naturally been proposed as a tool to track the biochemical reactions affecting chlorinated ethenes during their degradation as different processes differently affect their isotopic composition. More specifically, rate-limiting steps control the extent of isotopic enrichment during the course of biotransformation. Rate-limiting steps occurring during substrate-enzyme interactions are yet expected to equally affect both elements since such interactions are not bond-specific contrary to the purely chemical degradation reaction which involves a bond breakage. It was hence suggested that simultaneously considering the isotopic composition of two elements of a compound undergoing degradation via the dual C-Cl isotope slope associated with this compound strictly reflected the chemical reaction underlying this compound degradation contrary to single element isotopic data.

In view of getting more insight into the reaction mechanisms underlying reductive dechlorination of chlorinated ethenes, we studied the C and Cl isotopic evolution of PCE and TCE during their reductive dechlorination by two bacterial consortia (SL2-PCEc and SL2-PCEb) harbouring members of *Sulfurospirillum* spp. These consortia were specific in that they showed a different dechlorination pattern: SL2-PCEb was able to dechlorinate PCE or TCE until *c*DCE whereas SL2-PCEc only dechlorinated until TCE. Contrary to what was expected, two significantly different dual C-Cl isotope slopes of 2.7 ± 0.3 and 0.7 ± 0.2 associated with PCE reductive dechlorination were determined depending on the bacterial consortia. Such variability was attributed to the existence of two different reaction mechanisms underlying this reaction, under the assumption that dual C-Cl isotope slopes strictly reflect the chemical reaction. Two dual C-Cl isotope slopes associated with PCE reductive dechlorination in two field sites where each slope corresponded to one experimentally determined slope were also determined. This further supported the existence of two unique slopes and constituted another argument in favour of their corresponding to two different reaction mechanisms. It was moreover demonstrated that phylogenetically close bacteria could yield different C-Cl isotope slopes. The apparent kinetic isotope effect (AKIE) reflects the difference in reaction rates involving molecules containing light versus heavy isotopes of one element after correcting for non-reacting positions. Primary isotopic effects affect atoms located in reacting position as opposed to secondary isotopic effects which affect atoms located in non-reacting positions. Based on AKIEs calculations where secondary Cl isotopic effects were neglected, we furthermore suggested that one consortium (SL2-PCEc) more likely involved an electron-transfer or nucleophilic substitution as a first step of reaction mechanism than a nucleophilic addition. Comparing calculated AKIEs to the maximum theoretical kinetic isotope effects (or “semiclassical Streitwieser limits”) associated with C-Cl bond breakage suggested that either the primary Cl isotope effect was larger than the kinetic isotope effect given by the Streitwieser limit, or that a secondary Cl isotope effect occurred.

The Cl isotopic composition of TCE produced by PCE reductive dechlorination was further studied in order to explore in more details the possibility that secondary Cl isotope effects occur. A 1.4 ± 0.2 ‰

to 3.1 ± 0.6 ‰ lighter TCE than PCE at the beginning of the reaction indicated the presence of an inverse secondary effect or at least a difference of -10.6 ± 1 ‰ to -15.9 ± 2.8 ‰ between primary and secondary Cl isotopic effects.

In order reliably predict a chlorinated ethenes plume fate based on a modelling approach considering isotopic data, isotopic effects should be incorporated in a more comprehensive way than in the models so far proposed. A mathematical model aimed at simulating the evolution of C and Cl isotopic composition during sequential reductive dechlorination was thus developed where secondary isotopic effects were taken into account. So that the model reflects effectively occurring processes, Monod kinetics instead of first order kinetics were additionally considered. The rationale behind the approach consisted in considering all isotopocules (i.e. molecules differing in number and position of heavy and light isotopes) of each chlorinated ethene as individual species which were each degraded at different speed depending on the number and position of heavy and light isotopes in the isotopocule. Such difference in degradation rate between isotopocules was described by a matrix containing kinetic isotopocule fractionation factors. The definition of the latter is similar to that of the commonly used kinetic fractionation factor α which corresponds to the ratio between the degradation rate of heavy and light isotopes of a compound. More specifically, one comprehensive model (GM) considering C and Cl isotopes simultaneously was distinguished from a simplified model (SM) where C and Cl were considered separately. Both models almost identically simulated realistic C and Cl isotopic compositions of PCE, TCE and *c*DCE during sequential dechlorination when using experimentally plausible kinetic and isotopic parameters. They could additionally accurately reproduce our experimental data, leaving a promising future for the development of an integrative reactive transport model incorporating isotopic parameters. It also documented the slight impact of having different Cl secondary isotopic effects as well as the small effect induced by an unequal Cl isotopes distribution between positions of an asymmetric molecule on the produced compound Cl isotopic composition.

Finally, field investigations were performed at a site located in Denmark which was explored in a previous work, prior to source thermal remediation. C and Cl isotopic analysis of chlorinated ethenes from groundwater samples taken along the plume centreline were used to verify and improve the interpretation of redox and chlorinated ethenes concentration data. Dual C-Cl isotope slopes associated with PCE and TCE in the first part of the plume were similar to experimentally determined slopes during biotic reductive dechlorination. Based on the assumption that dual C-Cl isotope slopes directly reflect degradation pathways, it was suggested that steam injection enhanced PCE and TCE biotic reductive dechlorination in the first part of the plume. This was in agreement with the occurrence of more reducing conditions resulting from the release of organic matter likely triggered by the thermal remediation. On the other hand, we suggested based on the dual isotope slope approach that *c*DCE was probably primarily abiotically degraded by pyrite in the downstream part of the plume before and after the remediation event. This differed from the original postulation which suggested the occurrence of either *c*DCE anaerobic oxidation or complete reductive dechlorination prior to remediation. Such different conclusion could be drawn based on newly reported dual isotope slopes associated with *c*DCE abiotic degradation which were not available at the time of the study preceding source remediation. In the middle of the plume, a *c*DCE C isotopic composition lighter than the estimated initial one for PCE C documented the occurrence of further *c*DCE degradation despite the very low VC concentrations. On the contrary, a *c*DCE C isotopic composition equal to that of the

initially released PCE indicated the absence of or only little further *c*DCE degradation at the plume front. Such conclusion was in agreement with the observed plume expansion documented by larger concentration contours in the second campaign than in the first.

To sum up, this thesis reveals that dual C-Cl isotopic analysis should be applied with caution for pathway and source differentiation in the field. It yet demonstrates that such analysis constitutes a valuable complementary tool to explore biochemical processes affecting chlorinated ethenes in groundwater, provided that it is applied at sites where the hydrogeological and biogeochemical contexts are well characterised. The performed studies additionally put more light on C and Cl isotopic effects occurring during PCE and TCE biotic reductive dechlorination even though the specific kinetic processes controlling isotopic behaviours remain unclear. Finally, this work proposes a mathematical model which opens the door to a better incorporation of isotope data when evaluating a plume fate based on a modelling approach.

Keywords: chlorinated ethenes, reductive dechlorination, carbon and chlorine isotope analysis, groundwater, source delineation, simulations

Table of contents

Introduction

1. Chlorinated ethenes: the problem

1.1. History

While industrial development undeniably led to more comfortable living conditions, this period of history is also coated with some less positive consequences such as the environmental pollution it triggered. Due to the poor awareness of the toxic and ecotoxic effects of compounds used for numerous purposes, little action was taken to prevent their release to the environment. Accidental spills, careless disposal and various industrial processes thus contributed to the release of large amounts of chemicals in the environment. Today, countries all over the world are evaluating the number of potentially polluted sites they have inherited, and tremendous effort is put into investigating and eventually cleaning up those sites. As of 2011, an estimated amount of 2.5 million potentially polluted sites have been reported in Europe of which 340'000 are estimated to be contaminated and will thus have to be cleaned up *(Liedekerke, 2014)*. Even though mineral oils and heavy metals are reported to be the most frequently found contaminants in groundwater in Europe, chlorinated hydrocarbons (CHC) account for a considerable number of sites which will have to be remediated (34'000 in Europe *(Liedekerke, 2014)*, 1'100 in Switzerland *(FOEN, 2015)*), and much attention is brought to this contaminant category, as the occurrence of numerous guides focusing on these compounds issued from various environmental agencies suggests *(USEPA, 1993, EA, 2003, MEDD, 2004, ADEME, 2007, FOEN, 2008 (revised 2009))*.

More particularly, the chlorinated ethenes tetrachloroethylene (PCE) and trichloroethylene (TCE), which were commonly used for dry-cleaning, metal degreasing or quartering purposes but also as solvents in the chemical industry or in paints or glue, are the most ubiquitous CHC found in groundwater *(Pankow & Cherry, 1996, Wiedemeier et al., 1999, Bradley, 2000, Kilchmann, 2009)*. Their biodegradation products cis-dichloroethylene (*c*DCE) and vinyl chloride (VC), which is a known carcinogen, are also commonly found in groundwater. Chlorinated ethenes are (probable) carcinogens. They can affect fertility as well as the nervous, cardiac, digestive and respiratory systems, and they are skin and eye irritants (INRS toxicological records, Table A 2 of the Appendices). Consequently, their concentration in drinking water is nowadays regulated (in Switzerland < 20 $\mu g \cdot L^{-1}$, < 35 $\mu g \cdot L^{-1}$, < 25 $\mu g \cdot L^{-1}$, 0.05 $\mu g \cdot L^{-1}$ of PCE, TCE, *c*DCE and VC in groundwater intended for drinking *(OSites, 1998, OSEC, 1995)*).

1.2. Behaviour in the subsurface

Once chlorinated solvents (usually PCE or TCE) have been spilled on the ground, they migrate through the unsaturated zone where a fraction remains trapped in the soil interstitial pores or sorbed on soil organic matter to finally reach the water table *(Pankow & Cherry, 1996, Wiedemeier et al., 1999)*. Due to low water solubility and density higher than that of water (Table A 3, Appendices), these compounds migrate deeper in the aquifer and settle on impermeable layers, forming pools of so called Dense Non Aqueous Phase Liquids (DNAPL, Figure 1). Despite low water solubility, chlorinated solvents slowly dissolve in water and get transported by advection forming contaminant plumes. When solvents settle on less permeable layers such as clay, they also slowly penetrate these layers by diffusion, creating contaminant accumulations which are even more challenging to remediate due to the difficulty in accessing them *(Seyedabbasi et al., 2012)*. Finally, when adequate minerals or microbial communities are present associated with the occurrence of suitable redox and/or growing conditions, chlorinated solvents can get degraded either abiotically or biotically thus giving a chance for the contaminants to naturally get broken down by a destructive process *(Vogel et*

al., 1987, Bradley, 2000, Lee & Batchelor, 2002, Stroo, 2010). VC is the intermediate compound released during chlorinated ethenes biotic degradation which raises the most concern because it is a known carcinogen, and it is more volatile than other chlorinated ethenes, as its higher Henry-coefficient shows (Table A 3, Appendices). VC will hence more likely migrate and get released at the surface, potentially contaminating cellars or below-ground constructions *(Patterson et al., 2013)*. These transport, partitioning and transformation processes schematically summarised in Figure 1 control the contaminants distribution and fate in the subsurface *(Pankow & Cherry, 1996, Wiedemeier et al., 1999)*.

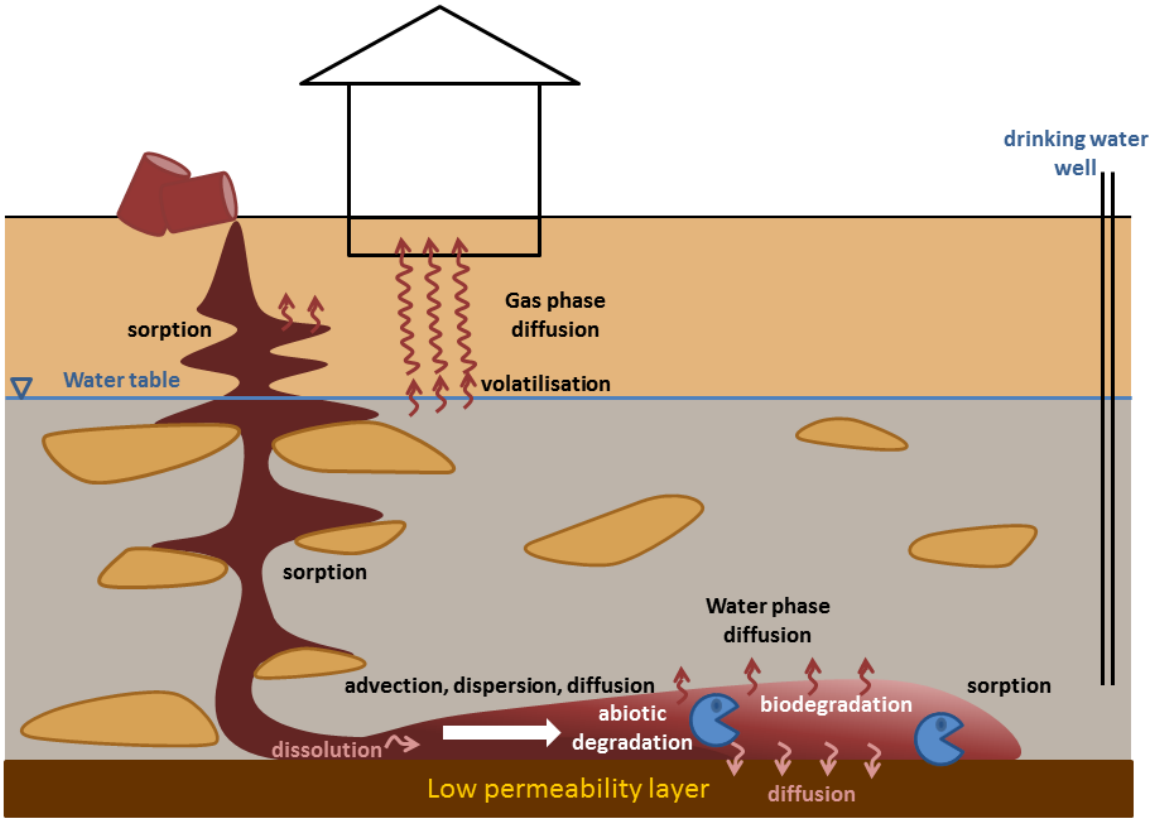

Figure 1. Summary of processes which can affect a contaminant spilled as a DNAPL in the subsurface.

1.3. Remediation

While identifying groundwater contamination by chlorinated ethenes remains relatively straightforward, localising their sources stays intricate. Source localisation is however essential as its removal alone can insure a long term solution. To perform a successful site remediation, different clean-up approaches are usually used for source and plume treatment *(Pankow & Cherry, 1996, Stroo, 2010)*. Source excavation (when constructions allow it), in situ thermal treatment *(von Schnakenburg, 2013)*(ISTT ; by thermal conductive heating, steam air injection or electric resistance heating), air sparging (oxygen injection to volatilize the volatile contaminants), in situ chemical oxidation *(ITRC, 2005, Huling, 2006)* (ISCO ; addition of chemical oxidants such as permanganate or peroxide) or in situ reduction *(Labeeuw, 2013)* (ISR; addition of reductants such as zero valent iron, natural presence of iron such as FeS) might be performed to remove or treat chlorinated solvent sources in situ. On the other hand, other strategies such as permeable reactive barriers *(ITRC, 1999)*

(construction of a wall in the subsurface consisting of materials supporting contaminant degradation), pump and treat (which efficiency is however questioned *(Pankow & Cherry, 1996)*), or bioremediation *(Wiedemeier et al., 1999, Stroo, 2010)* (which takes advantage of biotic degradation) are more adapted for the plume. All these remediation strategies may be divided in two categories of techniques, one relying on physical processes where the contaminant is physically removed (excavation, ISTT, sparging, pump and treat), the other relying on reactive (or degradation) processes where contaminants are transformed into non-toxic compounds (ISCO, ISR, reactive barrier, bioremediation). More particularly, bioremediation either consists in monitoring and leaving naturally occurring biodegradation degrade the contaminants (monitored natural attenuation), or in adding energy or carbon sources which will help microorganisms already present in the subsurface degrade the contaminants (enhanced bioremediation). Although contaminant removal by bioremediation usually takes longer than clean-up strategies employing physical processes, such methods are gaining massive interest when it comes to treating rather little concentrated residual plumes due to their financial and environmental advantages. Physical processes indeed often lead to incomplete decontamination (depending on the set remediation goals), and switching to a less expensive, more environmental friendly, softer technique which effect can spread over the entire plume area may be preferred after removing the larger part of contamination located in the source area. This is all the more so true in low permeability layers or in deep aquifers where physical processes (apart from excavation) are bound to show little efficiency. Finally, remediation by abiotic degradation where chemicals are added to trigger abiotic contaminant degradation, represents a cost-effective remediation approach which may be applied in the source zone rather than in the plume since the latter would require tremendous amounts of reactant.
The following section hence focuses on chlorinated ethenes degradation processes and sets out to compare their mode of action.

1.4. Degradation

1.4.1. Biotic degradation

A scheme summarising all degradation pathways for commonly encountered chlorinated solvents in groundwater is proposed in the Appendices (Figure A 1).

1.4.1.1. Reductive dechlorination

Due to their relatively oxidised state which they owe to the presence of electronegative chlorine substituents, chlorinated ethenes are known to act as terminal electron acceptors in a process called reductive dechlorination where chlorine substituents are sequentially being replaced by hydrogen atoms to finally yield non-toxic products such as ethene *(Vogel et al., 1987, Bradley, 2000)* (Figure 2). For thermodynamic reasons (Table 1), this process is known to occur in strictly anaerobic systems *(Wiedemeier et al., 1999, Bradley, 2000)*. The tendency of chlorinated ethenes to undergo reductive dechlorination generally decreases with decreasing number of chlorine substituents owing to the decreasing oxidant strength with decreasing number of chlorine substituents, with the exception of VC and *c*DCE where *c*DCE reductive dechlorination requires more reducing conditions than VC *(Wiedemeier et al., 1999)*. Laboratory and field observations lead to the conclusion that PCE could undergo reductive dechlorination in virtually any anaerobic conditions while TCE, *c*DCE and VC reductive dechlorination would generally occur in more reduced conditions such as iron-reducing for TCE and ideally sulfate-reducing to methanogenic for *c*DCE and VC *(Vogel et al., 1987, Chapelle, 1996,*

Bradley, 2000, Tiehm & Schmidt, 2011). Finally, while metabolic reductive dechlorination is the most commonly observed process, cometabolic reduction may also occur although it is characterised by a much less efficient use of electron donor *(Middeldorp et al., 1999)*.

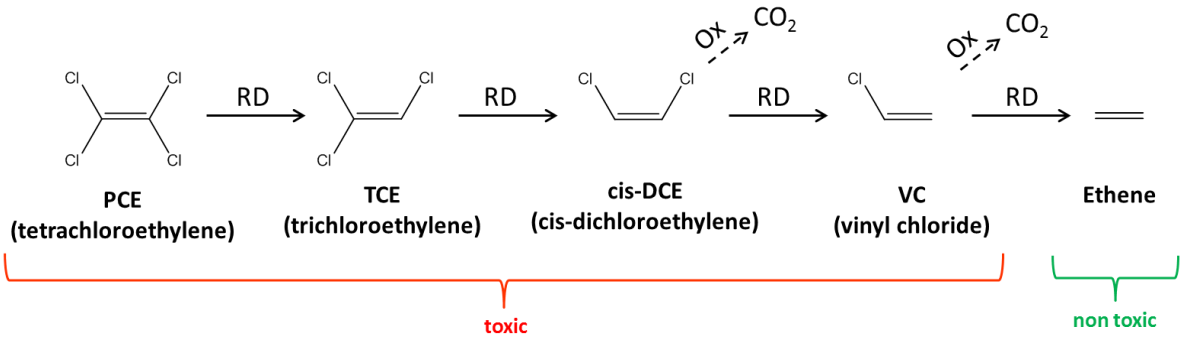

Figure 2. Chlorinated ethenes biotic degradation pathways. RD: reductive dechlorination; Ox: oxidation

1.4.1.2. Oxidation

While the tendency of chlorinated ethenes to undergo reductive dechlorination decreases with decreasing number of chlorine substituents, the contrary is observed for oxidation *(Vogel et al., 1987, Bradley, 2000)*. More particularly, *c*DCE and VC were demonstrated to serve as primary substrate for oxidation to CO_2 in aerobic *(Hartmans et al., 1985, Bradley & Chapelle, 1998, Bradley & Chapelle, 2000)* and anaerobic conditions *(Bradley & Chapelle, 1998, Bradley et al., 1998)*. Yet, the latter is quite controversial and could actually be attributed to aerobic oxidation taking place in the presence of very low O_2 concentration *(Gossett, 2010)*. Neither PCE nor TCE have been shown to undergo metabolic microbial aerobic oxidation *(Bradley, 2003)*. Clear advantages of oxidation are the absence of toxic intermediates and the higher *c*DCE and VC degradation rates compared to reductive dechlorination *(Suarez & Rifai, 1999)* (Table 2).

Finally, all chlorinated ethenes can be cometabolically oxidised to CO_2 in aerobic conditions even though such fortuitous degradation process is more frequently encountered for TCE, *c*DCE and VC *(Bradley, 2000, Tiehm & Schmidt, 2011)*. Disadvantages of this process over metabolic oxidation are the need for auxiliary substrates, lower degradation rates and lower concentration ranges *(Tiehm & Schmidt, 2011)*.

Whether metabolic or cometabolic, oxidation is unlikely to take place in the core of the plume whereas it is more likely that it occurs at the fringe where dissolved O_2 has not yet been totally depleted due to microbial respiration, or at the interface between groundwater and surface water *(Bradley, 2000)*.

1.4.2. Abiotic degradation

Abiotic degradation represents another relatively cost-efficient and environmental friendly clean-up method which mode of action is comparable to biodegradation in the sense that both are destructive processes. Contrary to biodegradation, abiotic degradation is usually implemented in the source area where the reactive compounds may be delivered in large quantities to reach the highest amount degraded possible per unit of time. They may be used to treat plumes when incorporated in reactive barriers through which the plume will flow. Such process can also sometimes naturally take place when the right minerals are present *(Lee & Batchelor, 2002)*.

1.4.2.1. Reductive degradation

Similarly to biotic reductive dechlorination, abiotic reductive degradation can occur in the presence of certain metals. In an attempt to design efficient remediation strategies relying on this process (e.g. permeable reactive barriers), considerable efforts have been made to investigate the optimal conditions for a rapid chlorinated ethenes removal without accumulation of toxic by-products *(Butler & Hayes, 1999, Arnold & Roberts, 2000, Butler & Hayes, 2001, Tobiszewski & Namieśnik, 2012)*. Various metals have been assessed such as zero valent iron (ZVI or Fe^0), zero valent zinc, nanoscale iron (nZVI) or palladium nanoparticles *(Tobiszewski & Namieśnik, 2012)*. However iron is usually preferred for field applications as it is less costly. Major products of chlorinated ethenes abiotic reductive degradation are chlorinated acetylenes resulting from a dihaloelimination pathway which rapidly get transformed into the non-toxic acetylene by hydrogenolysis (replacement of halogen by a hydrogen) and further to ethene by hydrogenation or to C_4 compounds by hydrogenolysis *(Arnold & Roberts, 2000)* (Figure A 1, Appendices). Although they are minor products, less chlorinated ethenes are also produced during abiotic reductive dechlorination. The branching varies depending on the type of iron, iron mineral or pH conditions, but they may account for up to 15-20% of abiotic reductive degradation products *(Butler & Hayes, 1999, Elsner et al., 2008)*. The rate, and therefore the efficiency, depends among others on the metal available surface for catalysis, the metal type, the temperature and the surrounding geochemical conditions *(Hwang et al., Su & Puls, 1999, Arnold & Roberts, 2000, Butler & Hayes, 2001, Tobiszewski & Namieśnik, 2012)*.

Abiotic reductive dechlorination can also take place naturally, provided that the adequate minerals and geochemical conditions occur. More particularly, iron sulphides such as Mackinawite ($Fe^{II}S$) or pyrite ($Fe^{II}S_2$), iron oxides such as magnetite ($Fe^{II}O{\cdot}Fe^{III}{}_2O_3$), and iron hydroxides such as green rusts which are corrosion products of iron or steel ($[Fe_{6-x}{}^{II}Fe_x{}^{III}(OH)_{12})]^{X+}[(A)_{x/n}yH_2O]^{X-}$ where A is an anion, typically $SO_4{}^{2-}$ or Cl^-) have been reported to catalyse abiotic reductive degradation *(Lee & Batchelor, 2002, Tobiszewski & Namieśnik, 2012)*. The latter is however generally slower than engineered abiotic degradation *(Tobiszewski & Namieśnik, 2012)*.

Finally, bacterial activity may change local redox conditions, thus affecting the redox potential of metals contained in minerals which might in turn affect the likelihood of abiotic degradation to take place *(Tobiszewski & Namieśnik, 2012)*.

1.4.2.2. In situ chemical oxidation

In situ chemical oxidation constitutes another abiotic degradation alternative. Artificially introduced oxidising agents are typically permanganate ($MnO_4{}^-$), Fenton's reagent ($H_2O_2 + Fe^{2+}$), ozone (O_3) and persulfate ($S_2O_8{}^{2-}$) *(Huling, 2006)*. Major advantages are the mineralisation of chlorinated ethenes to CO_2 without production of toxic intermediates, the short persistence of the reactive materials in groundwater (except for $MnO_4{}^-$) implying the absence of oxidant plume apparition, and their relatively low cost. Limitations are hydraulic preferential pathways which can make the delivery to the targeted zone difficult all the more so with gaseous O_3, main product accumulation near the injection well resulting in permeability reduction (e.g. MnO_2(s) produced by $MnO_4{}^-$ reduction), lack of contaminant targeting possibility due to the oxidants high reactivity and therefore use up of oxidant when they with natural organic matter for example, pH modification in some cases, and contaminant volatilisation in case of H_2O_2 and O_3. The stronger the oxidant, the shorter its residence time as it reacts rapidly and with a wide range of compounds (Figure 3).

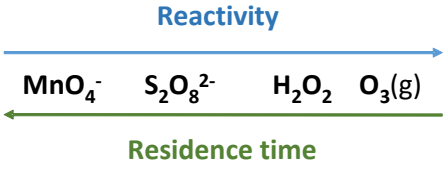

Figure 3. Comparison of reactivity and residence time in the subsurface between different oxidants

A major advantage of biodegradation over abiotic degradation resides in the fact that biodegradation naturally occurs in a wide range of conditions in the presence of chlorinated ethenes. More specifically, reductive dechlorination often naturally takes place, yet *c*DCE or VC are often found to be stalling products. On the contrary, natural abiotic degradation of chlorinated ethenes only takes place under very specific conditions. Understanding and controlling biodegradation thus raise high interests as it is the key to its successful implementation in the subsurface. An overview of the processes and factors currently assumed to govern the achievement of reductive dechlorination is hence proposed in the following section.

1.5. Factors and processes controlling the success of reductive dechlorination in the subsurface

1.5.1. Specific microorganisms

As metabolic reductive dechlorination is mediated by specific microorganisms, its occurrence first depends on the presence and the activity of such microorganisms. To date, members from various bacterial genera such as S*ulfurospirillum*, *Dehalobacter*, *Desulfitobacterium*, *Desulfuromonas* or *Geobacter* have been reported to catalyse some steps of chlorinated ethene reductive dechlorination *(Neumann et al., 1998, Seshadri et al., 2005, Nonaka et al., 2006, Wagner et al., 2012, Rupakula et al., 2013)*. However, only a few are able to dechlorinate further than *c*DCE, giving an explanation for commonly encountered *c*DCE stalling in plumes. While some enrichment cultures and consortia are able to dechlorinate down to ethene *(Flynn et al., 2000, Aulenta et al., 2002, Hoelen & Reinhard, 2004)*, to date, the only organism which have been reported to catalyse reductive dechlorination to ethene are of the genus *Dehalococcoides (Maymo-Gatell et al., 1997, Löffler, 2013)*. Despite their potential presence in the subsurface, such microorganisms may display a low activity, are sometimes inactive or even dormant *(Meckenstock et al., 2015)* which may additionally affect the achievement of reductive dechlorination.

1.5.2. Contaminant delivery to the microorganisms

All the processes responsible for the delivery of contaminants to the microorganisms, or in other words bioavailability (i.e. transport by groundwater and therefore residence time in the reactive zone, flow paths at the pore velocity scale, diffusion from the medium to the microorganisms), will then affect the likeliness and the rate at which contaminants will be degraded *(Meckenstock et al., 2015)*.

Once the microorganisms are present and the contaminants are delivered to them at a rate depending on the above-mentioned physical processes, their likelihood of mediating reductive dechlorination and the rate at which this process will occur seem to depend on the surrounding redox conditions (thermodynamic control), and kinetic limitations at the microorganism scale. The following sections discuss the influence of such thermodynamic and kinetic processes on the occurrence and rate of reductive dechlorination itself.

1.5.3. Electron donors

As dechlorinating bacteria need electron donors in order to respire on chlorinated ethenes, their availability is essential. Common electron donors used in this process are H_2, typically produced from fermentation of natural organic matter, pyruvate, formate, acetate or fumarate *(Gossett, 1996, Bhatt et al., 2006)*.

1.5.4. Thermodynamic control?

The capacity of chlorinated ethenes to act as electron acceptors can be understood from a thermodynamic perspective which also highlight the limitations of reductive dechlorination due to competition with other naturally present electron acceptors *(Wiedemeier et al., 1999)* (Table 1). From a thermodynamic viewpoint, PCE, which is a strong oxidant, should hence undergo reductive dechlorination to TCE in virtually all anaerobic conditions, while TCE, VC and *c*DCE should undergo reductive dechlorination in this order of prevalence under manganese to iron reducing conditions (Table 1). However, field and laboratory observations lead to different conclusions regarding the redox conditions under which chlorinated ethenes are readily degraded. TCE typically predominantly undergoes reductive dechlorination to *c*DCE and to a much lesser extent to trans-dichloroethyelene (tDCE) and 1,1-dichloroethylene (1,1-DCE) in iron-reducing conditions *(Bradley, 2000)*. *c*DCE reductive dechlorination to VC readily takes place in methanogenic conditions *(Bradley, 2000)* and requires at least sulfate-reducing conditions *(Vogel et al., 1987, Chapelle, 1996)*. Finally, some studies demonstrated that VC reductive dechlorination readily occurred under methanogenic conditions *(Wiedemeier et al., 1999, Bradley, 2000)* while other studies demonstrated that VC could be reductively dechlorinated to ethene in sulphate-reducing conditions *(Hoelen & Reinhard, 2004)*. Strongly reducing conditions in which *c*DCE and VC have so far been observed to be dechlorinated are not commonly encountered in groundwater. This could explain why incomplete chlorinated ethene reductive dechlorination may frequently occur, leading to *c*DCE and VC accumulation which is of greater health concern than PCE or TCE.

Traditionally, one refers to thermodynamics (i.e. redox conditions) when evaluating the likeliness of chlorinated ethenes to undergo reductive dechlorination. However, such considerations might not suffice as processes other than thermodynamics might control biodegradation. This was recently pointed out by Meckenstock et al., 2015 and is supported by the occurrence of reductive dechlorination observed in the field and the laboratory at more reduced conditions than necessary from a thermodynamic perspective.

Table 1. Standard reduction potentials at pH 7.0 (Wiedemeier *et al*., 1999)

Oxidants	Reductants	E_h^0 (V)
$O_2 + 4H^+ + 4e^-$	$2H_2O$	+0.81
$NO_3^- + 6H^+ + 6e^-$	½ $N_2 + 3H_2O$	+0.75
PCE + H^+ + e-	TCE + Cl^-	+0.58
$MnO_2 + 4H^+ + 2e^-$	$Mn^{2+} + 2H_2O$	+0.57
TCE + $H^+ + e^-$	*c*DCE + Cl^-	+0.55
VC + $H^+ + e^-$	Ethene + Cl^-	+0.49
*c*DCE + $H^+ + e^-$	VC + Cl^-	+0.36
$Fe(OH)_3 + 3H^+ + 3e^-$	$Fe_2+ + 3H_2O$	+0.06
$SO_4^{2-} + 9H^+ + 8e^-$	$HS^- + 4H_2O$	-0.22
$CO_2 + 8H^+ + 8e^-$	$CH_4 + 2H_2O$	-0.24
$H^+ + e^-$	½ H_2	-0.41

1.5.5. Kinetic control?

In terms of kinetic control at the microorganism scale, rates related to the contaminant transfer across the membrane, binding to the enzyme, and biochemical transformation influence the general microbial degradation kinetic *(Elsner, 2010, Thullner et al., 2013, Meckenstock et al., 2015)*. Depending on the conditions surrounding the microorganisms and the characteristics of the microorganisms themselves, one of these processes will be rate-limiting and will hence control the global degradation kinetic. For example, at high concentrations, kinetics are controlled by the degradation capacity of microorganisms since contaminants are relatively available. On the other hand, at low concentrations, kinetics are controlled by the mass transfer capacity of the environment since enzymes will catalyse the degradation faster than the compound uptake *(Thullner et al., 2013)*. The rate at which these processes take place may be quantified through Monod type kinetics, for example when looking primarily at the microorganism scale, or through simplified first order type kinetics, for example when looking at the subsurface scale. Less rate-controlling processes are considered when looking at the microorganism scale than at the subsurface scale.

It can be assumed that if redox conditions favourable for chlorinated ethenes reductive dechlorination in terms of a theoretical thermodynamic perspective are present (i.e. anaerobic for PCE and sulfate-reducing for TCE, *c*DCE and VC), the reason why reductive dechlorination might only be observed in more reduced conditions is that it is actually kinetically limited. Meckenstock *et al.*, 2015 also proposed that biodegradation in contaminated aquifers is largely kinetically controlled.

A successful reductive dechlorination of PCE to ethene in the subsurface is thus tributary, to a more or less large extent, of factors and processes encountered at different scales, i.e. the presence and activity of appropriate microorganisms, the electron donor availability, the contaminant availability to microorganisms, adequate redox conditions, and the kinetics associated with reductive dechlorination itself *(Bradley, 2000, Meckenstock et al., 2015)*.

1.6. Evaluating the potential for/performance of natural attenuation

In order to adequately evaluate whether natural attenuation is an appropriate management strategy for a site, i.e. it will efficiently and persistently protect the environment from harmful impacts *(Rügner et al., 2006)*, the potential for natural chlorinated ethenes degradation should be assessed.

1.7. Tracking the occurrence of reductive dechlorination

Various indicators may be evaluated in order to track the occurrence of reductive dechlorination in the subsurface.

Intermediate and end products as well as the concentration evolution thereof may for example be evaluated as their presence will indicate the occurrence of biodegradation. A limitation to its application however resides in the dilution of contaminants in groundwater which distorts the concentration relation to reductive dechlorination, as well as the potential occurrence of different degradation pathways. For example, *c*DCE as well as VC may both be reductively dechlorinated and oxidised to CO_2. This oxidation process might not easily be identified as the evolution of CO_2 is difficult to follow and especially to relate to chlorinated ethenes oxidation due to the intricate biogeochemical cycle CO_2 is involved in.

Redox conditions could also be considered to evaluate the potential for reductive dechlorination. An aquifer showing oxic conditions would definitely not host reductive dechlorination. Previous work

however showed that reductive dechlorination could occur under various redox conditions *(Vogel et al., 1987, Chapelle, 1996, Bradley, 2000, Hoelen & Reinhard, 2004, Tiehm & Schmidt, 2011)* and it may therefore be challenging to evaluate the potential for reductive dechlorination based primarily on redox conditions.

Molecular biology analysis aimed at identifying the presence and activity of dechlorinating microorganisms in the field may constitute an additional tool to track the occurrence of reductive dechlorination. Yet a restriction resides in the fact that not all microorganisms capable of carrying out reductive dechlorination have yet been identified, and that even if dechlorinating microorganisms are present and active, their activity might still be slow.

Although each of these indicators show uncertainties, combining the lines of evidence brought by each method and evaluating if the conclusions are coherent may eventually help tracking the occurrence of chlorinated ethenes reductive dechlorination.

1.7.1.1. Predicting the extent of reductive dechlorination

When dealing with contaminated sites, one may want to determine how long the source will persist, or evaluate the plume fate. As natural attenuation is rather adapted to treat the plume, the following work focuses on plume fate evaluation.

In terms of predicting the extent of reductive dechlorination, estimating degradation rates remains essential as this is currently virtually the only tool we possess to estimate the fate of contaminants in groundwater. Additionally, the choice of remediation approach partly depends on the rate at which the clean-up process will take place. So does the evaluation of whether or not a plume will reach a certain receptor. For bioremediation, such rates might concurrently account for several kinetic processes such as enzyme kinetics responsible for the contaminant biochemical transformation but also the residence time, the rate at which diffusion from sediments to water occurs or the mass transfer across the degrader cell membrane. Depending on whether they are measured in laboratory setup microcosms (which might or might not contain material from the field) or directly in the field, rates might hence differ in several orders of magnitude.

Numerous laboratory studies were performed where the degradation rates associated with microbial communities found in contaminated sites were estimated. Microbial metabolic rates are indeed usually found to be several orders of magnitude higher in the laboratory, where well-controlled and optimum conditions for microbial growth reside, than in the field *(Chapelle & Lovley, 1990, Suarez & Rifai, 1999)* (Table 2). This questions the pertinence of laboratory determined degradation constants to be representative of true field conditions *(Chapelle & Lovley, 1990, Madsen, 1991)*. As discussed in the previous section, various processes might affect the degradation rate. The best estimation approach consequently seems to be a field-based approach even though laboratory based determination of degradation constants is faster.

Although microbial growth is actually known to follow Monod kinetics which enzyme kinetics can be mathematically described by the Michaelis-Menten model, first order kinetics are usually assumed for simplification reasons when predicting plume fates undergoing reductive dechlorination. An approximate estimation of contaminants fate in groundwater may be conducted based on the range of formerly published degradation rate constants associated with reductive dechlorination as an alternative to estimating degradation rates from sites (Table 2) *(Aronson, 1997, Suarez & Rifai, 1999, Wiedemeier et al., 1999)*. Yet a relatively high uncertainty will remain.

Table 2. Summary of average half-lives (day) associated with first order degradation, after Suarez & Rifai, 1999; when mean values were not reported, averages were calculated weighted by the number of rates considered for the mean reported by Suarez & Rifai, 1999.

	Reductive dechlorination		**Aerobic degradation**	
	Lab	Field	Lab	Field
PCE	7	70	85	none
TCE	4	230	2	1.2
***c*DCE**	50	350	4	0.8
VC	2	230	4	0.4

Evaluating whether natural attenuation is an appropriate way to prevent contaminants from reaching a receptor thus remains challenging. Numerous parameters may influence the occurrence and rate at which reductive dechlorination of chlorinated ethenes might take place. The extent to which and the way how these parameters affect reductive dechlorination are not fully understood yet. Various tools may help identifying and quantifying reductive dechlorination in the field. Yet all show some limitations. Improving our understanding of how the various processes controlling in situ reductive dechlorination work and developing novel strategies to identify and quantify chlorinated ethenes degradation in the subsurface are thus essential steps for an optimal implementation of remediation strategies involving contaminant degradation. During the last two decades, increasing interest has been devoted to Compound Specific Isotope Analysis (CSIA) as this analytical method was proven a powerful tool when coming to elucidating the origin and fate of organic contaminants *(Schmidt et al., 2004, Elsner et al., 2005, Hunkeler, 2008, Thullner et al., 2012)*. This work will hence focus on the use of CSIA to address the limitations posed by the previously described traditional tools.

2. Compound specific isotopic analysis (CSIA)

2.1. Definition, natural abundance and standard notations

Isotopes are the set of different atoms of a same element presenting different number of neutrons. They are divided in two groups: radioactive and stable isotopes. Radioactive atoms are unstable, i.e. they decay by emitting radiation and releasing energy. In many cases, these emissions are accompanied by the transformation of the parent atom into an atom of lighter molecular weight with a known decay rate. This property can be very useful in the resolution of an identification issue involving time-scale affected processes. On the other hand, stable isotopes do not show measurable decay on geologic time scales, and elements currently found in nature such as hydrogen (H), carbon (C), nitrogen (N), oxygen (O), sulphur (S) and chlorine (Cl) are considered to have a constant mean stable isotopic composition. Natural isotopic abundances of H, C and Cl, which are of interest in the case of chlorinated ethenes, are listed in Table 3.

A molecule is made up of several atoms which can consist in one or another isotope of their corresponding element. Each molecule therefore presents a specific stable isotopic composition with regards to each element forming the molecule. Similarly, a bulk containing several molecules having each a specific isotopic composition will show an isotopic composition corresponding to the total amount of each isotope of each element forming the molecules of the bulk. The chemical species that differ only in the isotopic composition of their molecules or ions are called isotopologues (e.g.

HOD and HOH are two isotopologues of water and Figure 4) while isomers having the same number of each isotopic atom but differing in the isotopic atoms position are denominated as isotopomers (Figure 4). Isotopocules indicate all isotopomers of isotopologues. Isotopic compositions are measured in terms of isotopic ratios R which is determined as follows:

$$R = \frac{{}^{H}X}{{}^{L}X} \quad (1)$$

^{H}X and ^{L}X being the abundances of heavy and light isotopes of a given element X, respectively. For international standardisation purposes, stable isotope compositions of C, H, N, O, Cl are conventionally expressed by the delta notation as follows *(Coplen, 2011)*:

$$\delta^{n}X = \frac{R_{sample} - R_{standard}}{R_{standard}} \quad (2)$$

R_{sample} and $R_{standard}$ being the stable isotope ratios of the element X in the sample and in the corresponding international standard, respectively (see Table 3). n corresponds to the number of nucleons (i.e. protons + neutrons) of the heavy isotope. As $\delta^{n}X$ values are small they are usually reported in *per mil* (‰).

Table 3. Natural abundance and international references of H, C and Cl stable isotopes – modified from Höhener *et al.*, 2010 and de Laeter *et al*., 2003.

Element	Natural abundance of stable isotopes (%)	Isotope ratio (R)	International standard	International standard ratio ($R_{standard}$)
Hydrogen	^{1}H (99.9885) ^{2}H (0.0115)	$^{2}H/^{1}H$	Vienna Standard Mean Ocean Water (VSMOW)	1.5575×10^{-4}
Carbon	^{12}C (98.93) ^{13}C (1.07)	$^{13}C/^{12}C$	Carbonate from Vienna Pee Dee Belemnite (VPDB)	0.0111802 *(Hunkeler et al., 2009)*
Chlorine	^{35}Cl (75.76) ^{37}Cl (24.24)	$^{37}Cl/^{35}Cl$	Chloride ion in ocean water Standard Mean Ocean Chlorine (SMOC)	0.319766 *(Elsner et al., 2012)*

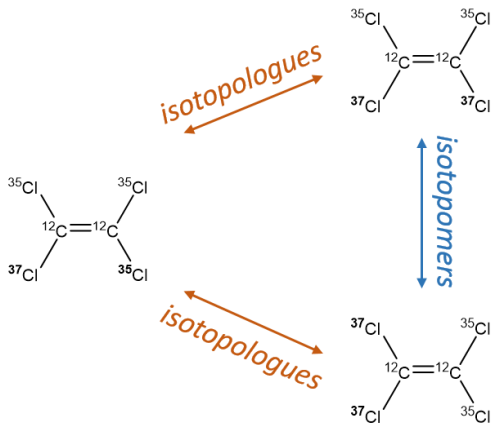

Figure 4. Illustration of some PCE isotopologues and isotopomers

2.2. Analytical measurements

Isotope ratios of organic compounds are most commonly measured with isotope ratio mass spectrometers (IRMS) that record the different masses in separate collectors to reach the highest precision *(Hunkeler et al., 2010)*. The element of interest can usually only be introduced in a specific chemical form. For isotopes of low molar weight (H, C, N, O), usually gaseous compounds are introduced such as H_2 for H, CO_2 for C, or N_2 for N. The corresponding instruments are denoted as gas-source isotope ratio mass-spectrometers. In the last decades, instruments were developed which allows for the direct transformation of a wide range of organic compounds into these measurement gases and transfer them directly to IRMS detectors. A common approach for volatile organic compounds consists of a GC separation of the compound followed by combustion of the compounds to CO_2 in case of C or pyrolysis to H_2 in case of H. These instruments are usually denoted as GC-IRMS and are the standard method to measure C, H and N isotope ratios in organic contaminants. As for non-volatile organic compounds, LC-IRMS has so far been commonly used for C isotope ratio analysis *(Godin & McCullagh, 2011)*. While detailed analytical methods will be described in the following chapters, an overall description of C and Cl isotopic analysis in volatile organic compounds is proposed in the following sections.
A summary of the measurement techniques, quantification limits, typical ranges and measurement accuracy can be found in Table 4.

2.2.1. C isotopic ratio

C isotopic ratios are commonly measured by isotope ratio mass spectrometry (IRMS). The general principle of such analytical setting relies on the deflection of ions with a different radius depending on their mass/charge ratio (m/z) by means of a magnet. After conversion of the compound of interest by combustion into the gaseous molecule of measurement (CO_2 in case of C isotopic analysis), the sample gas (produced CO_2) is introduced in the IRMS. The separated ions thus consisting of various isotopologues of CO_2 are then collected in separate Faraday cups where they are detected, after what the C isotopic ratio can be calculated.
Various instruments may be coupled to an IRMS which allow conducting compound C isotopic analysis in different type of materials. In order to determine the C isotopic ratio of a bulk material against the international standard VPDB with precision and accuracy, an elemental analyser IRMS (EA-IRMS) may be used where the sample is introduced in liquid or gas form. Calibration against VPDB is required to be performed by means of measuring at least two different international reference materials of known VPDB values, method known as two-point normalisation (e.g. NBS 19 calcium carbonate and L-SVEC lithium carbonate) *(Brand, 2014)*. It should be noted that only bulk measurements can be performed with EA-IRMS. An IRMS can also be coupled to a dual-inlet (DI-IRMS) where several pulses of reference and sample gas are injected in turn. The isotope ratio is then determined relative to the reference gas. This setup however does not allow compound mixture analysis and requires prior conversion of the sample and the reference material to CO_2 unless CO_2 previously calibrated in such a way is used as reference gas.
Finally, for compound mixtures, the currently most widely used setting is a gas chromatograph continuous flow IRMS (GC-CF-IRMS or GC-IRMS) which allows compound specific isotopic analysis by means of compounds separation in the GC. Compounds are then converted to CO_2 via a combustion interface and ion bombardment in the IRMS source contributes to charging CO_2 molecules which will further be detected depending on their m/z ratios. The reference gas is injected at the beginning and the end of each run, right before the helium flow enters the IRMS. It usually consists of CO_2

previously calibrated against the international standard by DI-IRMS thus preventing reference material exhaustion. Sample extraction prior to injection in the GC-IRMS can typically be carried out by purge-and-trap (P&T), solid phase microextraction (SPME) or headspace.

2.2.2. Cl isotopic ratio

In the 1990s, chlorinated ethenes were converted into CH_3Cl (g) through various methods *(vanWarmerdam, 1995, Holt et al., 1997)* and then introduced in a DI-IRMS for isotopic measurement where pulses of reference gas and sample were alternately injected so that the isotope ratio of the sample could be calculated relative to the international standard SMOC *(Hunkeler et al., 2010, Cincinelli et al., 2012)*. Another alternative consists in converting chlorinated ethenes into CsCl (s) and analyse the isotopic ratio using a thermal ionisation mass spectrometer (TIMS) *(Cincinelli et al., 2012)*. The reference material used for Cl isotopic ratio measurement is made from NaCl in pure water as the isotopic composition in seawater chloride is assumed to be very constant. For DI-IRMS measurements, chloride should then be transformed to CH_3Cl by precipitation with $AgNO_3$ followed by purification and reaction with CH_3I prior to injection in DI-IRMS. This method is nowadays used only to characterize external standards relative to the SMOC value which are necessary for further routine analysis. Cl isotopic ratio measurement has since then dramatically improved. To date, Cl isotopic ratios are being measured either by CF-IRMS or by GC quadrupole mass spectrometers (GCqMS). The first method involves an IRMS designed to detect specific mass fragments of the investigated compounds (so far developed for PCE, TCE, DCE *(Shouakar-Stash et al., 2006)*) after fragmentation by means of ion bombardment in the source. The reference gas of target compound previously calibrated against the SMOC by DI-IRMS is stored in the dual inlet bellows and pulses thereof are run at the beginning and at the end of each run. Dissolved compounds are typically injected after SPME extraction from water for the CF-IRMS settings and by headspace for the GCqMS. This method relies on the calculation of the Cl isotopic ratio based on the abundance of molecular and/or fragment ions of the targeted compound *(Sakaguchi-Söder et al., 2007, Aeppli et al., 2010, Jin et al., 2011)*. Measurement against the SMOC reference is made possible by injecting at least two SMOC calibrated external references during each sequence. A so-called two-point calibration is necessary for any accurate isotopic measurement, whether it is to determine exact values or shifts during a process affecting isotopic ratios *(Bernstein et al., 2011)*.

The advantage of these methods lies in the possibility to separate the compounds on-line, to reach lower measurement limits and without time consuming off-line chemical conversion steps prior to instrumental analysis. While CF-IRMS shows a higher precision than GCqMS (Table 4), a major drawback of CF-IRMS over GCqMS is the need to specifically adjust the Faraday cups for each compound, thus limiting the use of this method to a restricted set of compounds *(Cincinelli et al., 2012)*. Other advantages of GCqMS over CF-IRMS are its cost, the wide availability of GCqMS and the possibility to use one instrument for numerous organic compounds, provided that analytical methods are developed and SMOC calibrated standards are available for this compound.

Table 4. Summary of measurement techniques, quantification limits (QL, given in $\mu g \cdot l^{-1}$ as the concentration in water), typical ranges in chlorinated ethenes (in ‰) and measurement precision for each element of interest (in ‰); 1: 1σ ; 2: depending on the instrument (Agilent instruments showed higher precision than Thermo instruments); 3: reproducibility; 4: method detection limit (MDL, in $\mu g \cdot l^{-1}$); *(vanWarmerdam, 1995, Jendrzejewski et al., 2001, Jochmann et al., 2006, Shouakar-Stash et al., 2006, Abe et al., 2009, Bernstein et al., 2011, McHugh et al., 2011)*

Element	Measure-ment technique	Sample extraction	QL	Typical ranges in contaminants	Precision
C	GC-IRMS	P&T	PCE[4]: 1.3 TCE[4]: 1.2 *c*DCE[4]: 0.76	PCE: -37.4 to -23.2 TCE: -36.9 to -23.2	PCE[3]: 0.28 (n = 12-33) TCE[3]: 0.27 (n = 12-33) *c*DCE[3]: 0.28 (n = 12-33)
Cl	GC-IRMS	SPME	PCE: 20 TCE: 5 *c*DCE: 5	PCE: -4.4 to 1.2 TCE: -3.2 to 4.7	PCE[1]: 0.12 (n = 30) TCE[1]: 0.06 (n = 30) *c*DCE[1]: 0.08 (n = 15)
	GCqMS	Headspace injection	PCE: 50 – 100 TCE: 50 – 100		TCE[1,2]: 0.2 – 0.9

2.3. Contaminant isotopic fingerprints

Elements distributed across the Earth display various isotopic compositions depending on the location and the origins *(R.P, 2002, Komárek et al., 2008)*. Heavy isotopes of C (^{13}C) and H (^{2}H) naturally occur in nature in lower abundance compared to the corresponding light isotopes (Table 3) and are therefore expected to be present in lower proportions in molecules containing H and C such as petroleum hydrocarbons. As the conditions governing the formation of petroleum hydrocarbons vary depending on the geological reservoir, for one same compound originating from different reservoirs, different C and H isotopic signatures can be expected. Additionally, refinery treatments on petroleum hydrocarbons are expected to cause some variations in the isotopic signature *(O'Sullivan & Kalin, 2008)*. As chlorinated solvents are synthesised with petroleum hydrocarbons, differences in isotopic signatures are expected between manufacturers or even batches employing raw material from different origins and using different synthesis processes. This is supported by former work which revealed the existence of a wide range of manufacturer- and sometimes batch-specific C and Cl isotopic compositions of pure chlorinated solvents such as PCE, TCE, or 1,1,1-trichloroethane (1,1,1-TCA) (Figure 5)*(vanWarmerdam, 1995, Jendrzejewski et al., 1997, Beneteau et al., 1999, Jendrzejewski et al., 2001, Shouakar-Stash et al., 2003, McHugh et al., 2011)*.

A substantial advantage of this non uniformity is that isotopic signatures can serve as a fingerprint. They may indeed be used to elucidate which portion of a downgradient contamination is linked to which source of a polluted site impacted by several sources, provided that these sources have distinct isotopic compositions *(Beneteau et al., 1999)*. Higher accuracy will be attained for source discrimination with higher number of elements analysed in terms of isotopic composition (e.g. C and Cl) *(Lojkasek-Lima et al., 2012, Palau et al., 2014)*. The successful application of dual C-Cl isotopic

analysis to elucidate the contaminant origin in a few sites supports the potential power of such tool to address legal issues and apply the "polluter-pays" principle *(Lojkasek-Lima et al., 2012, Palau et al., 2014)*.

While the C-Cl isotopic fingerprint variability in some chlorinated solvents was demonstrated between manufacturers from North America, such data is lacking in Europe. Similarly, no study tracking the production and use of chlorinated solvents was carried out in Europe contrary to North America *(Doherty, 2000, Moran et al., 2007, Doherty, 2012)*. Such gap thus questions the applicability of C-Cl isotope analysis for source delineation purposes in Europe.

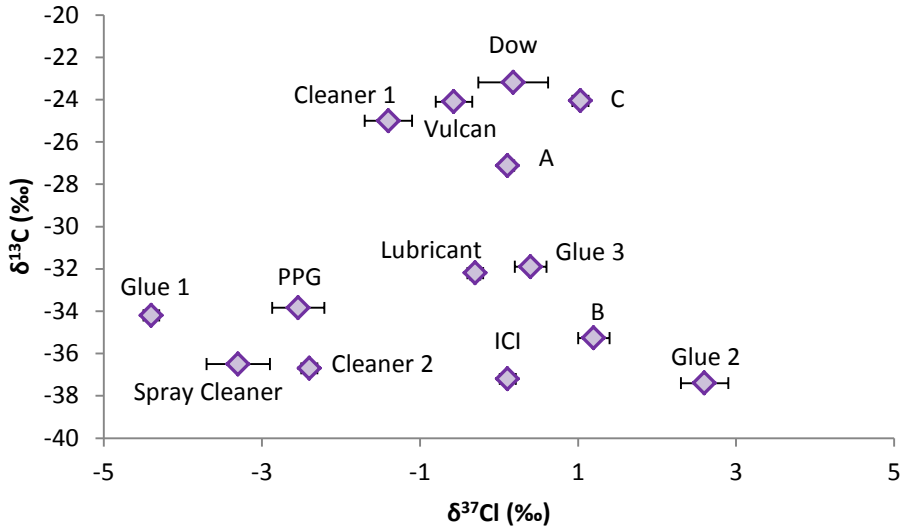

Figure 5. C and Cl isotopic composition variability among manufacturers of PCE, adapted from van Warmerdam *et al*., 1995, Jendrzejewski *et al*., 2001, and Mc Hugh *et al*., 2011.

2.4. Processes affecting isotopic ratios

Some processes affecting contaminants can induce an isotopic shift between the initial isotopic signature and the isotopic composition after the contaminant underwent such isotope fractionating process. This is due to the molecules undergoing kinetic processes at different rates depending on the isotopes present in the compound (kinetic isotope effect KIE) or simply to the different isotopic composition between one compound present at equilibrium in two phases (equilibrium isotope effect EIE). Even though isotope effects originate from processes affecting isotopologues or even isotopomers, isotopic fractionation is commonly estimated based on the bulk isotopic composition of all isotopologues without distinction between isotopologues.

In the subsurface and more particularly in groundwater, contaminants are affected by transport processes (advection, dispersion, diffusion), phase partitioning processes (sorption), NAPL-dissolution and biotically or abiotically mediated transformations (Figure 1). While it was demonstrated that sorption, dissolution, dispersion and advection have a small impact on isotopic compositions of organic compounds *(Clark, 1997, Hunkeler et al., 1999, Slater et al., 2000, Hunkeler et al., 2004, Elsner et al., 2005, Hunkeler et al., 2010)*, diffusion can change the isotopic composition of a contaminant when it becomes the dominant transport process, for instance at the dissolved

contaminant plume fringe or in a zone of low permeability *(Wanner & Hunkeler, 2015)*. This isotope fractionation process is however negligible with respect to biodegradation and not relevant in the plume centre in the saturated zone as advection dominates.

2.4.1. Isotope fractionation during biodegradation

Depending on various parameters previously discussed, biodegradation or abiotic degradation may occur in the subsurface. The activation energy required to break bonds involving lighter elements being less important than the energy required to break bonds involving heavier elements, molecules containing lighter isotopes will react faster than those containing heavier isotopes. Such difference in reaction rates induces a progressive enrichment in heavy isotopes of the remaining substrate during degradation. The extent of difference between degradation rates associated with molecules containing the broken bond involving light isotopes and molecules containing the broken bond involving heavy isotopes can be described by the kinetic fractionation factor α_{bulk}:

$$\alpha_{bulk} = \frac{^{H}k_{bulk}}{^{L}k_{bulk}} \quad (3)$$

where $^{H}k_{bulk}$ and $^{L}k_{bulk}$ are the degradation rate constants associated with the degradation of the molecules containing the heavy and the light isotopes, respectively.

Normal primary isotopic effects which reflect a faster bond breakage involving light elements than a bond breakage involving heavy elements ($\alpha_{bulk} < 1$) are usually observed during the course of a reaction. More unusual situations may nevertheless arise where a faster bond breakage involving heavy elements than a bond breakage involving light elements results in an *inverse* primary isotopic effect ($\alpha_{bulk} > 1$). Additionally, atoms which are not involved in the broken bond might affect the isotopologues degradation rates as well. This phenomenon is denoted as *secondary* isotopic effect.

2.4.2. Quantification of biodegradation by means of isotopes

Rather than the kinetic fractionation factor, the enrichment factor ε_{bulk} which reflects the isotopic fractionation amplitude is commonly derived:

$$\varepsilon_{bulk}(‰) = (\alpha_{bulk} - 1) \times 1000 \quad (4)$$

Unless specified otherwise, enrichment factors or fractionation factors discussed in this thesis are bulk factors denoted ε and α, respectively.

Furthermore, it was formerly demonstrated that the following Rayleigh equation, which describes the isotope enrichment phenomenon, could be used to evaluate isotope data and enabled to determine the enrichment factor associated with laboratory degradation studies *(Clark, 1997, Hunkeler et al., 1999)*:

$$\ln \frac{\delta E_t + 1000}{\delta E_0 + 1000} = \varepsilon_E \ln f \quad (5)$$

where E is the considered element, δE_t and δE_0 are the isotope ratios of the element E at times t and 0 reported against international standards, and f is the PCE remaining fraction at time t.

Wide ranges of enrichment factors associated with chlorinated ethenes degradation have been determined for each chlorinated ethene, particularly for C and to a lesser extent for Cl, as summarised in Table 5.

Enrichment factors may be chosen from the literature or determined based on a laboratory experiment set up with material from the field site to estimate the extent of degradation as well as the degradation rate constant (first order type) associated with the degradation process occurring in

a site *(Hunkeler, 2008, Hunkeler et al., 2010)* according to *(Meckenstock et al., 2004, Hunkeler et al., 2010)*:

$$B = 1 - \exp(\frac{\Delta\delta^{13}C}{\varepsilon}) \quad (6)$$

where B is the percent of biodegradation, $\Delta\delta^{13}C$ the difference between initial and final C isotopic ratio and ε the enrichment factor, and:

$$k_x = -\frac{\Delta\delta^{13}C \cdot v}{\varepsilon \cdot x} \quad (7)$$

where k_x is the first order degradation constant, $\Delta\delta^{13}C$ the difference between initial and C isotopic ratio at the distance x from the source, v the groundwater velocity and ε the enrichment factor.

Table 5. Range of enrichment factors given in ‰ associated with biotic and abiotic degradation of chlorinated ethenes *(Hunkeler et al., 1999, Barth et al., 2002, Hunkeler et al., 2002, Numata et al., 2002, Poulson and Naraoka 2002, Hunkeler et al., 2003, Chu et al., 2004, VanStone et al., 2004, Chartrand et al., 2005, Nijenhuis et al., 2005, Cichocka et al., 2007, Lee et al., 2007, Liang et al., 2007, Dong et al., 2008, Elsner et al., 2008, Tiehm et al., 2008, Abe et al., 2009, Fletcher et al., 2011, Marchesi et al., 2012, Audí-Miró et al., 2013, Cretnik et al., 2013, Badin et al., 2014, Cretnik et al., 2014, Liu et al., 2014)*. Enrichment factors reported between the beginning and the end of this work are also reported here. This table thus includes results from this thesis work. Median, minium and maximum values are given as well as the number of studies included.

	biotic		**abiotic**	
Com-pound	**Reductive dechlorination**	**Oxidation (metabolic/ cometabolic)**	**Reductive dechlorination (Fe0, FeS, FeS_2, green rust)**	**Oxidation (permanganate/ persulfate)**
PCE	ε_C : **-0.4 to -19** (-3.6, n = 31) ε_{Cl} : **-0.9 to -10.0** (-2.0, n = 5)	ε_C : - ε_{Cl} : -	ε_C : -5.7 to -30.2 (-15.5, n = 9) ε_{Cl} : -	ε_C : -17 (n = 1) / - ε_{Cl} : -
TCE	ε_C : -2.5 to -18.9 (-12.2, n = 31) ε_{Cl} : -2.7 to -5.7 (-4.3, n = 7)	ε_C : -1.1 to -18.2 (n = 2) ε_{Cl} : -	ε_C : -7.5 to -33.4 (-16.7, n = 17) ε_{Cl} : -2.6 (n = 1)	ε_C : -21.4 to -26.8 (-25.1, n = 3) / -3.6 (n = 1) ε_{Cl} : -
***c*DCE**	ε_C : -12 to -29.7 (-18.8, n = 17) ε_{Cl} : -1.5 (n = 1)	ε_C : -0.4 to -9.8 (-8.4, n = 6) ε_{Cl} : -0.3 (n = 1)	ε_C : -6.9 to -21.7 (-15.9, n = 7) ε_{Cl} : -6.2 (n = 1)	ε_C : -21.1 (n = 1) / -7.6 (n = 1) ε_{Cl} : -
VC	ε_C : -19.9 to -31.1 (-23.5, n = 14) ε_{Cl} : -1.7 (n=1)	ε_C : -3.2 to -8.2 (-6.3, n = 17) ε_{Cl} : -0.3 (n = 1)	ε_C : -6.9 to -19.4 (-16.6, n = 5) ε_{Cl} : -	ε_C : - ε_{Cl} : -

2.4.3. Factors controlling the magnitude of fractionation during biodegradation

Choosing an enrichment factor from the literature might be intricate as the large range of published factors associated with one compound degradation suggests. Understanding the relationship between degradation pathways and their corresponding enrichment factors is therefore of interest. Isotopic trends observed in compounds undergoing biodegradation result from the difference in degradation rates between molecules containing light isotopes compared to molecules containing

heavy isotopes. Isotopic behaviours and therefore enrichment factors thus reflect rate-limiting steps. These might as well be the rate-limiting step of the biochemical reaction (i.e. in the reaction mechanism) as other steps such as the contaminant transfer across the membrane or the contaminant binding to the enzyme. This could explain the large range of enrichment factors observed as the latter not only reflect the biochemical reaction (which cannot be expected to occur in as many different ways as there are enrichment factors) but also the transfer process across the cell membrane and the binding to the enzyme, all of which depend on the microorganisms and are therefore likely to vary between microorganisms. Relating enrichment factors to reaction mechanisms might help restraining the range of enrichment factors to ranges corresponding to each reaction mechanism. An interest thus resides in the use of isotopic data to gain mechanistic insights.

2.4.4. Mechanistic insight based on isotopes

It was recently precisely suggested that observing isotopic trends of two elements simultaneously may help getting more insight into the biochemical reaction itself. It may indeed be assumed that the difference in rate between light and heavy isotopologues at which the transfer across the membrane takes place may be indifferent to elements while the reaction mechanism which involves a bond breakage between two different elements might affect the two elements differently. Due to the relatively recent development of analytical methods enabling routine Cl isotope analysis, so far few studies explored the use of dual isotope analysis to gain such insight *(Cretnik et al., 2013, Kuder et al., 2013)*. Further investigations are therefore required to improve our understanding of the link between dual C-Cl isotope slopes and reaction mechanisms.

2.4.5. The particularity of reductive dechlorination

While isotopic trends displayed by parent compounds follow the Rayleigh equation where decreasing concentrations are accompanied by increasing isotopic ratios, compounds which are being both produced and degraded do not. The interpretation of isotopic ratios during sequential reductive dechlorination is thus intricate. In terms of C isotopic composition, the first produced compounds will be lighter than the initial parent compound with an offset equalling the enrichment factor. This results from the fact that the backbone of the produced compound is made of the backbone of the preferentially degraded lighter parent compound. The isotopic ratio of the daughter compound will then increase along with degradation as the degraded parent compound gets heavier. Another rule that can be observed during reductive dechlorination is that the isotopic balance should equal the initial compound isotopic signature at any time *(Nijenhuis et al., 2013)*. It follows that the C isotopic signature of the last degradation product when no further degradation is possible will equal that of the initial compound. For the same reasons, a non-constant isotope balance would be typical of a non-sequential degradation process (e.g. oxidation where CO_2 is produced). An illustration of the C isotopic composition evolution along with reductive dechlorination is proposed in Figure 6. Contrary to the case of C where atoms present in the parent compound remain in the daughter compound, a Cl atom gets cleaved out at each step of reductive dechlorination. It is hence expected that the Cl isotopic ratio in the produced compound at the beginning of degradation corresponds to the isotopic ratio of the Cl remaining in the molecule during the C-Cl bond cleavage and thus to the initial isotopic composition of the parent compound. This is particularly true when no secondary isotopic effects take place. Similarly to C, the Cl isotopic ratio of the daughter compound will then increase along with degradation (Figure 7). The evolution of Cl isotopic ratios was formerly simulated assuming first order kinetics and that no secondary isotopic effect occurred *(Hunkeler et al., 2009)*. Recent studies however support the existence of secondary isotopic effects *(Kuder et al., 2013, Cretnik et al., 2014)*,

and although first order kinetics are usually employed for simplifying reasons, microbial growth is actually associated with Monod type kinetics. There is thus a need to develop more advanced models taking into account these so far neglected phenomena.

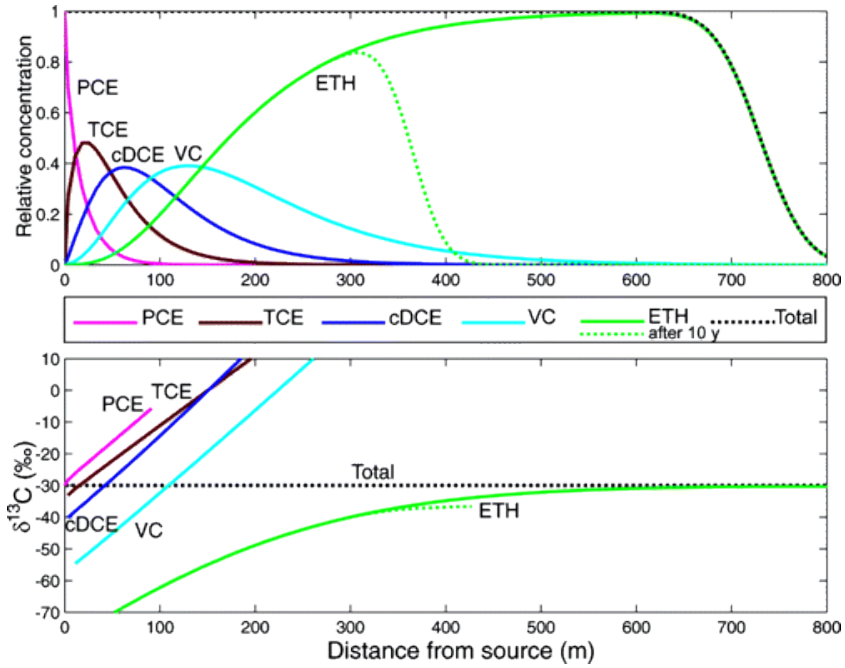

Figure 6. Evolution of chlorinated ethenes concentration and C isotopic composition during PCE reductive dechlorination based on transport simulation (reproduced from Environmental Science & Technology 39 (11), 4189-4197 (2005), by permission of the American Chemical Society *(Van Breukelen et al., 2005)*)

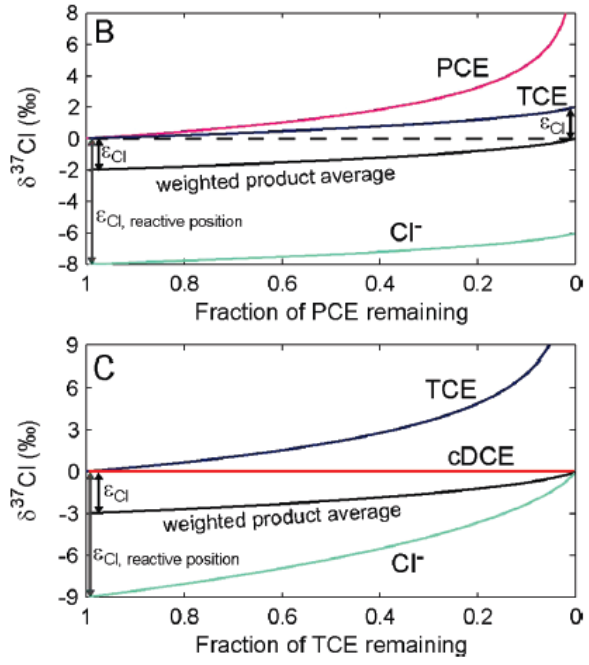

Figure 7. Evolution of Cl isotopic composition during PCE and TCE reductive dechlorination in function of the parent compound fraction remaining based on simulations (reproduced from Environmental Science & Technology 43 (17), 6750-6756 (2009), by permission of the American Chemical Society *(Hunkeler et al., 2009)*)

3. Thesis objectives

Despite the numerous successful applications of CSIA to solve various issues related to the origin and fate of chlorinated ethenes in the subsurface, some gaps remain in the understanding of how and which specific processes affect chlorinated ethenes isotopic composition. More particularly, improving our understanding of the processes underlying chlorinated ethenes isotopic trend during reductive dechlorination should eventually contribute to improve the evaluation of their natural attenuation potential in the subsurface. Additionally, as the extent of applicability of CSIA at the field scale has not yet been thoroughly explored, its applicability should be further tested.
The aim of this thesis was to address some of these gaps by exploring the use of C-Cl isotopic analysis as a complementary tool to more classical investigation methods commonly performed to evaluate the origin and fate of chlorinated ethenes in groundwater. A description of the gap addressed in each chapter and a short introduction thereof is presented below.

Chapter 1: Tetrachloroethene source delineation using C-Cl isotopic analysis: field investigations to assess the isotopic signature variability
The successful application of C-Cl isotopic analysis for source delineation purposes is tributary of a significantly different isotopic signature between sources. In Switzerland, data regarding the variability of chlorinated solvents manufacturers as well as of used chlorinated solvents isotopic fingerprint variability is lacking. In order to evaluate the extent of applicability of such method for source delineation purposes in Switzerland, the source isotopic signature variability between 10 sites contaminated with PCE and located in Switzerland was assessed.
This chapter was published in Grundwasser, 2015, 20 (4), 263-270.

Chapter 2: Multiple dual C-Cl isotope patterns associated with reductive dechlorination of tetrachloroethene
Estimating the extent of biodegradation in the field based on isotopic measurements requires choosing an adequate enrichment factor among the sometimes quite large range of values (e.g. PCE). Since three different reaction mechanisms have been postulated for the biotic reductive dechlorination of PCE, pinpointing more restricted enrichment factor ranges corresponding to each reaction mechanism could help choosing enrichment factors. The latter do not allow differentiating between chemical reaction (i.e. reaction mechanism) and other rate-limiting steps such as transfer across the cell membrane or enzyme-binding. On the contrary, dual C-Cl isotopic slopes are assumed to reflect the reaction mechanism *(Elsner et al., 2005, Abe et al., 2009)* and could thus be used to restrain the choice of enrichment factors. Additionally, they could help getting more insight into reaction mechanisms involved in biotic reductive dechlorination. This chapter aims at investigating the potential of dual C-Cl isotopic analysis to gain more insight in the reaction mechanism underlying PCE biotic reductive dechlorination in view of further choosing adequate enrichment factors to assess the extent of biodegradation in the field or to differentiate degradation processes. To this end, the behaviour of PCE in terms of C and Cl isotopic composition during reductive dechlorination by two bacterial consortia was studied.
This chapter was published in Environmental Science and Technology, 2014, 48, 9179-9186.

Chapter 3: Dual C-Cl isotope patterns associated with TCE as a reactant, product and intermediate of reductive dechlorination

The occurrence of secondary Cl isotopic effects during reductive dechlorination have so far been neglected. Their existence could however change the interpretation of isotope data with regards to processes affecting the contaminant during its biotransformation. Based on the Cl isotopic composition of TCE produced by PCE reductive dechlorination by the bacterial consortia presented in chapter 2, the possibility that secondary Cl isotope effects occur during PCE reductive dechlorination was explored in this chapter. Moreover, the interpretation of isotopic data is not always straightforward in the case of intermediate compounds which usually pose more concern than originally released compounds. Dual C-Cl isotope associated with TCE as a reactant, intermediate and product of reductive dechlorination were hence compared to further investigate which process controlled the slopes associated with TCE as an intermediate. To this end, an additional experiment where TCE was fed to one of the bacterial consortia used in chapter 2 was carried out.

Part of this chapter was submitted to Environmental Science and Technology with part of Chapter 4.

Chapter 4: Influence of secondary isotope effects and Monod kinetics when modelling Cl isotope trends in chlorinated ethenes biotic reductive dechlorination

In order to incorporate C and Cl isotopic data to reactive transport models to improve the estimation of the fate of chlorinated ethenes in groundwater, comprehensive models simulating the evolution of the isotopic composition of chlorinated ethenes during reductive dechlorination should be developed. So far, models describing the evolution of isotopic compositions were set up assuming first order kinetics and neglecting secondary isotopic effects. However, in reality, bacterial growth follows Monod-type kinetics and substrate degradation should be simulated accordingly. It was moreover discovered that secondary isotopic effects could play a non-negligible role in some cases. In an attempt to address this gap, a model including Monod kinetics and which considers secondary isotopic effects was set up to simulate the evolution of chlorinated ethenes isotopic compositions during biotic reductive dechlorination. In order to assess the model's applicability, the results were compared to the three laboratory experiments presented in chapters 2 and 3 where the reductive dechlorination of PCE to TCE by one consortium and the dechlorination of TCE to *c*DCE and PCE to *c*DCE by another consortium was conducted.

Part of this chapter was submitted to Environmental Science and Technology with part of Chapter 3.

Chapter 5: Plume characterisation after tetrachloroethene source in situ thermal treatment by means of isotopic and novel molecular biology tools

Finally, the contribution of C and Cl isotopic analysis to identify changes in redox processes further affecting chlorinated ethenes in groundwater was investigated when assessing the effect of source thermal remediation by steam injection on a chlorinated ethenes plume. For this purpose, field investigations were performed in a site located in Denmark which was explored in a previous work, prior to source thermal remediation. Redox conditions, chlorinated ethenes concentrations and isotopic compositions as well as the presence and activity of microbial populations were characterised along the plume centreline 7 years after the source thermal treatment. Results were compared to the plume characterisation performed prior to source remediation to document the effect of thereof.

This chapter will be submitted to Journal of Contaminant Hydrology.

Chapter 1

Tetrachloroethene source delineation using C-Cl isotopic analysis: field investigations to assess the isotopic signature variability

Alice Badin, Mario Schirmer, Christiane Wermeille, Daniel Hunkeler

Grundwasser, 2015, 20, 263-270

Abstract: When dealing with contaminated sites, identifying the source of contamination is critical for regulatory purposes. For chlorinated ethenes, previous studies have shown that dual carbon-chlorine (C-Cl) stable isotope analysis could be a key to address such issue as isotopic signatures vary between manufacturers and therefore, supposedly between sources. A successful application of this method relies on the assumption that different sources in the field will also show different signatures. Since the solvents used in the past are not available anymore, this study aimed at investigating the extent of applicability of C-Cl stable isotope measurements for source identification based on field investigations. 10 sites which covered whole Switzerland and various sectors employing tetrachloroethene (PCE) were chosen. Differences were observed between some sites, suggesting that this method could be successfully applied. Other sites showed very similar isotopic signatures, indicating that this method applicability is site-specific. Additionally, the isotopic signature variability between sites was less significant than between the values previously reported for various manufacturers from North America. It was also confirmed that PCE reductive dechlorination should be considered when applying C-Cl isotope analysis for source identification.

Keywords: chlorinated ethenes, isotopic signature, source identification, contaminated site

1. Introduction

Chlorinated solvents were widely used between the 1940s and 1970s for metal degreasing in the car or watch industry, as cleaning agents in dry-cleaning factories, as solvents in the chemical industry or during quartering processes. Their careless disposal and accidental spills lead to a large amount of contaminated sites which affect groundwater quality *(Pankow & Cherry, 1996)*. In Switzerland alone, an estimated amount of 12'300 sites including both industrial areas and landfills would be polluted with such chlorinated solvents.

Since the party responsible for a pollution is usually expected to cover the remediation costs, confidently identifying the latter becomes essential when a site requires remediation actions. A high interest resides in employing alternative methods for contamination source delineation since classical investigations involving hydrogeological and hydrochemical studies do not always suffice.

Previous studies have shown that carbon and chlorine isotopic compositions (C-Cl isotopic signatures) of pure tetrachloroethylene (PCE) significantly varied between manufacturers *(vanWarmerdam, 1995, Jendrzejewski et al., 2001, McHugh et al., 2011)*. Compound specific isotopic analysis thus represents a powerful tool for contaminant source delineation which was formerly successfully applied in a few studies *(McHugh et al., 2011, Lojkasek-Lima et al., 2012, Kaown et al., 2014, Palau et al., 2014)*. Moreover, some guidelines on how to apply this method were published *(Hunkeler, 2008, Eisenmann, 2010)*. Due to the only recent establishment of Cl isotopic analysis for field samples and to the lack of certified reference standard for organic compounds *(Sakaguchi-Söder et al., 2007, Aeppli et al., 2010, Bernstein et al., 2011, Hitzfeld et al., 2011, Jin et al., 2011)*, only a few studies employed dual C-Cl isotope analysis *(McHugh et al., 2011, Lojkasek-Lima et al., 2012, Kaown et al., 2014, Palau et al., 2014)* while the majority of so far reported source delineation studies applied single C isotope analysis *(Hunkeler et al., 2004, Eberts et al., 2008, Blessing et al., 2009, Amaral et al., 2011, Nijenhuis et al., 2013)*. The successful and routine application of C-Cl isotopic analysis for source delineation is however tributary of a C-Cl isotopic signature variability between sources in the field which should thus be verified. Moreover, while the isotopic signature variability between compounds produced by different manufacturers was shown in North America, such data is missing for Europe, including Switzerland. Additionally, unlike in the USA, no document referencing the origin of various PCE used in Switzerland and their corresponding isotopic signature exists *(Doherty, 2000, Moran et al., 2007)*. This work thus aims at investigating the PCE C-Cl isotopic composition variability in the field, i.e. in contaminated sites located in Switzerland. Groundwater samples were taken in the source zone of 10 sites located in Switzerland which were contaminated with PCE in order to assess their isotopic composition variability. The different sites hosted different branches of PCE use and are spread over the country. The measured C-Cl compositions were compared between each other and with PCE isotopic signatures of PCE produced by different manufacturers.

2. Materials and Methods

2.1. Choice of contaminated sites

Several criteria were used to choose the sites: (1) biodegradation should be negligible since its occurrence leads to a change in isotopic composition *(Hunkeler et al., 1999, Lollar et al., 1999, Bloom et al., 2000)*. Oxic conditions and/or only low metabolites concentrations should therefore be present. (2) Several sampling points should be available near the source. (3) The sites should represent different PCE application branches and cover various the whole country. (4) The owner

should allow data publication. (5) The PCE concentrations should comply with analytical requirements (i.e. > 100 µg·L^{-1}). 10 sites fulfilling these criteria could finally be identified. The chosen sites represent three typical branches employing chlorinated solvents, i.e. dry cleaning (7), metal degreasing (3) and processes applied during quartering (1) (Table 1). The sites main characteristics are summarized in Table 1.

2.2. Groundwater sampling

Groundwater sampling took place between March and August 2012 and each site was sampled within one day. Two to five sampling points were sampled per site, depending on the number of sampling points available close to the source and the corresponding PCE concentration. The wells were purged until field parameters (i.e. pH, conductivity, dissolved oxygen (DO)) were stable. Submersible pumps were used for purging and collecting samples except for multilevel wells where foot valve or peristaltic pumps were used. Teflon tubing was used for collecting samples to avoid any solvent sorption during sampling. Water samples for isotope and concentration analysis were collected in 40 mL glass vials sealed without headspace with PTFE-lined silicone septa and screw caps. Nitric acid (10 %) was added onsite to water samples to bring the pH to 2 in order to avoid any biodegradation during storage. Samples were transported in coolers topped with ice until their storage in a cold room at 4 °C. pH, conductivity and DO were measured on site with a probe dedicated to field measurements (HQ40D probe, HACH). Mn^{2+} and Fe^{2+} concentrations were measured on site via a portable colorimeter (DR 890, HACH) when DO contents were below 1 mg·L^{-1}, in order to evaluate to what extent the conditions were reducing.

.

Table 1. Summary of the geology, hydrogeology, geochemistry and history of the 10 studied sites; n: number of sampled wells; L: length; W: width; D: depth; unk.: unkown; DC: dry cleaning; GW: groundwater.

Site	Industry type	Site history	Plume description	Aquifer description	n	CE concentration interval ($\mu g \cdot l^{-1}$)	Redox conditions
SA	DC / machinery degreasing	* 1959-1990 * 1000 l tank * Phase suspected	* L: > 80 m * W: *unk.* * D: 40 m	* Sand and gravel aquifer containing clay lenses of low permeability * Water table: 5 m * Aquifer thickness: 34 m	3	[PCE]: 1'000 – 5'900 [TCE] < 1% [PCE] [*c*DCE] < 1% [PCE]	oxic to manganese reducing
SB	DC	* 1968 - 1983	* L: > 70 m * W: *unk.* * D: *unk.*	* Sand and gravel aquifer containing impermeable lentils * Water table: 5 m * Aquifer thickness: 4 m	5	[PCE]: 100 – 6'400 [TCE] < 5 [*c*DCE] < 5	oxic
SC	DC	* 1896 – 2006 * Accidental spills in 1989 and 1990	* L: 240 m * W: 140 m * D: < 4 m	* Silty sand and gravel aquifer * Water table: 2.5 - 3.5 m * Aquifer thickness: 0.5 - 1.5 m	2	[PCE]: 890 – 1'700 [TCE] < 5 [*c*DCE] < 5	oxic
SD	Metal degreasing	*unk.*	*unk.*	* Silty and sandy gravel aquifer * Water table: 2 m * Aquifer thickness: 6.5 m	4	[PCE]: 80 - 210 [TCE] < 5 [*c*DCE] < 5	oxic
SE	Metal degreasing	* 1955 - 1995 * Used amount: several t/year	* L: > 160 m * W: > 60 m * D: *unk.*	* Sand and gravel aquifer * Water table: 7-8 m * Aquifer thickness: 4-5 m	4	[PCE]: 380 - 570 [TCE] < 5 [*c*DCE] < 5	oxic
SF	Quartering	* 15 years use * Estimated spilled amount: 3'600 kg	* L: 750 m * W: 100 m * D: *unk.*	* Gravel aquifer * Water table: 2 – 3 m * Aquifer thickness: 2 – 4 m	2	[PCE]: 630 - 650 [TCE] < 5 [*c*DCE] < 5	oxic to manganese reducing
SG	DC	* 1974-1990	*unk.*	* Gravel and sand aquifer with silty and marl lenses * Water table: 4 – 5 m * Aquifer thickness: 3 m	3	[PCE]: 890 – 132'000 [TCE] < 4% [PCE] [*c*DCE] < 1% [PCE]	oxic
SH	DC	* 1966 - 1988	*unk.*	* Silty sand and gravel aquifer containing silt lenses * Water table: 6 m * Aquifer thickness: 1 m	2	[PCE]: 70 -600 [TCE] < 5 [*c*DCE] < 5	oxic
SI	DC	*unk.*	* L: 100 m * W: 35 m * D: *unk.*	* Silty sand and gravel aquifer with a cavity below the source area * Water table: 3 m * Aquifer thickness: 1 – 4 m	4	[PCE]: 37'000 – 150'000 [TCE] < 1% [PCE] [*c*DCE] < 1% [PCE]	oxic
SJ	DC	* 1954 - 1976 * Estimated used amount: 60 t	* L: 440 m * W: 100 m * D: < 7 m	* Gravel aquifer * Water table: 2 – 5 m * Aquifer thickness: 2 – 5 m	2	[PCE]: 20-40 [TCE] < 5 [*c*DCE] < 5	oxic

2.3. Analytical methods

A summary of the analytical methods for isotopic analysis is given in the Appendices (Appendix 1).

Chlorinated ethenes concentrations were measured with a Trace™ GC Ultra Gas Chromatograph (Thermo-Finnigan™) coupled with a DSQ II quadrupole mass spectrometer (GC-qMS, Thermo-Finnigan™). 500 µL headspace were injected by means of a CombiPal Autosampler (CTC Analytics) in the GC from a 20 mL glass vial filled with 10 mL water sample. Calibrations were performed with external standards containing 50, 100, 150, 200 and 300 $\mu g \cdot L^{-1}$ of each chlorinated ethene.

Cl isotope ratios were determined using the method described by Aeppli et al. based on gas chromatography quadrupole mass spectrometry (GC-qMS) *(Aeppli et al., 2010)*. A summary of the analytical methods can be found in the Appendices (Appendix 1). The instrumental setup consisted of an Agilent 7890 GC coupled to an Agilent 5975C quadrupole mass selective detector (Santa Clara, CA, USA). In order to ensure a high accuracy *(Bernstein et al., 2011)*, a calibration with two external standards ($\delta^{37}Cl_{EIL1}$ = +0.3 ‰ and $\delta^{37}Cl_{EIL2}$ = -2.5 ‰) which were formerly characterized by the Holt method *(Holt et al., 1997)* at the University of Waterloo was completed for each sequence to obtain δ values on the SMOC scale. A working PCE standard was measured after every 10 sample to check the measurement stability. To reach a high precision and in order to be largely above the quantification limit of 30 $\mu g \cdot L^{-1}$, samples were diluted to a constant concentration of 100 $\mu g \cdot L^{-1}$ and analysed 10 times by headspace injection using a CombiPal Autosampler (CTC Analytics, Zwingen, Switzerland). A DB-5 column (30 m, 0.25 mm, 0.25 µm, Agilent) with a constant helium flow of 1.2 $mL \cdot min^{-1}$ was used to perform chromatographic separation. Mass to charge ratios (m/z) of 166 and 164 were targeted in SIM mode for PCE. The Cl isotopic ratio in delta notation corresponds to the mean value of the 10 injections, and the uncertainty thereof is given by the standard deviation of the injections divided by the square root of the number of injections (i.e. the standard error of the mean).

C isotopic ratios were determined using an Agilent™ 7890a gas chromatograph (GC) coupled to an Isoprime™ 100 isotope ratio mass spectrometer (IRMS) via an Isoprime GC5 combustion interface and a purge-and-trap (P&T) system (Stratum, Teledyne Tekmar). Aqueous samples were diluted before analysis in 40 mL glas vials with a PTFE-lined screw cap to reach a final PCE concentration of 30 $\mu g \cdot L^{-1}$ (i.e. total 10 nmol C analysed). 25 mL of the diluted samples were purged with N_2 gas (40 $mL \cdot min^{-1}$) and the degassed compounds were retained on a Vocarb 3000 trap (VICI). After the purging step (10 min), the compounds were transferred into a cryogenic trap working with liquid N_2 (Tekmar Dohrmann) connected to the GC column (DB-VRX, 60 m, 0.25 mm, 1.4 µm). This step was followed by a rapid temperature increase (from -100 °C to 180 °C, using a ramp of 15 $°C \cdot s^{-1}$) which released the concentrated compounds to the column. Helium was used as a gas carrier (1.2 $mL \cdot min^{-1}$). Compounds were then separated in the GC oven, combusted to CO_2 in the combustion interface and sent to the IRMS for isotopic ratio ($^{13}C/^{12}C$) analysis. Samples were measured in duplicate and the average is given as final isotopic composition. In each sequence, samples containing reference compounds with known isotope ratios (EA-IRMS measurement) were included every 10 sample to check the method accuracy. Samples were corrected by subtracting the difference between the C isotopic composition of the reference compound measured by Isoprime GC-IRMS and by EA-IRMS. Standard deviation of the in-house reference material run every 10 sample was 0.2 ‰ for PCE (n=15). The analytical uncertainty is thus given as $\sigma = \frac{0.2}{\sqrt{2}}$ according to type A evaluation of standard uncertainty described in the ISO guidelines *(BIPM, 1993)*.

3. Results and discussion

3.1. Isotopic signature variability within sites

Isotopic compositions of PCE in groundwater of all sampled wells vary between -0.7 and 0.8 ‰ for Cl and -26.8 and -23.7 ‰ for C. Dual C-Cl isotopic compositions differ between each well of each site except for sites SC and SF where isotopic signatures are not significantly different between wells (Figure 1 and Table A 4, Appendices). The most important shift observed between the minimum and the maximum C and Cl isotopic ratios are of 1.3 ‰ (site SE) and 0.6 ‰ (sites SB, SE and SG) for C and Cl, respectively (Table 2). On the other hand, the maximum isotopic shift observed for PCE undergoing reductive dechlorination at the field scale is larger than the maximum shifts observed within the 10 sites for at least one element (C or Cl) (Table 2) *(Wiegert et al., 2012, Badin et al., 2014)*. Additionally, no linear trend is observed when plotting C against Cl isotopic values in 8 out of 10 sites. As such behaviour is typically observed during biodegradation, it may be discarded that the difference observed between wells within these 8 sites is due to biodegradation. The little intra-site isotopic signature variability observed may thus either be attributed to various physical processes (e.g. diffusion, sorption, partitioning to the unsaturated zone) or to the existence of multiple sources having slightly different initial isotopic signatures. Although the effect of such processes on the isotopic composition is expected to be negligible compared to the effect of biodegradation *(Slater et al., 1999, Jeannottat & Hunkeler, 2012, Jeannottat & Hunkeler, 2013)*, they could be responsible for the little intra-site isotopic signature variability. Even though sites which showed little reductive dechlorination were chosen, it seems that this process still takes place in 2 out of 10 sites. Dual C-Cl isotope slopes likely reflecting biodegradation along the flow path can indeed be observed in sites SA and SB (Figure 2 and Figure 3). The maximum C, respectively Cl, isotopic shifts in sites SA and SB are however smaller than previously reported shifts associated with PCE reductive dechlorination occurring in the field (Table 2) *(Wiegert et al., 2012, Badin et al., 2014)*.

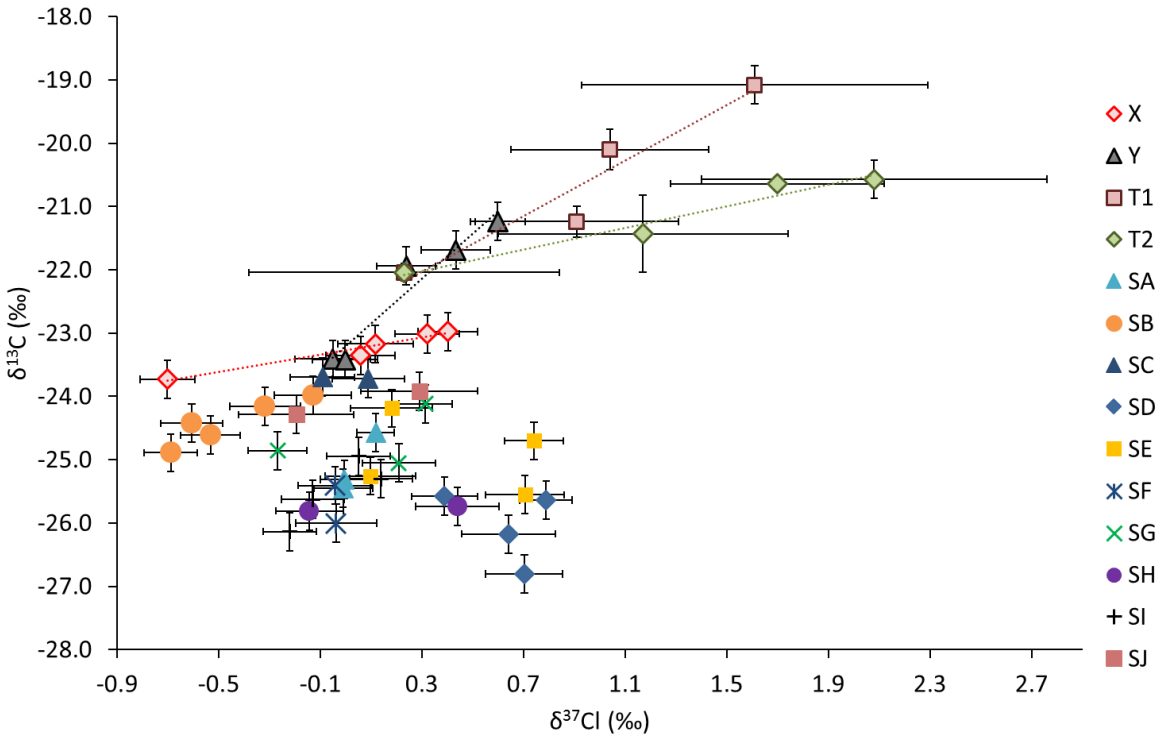

Figure 1. C-Cl isotopic composition of each sampling point of each investigated site (sites SA to SJ) and C-Cl isotopic composition of PCE undergoing reductive dechlorination in the field reported in former work, i.e. for sites X and Y (after Badin *et al.*, 2014), and for transects 1 and 2 (T1 and T2; after Wiegert *et al.*, 2012). Dotted lines are associated with the reductive dechlorination data reported in former studies.

Table 2. C-Cl isotopic signature of 10 sites located in Switzerland and contaminated with PCE. Maximum C and Cl isotopic shifts within each studied site and within sites previously studied in former work where PCE undergoes reductive dechlorination (after Wiegert *et al.*, 2012, Badin *et al.*, 2014). The uncertainty is given by the standard uncertainty between wells of a site or the analytical uncertainty in case the latter is larger than the standard uncertainty between wells. a.u: analytical uncertainty.

Site	**δ^{37}Cl (‰)**	δ^{37}Cl maximum shift between min. and max.	**δ^{13}C (‰)**	δ^{13}C maximum shift between min. and max.
SA	**0.1 ± 0.1**	0.3	**-25.1 ± 0.5**	1.2
SB	**-0.5 ± 0.2**	0.6	**-24.4 ± 0.4**	0.9
SC	**0.0 ± 0.1**	0.2	**-23.7 ± 0.1**	0 < a.u.
SD	**0.6 ± 0.2**	0.4	**-26.0 ± 0.6**	1.2
SE	**0.4 ± 0.3**	0.6	**-24.9 ± 0.6**	1.3
SF	**0.0 ± 0.2**	0 < a.u.	**-25.7 ± 0.3**	0.6
SG	**0.1 ± 0.3**	0.6	**-24.7 ± 0.5**	0.9
SH	**0.1 ± 0.4**	0.5	**-25.8 ± 0.1**	0.1
SI	**0.0 ± 0.2**	0.3	**-25.5 ± 0.5**	1.2
SJ	**0.0 ± 0.3**	0.5	**-24.1 ± 0.2**	0.4
X (Badin *et al.*, 2014)		1.1		0.8
Y (Badin *et al.*, 2014)		0.7		2.2
T1 (Wiegert *et al.*, 2012)		1.4		3.0
T2 (Wiegert *et al.*, 2012)		1.9		1.5

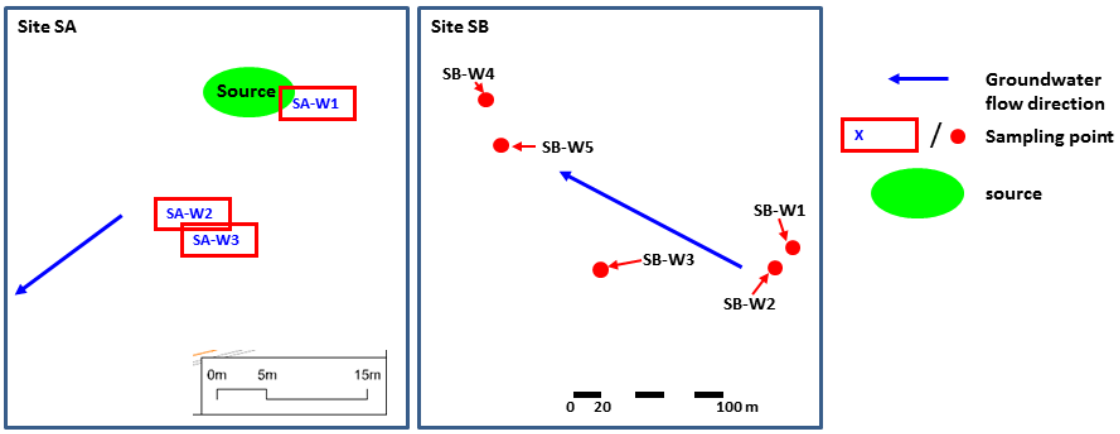

Figure 2. Description of sites SA and SB; the location of the PCE source in site SB is unsure.

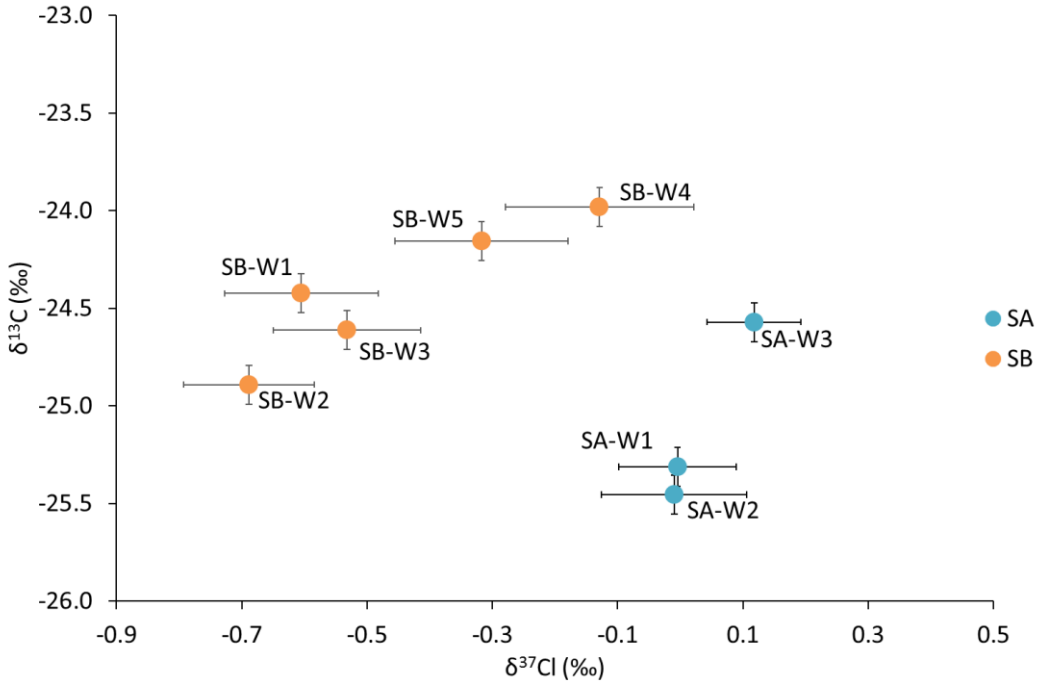

Figure 3. C and Cl isotopic compositions in sampling points of sites SA and SB.

3.2. Isotopic signature variability between sites

The site isotopic signature was defined as the average isotopic signature of all wells of a site since physical processes may lead to small isotopic shifts in both directions (Table 2, Figure 4 and Figure 5). The uncertainty is given by the standard uncertainty between wells of a site or the analytical uncertainty in case the latter is larger than the standard uncertainty between wells.

The C-Cl isotopic signature variability between the 10 studied sites located in Switzerland is smaller than between PCE produced by different manufacturers *(vanWarmerdam, 1995, Jendrzejewski et al., 2001, McHugh et al., 2011)* and is independent from the former PCE purpose of use and from the site location (Figure 4). PCE was used in sites SA, SD and SE for metal degreasing purposes, while it was used during quartering processes in site SF and as a dry-cleaning agent in sites SA, SB, SC, SG, SH, SI and SJ. No isotopic signature cluster specific to PCE purpose of use can be identified. Sites SA (-25.1 ± 0.5 ‰; 0.1 ± 0.1 ‰)[1] and SE (-24.9 ± 0.6 ‰; 0.4 ± 0.3 ‰) are ca. 250 km apart from each other but show similar isotopic signatures. Similarly, sites SA (-25.1 ± 0.5 ‰; 0.1 ± 0.1 ‰) and SC (-23.7 ± 0.1 ‰; 0.0 ± 0.1 ‰) which are located 300 km apart from each other show similar isotopic signatures while sites SD (-26.0 ± 0.6 ‰; 0.6 ± 0.2 ‰) and SC (-23.7 ± 0.1 ‰; 0.0 ± 0.1 ‰) which are only located 80 km apart from each other show a different isotopic signature. Although the variability is small, some sites show different signatures (i.e. sites SB (-24.4 ± 0.4 ‰; -0.5 ± 0.2 ‰) and SD (-26.0 ± 0.6 ‰; 0.6 ± 0.2 ‰)) while others cannot be differentiated (i.e. sites SF (-25.7 ± 0.3 ‰; 0.0 ± 0.2 ‰) and SI (-25.5 ± 0.5 ‰; 0.0 ± 0.2 ‰)) (Figure 5 and Table 2). Despite the good representability of PCE purpose of use and the sites wide geographical spreading, these results apply for 10 out of ca. 12'300 sites estimated to be polluted with chlorinated solvents in Switzerland. A larger isotopic signature variability between other Swiss sites can thus not be discarded.

[1] To improve the reading, isotopic signatures are given as ($\delta^{13}C$ (‰); $\delta^{37}Cl$ (‰)).

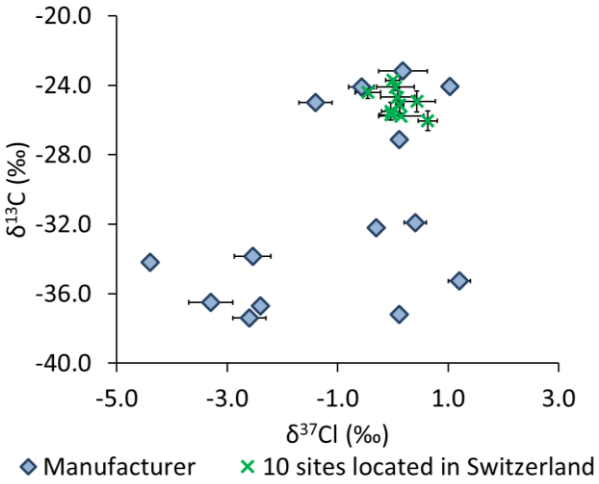

Figure 4. Difference in PCE C-Cl isotopic signature between 10 Swiss sites (this study) and PCE from various manufacturers *(vanWarmerdam, 1995, Jendrzejewski et al., 2001, McHugh et al., 2011)*. The uncertainty is given by the standard uncertainty between wells of a site or the analytical uncertainty in case the latter is larger than the standard uncertainty between wells.

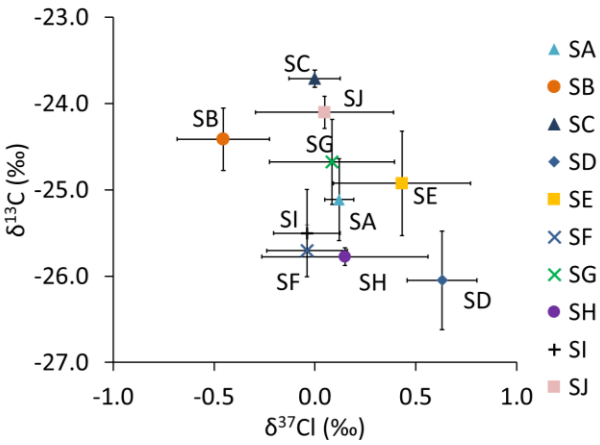

Figure 5. PCE isotopic signature of 10 Swiss sites. The uncertainty is given by the standard uncertainty between wells of a site or the analytical uncertainty in case the latter is larger than the standard uncertainty between wells.

4. Implications for the application of isotopic analysis

C-Cl isotopic analysis may generally be used for source delineation as PCE C-Cl isotopic signatures between sites are often different. However, the current results suggest a limited applicability of this method in Switzerland as signatures between sources are not always different. It is for example not because PCE was used for different purposes in two sites that the isotopic signatures will necessarily vary between those two sites. Yet, as C-Cl isotopic analysis was successfully applied for source delineation in some cases *(Palau et al., 2014)* and as some of the studied sites display different signatures, it may be concluded that this method success is site specific. In order to evaluate the potential success of this method for source delineation on a site, a pre-study where the difference in isotopic signature between the suspected sources should be verified. These conclusions are particularly valid for PCE as no data for other compounds were collected.

This method should thus be considered as a complementary tool after a thorough site characterization was performed or when taking a few additional samples for isotopic analysis in the source area does not require much effort. Guidelines for the application of isotopic methods for source delineation in which various scenarios are differentiated were previously made available *(Hunkeler et al., 2008, Eisenmann, 2010)*. As chlorinated ethenes biodegradation leads to shifts in isotopic compositions, samples should be taken as close as possible to the source where the least degradation is expected. Biodegradation should be taken into account when linking a suspected source with a downstream contamination. Samples should be taken at two different time points and compared to each other in order to ensure that the isotopic composition measured in the source

area corresponds to the initial isotopic signature and does not change with time, thus preventing any misinterpretation.

Acknowledgements: This research was completed within the framework of the Marie Curie Initial Training Network ADVOCATE - Advancing sustainable *in situ* remediation for contaminated land and groundwater, funded by the European Commission, Marie Curie Actions Project No. 265063. Site owners, collaborators from consulting companies and from the cantons who shared sites data and patiently explained previous work carried out in the sites are sincerely thanked. Jordi Palau and Dimitri Boulaz are also thanked for their help in the field, and Daniel Bouchard, Jordi Palau and Simon Jeannottat for their help in measuring isotopic compositions. Many thanks to Vivien Hakoun and Radu Slobodeanu for the constructive discussions regarding data evaluation.

Chapter 2

Multiple dual C-Cl isotope patterns associated with reductive dechlorination of tetrachloroethene

Alice Badin, Géraldine Buttet, Julien Maillard, Christof Holliger, Daniel Hunkeler

Environmental Science and Technology, 2014, 48, 9179–9186

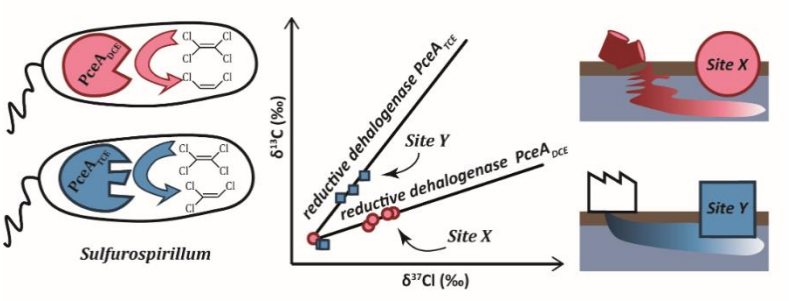

Abstract: Dual isotope slopes are increasingly used to identify transformation pathways of contaminants. We investigated if reductive dechlorination of tetrachloroethene (PCE) by consortia containing bacteria with different reductive dehalogenases (*rdhA*) genes can lead to variable dual C-Cl isotope slopes and if different slopes also occur in the field. Two bacterial enrichments harbouring *Sulfurospirillum* spp. but different *rdhA* genes yielded two distinct $\delta^{13}C$ to $\delta^{37}Cl$ slopes of 2.7 ± 0.3 and 0.7 ± 0.2 despite a high similarity in gene sequences. This suggests that PCE reductive dechlorination could be catalysed according to at least two distinct reaction mechanisms or that rate-limiting steps might vary. At two field sites, two distinct dual isotope slopes of 0.7 ± 0.3 and 3.5 ± 1.6 were obtained, which each fits one of the laboratory slopes within the range of uncertainty. This study hence provides additional insight into multiple reaction mechanisms underlying PCE reductive dechlorination. It also demonstrates that caution is necessary if a dual isotope approach is used to differentiate between transformation pathways of chlorinated ethenes.

1. Introduction

Chlorinated ethenes are widespread persistent groundwater contaminants. Their occurrence in groundwater results from their common industrial use as solvents *(Pankow & Cherry, 1996)*. Accidental spills and careless disposal led to a high number of contaminated sites.

In order to comply with regulations and ensure human safety, risk assessment if not remediation must be carried out. Among all clean-up strategies, approaches involving bacteria-mediated contaminant degradation, also denoted as bioremediation, are particularly attractive as they are cost-effective and have a low environmental impact *(Wiedemeier et al., 1999)*. A major drawback of this technique lies in the often incomplete dechlorination of the commonly encountered tetrachloroethene (PCE) or trichloroethene (TCE) due to the slow bioremediation of its toxic metabolites cis-dichloroethene (*c*DCE) or vinyl chloride (VC), resulting in an accumulation of these compounds.

Understanding the mechanisms underlying dechlorination of chlorinated ethenes is a current scientific challenge. Enzymes belonging to the reductive dehalogenase (RdhA) family which are present in virtually all chlorinated ethenes-degrading anaerobic bacteria are known to contain a corrinoid and two iron-sulfur centers as cofactors *(Hug et al., 2013)*. For PCE, three possible reaction mechanisms (Figure 1) involving the active corrinoid cofactor have been suggested *(Glod et al., 1997, Glod et al., 1997, Schmitz et al., 2007, Kliegman & McNeill, 2008)*. The first one involves the formation of a trichlorovinyl radical as a first and rate-limiting step (*scenario C*). The other two consist of a first nucleophilic attack of the cobalt (Co) center on a carbon (C) atom. This step can then either lead to the intermediate 1,1,2,2-tetrachloroethyl complex further undergoing the elimination of a chlorine (Cl) substituent from the Co center (addition-elimination type mechanism, *scenario B*), or to the substitution of a Cl substituent by this Co center followed by the elimination of the Co ligand and addition of a proton to yield TCE (S_N2-like mechanism, *scenario A*). However, there is no evidence so far to what extent each of these mechanisms are actually involved in the dechlorination process of PCE *(Kliegman & McNeill, 2008)*.

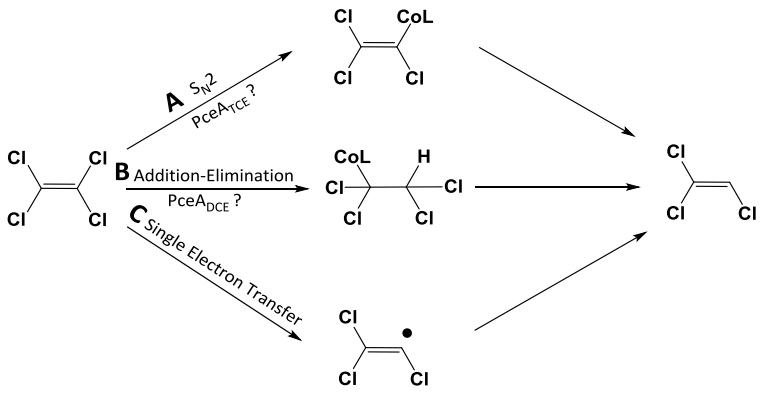

Figure 1. Proposed mechanisms for reductive dechlorination of PCE. See text for details.

Recent studies revealed the potential use of a C-Cl dual isotope approach to gain mechanistic insight in the dechlorination reaction of chlorinated ethenes *(Abe et al., 2009, Cretnik et al., 2013)*. As chemical bond breakage or formation controls the extent of isotope effects, this approach represents a valuable tool to differentiate the rate-limiting step in reaction mechanisms. In earlier studies, the sole use of C isotope data showed limitations as the magnitude of isotope fractionation not only reflects the actual reactive step but may be influenced by rate-limiting preceding steps *(Nijenhuis et*

al., 2005). In particular for PCE, C isotope enrichment factors have been shown to vary consequently (i.e. from 0.4 to -16.7 ‰ *(Nijenhuis et al., 2005, Cichocka et al., 2008)*). Isotope enrichment factor correspond to the change of the isotope ratio per unit of transformation. Conversely, the dual isotope approach is believed not to be affected by masking effects and is thus a promising tool to explore the mechanisms involved during chlorinated ethene reductive dechlorination *(Elsner et al., 2005, Cretnik et al., 2013)*. Abe *et al*. demonstrated that C and Cl isotope ratios ($\delta^{13}C$ and $\delta^{37}Cl$) of *c*DCE and VC showed a linear correlation with different dual isotope slopes $m \approx \varepsilon_C/\varepsilon_{Cl}$ (ratio between C and Cl enrichment factors) for reductive dechlorination and aerobic oxidation, suggesting the slope to be characteristic of the reaction mechanism *(Abe et al., 2009)*. For PCE, the C-Cl dual isotope approach was recently investigated by Wiegert *et al*. at the field and laboratory scales *(Wiegert et al., 2012, Wiegert et al., 2013)*. At the field site undergoing PCE reductive dechlorination, two different isotope patterns occurred along two different groundwater flow paths corresponding to dual isotope slopes of 2.2 ± 2.0 and 0.9 ± 0.7 (95% confidence interval) *(Wiegert et al., 2012)*. On the other hand, a unique dual isotope slope of 2.5 ± 0.8 was determined for a bacterial consortium dominated by a bacterium closely related to *Desulfitobacterium aromaticivorans* strain UKTL (mentioned as *Desulfitobacterium*-containing consortium in the present study) *(Wiegert et al., 2013)*. According to the previous mechanistic assumptions, the two field slopes could be attributed to different reductive dechlorination mechanisms. However, in addition to dechlorination, isotopes can be affected by various processes in the field such as diffusion *(Van Breukelen & Rolle, 2012)* and thus the isotopic data might not only reflect reactive processes. In order to evaluate whether different reaction mechanisms are associated with different dual isotope slopes, additional laboratory studies are necessary that yield well-constrained dual isotope slopes. In addition to providing insight into reaction mechanisms, such studies are also required to establish reference data sets for dual isotope approaches in order to differentiate between biotic (e.g. bacterial dechlorination) and abiotic (e.g. in situ chemical oxidation) processes. As RdhAs are controlling the biotic dechlorination mechanisms, the comparison of dual isotope slopes generated by bacterial populations containing different active RdhAs might bring answers to these questions.

The main objective of this study was to evaluate if (i) consortia with bacteria expressing different *RdhA* enzymes are associated with different dual C-Cl isotope slopes for reductive dechlorination of PCE and (ii) corresponding differences in slopes can also be observed at the field scale. For this purpose, we investigated C and Cl isotope fractionation in two bacterial consortia containing members of the S*ulfurospirillum* genus expressing different RdhA enzymes that were previously characterized *(Buttet et al., 2013)*. In addition, we analysed C and Cl isotope ratios of PCE in samples from two field sites, at which reductive dechlorination was expected to occur based on redox conditions.

2. Materials and Methods

2.1. Sites description

C and Cl isotope ratios of PCE were determined for two sites located in Switzerland. At site X, PCE was formerly used for the processing of slaughterhouse waste. The subsurface consists of an impermeable clay silt layer overlain by a 3.5 m thick sandy gravel aquifer which is covered by a 4 m thick silt layer. The first 2.5 m of the aquifer consist of coarse gravel. Based on previous campaigns and a site characterisation performed by consultants, five wells representing various proportions of PCE and its three dechlorination products TCE, cDCE and VC were chosen in view of covering

different stages of dechlorination. The wells are located along the plume central line covering a distance of 800 m (Figure 2 and Table A 5 of the Appendices).

At site Y, PCE was used for dry cleaning purposes. The subsurface consists of a Tertiary fine sand (Molasse) base acting as an aquitard overlain by a 2.5 to 25 m thick layer of unconsolidated Quaternary fluvio-glacial sediments forming the aquifer *(Ducommun et al., 2013)*. The latter includes a layer of sandy gravel (5 to 25 m) with a high hydraulic conductivity (10^{-3} to 10^{-4} m·s^{-1}) covered by a clay-silty sand sheet rich in organic matter located 2.5 to 5 m below surface which exhibits a low hydraulic conductivity (10^{-5} to 10^{-6} m·s^{-1}). The water table is located between 2.0 and 2.3 m below surface. Based on former sampling campaigns, wells representing various proportions of the PCE and its three dechlorination products TCE, *c*DCE and VC were chosen in view of covering different stages of dechlorination. Samples were taken in four wells: three multilevel wells (ML13, ML14, ML15) situated on a transect perpendicular to the groundwater flow direction and located 7 m downstream of the source area, and one (P13) located 28 m downstream of the source area (Figure 3). The multilevel installation allowed sampling at different depths in the well ML13. The various sampled depths are summarised in Table A 5, Appendices.

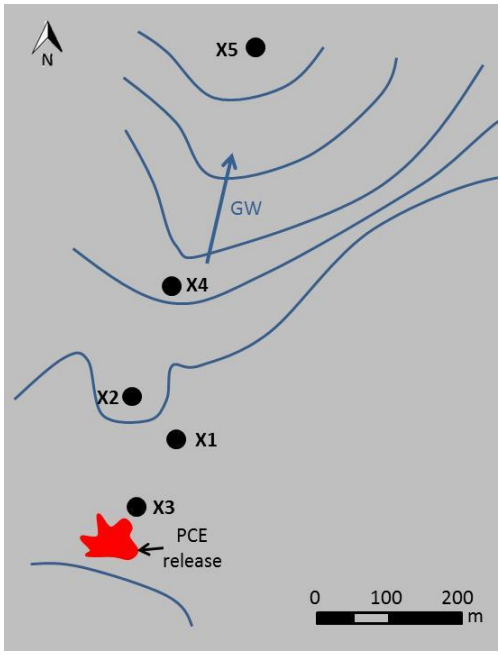

Figure 2. Site X description

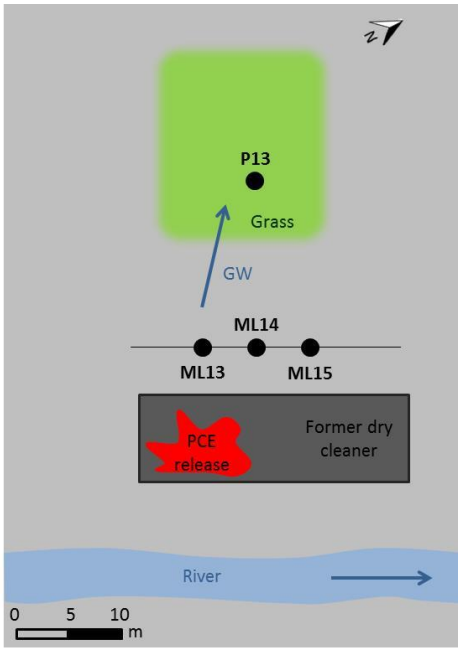

Figure 3. Site Y description

2.2. Groundwater sampling

Sites X and Y were sampled in June and July 2013, respectively. The wells were purged until field parameters (i.e. pH, conductivity, dissolved oxygen (DO)) were stable. Submersible pumps were used for purging and collecting samples except for multilevel wells where foot valve or peristaltic pumps were used. Teflon and PVC tubing were used for collecting samples in sites Y and X, respectively. Samples for concentration analysis were collected in 40 mL glass vials sealed without headspace with PTFE-lined silicone septa and screw caps. Nitric acid (10%) was added onsite to water samples to bring the pH to 2 in order to avoid any biodegradation during storage. Samples were transported in

coolers topped with ice until their storage in a cold room at 4 °C. pH, conductivity and DO were measured onsite (HD40Q probe, HACH LANGE).

2.3. Chemicals

The PCE used in the dechlorination experiment was purchased from Acros Organics (extra pure, 99%, Geel, Belgium) while the PCE used as a working standard for $\delta^{13}C$ and $\delta^{37}Cl$ measurements was purchased from Riedel-de-Haën (min. 99.5% purity, Seelze, Germany).

2.4. Cultivation of bacterial consortia, sampling and detection of *rdhA* genes

Two bacterial consortia (SL2-PCEb and the subculture thereof SL2-PCEc) which harbour members of the *Sulfurospirillum* genus and were recently described for their distinct PCE dechlorination pattern *(Buttet et al., 2013)* were used for the laboratory scale experiments.

The consortia were cultivated in serum bottles of 1000 mL (VWR international AG, Merck, Dietikon, Switzerland) sealed with butyl rubber stoppers which contained 900 mL of anaerobic medium that has been adapted from previously described methods *(Buttet et al., 2013)*. Briefly, the cultivation was performed in presence of PCE in a phosphate-bicarbonate-buffered medium. Addition of 5 mL of 100 mM PCE dissolved in ethanol yielded a final PCE concentration of 560 µM in the aqueous phase of the culture. Formate and acetate were used at 20 mM and 2 mM final concentration as electron donor and C source, respectively. As inoculum, 20 mL of similarly cultivated culture were added per bottle. The cultures were incubated at 30 °C in the dark and agitated on a rotary shaker at 100 rpm.

During dechlorination of PCE to *c*DCE by SL2-PCEb, 5 mL samples were taken from one of the three replicate cultures at times when the fractions of remaining PCE were 82, 60, 20 and 0%, which were subjected to DNA extraction by using the DNA Tissue Kit according to the manufacturer's instructions (Qiagen). A terminal-restriction fragment length polymorphism (T-RFLP) analysis dedicated to the detection of *Sulfurospirillum*-specific reductive dehalogenase genes was applied as described earlier *(Buttet et al., 2013)*. Briefly, a fragment of the *rdhA* genes was amplified by PCR from 5 ng of DNA with primers targeting conserved regions of all *Sulfurospirillum*-specific *rdhA* genes. The fluorescently-labeled PCR product was digested with *Taq*I enzyme and the obtained terminal restriction fragments (TRFs) analysed on a capillary sequencer (Applied Biosystems) allowing to distinguish between $pceA_{DCE}$ (284-bp) and $pceA_{TCE}$ (272-bp) genes.

2.5. Quantification of stable isotope fractionation

For each consortium, isotope fractionation was characterized in three to four replicate assays. Control experiments which were not inoculated were also included. The PCE concentration in the cultures was followed by sampling the headspace for GC-FID analysis. Aqueous samples for isotope and concentration analysis were taken at six to ten time points per bottle, for PCE remaining fractions ranging from 100 to 5%. A total amount of 20 mL was taken at each sampling step and distributed in 2 mL glass vials closed with PTFE-lined screw caps in which 50 µL of NaOH 20 M was added to stop the dechlorination. The vials intended for concentration analysis were filled without headspace, stored at 4 °C, and analysed within six days by GC-MS. The concentrations yielded by these measurements were used to determine the enrichment factors. The vials for isotope analysis were frozen upside down with a small headspace to allow for expansion during freezing *(Elsner et al., 2006)*.

The enrichment factor ε_E of each replicate was determined according to the following form of the Rayleigh equation:

$$\ln\frac{\delta E_t + 1000}{\delta E_0 + 1000} = \varepsilon_E \cdot \ln f \quad (1)$$

where f is the PCE remaining fraction at time t, E the considered element, δ_t and δ_0 are the isotope ratios of one element at time t and time 0 reported against international standards (Vienna Pee Dee Belemnite, VPDB or Standard Mean Ocean Chloride, SMOC for C and Cl, respectively) according to the following expression:

$$\delta E = \left(\frac{R}{R_{std}} - 1\right) \cdot 1000\ [‰] \quad (2)$$

where R and R_{std} are the isotope ratios of the sample and the standard, respectively.
The enrichment factors and dual isotope slopes were calculated by combining $\delta^{13}C$ and $\delta^{37}Cl$ data from all replicates and results were given with a 95% confidence interval.

2.6. Analytical methods

A summary of the analytical methods for isotopic measurements is given in the Appendices (Appendix 1).
Concentration analysis of the aqueous samples was performed using a Thermo-Finnigan™ Trace GC Ultra gas chromatograph coupled to a Thermo-Finnigan™ DSQ II quadrupole mass spectrometry (GC-qMS). Headspace injections of 500 µL from 10 mL were carried out using a CombiPal Autosampler (CTC Analytics, Zwingen, Switzerland), and concentration values were corrected in order to take the equilibrium between the gas and the aqueous phase into account.
C isotope ratios were determined using an Agilent™ 7890a gas chromatograph (GC) coupled to an Isoprime™ 100 isotope ratio mass spectrometer (IRMS) via an Isoprime GC5 combustion interface and a purge-and-trap (P&T) system (Stratum, Teledyne Tekmar). Before analysis, aqueous samples were diluted in 40 mL glas vials with a PTFE-lined screw cap to reach a final PCE concentration of 30 $\mu g \cdot L^{-1}$. 25 mL of the diluted samples were purged with N_2 gas (40 $mL \cdot min^{-1}$) and the degassed compounds were retained on a Vocarb 3000 trap (VICI). After the purging step (10 min), the compounds were transferred into a cryogenic trap (Tekmar Dohrmann) connected to the GC column (DB-VRX, 60 m, 0.25 mm, 1.4 µm). This step was followed by a rapid temperature increase (from -100 °C to 180 °C, using a ramp of 15 $°C \cdot s^{-1}$) which released the concentrated compounds to the column. Helium was used as a gas carrier (1.2 $mL \cdot min^{-1}$). Samples were measured in duplicate unless their concentration was too low and enabled only one measurement. Standard deviation of the in-house reference material was 0.3 ‰ (n=47). In each sequence, samples containing reference compounds with known isotope ratios (EA-IRMS measurement) were included to check the accuracy of the method.
Cl isotope ratios were determined using the method based on gas chromatography quadrupole mass spectrometry (GC-qMS) previously described *(Sakaguchi-Söder et al., 2007, Aeppli et al., 2010)*. An Agilent 78901 GC coupled to an Agilent 5975C quadrupole mass selective detector (Santa Clara, CA, USA) was used for the analysis. A recent inter-laboratory study showed that the use of two standards improved the accuracy of $\delta^{37}Cl$ *(Bernstein et al., 2011)*. Thus, a calibration with two external PCE standards ($\delta^{37}Cl_{EIL1}$ = 0.3 ‰ and $\delta^{37}Cl_{EIL2}$ = -2.5 ‰) which were formerly characterized by the Holt

method *(Holt et al., 1997)* at the University of Waterloo was completed for each sequence to obtain δ values on the SMOC scale. A working PCE standard was measured after every ten sample to check the measurement stability. To reach a high precision and in order to be largely above the quantification limit of 30 $\mu g \cdot L^{-1}$, samples were diluted to a constant concentration of 100 $\mu g \cdot L^{-1}$ and analyzed five to ten times by headspace injection using a CombiPal Autosampler (CTC Analytics, Zwingen, Switzerland). Only two samples from the field showing concentrations between 80 and 90 $\mu g \cdot L^{-1}$ were measured without dilution. A DB-5 column (30 m, 0.25 mm, 0.25 µm, Agilent) with a constant helium flow of 1.2 $mL \cdot min^{-1}$ was used to perform chromatographic separation. As chlorinated ethenes were the only contaminants present in the sites and the retention times for PCE, TCE, *c*DCE and VC being sufficiently different, the PCE peak could be resolved without any problem (Figure A 2). In samples from the control experiment that were stored similarly as samples from the active assays, isotope ratios remained within the range of uncertainty of the measurement.

2.7. Calculation of AKIEs and theoretical dual isotope slopes for radical mechanism

In order to gain more insight into the mechanism underlying PCE reductive dechlorination, C and Cl kinetic isotope effects (KIEs) associated to the C and Cl involved in the reaction can be compared. Enrichment factors were transformed to apparent kinetic isotope effects (AKIEs) to take into account the effect of non-reacting positions and reactive positions which are in intramolecular competition *(Elsner et al., 2005, Abe et al., 2009, Elsner, 2010, Kuder et al., 2013)*. The following equation was applied to obtain AKIE values:

$$AKIE_E = \frac{1}{1 + z \cdot \frac{n}{x} \cdot \varepsilon} \quad (3)$$

where E is the considered element (C or Cl), n the number of atoms of the considered element in the molecule, x the number of these atoms located at reactive sites, and z the number of atoms located at the reactive sites and being in intramolecular competition. Thus, for *scenarios C* (radical mechanism) and *A* (S_N2), n=2, x=2, z=2 and n=4, x=4, z=4 were applied for C and Cl, respectively, as in both cases, all C and Cl atoms are located at reactive sites and are in intramolecular competition.
For *scenario B* (nucleophilic addition), bond strengths to both carbons are altered during the initial step. Therefore, an average $AKIE_C$ for the two position was calculated although the AKIE is likely not exactly the same for both positions (n=2, x=2, z=1). The calculated $AKIE_{Cl}$ in this scenario corresponds to a secondary isotope effect as Cl atoms are not involved in any bond formation or breakage during the rate-limiting step (n=4, x=4, z=1).

3. Results and Discussion

3.1. Sulfurospirillum consortia and *rdhA* genes detection in laboratory experiment

The consortium SL2-PCEb catalyses the reduction of PCE to *c*DCE and contains at least two different *Sulfurospirillum* populations, each of them displaying one distinct PceA enzyme ($PceA_{DCE}$ and $PceA_{TCE}$). In the present study, this consortium was completely dominated by the *Sulfurospirillum* population harbouring $PceA_{DCE}$. This situation was demonstrated by T-RFLP analysis of SL2-PCEb targeting the *rdhA* genes of *Sulfurospirillum* showing that the $PceA_{DCE}$ gene amounted to ≥99.5% of the *rdhA* genes (Table 1). The consortium SL2-PCEc on the other hand, has been obtained from SL2-

PCEb after selecting the *Sulfurospirillum* population that is dechlorinating PCE only until TCE *(Buttet et al., 2013)*. This population displays only one PceA enzyme, namely $PceA_{TCE}$ *(Buttet et al., 2013)*.

Table 1. Relative abundance of pceATCE and pceADCE genes during PCE dechlorination in the consortium SL2-PCEb determined by T-RFLP

f_{PCE} (%) [a]	$pceA_{DCE}$	$pceA_{TCE}$
90	99.5	0.5
70	99.6	0.4
25	100.0	n.d.
0	100.0	n.d.

[a] f_{PCE}: fraction of the remaining PCE; n.d. not detected.

3.2. Concentration and isotope ratios of laboratory experiments

For both consortia, a similar reaction kinetics was observed for PCE (Figure 4). PCE was consumed within about 95h (SL2-PCEc) and 80h (SL2-PCEb), respectively. As expected, SL2-PCEc produced TCE only while in the SL2-PCEb bottles both TCE and *c*DCE were observed. The two consortia showed distinctly different isotope patterns as a function of reaction progress (Figure 5). For SL2-PCEc, changes in isotope ratios were about three times large for C (maximum 9.5 ‰ for all replicates) than for Cl (maximum 3.6 ‰). In contrast, SL2-PCEb showed a similar shift for C (maximum 2.7 ‰) and Cl (maximum 2.9 ‰). The C isotope enrichment factor for PCE was -3.6 ± 0.2 ‰ for the consortium SL2-PCEc harbouring the enzyme $PceA_{TCE}$ and -0.7 ± 0.1 ‰ for the consortium SL2-PCEb dominated by $PceA_{DCE}$ (Table 1). The values are within the range of those obtained by previous authors (i.e. from -0.4 ‰ to -16.7 ‰ *(Nijenhuis et al., 2005, Cichocka et al., 2008)*) and are significantly different from each other. The Cl isotope enrichment factors were -1.2 ± 0.1 ‰ for SL2-PCEc and -0.9 ± 0.1 ‰ for SL2-PCEb, which is also comparable to the value of -2.0 ± 0.5 ‰ recently reported for a *Desulfitobacterium*-containing consortium studied by Wiegert *et al.*, 2013 (Table 2). To date, in addition to the study from Wiegert *et al*., the only other Cl isotope enrichment factor determined for PCE reductive dechlorination is of -10 ‰ *(Numata et al., 2002)*, which is much larger than what was obtained in this study and by Wiegert *et al*., 2013 The variation could be explained by the difference in methods as Numata *et al*., 2002 performed $\delta^{37}Cl$ analysis without separating the chlorinated ethenes.

When applying the dual isotope approach, significantly different (ANCOVA, $p < 0.05$) slopes were obtained with a value of 2.7 ± 0.3 (95% confidence interval) for SL2-PCEc and 0.7 ± 0.2 (95% confidence interval) SL2-PCEb (Table 2, Figure 6). The dual isotope slope obtained for SL2-PCEc agrees with the value obtained by Wiegert *et al*., 2013, i.e. 2.5 ± 0.8.

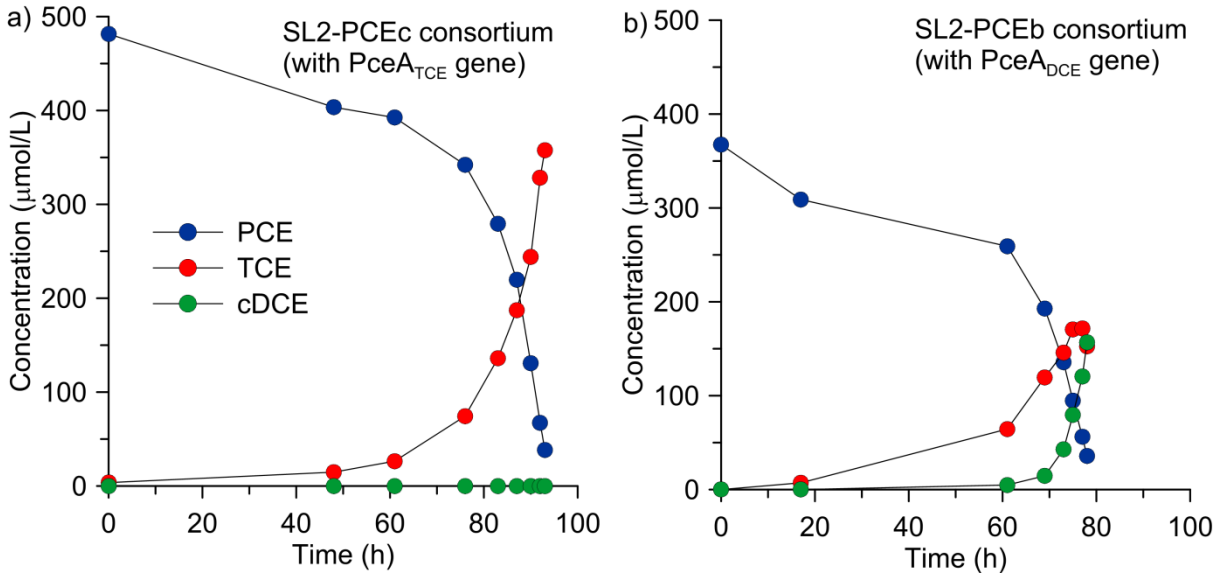

Figure 4. Concentration evolution of PCE, TCE and cDCE for a representative replicate of consortium SL2-PCEc (a) and SL2-PCEb (b).

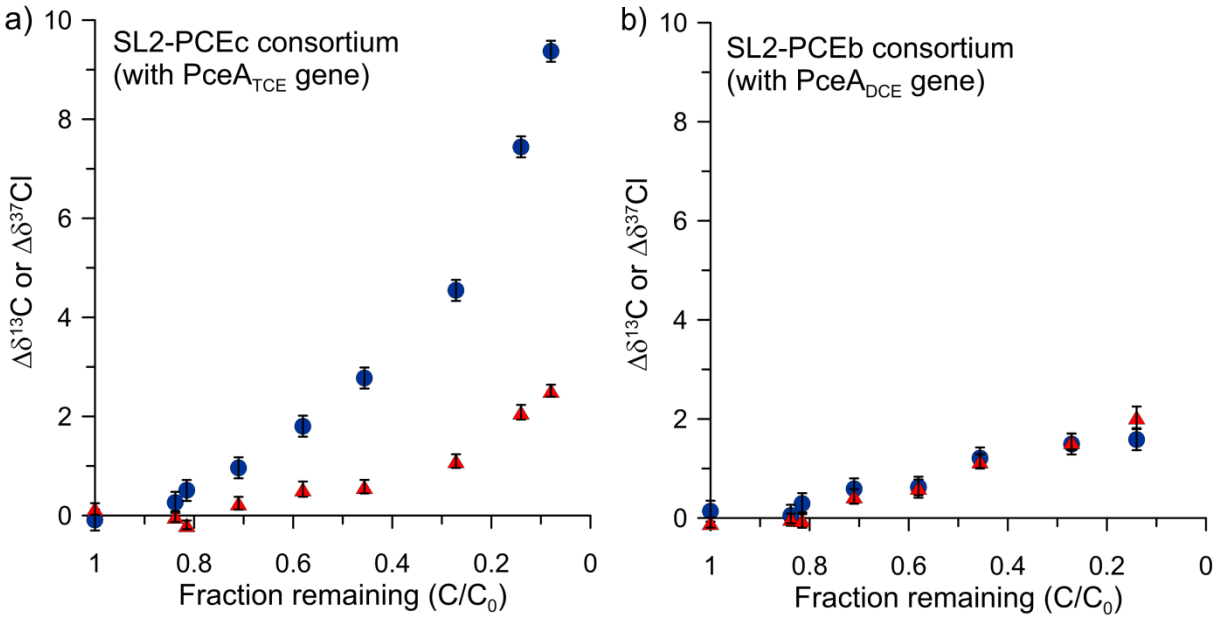

Figure 5. Change in C (blue circle) and Cl (red triangle) isotope ratio as a function of reaction progress for a representative replicate of consortium SL2-PCEc (a) and SL2-PCEb (b). Error bars correspond to the standard uncertainty.

Table 2. Summary of enrichment factors and dual isotope slopes for reductive dechlorination of PCE in various laboratory and field studies. [a] 95% Confidence interval ; N.A.: not available.

Studied system (genus, enzyme)	Substrate to final product	Enrichment factor ε (‰)	Dual isotope slope $\Delta\delta^{13}C/\Delta\delta^{37}Cl$	Reference
Consortium SL2-PCEc (*Sulfurospirillum*, $PceA_{TCE}$)	PCE to TCE	ε_C = -3.6 ± 0.2[a] ε_{Cl} = -1.2 ± 0.1[a]	2.7 ± 0.3[a] *(R^2=0.94 ; n=23)*	This study
Consortium SL2-PCEb (*Sulfurospirillum*, $PceA_{DCE}$)	PCE to *c*DCE	ε_C = -0.7 ± 0.1[a] ε_{Cl} = -0.9 ± 0.1[a]	0.7 ± 0.2[a] *(R^2=0.74 ; n=29)*	This study
Consortium (*Desulfitobacterium*)	PCE to *c*DCE	ε_C = -5.6 ± 0.7[a] ε_{Cl} = -2.0 ± 0.5[a]	2.5 ± 0.8[a] *(R^2=0.88 ; n=10)*	*(Wiegert et al., 2013)*
Field site X	PCE to VC	N.A.	0.7 ± 0.3[a] *(R^2= 0.95 ; n=5)*	This study
Field site Y	PCE to VC	N.A.	3.5 ± 1.6[a] *(R^2=0.94 ; n=5)*	This study

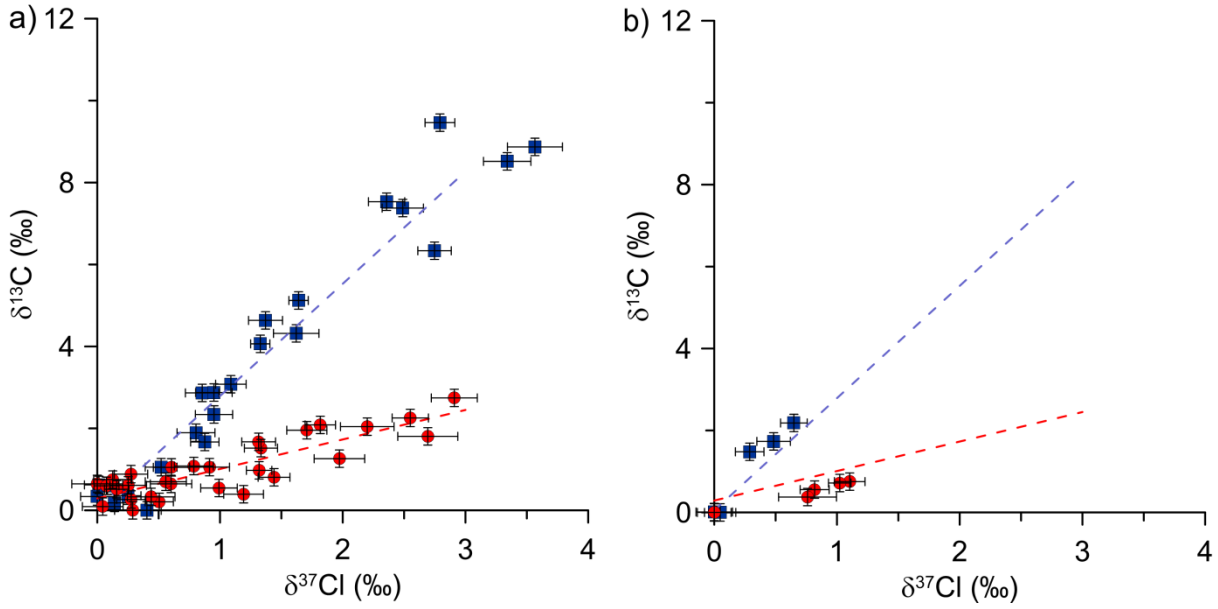

Figure 6. a) Dual isotope plot for reductive dechlorination of PCE by consortium SL2-PCEc (blue squares) and SL2-PCEb (red circles); b) Dual isotope plot for reductive dechlorination of PCE at field site Y (blue squares) and X (red circles). The dashed lines represent the dual isotope slope from the laboratory experiment. Error bars correspond to the standard uncertainty.

3.3. Potential reaction mechanisms

In order to be able to relate isotope fractionation to reaction mechanisms, AKIE values were calculated making some unavoidable simplifying assumptions *(Elsner et al., 2005)*. The calculated values can be considered as limiting values that help to identify additional contributions that do not enter into the calculations and will be discussed accordingly. The obtained AKIE values cannot be directly compared to KIE values for specific reactions as they are often masked by rate-limiting steps *(Elsner et al., 2005)*. An advantage of a dual isotope effect is however that ratios of AKIE-1 values for

two elements are calculated which should correspond to ratios of KIE-1 values for reference reactions as rate-limiting effects cancel *(Elsner et al., 2005)*. Scenario A/C were grouped as they both involve cleavage of a C-Cl bond in an initial step. For scenario A/C, it was assumed that only primary isotope effects occur during cleavage of C-Cl bond. The obtained AKIE-1 ratio for SL2-PCEc (1.39, Table 3) is closer to the KIE-1 ratio for simple C-Cl bond cleavage (4.38) than the ratio of SL2-PCEb (0.78) suggesting that mechanism A/C is more likely for SL2-PCEc. However the ratio for SL2-PCEc (1.39) remains below the reference ratio (4.38) suggesting that either the primary Cl isotope effect is larger than given by the Streitwieser limit or secondary Cl isotope effects occur. Both explanations are plausible. A recent study has suggested that primary Cl isotope effect as high as 1.028 and secondary isotope effects as high as 1.005 might occur *(Świderek & Paneth, 2012)*. For SL2-PCEb, scenario B is more likely as C and Cl AKIE in the same range are more plausible than a Cl AKIE four–times that of the C. However, the difference in dual isotope slope could also be related to a shift of the rate-limiting step within a reaction sequence rather than two distinct reaction mechanisms.

Table 3. Apparent kinetic isotope effects (AKIE) calculated with simplifying assumptions. For scenario A/C it was assumed that only a primary isotope effect during C-Cl bond cleavage occurred. For scenario B, an average AKIE over all positions was calculated. See text for more explanations.

Studied system (genus, enzyme)	Scenario	Isotope	Factors n/x/z	AKIE	$((A)KIE_C-1)/((A)KIE_{Cl}-1)$	Reference
Consortium SL2-PCEc (*Sulfurospirillum*, $PceA_{TCE}$)	A/C	C	2/2/2	1.007	1.39	This study
		Cl	4/4/4	1.005		
	B	C	2/2/1	1.004	2.78	
		Cl	4/4/1	1.001		
Consortium SL2-PCEb (*Sulfurospirillum*, $PceA_{DCE}$)	A/C	C	2/2/2	1.001	0.39	This study
		Cl	4/4/4	1.004		
	B	C	2/2/1	1.001	0.78	
		Cl	4/4/1	1.001		
Consortium (*Desulfitobacterium*)	A/C	C	2/2/2	1.011	1.40	*(Wiegert et al., 2013)*
		Cl	4/4/4	1.008		
	B	C	2/2/1	1.006	2.81	
		Cl	4/4/4	1.002		
Streitwieser limit for C-Cl bond cleavage		C		1.057	4.38	
		Cl		1.013		

3.4. Correlation between RdhA protein sequence and reaction mechanism

Furthermore, despite their highly similar protein sequences *(Buttet et al., 2013)*, SL2-PCEc ($PceA_{TCE}$) and SL2-PCEb ($PceA_{DCE}$) each seem to catalyse PCE reductive dechlorination according to a different mechanism as suggested by the distinct dual isotope slopes. Conversely, SL2-PCEb and the *Desulfitobacterium*-containing consortium *(Wiegert et al., 2013)* seem to catalyse this reaction

according to the same reaction mechanism, although the RdhA protein sequence of this consortium is expected to be significantly different from PceATCE and PceADCE as RdhA sequences observed so far in *Sulfurospirillum* are different from those observed in *Desulfitobacterium (Hug et al., 2013)*. In previous studies, different C isotope enrichments within the same genera have been measured *(Nijenhuis et al., 2005, Cichocka et al., 2008)*. However, if only one element is analysed, it remains unclear to what extent the variability in isotope fractionation is due to rate-limiting step preceding that actual fractionating step or due to different reaction mechanisms. Our study demonstrates for the first time that some of the variability can be explained by different reaction mechanisms occurring even within the same genus. Finally, the results suggest that the reaction mechanism is not related to the level of *RdhA* sequence identity. This goes in the same direction as what was previously shown regarding similarities between *RdhA* protein sequences and their substrate specificity (i.e. between different chlorinated compounds): *RdhAs* showing comparable substrate specificity do not necessarily show high sequence identity and highly similar sequences do not imply equivalent substrate specificity *(Marzorati et al., 2007, Buttet et al., 2013, Hug et al., 2013)*.

3.5. Reductive dechlorination of PCE at two field sites

At site X (Figure 2), PCE concentrations vary from 83 to 1500 $\mu g \cdot L^{-1}$ at site Y (Figure 3) from 88 to 321 $\mu g \cdot L^{-1}$ (Table A 5, Appendices). At both sites, the presence of the dechlorination products TCE, *c*DCE and VC is a clear sign of on-going PCE dechlorination (Table A 5, Appendices). There is no correlation between PCE concentrations and isotope ratios as concentrations are likely also influenced by difference in screen length and geological heterogeneity. The dual C-Cl isotope plots obtained from five wells in each site yielded two significantly different (ANCOVA, $p < 0.05$) dual isotope slopes of 0.7 ± 0.3 (95% confidence interval) and 3.5 ± 1.6 (95% confidence interval) for site X and site Y, respectively (Table 2). The slope for site X is statistically similar (ANCOVA, $p < 0.05$) to the slope of SL2-PCEb, the slope of site Y similar to SL2-PCEc. This suggests that PCE is degraded by different mechanisms at the two sites, analogously as in the laboratory study. Similarly as for *c*DCE at another site *(Hunkeler et al., 2011)*, a single linear trend, and thus a single mechanism, per site were identified. Conversely, Wiegert *et al*., 2012 identified a wider range of slopes for a single site reaching from 0.8 to 2.2 suggesting that different reaction mechanisms might occur at a given site. Indeed, bioremediation in the field generally occurs in a system which usually involves several bacterial genera *(Imfeld et al., 2008, Shani, 2012)* each harbouring various *RdhAs* possibly involved in different reaction mechanisms.

Although the collection of dual isotope slopes is still limited, the dual isotope approach potentially helps to select an appropriate value (or range of values) for calculating the degree of contaminant transformation. For example, at site Y, a maximal shift in $\delta^{13}C$ of 2.2 ‰ is obtained (Table A 5, Appendices). Using the C isotope enrichment factors of SL2-PCEc (-3.6 ‰, Table 2), SL2-PCEb (-0.7 ‰) and the consortium of Wiegert *et al.*, 2013 (-5.6 ‰), fractions remaining of 0.54, 0.04 and 0.68, respectively are calculated using the Rayleigh equation. Based on the dual isotope slope of site Y, the second value can be discarded and thus the fraction remaining narrowed to 0.54 to 0.68.

4. Advances in understanding the mechanisms underlying PCE reductive dechlorination and implications for environmental studies

The study provides for the first time evidence that reductive dechlorination of PCE can be associated with different dual isotope slopes likely due to different reaction mechanisms. This has an incidence on the use of dual isotope measurements to distinguish abiotic from biotic dechlorination processes in the field as the dual isotope slope for reductive dechlorination covers an interval rather than a unique value. It is yet to be seen if this interval is significantly different from slopes for other processes such as in situ chemical oxidation. For process quantification using isotope data, an appropriate isotope enrichment factor has to be chosen *(Meckenstock et al., 2004, Elsner et al., 2005)*, which is challenging when a compound is degraded by multiple mechanisms. Previous studies on 1,2-DCA have shown that mechanisms with different dual isotope slopes also show distinctly different absolute values of enrichment factors helping to choose appropriate enrichment factors *(Hirschorn et al., 2004)*. In the case of PCE, it seems that enrichment factors partition into two groups (Table 2) although additional data is required to confirm this pattern. As shown by the example given above, a dual isotope approach can potentially help to narrow the calculated fraction remaining for a specific site.

Pinpointing two distinct dual isotope slopes associated to RdhAs with similar protein sequence also constitutes an additional step to the understanding of fundamental aspects of RdhAs activity. Our results show that similarities in RdhA protein sequences do not necessarily imply similarities in reductive dehalogenation mechanisms. Thus, enzymes which show less sequence similarities might use the same mechanism while others which share high sequence similarities might catalyse different reaction mechanisms.

Yet, further investigations are required to confidently link field slopes to their relative reaction mechanism. Determining dual isotope slopes obtained for chemical models mimicking the three conjectured dechlorination mechanisms might for example allow associating reaction mechanisms to slopes.

Acknowledgements: This research was completed within the framework of the Marie Curie Initial Training Network ADVOCATE - Advancing sustainable *in situ* remediation for contaminated land and groundwater, funded by the European Commission, Marie Curie Actions Project No. 265063. Géraldine Buttet is financed by the Swiss National Science Foundation grant 31003A_138114. Jordi Palau, Daniel Bouchard, Simon Jeannottat, Roberto Costa, Bibiane Schlunegger and Radu Slobodeanu are thankfully acknowledged for their support. Members from cantonal offices and consultants are gratefully acknowledged for their help in finding appropriate sites. The authors would like to thank three anonymous reviewers for their constructive comments.

Chapter 3

Dual C-Cl isotope patterns asssociated with TCE as a reactant, product and intermediate of reductive dechlorination

Alice Badin, Fabian Braun, Julien Maillard, Daniel Hunkeler

Abstract: What controls the dual C-Cl isotope slope associated with TCE as a reactant, intermediate and product of reductive dechlorination is still poorly understood. So is the occurrence of secondary Cl isotope effects during PCE reductive dechlorination which arose in the previous chapter. We thus performed C and Cl isotopic analysis of TCE from experiments described in chapter 2 as well as from an additional experiment where TCE was dechlorinated to *c*DCE by the bacterial consortia SL2-PCEb. Dual isotope slopes of 3.7 ± 0.4 and 4.3 ± 0.3 were obtained for TCE from reductive dechlorination of PCE to *c*DCE and TCE to *c*DCE, respectively, suggesting that the slope associated with an accumulating intermediate product is controlled by its degradation. These results additionally confirm the existence of a restricted TCE dual C-Cl isotope slope variability which supports the assumption according to which such slopes reflect the reaction mechanism underlying TCE reductive dechlorination. Finally, the existence of secondary isotopic effects was confirmed as inverse effects of 1.4 ± 0.2 and 3.1 ± 0.6 were obtained, thus indicating that such effect should not be neglected.

1. Introduction

In the previous chapter, the possible occurrence of secondary Cl isotopic effects during PCE reductive dechlorination by the bacterial consortia SL2-PCEb and SL2-PCEc harbouring members of the *Sulfurospirillum* genus was raised. In parallel to the work presented in Chapter 2, Cretnik *et al.*, 2014 suggested a method enabling to identify and quantify secondary Cl isotope effects (i.e. affecting non-reacting positions) based on the analysis of the Cl isotopic composition of compounds merely produced by sequential reductive dechlorination *(Cretnik et al., 2014)*. More particularly in the case of TCE produced by PCE reductive dechlorination, the proposed approach relies on the fact that TCE reflects merely secondary isotopic effects while the released chloride (Cl^-) contains information relative to primary isotopic effects (i.e. affecting reacting positions). Applying such method would hence allow answering the question raised in chapter 2.

Additionally, concomitantly to the previous chapter, Renpenning *et al., 2014* reported new dual C-Cl isotope slopes associated with reductive dechlorination of TCE performed by purified enzymes and corrinoids. Corrinoid cofactors are the centre where the chemical reaction itself is catalysed in the enzyme. Their work hence permitted to explore further the different processes controlling dual C-Cl isotope trends during biotic reductive dechlorination by "separating" each step of the global biochemical process carried out by bacteria. Cretnik *et al.*, 2013 previously also investigated the variability of dual C-Cl isotope slopes associated with TCE reductive dechlorination by different bacterial strains and chemical models mimicing microbial dechlorination. Both studies reported by Cretnik et al. and Renpenning et al. converge to conclude that dual C-Cl isotope slopes associated with TCE reductive dechlorination reflect the underlying reaction mechanism. This was supported by the narrow range observed for TCE dual C-Cl isotope slopes associated with TCE reductive dechlorination performed by different bacterial strains, purified enzymes as well as different purified corrinoids, as summarised in Table 1.

Finally, few studies discussed the evolution of intermediate compounds during the course of reductive dechlorination. However, knowing how to interpret them might be useful as one is usually mainly confronted with intermediate products in the field rather than with sole reactants. Hunkeler *et al.*, 2009 previously suggested based on a modelling approach that the slope of intermediate compounds is controlled by its degradation when the compound is accumulating, contrary to when it is being rapidly degraded after its production.

In this chapter, we thus propose to go a step further in the interpretation of dual C-Cl isotope slopes by focusing on TCE being either a reactant, an intermediate or a product of biotic reductive dechlorination, based on the mentioned additional references. More specifically, we will present and discuss the evolution of such TCE C and Cl isotopic composition in view of (i) adding a stone to build the general understanding of what controls dual C-Cl isotope slopes (ii) verifying the hypothesis from the previous chapter according to which Cl secondary isotopic effects may occur during PCE reductive dechlorination by the studied consortia; this will be performed by applying the method developed by Cretnik *et al.*, 2014, and (iii) experimentally verify the prediction proposed by Hunkeler *et al.*, 2009 with regards to which step controls the dual C-Cl isotope slope of an intermediate product.

Table 1. Summary of dual C-Cl isotope slopes associated with PCE, TCE, *c*DCE and VC biotic reductive dechlorination so far reported. Values are reported for studies employing reductive dechlorination "catalysers" (i.e. degraders) at the bacteria, enzyme and corrinoid (synthetic or purified) level. In the case of TCE, *c*DCE and VC, slope values observed for TCE, *c*DCE and VC as products and as intermediates are also reported.

Compound	« Catalyser » level	« Catalyser »	slope	±	ref
PCE (reactant)	Bacteria	*Sulfurospirillum* (consortium; $PceA_{TCE}$)	2.7	0.3	*(Badin et al., 2014)*
PCE (reactant)	Bacteria	*Sulfurospirillum* (consortium; $PceA_{DCE}$)	0.7	0.2	*(Badin et al., 2014)*
PCE (reactant)	Bacteria	*Desulfitobacterium* mixed culture	2.5	0.8	*(Wiegert et al., 2013)*
PCE (reactant)	Bacteria	*Desulfitobacterium* sp. Strain Viet 1	3.8	0.2	*(Cretnik et al., 2014)*
PCE (reactant)	Enzyme	PceA enzyme (norpseudo-B12 type)	2.2	0.7	*(Renpenning et al., 2014)*
PCE (reactant)	Enzyme	PceA enzyme (nor-B12 type)	2.8	0.5	*(Renpenning et al., 2014)*
PCE (reactant)	purified corrinoid	from PceA enzyme (norpseudo-B12 type)	6.9	0.7	*(Renpenning et al., 2014)*
PCE (reactant)	purified corrinoid	from PceA enzyme (nor-B12 type)	5	0.8	*(Renpenning et al., 2014)*
PCE (reactant)	synthetic corrinoid	cyano-B12	4.6	0.2	*(Renpenning et al., 2014)*
PCE (reactant)	synthetic corrinoid	dicyanocobinamid	7	0.8	*(Renpenning et al., 2014)*
TCE (reactant)	Bacteria	*Dehalococcoides* mixed culture	4.8		*(Kuder & Philp, 2013)*
TCE (reactant)	Bacteria	*Desulfitobacterium hafniense* Y51	3.4	0.2	*(Cretnik et al., 2013)*
TCE (reactant)	Bacteria	*Geobacter lovleyi* strain SZ	3.8	0.2	*(Cretnik et al., 2013)*
TCE (reactant)	Bacteria	*Geobacter lovleyi* strain SZ	3.4	0.2	*(Cretnik et al., 2013)*
TCE (reactant)	Bacteria	*Sulfurospirillum* (consortium; $PceA_{DCE}$)	4.3	0.2	this study
TCE (intermediate)	Bacteria	*Sulfurospirillum* (consortium; $PceA_{DCE}$)	3.7	0.4	this study
TCE (product)	Bacteria	*Desulfitobacterium* sp. Strain Viet 1	3.9	0.5	*(Cretnik et al., 2013)*
TCE (product)	Bacteria	*Sulfurospirillum* (consortium; $PceA_{TCE}$)	not clear		this study
TCE (reactant)	Enzyme	PceA enzyme (nor-B12 type)	5	0.8	*(Renpenning et al., 2014)*
TCE (reactant)	Enzyme	PceA enzyme (norpseudo-B12 type)	5.3	0.3	*(Renpenning et al., 2014)*
TCE (reactant)	synthetic corrinoid	cobalamin	3.9	0.2	*(Cretnik et al., 2013)*
TCE (reactant)	synthetic corrinoid	cobaloxime	6.1	0.5	*(Cretnik et al., 2013)*
TCE (reactant)	purified corrinoid	from PceA enzyme (nor-B12 type)	3.7	0.3	*(Renpenning et al., 2014)*
TCE (reactant)	purified corrinoid	from PceA enzyme (norpseudo-B12 type)	4.5	0.8	*(Renpenning et al., 2014)*
TCE (reactant)	synthetic corrinoid	cyano-B12	4.4	0.7	*(Renpenning et al., 2014)*
TCE (reactant)	synthetic corrinoid	dicyanocobinamid	4.2	0.6	*(Renpenning et al., 2014)*
cDCE (reactant)	Bacteria	*ß-Proteobacterium* strain JS666	32.3		(Abe *et al.*, 2009)
cDCE (reactant)	Bacteria	*Dehalococcoides*-containing KB-1 culture	11.4 to 13.7		(Abe *et al.*, 2009)

Compound	« Catalyser » level	« Catalyser »	slope	±	ref
cDCE (product)	Bacteria	*Geobacter lovleyi* strain SZ	4	0.5	(Cretnik *et al.*, 2014)
VC (reactant)	Bacteria	*Nocardioides* strain JS614	25.6 to 27.0		(Abe *et al.*, 2009)
VC (reactant)	Bacteria	*Dehalococcoides*-containing KB-1 culture	13.7 to 14.5		(Abe *et al.*, 2009)

2. Material and methods

2.1. Cultivation of bacterial consortia and sampling

In addition to the experiments described in chapter 2, a third set of experiments was performed where TCE was fed to the consortium SL2-PCEb which carried out reductive dechlorination down to *c*DCE by means of the $PceA_{DCE}$ enzyme. The consortia cultivation and sampling was performed as described in chapter 2. Briefly, cultivation was carried out in 1000 mL serum bottles containing 900 mL of anaerobic medium in presence of PCE (560 µM) or TCE (560 µM) in a phosphate-bicarbonate-buffered medium where formate and acetate acted as electron donor and C source, respectively. It should be noted that accumulation of TCE occurred during PCE to *c*DCE dechlorination by SL2-PCEb.

2.2. Analytical methods

The methods described in chapter 2 were used for PCE and TCE C and Cl isotopic analysis. A summary of the analytical methods is furthermore given in the Appendices (Appendix 1).
More specifically in the case of TCE, the standard deviation σ of the in-house reference material associated with C isotopic analysis was 0.9 ‰ (n=37). A two-point calibration was performed for TCE Cl isotopic analysis with standards formerly characterized by the Holt method *(Holt et al., 1997)* at the University of Waterloo ($\delta^{37}Cl_{EIL1,\,TCE}$ = +3.05 ‰ and $\delta^{37}Cl_{EIL2,\,TCE}$ = -2.70 ‰).

2.3. Isotopic results treatment

Enrichment factors and dual C-Cl isotope slopes were determined as described in chapter 2.
Additionally, primary and secondary isotopic effects were determined from PCE and TCE data according to Cretnik *et al.*, 2014 who demonstrated that primary and secondary isotopic effects during PCE biotic reductive dechlorination can be estimated based on the difference in Cl isotopic composition between the substrate PCE and the produced TCE and Cl^-. This is based on the assumption that the products mirror the Cl isotope enrichment behaviour of the four chemically equivalent positions of PCE from which they origin. It was among others demonstrated that:

$$\delta^{37}Cl_{TCE,t} = \delta^{37}Cl_{PCE,0} - \frac{1}{4}\varepsilon_{diff} - \varepsilon_{PCE} \cdot \frac{f \cdot \ln(f)}{1-f} \quad (1)$$

After determining the Cl enrichment factor ε_{PCE} associated with PCE reductive dechlorination to TCE by means of the Rayleigh equation, ε_{diff} could hence be determined based on the expression above at time 0 where:

$$\lim_{f \to 1}\left(\frac{f \cdot \ln(f)}{1-f}\right) = -1 \quad (2)$$

The primary and secondary isotopic enrichments were consecutively determined based on the following expressions, assuming a one-step dechlorination scenario where no intermediate specie exists between PCE and TCE:

$$\varepsilon_{PCE,P} = \delta^{37}Cl_{Cl-,0} - \delta^{37}Cl_{PCE,0} = \frac{3}{4}\varepsilon_{diff} + \varepsilon_{PCE} \quad (3)$$

$$\varepsilon_{PCE,S} = \delta^{37}Cl_{TCE,0} - \delta^{37}Cl_{PCE,0} = -\frac{1}{4}\varepsilon_{diff} + \varepsilon_{PCE} \quad (4)$$

where $\varepsilon_{PCE,P}$ and $\varepsilon_{PCE,S}$ correspond to the primary and secondary isotopic effects associated with PCE reductive dechlorination to TCE in the case of a one-step scenario, respectively.
In case of a two-step scenario where an intermediate product is formed and the rate-limiting step is the transformation from intermediate to products TCE and Cl^-, TCE does not reflect the secondary isotope effect any more but both the secondary and additional effect from the rate-limiting transformation of intermediate to TCE and Cl^-. Determining the absolute primary and secondary isotope effects may then not be possible anymore. Instead, the sole difference between primary and secondary isotope effects ε_{diff} may be determined *(Cretnik et al., 2014)*. $\varepsilon_{PCE,P}$, $\varepsilon_{PCE,S}$, and ε_{diff} are given as the average between values obtained for each replicate and the uncertainties were determined by error propagation.
Since $\delta^{37}Cl$ of *c*DCE could not be measured, no information regarding secondary and primary isotopic effects during PCE dechlorination to *c*DCE or TCE dechlorination to *c*DCE could be determined.

3. Results and discussion

3.1. General evolution of concentration and single element isotope data

The evolution of chlorinated ethenes concentrations are given in Figure 1, A, B, C. Whether PCE was dechlorinated by consortium SL2-PCEb or SL2-PCEc, the lag phase lasted between 20 and 50 h while the lag phase preceding TCE dechlorination lasted one to two orders of magnitude longer, i.e. from 300 to 1500 h depending on the replicate. Traces of *t*DCE were detected together with *c*DCE. The evolution of C and Cl isotopic composition of PCE, TCE and *c*DCE in all replicates are represented in the Appendices (Figure A 4 and Figure A 5) while the latter is represented for one replicate of each experiment in Figure 1 D to L.
As reported in the previous chapter, PCE was slightly enriched in heavy C and Cl during its dechlorination by both consortia, with maximum enrichment factors of -3.6 ± 0.2 ‰ for C and -1.2 ± 0.1 ‰ for Cl associated with consortium SL2-PCEc (Table 2). Conversely, both C and Cl enrichments were stronger for TCE dechlorination by consortium SL2-PCEb where a C enrichment factor of -18.9 ± 1.3 ‰ and a Cl enrichment factor of -4.3 ± 0.4 ‰ were determined (Table 2). While C enrichment factors of PCE are in the lower range of the so far available values *(Hunkeler et al., 2010)*, both C and Cl enrichment factors associated with TCE dechlorination are higher than the maximum values available of -18.5 ‰ for C *(Cichocka et al., 2007)* and -3.6 ‰ for Cl *(Cretnik et al., 2013, Kuder et al., 2013)*.

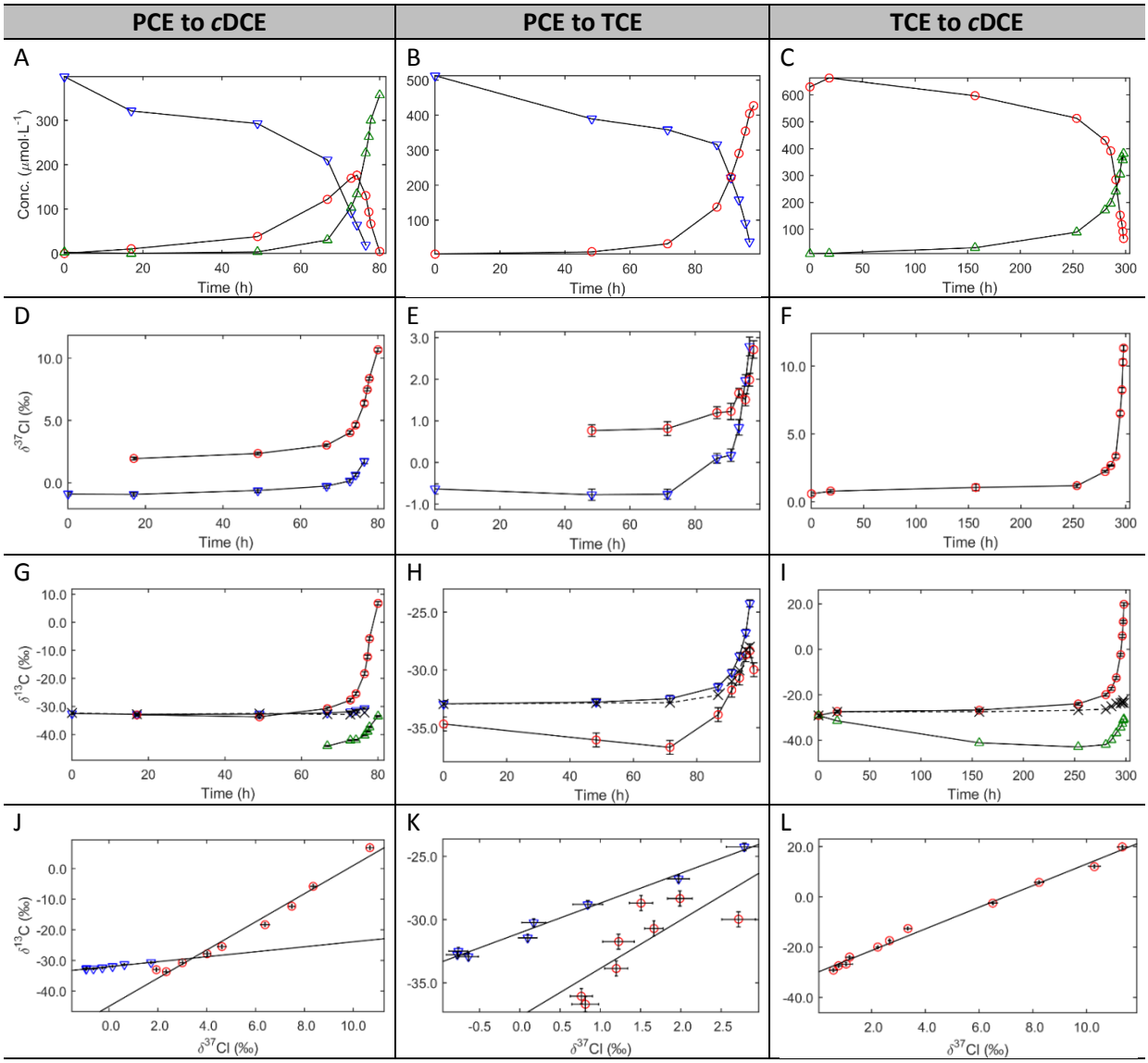

Figure 1. PCE, TCE and cDCE C and Cl isotopic composition during reductive dechlorination of PCE to TCE by SL2-PCEc, PCE to cDCE with TCE accumulation by SL2-PCEb and TCE to cDCE by SL2-PCEb. Blue triangles, red circles and green triangles represent PCE, TCE and cDCE, respectively. Black crosses represent the C isotope balance.

3.2. Dual isotope slopes

Dual isotope slope results are given in Table 2 and represented in Figure 1 J, K, L and Figure 2.

The TCE dual C-Cl isotope slopes of 4.3 ± 0.2 and 3.7 ± 0.4 associated with dechlorination of TCE to *c*DCE and PCE to *c*DCE with accumulation of TCE, respectively, are similar within the range of uncertainty. The degradation step from TCE to *c*DCE is known to be catalysed by the same enzyme $PceA_{DCE}$ in both experiments *(Buttet et al., 2013)*. As TCE accumulated during PCE dechlorination to *c*DCE, the existence of similar dual C-Cl slopes associated with TCE supports the conclusion from Hunkeler *et al.*, 2009 according to which the slope associated with an intermediate compound is controlled by its degradation rather than its production when the latter accumulates.

These two slope values moreover fall in the range corresponding to dual C-Cl isotope slopes associated with TCE reductive dechlorination by different bacterial strains, purified enzymes and purified corrinoids which range from 3.4 ± 0.2 *(Cretnik et al., 2013)* to 5.3 ± 0.3 *(Renpenning et al.,*

2014). Our results thus support the previous conclusions from Cretnik *et al.* and Repenning *et al.* according to which no other rate-limiting step affect dual C-Cl isotope slopes associated with TCE bacterial reductive dechlorination which thus may be assumed to reflect the underlying reaction mechanism.

No clear C-Cl dual isotope slope could be determined for TCE from PCE dechlorination to TCE by SL2-PCEc (Figure 2). Slopes ranging from 2.1 ± 1.1 to 3.8 ± 3.2 with a R^2 varying from 0.59 to 0.89 could be determined for each replicate (Table A 6 of the Appendices), yet a dual C-Cl slope determined based on the combination of data from all replicates has no meaning as its associated R^2 is of 0.16. This is very likely due to the not respected C isotope balance as illustrated in Figure 1 H. Such violation of C isotope balance is not equally reproduced in all the replicates and seems to be due to the TCE C isotopic composition which is less consistent between replicates than the PCE C isotopic composition (Figure A 4, Appendices).

3.3. Primary and secondary Cl isotope effects

Although primary and secondary Cl isotope effects could not be determined for TCE dechlorination to *c*DCE by SL2-PCEb due to the lack of Cl isotope data for *c*DCE, such isotope effects were determined for PCE dechlorination to TCE by SL2-PCEc and to *c*DCE by SL2-PCEb (Table 2). In the case of PCE dechlorination to *c*DCE, primary and secondary isotope effects were determined similarly as for PCE dechlorination to TCE. We justify such procedure by the fact that TCE was not affected by its degradation for the first Cl isotopic measurements since *c*DCE was not yet present (Figure 1 A and D). When considering a one-step scenario, primary isotopic effects of -9.0 ± 0.9 ‰ and -12.8 ± 2.1 ‰ are obtained for PCE dechlorination to TCE and *c*DCE, respectively (Table 2). These values are slightly to twice smaller than the previously reported value of -17.0 ± 1.6 ‰ for PCE to TCE reductive dehalogenation by *Desulfitobacterium* sp. Strain Viet1 *(Cretnik et al., 2014)*. Secondary isotopic effects of 1.4 ± 0.2 ‰ and 3.1 ± 0.6 ‰ associated with PCE dechlorination to TCE and *c*DCE, respectively, are on the other hand different from the formerly reported value of -1.0 ± 0.5 ‰ *(Cretnik et al., 2014)*, and reflect an unexpected inverse secondary isotope effect. Such effect was previously reported during TCE abiotic reduction by zero valent iron at the laboratory scale *(Audí-Miró et al., 2013)* and twice in the field where *c*DCE was found to be 1 to 1.5 ‰ more enriched than TCE assumed to be biotically dechlorinated *(Lojkasek-Lima et al., 2012)*. Finally, in case a two-step scenario is taking place, only differences between primary and secondary isotope effects of -10.6 ± 1 ‰ and -15.9 ± 2.8 ‰ for PCE dechlorination to TCE and *c*DCE, respectively, can be determined. These values are from equal to smaller than the formerly reported value of -16.3 ± 1.4 ‰ for PCE to TCE reductive dehalogenation by *Desulfitobacterium* sp. Strain Viet1 *(Cretnik et al., 2014)*, and indicate that primary chlorine isotope effects are larger than secondary effects though sometimes only 4-fold larger.

Table 2. Summary of C and Cl enrichment factors, primary and secondary Cl isotopic effects associated with one-step scenario denoted as εCl,prim and εCl,sec, respectively, difference between primary and secondary Cl isotopic effects εCl,diff, and dual C-Cl isotope slopes associated with reductive dechlorination of PCE to TCE (SL2-PCEc), PCE to cDCE (SL2-PCEb), and TCE to cDCE (SL2-PCEb).a: (Badin *et al.*, 2014 or Chapter 2)

Substrate to final product Consortium	ε_C (‰)	ε_{Cl} (‰)	$\varepsilon_{Cl,prim}$ (‰) $\varepsilon_{Cl,sec}$ (‰)	$\varepsilon_{Cl,diff}$ (‰)	dual C-Cl PCE	dual C-Cl TCE
PCE to TCE SL2-PCEc	**-3.6 ± 0.2**[1]	**-1.2 ± 0.1**[1]	**$\varepsilon_{Cl,prim}$ = -9.2 ± 0.9** **$\varepsilon_{Cl,sec}$ = 1.4 ± 0.2**	**-10.6 ± 1**	**2.7 ± 0.3**[a] (R^2 = 0.94, n=23)	
PCE to cDCE SL2-PCEb	**-0.7 ± 0.1**[1]	**-0.9 ± 0.1**[1]	**$\varepsilon_{Cl,prim}$ = -12.8 ± 2.1** **$\varepsilon_{Cl,sec}$ = 3.1 ± 0.6**	**-15.9 ± 2.8**	**0.7 ± 0.2**[a] (R^2 = 0.74, n=29)	**3.7 ± 0.4** (R^2 = 0.93, n=30)
TCE to *c*DCE SL2-PCEb	**-18.9 ± 1.3**	**-4.3 ± 0.4**				**4.3 ± 0.2** (R^2 = 0.99, n=29)

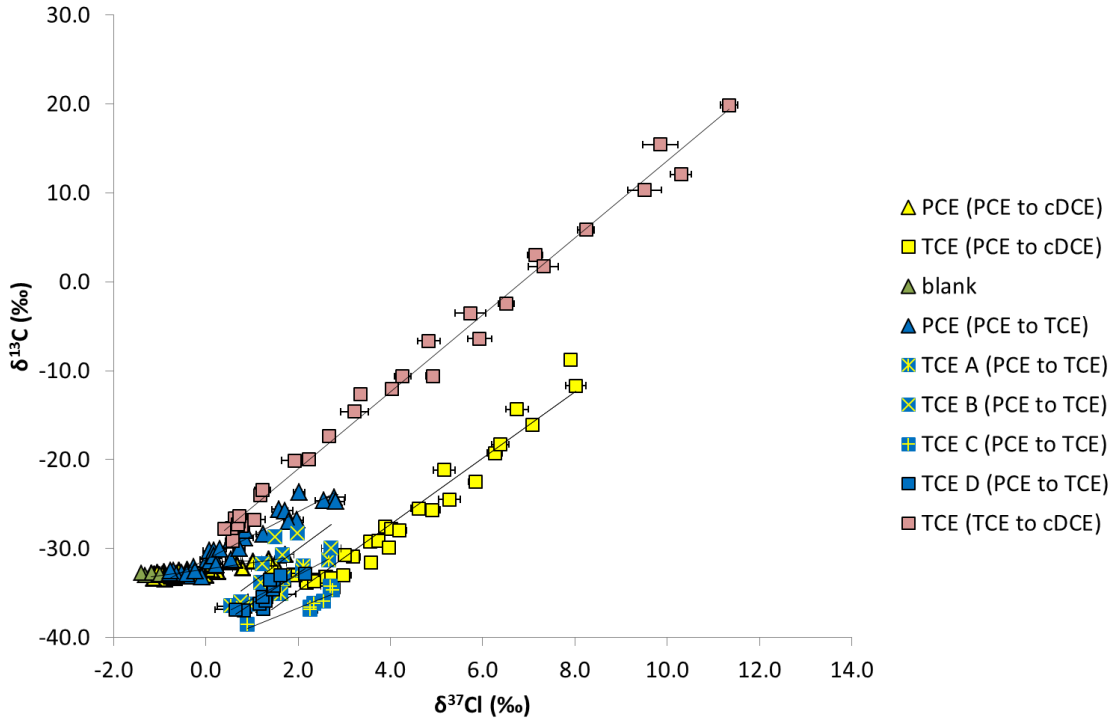

Figure 2. Dual C-Cl isotope slopes for PCE and TCE for reductive dechlorination of PCE to TCE (SL2-PCEc), PCE to cDCE (SL2-PCEb), and TCE to cDCE (SL2-PCEb). Except for TCE from PCE to TCE reductive dechlorination, all replicates are plotted together. For TCE from PCE to TCE reductive dechlorination, replicates A, B, C and D are plotted separately.

4. Conclusion

As predicted by Hunkeler *et al.*, 2009 based on a modelling approach, the present experimental data confirm that the dual C-Cl isotope slope associated with an intermediate which accumulates in the course of reductive dechlorination is controlled by its degradation. This is supported by the similar TCE C-Cl isotope slope associated with TCE from PCE to *c*DCE and from TCE to *c*DCE dechlorination where the transformation step from TCE to *c*DCE is catalyzed by $PceA_{DCE}$.

The TCE dual C-Cl isotope slopes determined for PCE to *c*DCE and TCE to *c*DCE reductive dechlorination contribute to the building dual isotope slopes data-base associated with chlorinated ethenes reductive dechlorination. They additionally support the conclusions so far drawn by Cretnik *et al.*, 2013 and Renpenning *et al.*, 2014 according to which dual slopes associated with TCE microbial reductive dechlorination reflect the chemical reaction contrary to PCE where the interpretation of dual slopes remains uncertain.

Based on the Cl isotopic analysis of merely produced or intermediate TCE, it was furthermore demonstrated that secondary isotopic effects take place during PCE reductive dechlorination. Depending on whether a one-step or a two-step scenario is considered, the observed results would even indicate the existence of a so far unexpected inverse Cl secondary isotope effect. The differences between primary and secondary isotope effects observed for consortia harbouring members of the *Sulfurospirillum* genus are from equal to smaller than the value formerly reported for PCE dechlorination by *Desulfitobacterium* sp. Strain Viet1 *(Cretnik et al., 2014)*. As primary isotopic effects are sometimes only 4-fold larger than secondary isotopic effects, the latter should not be disregarded and should be incorporated in models involving chlorinated ethenes isotopic behavior during reductive dechlorination.

Chapter 4

Influence of secondary isotope effects and Monod kinetics when modelling chloroethenes C/Cl isotope trends during biotic reductive dechlorination

Alice Badin, Fabian Braun, Julien Maillard, Daniel Hunkeler

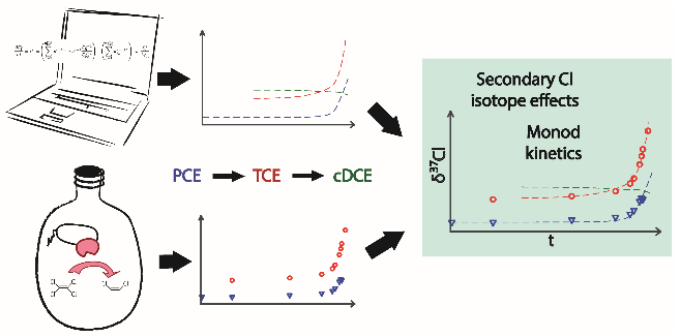

Abstract: Predicting the fate of chlorinated ethenes in groundwater is essential when evaluating remediation strategies. Such predictions are expected to be more accurate when incorporating isotopic parameters. However, current models simulating isotopic behaviour fail to describe recent observations such as secondary chlorine isotope effects. We propose a novel mathematical framework to simulate the C/Cl isotopic fractionation during chlorinated ethenes reductive dechlorination, which differs from existing models by taking into account both secondary isotopic effects as well as Monod kinetics. The approach consists in considering all isotopocules (i.e. molecules differing in number and position of heavy and light isotopes) of each chlorinated ethene as individual species, of which each is degraded at a different speed. One comprehensive model (GM) considering C and Cl isotopes simultaneously was developed and further simplified to a computationally less intensive model (SM). Both models simulated plausible C/Cl isotopic compositions of PCE, TCE and cDCE during sequential dechlorination when using experimentally plausible kinetic and isotopic parameters. Besides, these models could accurately reproduce our experimental data obtained during reductive dechlorination by bacterial enrichments harbouring *Sulfurospirillum* spp. where secondary isotope effects indeed occurred. These findings leave a promising future for the development of areactive transport model incorporating isotopic parameters.

1. Introduction

Owing to recent analytical methods development *(Shouakar-Stash et al., 2003, Sakaguchi-Söder et al., 2007, Aeppli et al., 2010, Bernstein et al., 2011, Jin et al., 2011)* and to numerous studies demonstrating the application potential of compound specific isotopic analysis (CSIA) to estimate the origin and fate of chlorinated solvents in the subsurface *(Hunkeler et al., 2004, Hunkeler et al., 2011, Palau et al., 2014)*, environmental samples are increasingly being submitted to isotopic analysis. Previous studies showed that such analysis may allow determining the extent of biodegradation in groundwater based on isotopic enrichment factors determined via the Rayleigh equation. The latter translates the fact that molecules containing different proportions of isotopes of one element (i.e. isotopologues) follow different reaction kinetics. This is due to the different energy required for breaking bonds binding elements with heavy or light isotopes and eventually induces the observed variation in isotopic composition along biodegradation.

An accurate simulation of the isotopic ratios evolution during biodegradation may allow a better integration of isotopic data to estimate the fate of a plume undergoing natural attenuation. Several studies were carried out to address this challenge some of which additionally successfully applied models to evaluate the fate of chlorinated ethenes plumes. *(Van Breukelen, 2007, Atteia et al., 2008, Hunkeler et al., 2009, Höhener & Atteia, 2010, Jin et al., 2013)* However, for simplification purposes, most models considered one element only *(Van Breukelen et al., 2005, Van Breukelen, 2007, Aeppli et al., 2009, Hunkeler et al., 2009)*, and some models simulated heavy and light isotopes of one element of each compound as separate species *(Van Breukelen et al., 2005, Aeppli et al., 2009)* while others considered isotopologues. *(Hunkeler et al., 2009, Jin et al., 2013)* Such a variety of simplification types reflects the need for a trade-off between including all isotopologues or isotopocules (i.e. isomers of all isotopologues of one compound; isotopomers being isomers of isotopologues) and avoiding an excessive complexity leading to computationally demanding models. The most recently developed model successfully simulated the isotopic behaviour of two elements simultaneously via considering isotopologues and their isotopomers as well as first order kinetics but no secondary isotopic effects. Jin *et al.*, 2013 more specifically demonstrated that considering simultaneously combined C-Cl isotopologues could change simulated isotopic behaviours at late reaction times and for large differences between the C and Cl enrichment factors compared to the simplified method developed by Hunkeler *et al.*, 2009 where Cl isotopologues/isotopes only were considered. Finally, in order to reflect the reality more accurately, some authors applied Monod kinetics which describe biodegradation kinetics more faithfully instead of the simplifying first order kinetics assumption *(Van Breukelen, 2007, Aeppli et al., 2009).* Recent studies showed that secondary isotopic effects which affect elements located in non-reacting bonds were measurable and should therefore not be discounted, *(Kuder et al., 2013, Cretnik et al., 2014)*. However, no model so far considered secondary isotopic effects since their effect was formerly often assumed to be negligible. *(Elsner et al., 2005, Cretnik et al., 2013)*

The challenging task of concurrently considering (i) Monod kinetics, (ii) several elements simultaneously and the corresponding isotopocules they belong to, and (iii) secondary isotopic effects, remains so far unaddressed in the simulation of the evolution of chlorinated ethenes isotopic composition during reductive dechlorination. Addressing this gap may help integrating isotopic data from field sample measurements in reactive transport models for an improved plume fate prediction. To this end, the present contribution proposes a novel isotope modelling framework which is more comprehensive than the current state of the art. With a focus on reductive dechlorination of chlorinated ethenes, this study more particularly aimed at (i) setting up a comprehensive general

model (GM) which allows simulating the simultaneous evolution of C and Cl isotopic composition in chlorinated ethenes during sequential reductive dechlorination considering Monod kinetics and taking secondary isotopic effects into account, (ii) setting up a computationally less demanding simplified model (SM) matching the comprehensive general model which meets the same requirements with regards to Monod kinetics and secondary isotopic effects, and (iii) verifying whether these models could accurately represent experimentally obtained isotopic data during reductive dechlorination of chlorinated ethenes by two different bacterial consortia. For this purpose, the manuscript was structured as follows: (i) description of models mathematical framework, (ii) general and simplified models implementation, evaluation and comparison, (iii) assessment of the feasibility of real experimental data simulation, (iv) environmental significance.

2. Mathematical model development

In this section, the general (GM) and simplified (SM) models developed to simulate isotope trends taking into account primary and secondary isotope effects as well as Monod kinetics are described. Isotopocules designate all isotopomers of all isotopologues, i.e. all the molecules differing both in the number and position of light and heavy isotopes.

2.1. General model (GM): simultaneous consideration of C and Cl isotopes

2.1.1. General expression

Traditionally, fractionation between isotopes rather than between isotopocules is considered *(Hunkeler et al., 2010)*. Such fractionation is described by the kinetic isotope fractionation factor α_k relating the isotope ratio of the instantaneous product to the isotope ratio of the substrate. The difference in rate transfer from reactant to product pool associated with heavy and light isotopes, ${}^{H}k_{\mathrm{bulk}}$ and ${}^{L}k_{\mathrm{bulk}}$, respectively, can also be described by α_k which equals the ratio ${}^{H}k_{\mathrm{bulk}}/{}^{L}k_{\mathrm{bulk}}$ *(Hunkeler et al., 2010)*. In order to incorporate isotope fractionation during sequential dechlorination in a reactive transport model, Van Breukelen *et al.*, 2005, previously established the following expression relating the ^{13}C isotope reaction rate ${}^{13}r_S$ of a consumed substrate (S) to overall reaction rate r_S of S:

$$ {}^{13}r_S = r_S \frac{[{}^{13}S]}{[S]} \alpha_k \qquad (1) $$

This equation is valid under the assumption that the degradation rate of the predominant ^{12}C isotope corresponds to the overall degradation rate of S corrected for the proportion of ^{12}C to total carbon *(Van Breukelen et al., 2005)*. The terms $[{}^{13}S]$ and $[S]$ correspond to the ^{13}C concentration in S and S concentrations, respectively. A similar approach was applied in the present work to simulate the evolution of a compound isotopic composition considering simultaneously all elements affected by isotopic fractionation and including secondary isotope effects. In this case, instead of two isotopes, each isotopocule was considered as an individual entity undergoing the reaction at a specific rate related to its isotopic composition and therefore to the "isotopocule fractionation" it undergoes. We thus expanded the expression suggested by Van Breukelen *et al.*, 2005 for isotopocules of a both produced and degraded compound. More particularly, the fact that an isotopocule of a produced compound is yielded by specific isotopocules of its precursor compound should appear in the expanded expression.

The reaction rate of each isotopocule i of intermediate (i.e. both produced and degraded) compound c resulting from the degradation of isotopocules h of compound c-1 and being further degraded to isotopocules j of compound c+1 can then be described by the following general equation:

$$\frac{\partial C_i^c}{\partial t} = r_i^c = \underbrace{\left(\sum_{h=1}^{n_{\mathrm{Iso}}^{c-1}} \boldsymbol{\kappa}_{h,i}^{c-1\to c} \cdot v^{c-1} \frac{C_h^{c-1}}{C_{\mathrm{tot}}^{c-1}}\right)}_{\text{produced from } c-1} - \underbrace{\left(\sum_{j=1}^{n_{\mathrm{Iso}}^{c+1}} \boldsymbol{\kappa}_{i,j}^{c\to c+1}\right) \cdot v^c \frac{C_i^c}{C_{\mathrm{tot}}^c}}_{\text{degraded to } c+1} \qquad \forall i \in [1, \dots, n_{\mathrm{Iso}}^c] \tag{2}$$

where C_i and C_{tot} are the isotopocule i and total compound concentrations (i.e. $C_{\mathrm{tot}}^c = \sum_{i=1}^{n_{\mathrm{Iso}}^c} C_i^c$ and $C_{\mathrm{tot}}^{c-1} = \sum_{h=1}^{n_{\mathrm{Iso}}^{c-1}} C_h^{c-1}$ where n_{Iso}^c and n_{Iso}^{c-1} are the number of isotopocules of compound c and c-1), r is the isotopocule reaction rate, v is the total compound reaction rate. The matrix $\boldsymbol{\kappa}$ describes the difference in isotopocule reaction rates due to the presence of light or heavy atoms in reacting (primary isotope effect) and/or non-reacting positions (secondary isotope effect). It is hence similar to α_k except that it applies to isotopocules instead of isotopes. It theoretically allows any transition from one isotopocule of a degraded compound (i.e. breaking any reactive bond) to any isotopocule of the compound it produces. As there are in reality only a few possible transitions from isotopocules of degraded compound to isotopocules of produced compound (e.g. maximum 4 transitions for 1 PCE isotopocule degraded to TCE) the matrix is mostly filled with zero elements which inhibit non-existing transitions. On the contrary, the non-zero elements represent the isotopocule fractionation factors. Here $\boldsymbol{\kappa}_{h,i}^{c-1\to c}$ thus represents an element of the isotopocule fractionation matrix $\boldsymbol{\kappa}^{c-1\to c} (\in \mathbb{R}^{n_{\mathrm{Iso}}^{c-1} \times n_{\mathrm{Iso}}^c})$ containing kinetic isotopocule fractionation factors associated with isotopocules h of compound c-1 leading to isotopocule i of compound c. Analogously, the matrix $\boldsymbol{\kappa}^{c\to c+1} (\in \mathbb{R}^{n_{\mathrm{Iso}}^c \times n_{\mathrm{Iso}}^{c+1}})$ describes the transitions from compound c leading to compound c+1. $\boldsymbol{\kappa}$ is more specifically defined as:

$$\boldsymbol{\kappa}_{h,i}^{c-1\to c} = \begin{cases} \dfrac{1}{n_{RB}^{c-1}} \displaystyle\prod_{p=1}^{n_{\mathrm{Atoms}}^{c-1}} \left(\frac{1}{\mathrm{AKIE}_p^{c-1}}\right)^{\left(\boldsymbol{W}^{c-1},\, {}^{X}\boldsymbol{T}^{c-1}\right)_{h,p}}, & \text{if removing atom at absolute position X of isotopocule h (of compound c-1) leads to isotopocule i (of compound c)} \\ 0, & \text{else} \end{cases} \tag{3}$$

where c and and $c-1$ designate the produced and degraded compounds, respectively, and h and i the isotopocules of c and and $c-1$, respectively. n_{RB} is the number of reactive bonds, AKIE_p the position-specific apparent kinetic isotopic effect associated with the atom at relative position p when removing the atom at absolute position X. The weight coefficient matrix $\boldsymbol{W}^{c-1}$ $(\in \mathbb{R}^{n^{c-1} \times n_{\mathrm{Atoms}}^{c-1}})$ accounts for all possible combinations of heavy (weight = 1) and light (weight = 0) isotopes in the molecule and thus describes all possible isotopocules. For each of the possible bond breakage positions (removal of atom X) a transformation matrix ${}^{X}\boldsymbol{T}^{c-1}$ $(\in \mathbb{R}^{n_{\mathrm{Atoms}}^c \times n_{\mathrm{Atoms}}^c})$ exists, which transforms **W** from an absolute reference system (geographically fixed) to a relative reference system (relative to the bond breakage position) as illustrated for PCE in Figure 2. This transformation step is necessary as the vector AKIE is arranged in the relative reference system. Furthermore, two

examples of $\boldsymbol{\kappa}$ associated with PCE reductive dechlorination to *c*DCE ($\boldsymbol{\kappa}^{\mathrm{PCE}\rightarrow\mathrm{TCE}}$ and $\boldsymbol{\kappa}^{\mathrm{TCE}\rightarrow c\mathrm{DCE}}$) are illustrated below (Figure 1).

The product in each non-zero element of $\boldsymbol{\kappa}$ takes into account the position-specific apparent kinetic isotopic effects (AKIEs) associated with each atom of the isotopocule of the degraded compound. The latter accounts for primary and secondary isotopic effects in isotopocule fractionation factors and is defined as follows:

$$\mathrm{AKIE}^{c} = \left[\frac{1}{1+\frac{\epsilon_1}{1000}}, \dots, \frac{1}{1+\frac{\epsilon_{n^c_{\mathrm{Atoms}}}}{1000}}\right] \in \mathbb{R}^{n^c_{\mathrm{Atoms}}} \quad (4)$$

where ε_p (with $p \in [1, \dots, n^c_{\mathrm{Atoms}}]$) corresponds to the degradation-related position specific isotopic effect (either primary or secondary) of the atom at relative position p.

Additionally, clumped isotope effects, where the isotope effect associated with the presence of a heavy atom at a certain position depends on the presence of heavy atoms at other positions, could be included in order to have a more comprehensive model. They were however not included when determining $\boldsymbol{\kappa}$ due to the lack of experimental evidence for the occurrence of such effects. Yet, as each isotopocule is considered separately, the approach could be adapted to include clumped isotope effects. The only modification necessary would consist in adapting the non-zero elements of $\boldsymbol{\kappa}$.

2.1.2. Application of GM to PCE reductive dechlorination

First the general concept of GM applied to the reductive dechlorination of PCE to *c*DCE is presented followed by a more detailed explanation of how the matrix $\boldsymbol{\kappa}$ was generated for the PCE to TCE transformation step. Figure 1-B illustrates the sequential reductive dechlorination of PCE isotopocules to TCE and consecutively to *c*DCE isotopocules. Figure 1-A illustrates the corresponding isotopocule fractionation matrices $\boldsymbol{\kappa}^{\mathrm{PCE}\rightarrow\mathrm{TCE}} \in \mathbb{R}^{64\times32}$ and $\boldsymbol{\kappa}^{\mathrm{TCE}\rightarrow c\mathrm{DCE}} \in \mathbb{R}^{32\times16}$. The number of lines in each matrix corresponds to the number of isotopocules of the degraded compound. Conversely, the number of columns in each matrix corresponds to the number of isotopocules of produced compound. In each line corresponding to the degradation of one isotopocule, each non-zero element corresponds to the isotopocule fractionation factor associated with each breakable bond position. In the case of PCE to *c*DCE reductive dechlorination, a total number of $n^{\mathrm{PCE}}_{\mathrm{Iso}} = 2^6 = 64$ (6 atoms, each having two possible states, i.e. either a heavy or a light isotope) isotopocules of PCE each yield 4 possible TCE isotopocules (= 4 breakable bonds) among a total number of $n^{\mathrm{TCE}}_{\mathrm{Iso}} = 2^5 = 32$ isotopocules of TCE. In $\boldsymbol{\kappa}^{\mathrm{PCE}\rightarrow\mathrm{TCE}}$, each line will thus contain 4 non-zero elements corresponding to the different possible bond breakage positions. Each TCE isotopocule will in turn yield 1 *c*DCE isotopocule (= 1 breakable bond) among a total number of $n^{c\mathrm{DCE}}_{\mathrm{Iso}} = 2^4 = 16$ isotopocules of *c*DCE. Similarly, in $\boldsymbol{\kappa}^{\mathrm{TCE}\rightarrow c\mathrm{DCE}}$, each line will thus contain 1 non-zero element corresponding to the different possible bond breakage positions. It should be noted that different isotopocules of degraded compound might yield the same isotopocule of produced compound. Furthermore, for symmetric molecules such as PCE and *c*DCE, the total number of isotopocules may be reduced due to symmetries.

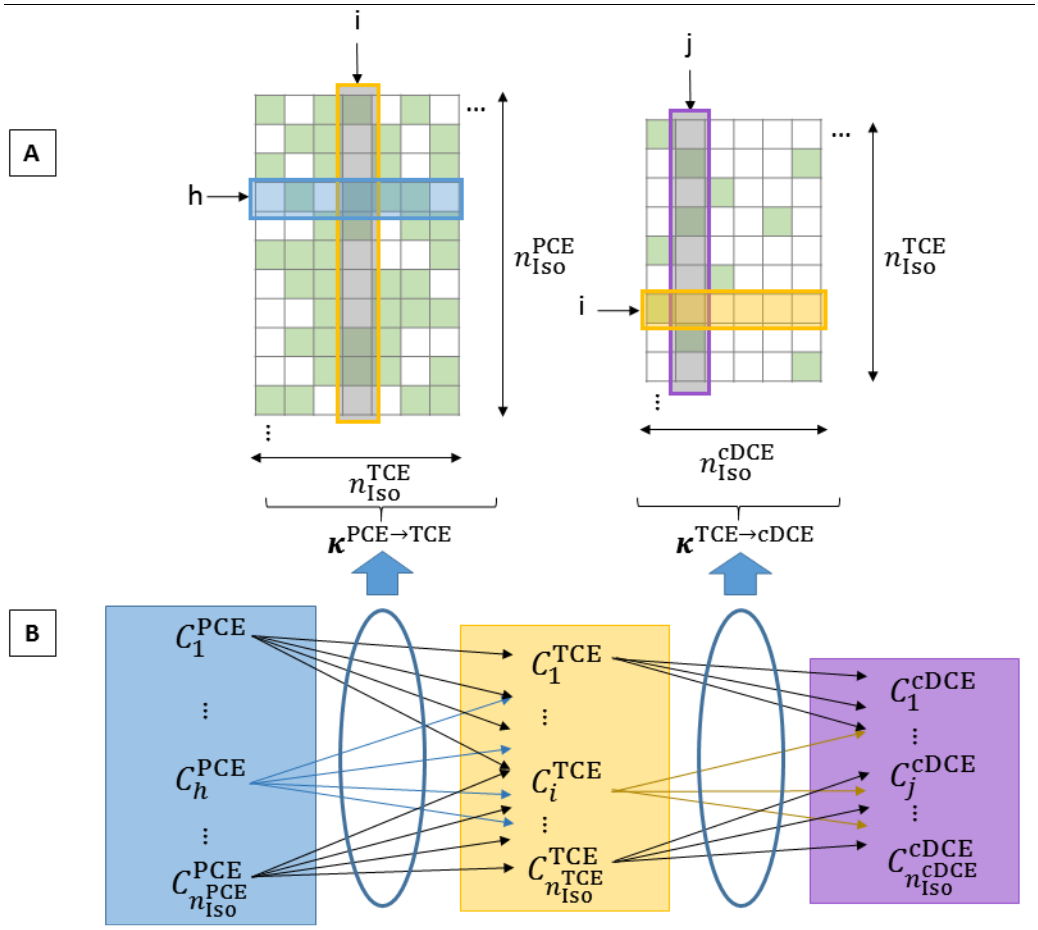

Figure 1. Schematic explanation of matrices $\boldsymbol{\kappa}^{\mathrm{PCE}\rightarrow\mathrm{TCE}}$ ($\in \mathbb{R}^{64\times32}$) and $\boldsymbol{\kappa}^{\mathrm{TCE}\rightarrow c\mathrm{DCE}}$ ($\in \mathbb{R}^{32\times16}$) containing kinetic isotopic coefficients $\boldsymbol{\kappa}_{h,i}^{\mathrm{PCE}\rightarrow\mathrm{TCE}}$ and $\boldsymbol{\kappa}_{i,j}^{\mathrm{TCE}\rightarrow c\mathrm{DCE}}$, associated with reductive dechlorination of PCE to TCE and TCE to cDCE, respectively. Panel A: For the sake of simplicity, smaller matrices than the actual ones are here represented. The green and white squares represent isotopocule fractionation factors different from zero and equal to zero, respectively. Columns i and j correspond to the column of factors associated with the production of the ith isotopocule of TCE from PCE and the jth isotopocule of cDCE from TCE, respectively. The blue shade in panel A corresponds to the factors associated with degradation of the hth isotopocule of PCE to TCE which are further illustrated by the blue arrows in panel B. Similarly, the orange shade in panel A corresponds to the factors associated with degradation of the ith isotopocule of TCE to cDCE which are illustrated by the orange arrows in panel B.

In the following section, PCE reductive dechlorination to TCE denoted as PT is considered (without any subsequent degradation to *c*DCE) to illustrate the application of equation (2). PCE being degraded, the concentration of its isotopocules h will thus follow:

$$\frac{\partial C_h^{\mathrm{PCE}}}{\partial t} = -\left(\sum_{i=1}^{n_{\mathrm{Iso}}^{\mathrm{TCE}}} \boldsymbol{\kappa}_{h,i}^{\mathrm{PCE}\rightarrow\mathrm{TCE}}\right) \cdot v^{\mathrm{PCE}} \frac{C_h^{\mathrm{PCE}}}{C_{\mathrm{tot}}^{\mathrm{PCE}}}, \qquad \forall h \in [1,\ldots,n_{\mathrm{Iso}}^{\mathrm{PCE}}] \tag{5}$$

Conversely, the concentration of isotopocules i of produced TCE will follow:

$$\frac{\partial C_i^{\mathrm{TCE}}}{\partial t} = \sum_{h=1}^{n_{\mathrm{Iso}}^{\mathrm{PCE}}} \left(\boldsymbol{\kappa}_{h,i}^{\mathrm{PCE}\rightarrow\mathrm{TCE}} \cdot v^{\mathrm{PCE}} \frac{C_h^{\mathrm{PCE}}}{C_{\mathrm{tot}}^{\mathrm{PCE}}} \right), \qquad \forall i \in [1, \dots, n_{\mathrm{Iso}}^{\mathrm{TCE}}] \tag{6}$$

These equations are based on the general equation (2). Equations (11), (12) and (13) describing PCE, TCE and *c*DCE isotopocules during sequential reductive dechlorination are given in the case of Monod kinetics in part 2.3. In order to generate $\boldsymbol{\kappa}^{\mathrm{PCE}\rightarrow\mathrm{TCE}}$, the weight coefficient matrix $\boldsymbol{W}^{\mathrm{PCE}}$ ($\in \mathbb{R}^{64\times 6}$) is created to describe the position of heavy (weight = 1) and light (weight = 0) isotopes in all degraded PCE isotopocules by means of an absolute reference system where the position of all atoms in the molecule are "geographically" fixed (Figure 2, molecule 1). Each of the 64 lines in $\boldsymbol{W}^{\mathrm{PCE}}$ represents an isotopocule whereas each of the 6 columns correspond to one atom at absolute position X being light or heavy. This matrix is then transformed into the aforementioned relative reference system by using one of the four transformation matrices ${}^{\boldsymbol{C}}\boldsymbol{T}^{\mathrm{PCE}}$, ${}^{\boldsymbol{D}}\boldsymbol{T}^{\mathrm{PCE}}$, ${}^{\boldsymbol{E}}\boldsymbol{T}^{\mathrm{PCE}}$, or ${}^{\boldsymbol{F}}\boldsymbol{T}^{\mathrm{PCE}}$ enabling to take into account the broken bond at absolute position X = C, D, E, or F, respectively (Figure 2, molecules 3 to 6).

The AKIEs themselves are given in the relative system (Figure 2, molecule 2) and correspond to the kinetic isotopic effects associated with each atom at relative position p ∈ $[1, \dots, 6]$.

Typically, $\mathrm{AKIE} = \left[\mathrm{AKIE}_{\mathrm{C}\alpha}, \mathrm{AKIE}_{\mathrm{C}\beta}, \mathrm{AKIE}_{\mathrm{Cl}\alpha 1}, \mathrm{AKIE}_{\mathrm{Cl}\alpha 2}, \mathrm{AKIE}_{\mathrm{Cl}\beta 1}, \mathrm{AKIE}_{\mathrm{Cl}\beta 2}\right]$, where C_α undergoes a primary C isotopic effect and C_β a secondary C isotopic effect; $Cl_{\alpha 1}$ undergoes a primary Cl isotopic effect while $Cl_{\alpha 2}$, $Cl_{\beta 1}$ and $Cl_{\beta 2}$ undergo secondary Cl isotopic effects. Thanks to the transformed weight coefficient matrix $\boldsymbol{W}^{\mathrm{PCE}} \cdot {}^{\boldsymbol{X}}\boldsymbol{T}^{\mathrm{PCE}}$, these AKIEs will be accounted for (weight = 1) or not (weight = 0) in $\boldsymbol{\kappa}^{\mathrm{PCE}\rightarrow\mathrm{TCE}}$ depending on whether a heavy or a light isotope is present in the absolute position X as described earlier in equation (3).

2.2. Separate consideration of C and Cl isotopes (SM)

In view of incorporating the change of isotopic ratios during degradation in a reactive transport model for example, the general model (GM) was simplified to a computationally less expensive model (SM). This simplification was achieved by simulating less species simultaneously.

This model is explained in the following for chlorinated ethenes and is illustrated in Figure 3. First, C and Cl atoms were considered separately. Second, as the bond cleavage can take place at any position involving a Cl atom (non regioselective reaction) for symmetric chlorinated ethenes (e.g. PCE), the positions of heavy and light Cl and C isotopes in the molecule do not matter anymore and we thus considered isotopologues relative to C and Cl instead of isotopocules. Since the secondary positions are not differentiated anymore, a single secondary isotopic effect ($\mathrm{AKIE}_{\mathrm{ClSec}}^{\mathrm{c}}$) is considered which reflects all position-specific secondary isotopic effects associated with all Cl atoms located in remaining positions (e.g. for PCE: $\mathrm{AKIE}_{\mathrm{Cl}\alpha 2}^{\mathrm{PCE}}$ = $\mathrm{AKIE}_{\mathrm{Cl}\beta 1}^{\mathrm{PCE}}$ = $\mathrm{AKIE}_{\mathrm{Cl}\beta 2}^{\mathrm{PCE}}$ = $\mathrm{AKIE}_{\mathrm{ClSec}}^{\mathrm{PCE}}$). This assumption was made according to the recent explanations of Cretnik *et al.*, 2014 who showed that the overall secondary isotopic effect corresponds to the average between all secondary isotopic effects. Finally, symmetric molecules were distinguished from asymmetric molecules.

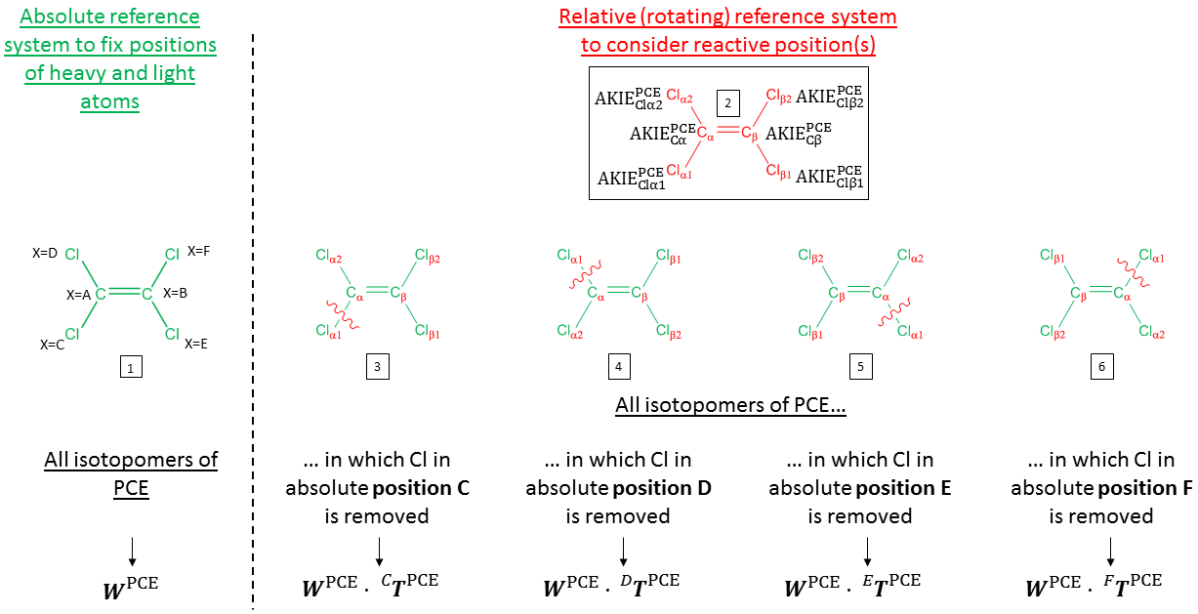

Figure 2. Absolute and relative reference systems used to determine weight coefficients associated with AKIEp for further calculation of isotopocule fractionation factors. Molecule 1 illustrates the absolute reference system where each of the 6 atoms adopt absolute positions and based on which all 64 isotopocules of PCE are determined. This absolute reference system is described by $\boldsymbol{W}^{\mathrm{PCE}}$. Molecule 2 illustrates the relative reference system based on which each reactive bond can be distinctly considered. Molecules 3 to 6 illustrate the result of transformation of the absolute system with a rotating reference system required to determine position-specific AKIEs related to the removed atom at absolute position X = C, E, F, and D, respectively. Clα1 will typically undergo a primary Cl isotopic effect while Clα2, Clβ1 and Clβ2 will undergo secondary Cl isotopic effects. Similarly, Cα will undergo a primary C isotopic effect and Cβ a secondary C isotopic effect. The green color indicates the absolute reference system; the red color indicates the relative reference system.

Based on these considerations, the corresponding fractionation factor associated with Cl thus reflects (i) both the isotopic effects induced when cleaving a bond involving a heavy Cl isotope (primary isotopic effect) and the isotopic effect induced by the presence of heavy Cl isotopes in the remaining positions which did not react (secondary isotopic effect) (first condition of $\boldsymbol{\kappa}^{c\to c+1}$ described in equation (7)) or (ii) the isotopic effects induced only by the presence of heavy Cl isotopes in the positions which did not react when cleaving a bond involving a light Cl isotope (second condition of $\boldsymbol{\kappa}^{c\to c+1}$ described in equation (7)).

Isotopologue fractionation factors relative to Cl were hence calculated as follows:

$$\boldsymbol{\kappa}_{i,j}^{c\to c+1} = \begin{cases} \dfrac{1}{\mathrm{AKIE}_{\mathrm{ClPrim}}^{c}} \cdot \left(\dfrac{1}{\mathrm{AKIE}_{\mathrm{ClSec}}^{c}}\right)^{n_{^{37}\mathrm{Cl}_i}^{c}-1} \cdot \left(\dfrac{n_{^{37}\mathrm{Cl}_i}^{c}}{n_{\mathrm{Cl}}^{c}}\right), & \text{if bond breakage involving heavy isotope in isotopologue i leads to isotopologue j (c+1)} \\ \left(\dfrac{1}{\mathrm{AKIE}_{\mathrm{ClSec}}^{c}}\right)^{n_{^{37}\mathrm{Cl}_i}^{c}} \cdot \left(1-\dfrac{n_{^{37}\mathrm{Cl}_i}^{c}}{n_{\mathrm{Cl}}^{c}}\right), & \text{if bond breakage involving light isotope in isotpologue i leads to isotopologue j (c+1)} \\ 0, & \text{else} \end{cases} \quad (7)$$

On the other hand, C atoms are not removed during the reaction contrary to Cl, isotopologue fractionation factors associated with C were hence determined as follows:

$$\boldsymbol{\kappa}_{i,j}^{c\to c+1} = \begin{cases} \frac{1}{\mathrm{AKIE}_{\mathrm{CPrim}}^{c}} \cdot \left(\frac{1}{\mathrm{AKIE}_{\mathrm{CSec}}^{c}}\right)^{n_{^{13}\mathrm{C}_i}^{c}-1} \cdot \left(\frac{n_{^{13}\mathrm{C}_i}^{c}}{n_{\mathrm{C}}^{c}}\right) \\ \quad + \left(\frac{1}{\mathrm{AKIE}_{\mathrm{CSec}}^{c}}\right)^{n_{^{13}\mathrm{C}_i}^{c}} \cdot \left(1 - \frac{n_{^{13}\mathrm{C}_i}^{c}}{n_{\mathrm{C}}^{c}}\right), & \text{if isotopologue i leads to isotopologue j} \\ 0, \text{ else} \end{cases} \quad (8)$$

where i and j correspond to isotopologues of compound c and c+1. The specific matrices $\boldsymbol{\kappa}$ containing isotopologue fractionation factors associated with sequential reductive dechlorination of PCE to *c*DCE are given in Figure 4. The latter slightly differ from their definitions in equations (7) and (8) as they were further modified to meet the requirements for asymmetric molecules as explained in the following.

Contrary to symmetric molecules, the bond cleavage is regioselective for asymmetric chlorinated ethenes (e.g. TCE). For isotopologues containing both heavy and light Cl (respectively C) isotopes, the positions thereof should therefore be taken into account so that the fact that the bond breakage takes place only where the isotope located in the only reactive position may be considered. "Isotopocules" relative to Cl (respectively to C) were hence considered in the case of asymmetric chlorinated ethenes instead of isotopologues. The fractionation factors were determined similarly as for symmetric molecules with the exception that instead of considering any Cl position, the presence of heavy or light Cl isotope in the only possible cleaved position (α1) was taken into account separately from heavy or light Cl isotopes located in non-reacting positions (Figure 3, Figure 4). In the case of C which consistutes the backbone during sequential dechlorination, the probability that a heavy or a light atom is involved in the bond breakage is considered equal when both a light and a heavy isotope are present in the molecule for symmetric molecules (e.g. PCE). Conversely for asymmetric molecules (e.g. TCE), since only one C is involved in the bond-breakage in one isotopocule, the occurrence of primary and secondary isotopic effect is not distributed between the two positions as illustrated for the case of TCE ($\boldsymbol{\kappa}^{\mathrm{TCE_C}\to c\mathrm{DCE_C}}$) in Figure 4.

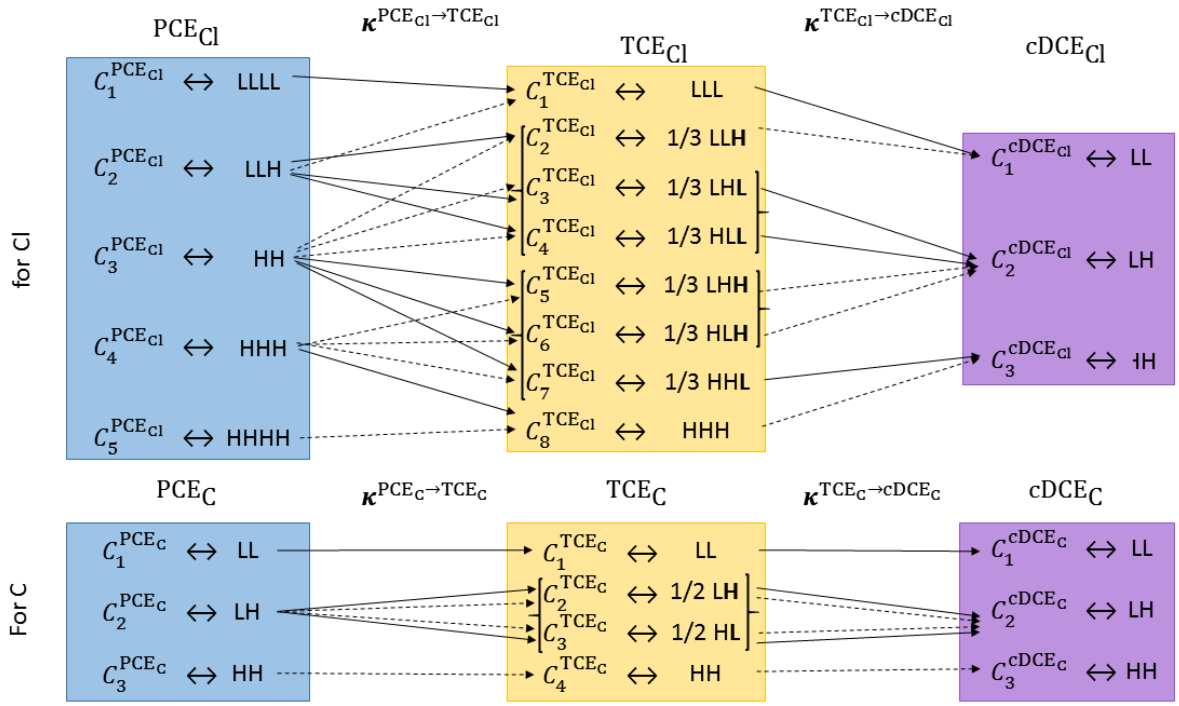

Figure 3. Transitions considered between isotopologues of PCE, TCE and *c*DCE during PCE reductive dechlorination for the simplified model (SM). A more intuitive notation was used in this scheme based on the scheme suggested by Hunkeler *et al.*, 2009: L designates light isotopes while H designates heavy isotopes (of either C or Cl). Solid arrows correspond to transitions where bond breakage involves a light isotope of the considered element while dotted arrows correspond to transitions involving heavy isotopes. $\boldsymbol{\kappa}$ are the matrices containing the isotopologue fractionation factors relative to Cl and C associated with each transition. The corresponding matrices are given in Figure 4.

$$\boldsymbol{\kappa}^{\mathrm{PCE}_C\rightarrow\mathrm{TCE}_C}=\begin{array}{c}\begin{matrix}\mathrm{LL} & \mathrm{L\mathbf{H}} & \mathrm{H\mathbf{L}} & \mathrm{HH}\end{matrix}\\ \begin{pmatrix}1 & 0 & 0 & 0\\ 0 & \frac{1}{4\,\mathrm{A}_p^C}+\frac{1}{4\,\mathrm{A}_s^C} & \frac{1}{4\,\mathrm{A}_p^C}+\frac{1}{4\,\mathrm{A}_s^C} & 0\\ 0 & 0 & 0 & \frac{1}{\mathrm{A}_p^C\,\mathrm{A}_s^C}\end{pmatrix}\end{array}\begin{matrix}\mathrm{LL}\\ \mathrm{LH}\\ \mathrm{HH}\end{matrix}$$

$$\boldsymbol{\kappa}^{\mathrm{PCE}_{Cl}\rightarrow\mathrm{TCE}_{Cl}}=\begin{array}{c}\begin{matrix}\mathrm{LLL} & \mathrm{LL\mathbf{H}} & \mathrm{LH\mathbf{L}} & \mathrm{HL\mathbf{L}} & \mathrm{LH\mathbf{H}} & \mathrm{HL\mathbf{H}} & \mathrm{HH\mathbf{L}} & \mathrm{HHH}\end{matrix}\\ \begin{pmatrix}1 & 0 & 0 & 0 & 0 & 0 & 0 & 0\\ \frac{1}{4\,\mathrm{A}_p^{Cl}} & \frac{1}{4\,\mathrm{A}_s^{Cl}} & \frac{1}{4\,\mathrm{A}_s^{Cl}} & \frac{1}{4\,\mathrm{A}_s^{Cl}} & 0 & 0 & 0 & 0\\ 0 & \frac{1}{6\,\mathrm{A}_p^{Cl}\,\mathrm{A}_s^{Cl}} & \frac{1}{6\,\mathrm{A}_p^{Cl}\,\mathrm{A}_s^{Cl}} & \frac{1}{6\,\mathrm{A}_p^{Cl}\,\mathrm{A}_s^{Cl}} & \frac{1}{6\,(\mathrm{A}_s^{Cl})^2} & \frac{1}{6\,(\mathrm{A}_s^{Cl})^2} & \frac{1}{6\,(\mathrm{A}_s^{Cl})^2} & 0\\ 0 & 0 & 0 & 0 & \frac{1}{4\,\mathrm{A}_p^{Cl}\,(\mathrm{A}_s^{Cl})^2} & \frac{1}{4\,\mathrm{A}_p^{Cl}\,(\mathrm{A}_s^{Cl})^2} & \frac{1}{4\,\mathrm{A}_p^{Cl}\,(\mathrm{A}_s^{Cl})^2} & \frac{1}{4\,(\mathrm{A}_s^{Cl})^3}\\ 0 & 0 & 0 & 0 & 0 & 0 & 0 & \frac{1}{\mathrm{A}_p^{Cl}\,(\mathrm{A}_s^{Cl})^3}\end{pmatrix}\end{array}\begin{matrix}\mathrm{LLLL}\\ \mathrm{LLLH}\\ \mathrm{LLHH}\\ \mathrm{LHHH}\\ \mathrm{HHHH}\end{matrix}$$

$$\boldsymbol{\kappa}^{\mathrm{TCE}_C\rightarrow\mathrm{cDCE}_C}=\begin{array}{c}\begin{matrix}\mathrm{LL} & \mathrm{LH} & \mathrm{HL}\end{matrix}\\ \begin{pmatrix}1 & 0 & 0\\ 0 & \frac{1}{\mathrm{A}_p^C} & 0\\ 0 & \frac{1}{\mathrm{A}_s^C} & 0\\ 0 & 0 & \frac{1}{\mathrm{A}_p^C\,\mathrm{A}_s^C}\end{pmatrix}\end{array}\begin{matrix}\mathrm{LL}\\ \mathrm{L\mathbf{H}}\\ \mathrm{H\mathbf{L}}\\ \mathrm{HH}\end{matrix}$$

$$\boldsymbol{\kappa}^{\mathrm{TCE}_{Cl}\rightarrow\mathrm{cDCE}_{Cl}}=\begin{array}{c}\begin{matrix}\mathrm{LL} & \mathrm{LH} & \mathrm{HL}\end{matrix}\\ \begin{pmatrix}1 & 0 & 0\\ \frac{1}{\mathrm{A}_p^{Cl}} & 0 & 0\\ 0 & \frac{1}{\mathrm{A}_s^{Cl}} & 0\\ 0 & \frac{1}{\mathrm{A}_s^{Cl}} & 0\\ 0 & \frac{1}{\mathrm{A}_p^{Cl}\,\mathrm{A}_s^{Cl}} & 0\\ 0 & \frac{1}{\mathrm{A}_p^{Cl}\,\mathrm{A}_s^{Cl}} & 0\\ 0 & 0 & \frac{1}{(\mathrm{A}_s^{Cl})^2}\\ 0 & 0 & \frac{1}{\mathrm{A}_p^{Cl}\,(\mathrm{A}_s^{Cl})^2}\end{pmatrix}\end{array}\begin{matrix}\mathrm{LLL}\\ \mathrm{LL\mathbf{H}}\\ \mathrm{LH\mathbf{L}}\\ \mathrm{HL\mathbf{L}}\\ \mathrm{LH\mathbf{H}}\\ \mathrm{HL\mathbf{H}}\\ \mathrm{HH\mathbf{L}}\\ \mathrm{HHH}\end{matrix}$$

Figure 4. Matrices of isotopologue/isotopocule fractionation factors used in SM associated with each step of reductive dechlorination of PCE to *c*DCE. Unlike in GM where C and Cl are considered simultaneously, C and Cl are here treated separately. Each matrix thus represents the transition between isotopologues/ isotopocules of degraded to produced compound relative to either C or Cl. Letters in bold represent the reaction position. A stands for AKIE, p for primary, s for secondary. $\boldsymbol{\kappa}^{\mathrm{PCE_C\rightarrow TCE_C}}$ and $\boldsymbol{\kappa}^{\mathrm{PCE_{Cl}\rightarrow TCE_{Cl}}}$ thus describe the transition of PCE to TCE relative to C and Cl, respectively, while $\boldsymbol{\kappa}^{\mathrm{TCE_C\rightarrow cDCE_C}}$ and $\boldsymbol{\kappa}^{\mathrm{TCE_{Cl}\rightarrow cDCE_{Cl}}}$ describe the transition of TCE to *c*DCE relative to C and Cl, respectively. Symmetries (PCE and *c*DCE) and asymmetries (TCE) are also taken into account. More particularly for C where no atom is removed during the transition, it is considered during PCE transformation to TCE that primary and secondary effects are equally distributed between the two positions. On the contrary, during TCE transformation to *c*DCE, it is considered that one C either undergoes a primary or a secondary isotopic effect since the reaction is regioselective and there are therefore no equal possibilities of cleaving the bond from one or the other C.

2.3. The case of Monod kinetics

The bacterial growth on sequential or simultaneous substrates following Monod kinetics can be described as by Kompala *et al.*, 1984:

$$\frac{\partial X}{\partial t}=\sum_{c=1}^{n_{\mathrm{Comps}}-1}\left(\mu_{\mathrm{MAX}}^{c}\frac{X\cdot C_{\mathrm{tot}}^{c}}{K_m^{c}+C_{\mathrm{tot}}^{c}}\right)-\mu_{\mathrm{DEC}}\cdot X \qquad (9)$$

where n_{Comps} is the total number of compounds used for growth, X [g of protein·L^{-1}] is the biomass concentration growing on all compounds, C_{tot} [µmol·L^{-1}] is the concentration, μ_{MAX} [µmol·g of protein^{-1}·s^{-1}] is the maximum growth rate, K_m [µmol·L^{-1}] is the half saturation constant, and μ_{DEC} [s^{-1}] is the biomass decay rate constant associated with growth on chlorinated ethenes. As the isotopic shifts triggered by compound consumption constitute the primary interests, we are focusing on the biomass growth phase. The biomass decay rate constant (μ_{DEC}) associated with growth is thus assumed to be zero here.

If Monod kinetics are assumed, the following expression for isotopocules (respectively isotopologues for SM) rates may be expressed based on equation (2) and considering growth on sequential or simultaneous substrates where substrates correspond to isotopocules:

$$\frac{\partial C_i^c}{\partial t} = \underbrace{\left(\sum_{h=1}^{n_{\mathrm{iso}}^{c-1}} \boldsymbol{\kappa}_{h,i}^{c-1\to c} \cdot \frac{\mu_{\mathrm{MAX}}^{c-1} \cdot X \cdot C_h^{c-1}}{Y^{c-1} \cdot (K_m^{c-1} + C_{\mathrm{tot}}^{c-1})}\right)}_{\text{produced from } c-1} - \underbrace{\left(\sum_{j=1}^{n_{\mathrm{iso}}^{c+1}} \boldsymbol{\kappa}_{i,j}^{c\to c+1}\right) \cdot \frac{\mu_{\mathrm{MAX}}^{c} \cdot X \cdot C_i^{c}}{Y^{c} \cdot (K_m^{c} + C_{\mathrm{tot}}^{c})}}_{\text{degraded to } c+1}, \quad \forall i \in [1, \dots, n_{\mathrm{iso}}^{c}] \tag{10}$$

where Y [g of protein·µmol of released chloride^{-1}] represents the biomass yield. The first term corresponds to the production of compound c from $c-1$ and the second term to its degradation to $c+1$.

For PCE reductive dechlorination to *c*DCE, the following equations thus apply. For PCE:

$$\frac{\partial C_i^{PCE}}{\partial t} = \underbrace{\left(\sum_{h=1}^{n^{c-1}} \boldsymbol{\kappa}_{h,i}^{c-1\to c} \cdot v^{c-1} \cdot \frac{C_h^{c-1}}{C_{tot}^{c-1}}\right)}_{\text{produced from c-1}} - \underbrace{\left(\sum_{j=1}^{n^{PCE}} \boldsymbol{\kappa}_{i,j}^{PCE\to TCE}\right) \cdot v^{PCE} \cdot \frac{C_i^{PCE}}{C_{tot}^{PCE}}}_{\text{degraded to TCE}}, \quad \forall i \in [1, \dots, n^{PCE}] \tag{11}$$

The first term in grey is left here to remind of equation (10) but does not apply to PCE which is only being degraded.

For TCE :

$$\frac{\partial C_i^{TCE}}{\partial t} = \underbrace{\left(\sum_{h=1}^{n^{PCE}} \boldsymbol{\kappa}_{h,i}^{TCE\to PCE} \cdot v^{PCE} \cdot \frac{C_h^{PCE}}{C_{tot}^{PCE}}\right)}_{\text{produced from PCE}} - \underbrace{\left(\sum_{j=1}^{n^{TCE}} \boldsymbol{\kappa}_{i,j}^{TCE\to cDCE}\right) \cdot v^{TCE} \cdot \frac{C_i^{TCE}}{C_{tot}^{TCE}}}_{\text{degraded to } c\text{DCE}}, \quad \forall i \in [1, \dots, n^{TCE}] \tag{12}$$

And for *c*DCE :

$$\frac{\partial C_i^{cDCE}}{\partial t} = \underbrace{\left(\sum_{h=1}^{n^{TCE}} \boldsymbol{\kappa}_{h,i}^{TCE\to cDCE} \cdot v^{TCE} \cdot \frac{C_h^{TCE}}{C_{tot}^{TCE}}\right)}_{\text{produced from TCE}} - \underbrace{\left(\sum_{j=1}^{n_i^c} \boldsymbol{\kappa}_{i,j}^{c\to c+1}\right) \cdot v^{c} \cdot \frac{C_i^c}{C_{tot}^c}}_{\text{degraded to c+1}}, \quad \forall i \in [1, \dots, n^{cDCE}] \tag{13}$$

The second term in grey is left here to remind of equation (10) but does not apply to *c*DCE which is only being produced.

2.4. Initial isotopocules/isotopologues concentrations calculation

From now on, all the equations are applicable to any of the compounds c simulated (i.e. PCE, TCE or *c*DCE). Therefore, for the sake of readability, the c in the superscript of the corresponding variables has been omitted. In the case of GM, the initial isotopocules concentrations can be calculated based on the initial isotopic compositions $\delta^{37}Cl_0$ and $\delta^{13}C_0$ of degraded compound and the total initial concentration thereof. Initial isotopocules concentrations C_h can be determined from the total compound concentration C_0 based on the relative abundance of isotopocule h as formerly suggested by Jin *et al.*, 2013:

$$C_h = C_0 \cdot p_h, \text{ with } p_h = \left(P_{^{13}\mathrm{C}}\right)^{n_{^{13}\mathrm{C}_h}} \left(P_{^{12}\mathrm{C}}\right)^{n_{^{12}\mathrm{C}_h}} \left(P_{^{37}\mathrm{Cl}}\right)^{n_{^{37}\mathrm{Cl}_h}} \left(P_{^{35}Cl}\right)^{n_{^{35}\mathrm{Cl}_h}} \quad (14)$$

Where p_h is the relative abundance of the isotopocule h containing $n_{^{13}\mathrm{C}_h} (= \sum_{(i \in \mathrm{C\ Atoms})} \boldsymbol{W}_{h,i})$ ^{13}C from a total of n_{C} $(= n_{^{13}\mathrm{C}_h} + n_{^{12}\mathrm{C}_h})$ C and $n_{^{37}\mathrm{Cl}_h} (= \sum_{(i \in \mathrm{Cl\ Atoms})} \boldsymbol{W}_{h,i})$ ^{37}Cl from a total of n_{Cl} $(= n_{^{37}\mathrm{Cl}_h} + n_{^{35}\mathrm{Cl}_h})$ Cl atoms.

When C and Cl are considered separately, the relative abundance of isotopologues relative to C and Cl can be determined separately by the probability mass function, as previously described by Hunkeler, van Breukelen and Elsner according to *(Hunkeler et al., 2009)*:

$$p_h = \binom{n_{\mathrm{C}}}{n_{^{13}\mathrm{C}_h}} \left(P_{^{13}\mathrm{C}}\right)^{n_{^{13}\mathrm{C}_h}} \left(P_{^{12}\mathrm{C}}\right)^{n_{^{12}\mathrm{C}_h}}, \text{ for isotopologues relative to C} \quad (15)$$

$$p_h = \binom{n_{\mathrm{Cl}}}{n_{^{37}\mathrm{Cl}_h}} \left(P_{^{37}\mathrm{Cl}}\right)^{n_{^{37}\mathrm{Cl}_h}} \left(P_{^{35}\mathrm{Cl}}\right)^{n_{^{35}\mathrm{Cl}_h}}, \text{ for isotopologues relative to Cl} \quad (16)$$

where p_h is the relative abundance of isotopologue (or isotopocule for asymmetric molecules) h. Such simplification is possible when C and Cl are considered separately since the atoms positions relative to each other are not any more taken into consideration (isotopologues) contrary to when C and Cl are considered simultaneously as in equation (14) (isotopocules). For asymmetric chlorinated ethenes (e.g. TCE) the relative abundances are equally distributed between isotopocules arising due to asymmetry.

Isotopic ratios of an element E are usually given by the delta notation δEreported against international standards (VPDB or SMOC for C and Cl, respectively) defined as:

$$\delta E = \left(\frac{R}{R_{\mathrm{std}}} - 1\right) \cdot 1000\ [‰] \quad (17)$$

where R and R_{std} are the isotope ratios of the element E of the sample and the standard, respectively (R_{VPDB} = 0.0111802 *(Elsner et al., 2012)* and R_{SMOC} = 0.319766 *(Hunkeler et al., 2009)*).

The relative abundance of C and Cl isotopes in isotopocules or isotopologues h is therefore calculated based on the initial isotopic compositions $\delta^{13}\mathrm{C}_0$ and $\delta^{37}\mathrm{Cl}_0$ as:

$$P_{^{13}\mathrm{C}} = \frac{\left(\frac{\delta^{13}\mathrm{C}_0}{1000} + 1\right) \cdot R_{\mathrm{VPDB}}}{\left(\frac{\delta^{13}\mathrm{C}_0}{1000} + 1\right) \cdot R_{\mathrm{VPDB}} + 1} \quad (18)$$

$$P_{^{37}\mathrm{Cl}} = \frac{\left(\frac{\delta^{37}\mathrm{Cl}_0}{1000} + 1\right) \cdot R_{\mathrm{SMOC}}}{\left(\frac{\delta^{37}\mathrm{Cl}_0}{1000} + 1\right) \cdot R_{\mathrm{SMOC}} + 1} \quad (19)$$

2.5. Final C and Cl isotopic composition

Finally, the C and Cl isotopic compositions of each compound can be computed based on the simulated isotopocule/isotopologue concentrations according to:

$$\delta^{13}\mathrm{C} = \left(\frac{R_{\mathrm{C}}}{R_{\mathrm{VPDB}}} - 1\right) \cdot 1000\ [‰], \text{ with } R_{\mathrm{C}} = \sum_{\forall h}\left(\frac{n_{13\mathrm{C}_h}}{n_{12\mathrm{C}_h}} C_h\right) \quad (20)$$

$$\delta^{37}\mathrm{Cl} = \left(\frac{R_{\mathrm{Cl}}}{R_{\mathrm{SMOC}}} - 1\right) \cdot 1000\ [‰], \text{ with } R_{\mathrm{Cl}} = \sum_{\forall h}\left(\frac{n_{37\mathrm{Cl}_h}}{n_{35\mathrm{Cl}_h}} C_h\right) \quad (21)$$

2.6. Models implementation, evaluation and comparison

2.6.1. Implementation method

Both models GM and SM were applied to simulate dechlorination of PCE to TCE (PT), PCE to *c*DCE with TCE accumulation (PTD), and TCE to *c*DCE (TD). Simulations with GM were performed with Matlab while simulations with SM were performed both with Matlab and COMSOL Multiphysics. Differential equations used in COMSOL are given in the Appendices (Table A 8 to Table A 13). Considering TCE dechlorination to *c*DCE (i.e. in TD and PTD), we assume that the Cl positions in TCE are strictly distinguished between reactive and non-reactive positions. The *c*DCE Cl isotopic composition thus reflects the secondary isotopic effect only. *(Cretnik et al., 2014)* For simplification purposes, it is also assumed that no selective interconversion of *cis*/*trans*-DCE intermediates occur.
The kinetic parameters (i.e. μ_{MAX} and K_m) chosen for all simulations were comparable to those shared by Yu and Semprini, 2004, and Maymo-Gatell *et al.,* 1997 while C and Cl enrichment factors chosen are in the usually observed experimental range *(Meckenstock et al., 2004, Hunkeler et al., 2010)* (Figure 5 and Table A 7 of the Appendices). Simulations were performed until the concentratioin of the degraded compound reached 1 % of the initial concentration, thus allowing to stay in an experimentally representative context.

2.6.2. Comparison method

In order to compare both models, 31 different sets of isotopic parameters were defined e.g. some which differed in C and Cl enrichment factors, some with no secondary isotopic effect, some with normal/inverse secondary isotopic effects. Simulations were then performed for each set of parameters with both models (GM and SM). The average isotopic effect of the three Cl atoms located in non-reacting positions was used as Cl secondary isotopic effect in SM. These isotopic parameters are summarised in Table 1.
In order to evaluate the goodness of fit between SM and GM with regards to chlorinated ethenes concentration and isotopic behaviour along degradation, the Nash-Sutcliff efficiency coefficient (NSE) *(Krause et al., 2005)* and a normalised maximal absolute error coefficient (NME) were determined. The NSE varies between - ∞ and 1, a value of 1 corresponding to a perfect fit and is given by:

$$NSE = 1 - \frac{\sum_{i=1}^{N}(S_i - Q_i)^2}{\sum_{i=1}^{N}(Q_i - Q)^2} \quad (22)$$

The NME is given in percent and corresponds to the maximal absolute difference between GM and SM, divided by the maximal amplitude of GM. Compared to the established NSE coefficient, the NME allows a more conservative comparison between the two models and represents the worst case error. The discrepancy ratio η previously defined by Jin *et al*., 2013 was additionally used to evaluate the bias in SM due to the fact that we are solving the differential equations for C and Cl

isotopologues of a compound independently and thus simulating twice this compound. The more the value of η deviates from 1, the higher is the discrepancy between compound concentrations simulated with the C and Cl systems. NSE, NME and η determined for all parameter sets are given in Table 2 and Table 3.

2.6.3. Results of GM vs. SM comparison

NSEs of 0.995 to 1 were obtained for all simulated species (i.e. biomass, chlorinated ethenes concentrations and isotopic ratios) when comparing GM and SM simulated data using the same set of parameters. This indicates that both models simulate chlorinated ethenes concentrations and isotopic behaviours almost identically. An exception is observed in the case of *c*DCE Cl isotopic composition where some NSEs ranging from -3 to -16 are obtained. Such deviation however occurs only when non-reactive Cl atoms in PCE show different secondary isotope effects depending on their position relative to the reacting bond (PTD_diff_sec, Table 2). The observed discrepancy results from the unequal Cl isotope distribution in TCE due to the occurrence of different secondary Cl isotopic effects during transformation of PCE to TCE. The fact that this degradation step further affects *c*DCE Cl isotopic composition is taken into account when applying GM but is lost when applying SM, hence explaining the discrepancy. This *c*DCE specific discrepancy is reflected by NME ranging from 47 to 94% as well (Table 3). However, the absolute maximum difference in cDCE Cl isotopic composition between GM and SM is actually of 2 ‰ which is only slightly higher than the analytical uncertainty. Such discrepancy thus poses a problem primarily when little overall shifts are observed in cDCE Cl isotopic composition. Apart from this special case, a maximum NME of 2 % was found associated with *c*DCE C isotopic composition during TCE degradation to *c*DCE where inverse secondary isotopic effects were considered. Among the 31 simulations with different parameter sets, NME was < 1 % in 96 % of the cases (Table 3). These results confirm that GM and SM both simulate chlorinated ethenes concentrations and isotopic behaviours almost identically except for *c*DCE Cl isotopic composition when different secondary isotopic effects occur during the transformation step of PCE to TCE in the overall degradation of PCE to *c*DCE. Finally, acceptable discrepancy values η related to the simultaneous resolution of differential equation systems for compounds relatively to C and Cl ranging from 0.979 to 1.008 were observed.

As the discrepancy between SM and GM is little in most cases and as η remains in a reasonable range for the 31 sets of simulations, SM can be considered as a representative enough model for most cases. *c*DCE Cl isotopic composition from PCE to *c*DCE degradation where different secondary isotopic effects are considered during the transformation step of PCE to TCE constitutes the only exception. As the occurrence of different secondary isotopic effects is not yet experimentally proven, such exception is currently not problematic. Finally, depending on the required simulation accuracy, GM or SM may be chosen.

Table 1. Sets of isotopic effect parameters with which both GM and SM were run. εCα, εCβ, εClα1, εClα2, εClβ1, εClβ2 correspond to C primary, C secondary, Cl primary, Cl secondary in geminal position, Cl secondary in vicinal positions (β1 and β2), respectively. f corresponds to the fraction remaining of initial compound. No_sec, normal_sec, inv_sec, diff_sec, diff_secB, diff_secP, diff_secT are relative to secondary isotope effects and stand for no, normal, inverse, different secondary effects. Different cases are differentiated for different secondary effects associated with PTD: B means that both PCE and TCE undergo secondary effects while P and T mean that either PCE or TCE undergoes secondary effects, respectively.

	PCE						TCE						PCE	TCE
	εCα	εCβ	εClα1	εClα2	εClβ1	εClβ2	εCα	εCβ	εClα1	εClα2	εClβ1	εClβ2	f	f
Simulation type													**%**	**%**
PT_1no_sec	-20	0	-0.2	0	0	0							0.9	
PT_2no_sec	-20	0	-2	0	0	0							0.9	
PT_3no_sec	-4	0	-2	0	0	0							0.9	
TD_1no_sec							-20	0	-0.2	0	0	0		0.9
TD_2no_sec							-20	0	-2	0	0	0		0.9
TD_3no_sec							-4	0	-2	0	0	0		0.9
PTD_1no_sec	-20	0	-0.2	0	0	0	-20	0	-0.2	0	0	0	1.0	
PTD_2no_sec	-20	0	-2	0	0	0	-20	0	-2	0	0	0	1.0	
PTD_3no_sec	-4	0	-2	0	0	0	-4	0	-2	0	0	0	1.0	
PT_1normal_sec	-20	-10	-10	-3	-3	-3							1.0	
PT_3normal_sec	-4	-5	-2	-3	-3	-3							0.9	
TD_1normal_sec							-20	-10	-0.2	-3	-3	-3		1.0
TD_3normal_sec							-4	-5	-2	-3	-3	-3		1.0
PTD_1normal_sec	-20	-10	-10	-3	-3	-3	-20	-10	-0.2	-3	-3	-3	0.9	
PTD_3normal_sec	-4	-5	-2	-3	-3	-3	-4	-5	-2	-3	-3	-3	1.0	
PT_1inv_sec	-20	5	-10	3	3	3							0.9	
PT_3inv_sec	-4	2	-2	3	3	3							0.9	
TD_1inv_sec							-20	5	-0.2	3	3	3		0.9
TD_3inv_sec							-4	2	-2	3	3	3		0.9
PTD_1inv_sec	-20	5	-10	3	3	3	-20	5	-0.2	3	3	3	1.0	
PTD_3inv_sec	-4	2	-2	3	3	3	-4	2	-2	3	3	3	0.9	
PT_1diff_sec	-20	3	-10	-5	2	-3							1.0	
PT_3diff_sec	-4	-3	-2	-5	2	-3							0.9	
TD_1diff_sec							-20	3	-0.2	-5	-3	2		0.9
TD_3diff_sec							-4	-3	-2	-5	-3	2		0.9
PTD_1diff_secB	-20	3	-10	-5	2	-3	-20	3	-0.2	-5	-3	2	1.0	
PTD_3diff_secB	-4	-3	-2	-5	2	-3	-4	-3	-2	-5	-3	2	1.0	
PTD_1diff_secT	-20	3	-10	-3	-3	-3	-20	3	-0.2	-5	2	2	0.9	
PTD_3diff_secT	-4	-3	-2	-3	-3	-3	-4	-3	-2	-5	2	2	1.0	
PTD_1diff_secP	-20	3	-10	-5	2	-3	-20	3	-0.2	-3	-3	-3	1.0	
PTD_3diff_secP	-4	-3	-2	-5	2	-3	-4	-3	-2	-3	-3	-3	1.0	
PT_exp	-5	0	-10	1.8	1.8	1.8							0.9	
TD_exp							-30.0	-5.0	-5.3	-3.0	-3.0	-3.0		0.8
PTD_exp	-0.7	0	-11.1	3.1	3.1	3.1	-29.1	0	-12.8	1.4	1.4	1.4	1.0	

Table 2. Nash-Sutcliff efficiency coefficients (NSE) associated with the comparison of GM and SM for all sets of parameters used for simulations. No NSE was calculated for *c*DCE Cl isotopic composition associated with TD when no secondary effect occurred since the Cl isotopic composition is then constant and equal to the initial TCE Cl isotopic composition.

Simulation type	X []	PCE []	TCE []	*c*DCE []	PCE $\delta^{13}C$	TCE $\delta^{13}C$	*c*DCE $\delta^{13}C$	PCE $\delta^{37}Cl$	TCE $\delta^{37}Cl$	*c*DCE $\delta^{37}Cl$
PT_1no_sec	1.00	1.00	1.00		1.00	1.00		1.00	1.00	
PT_2no_sec	1.00	1.00	1.00		1.00	1.00		1.00	1.00	
PT_3no_sec	1.00	1.00	1.00		1.00	1.00		1.00	1.00	
TD_1no_sec	1.00		1.00	1.00		1.00	1.00		1.00	X
TD_2no_sec	1.00		1.00	1.00		1.00	1.00		1.00	X
TD_3no_sec	1.00		1.00	1.00		1.00	1.00		1.00	X
PTD_1no_sec	1.00	1.00	1.00	1.00	1.00	1.00	1.00	1.00	1.00	1.00
PTD_2no_sec	1.00	1.00	1.00	1.00	1.00	1.00	1.00	1.00	1.00	1.00
PTD_3no_sec	1.00	1.00	1.00	1.00	1.00	1.00	1.00	1.00	1.00	1.00
PT_1normal_sec	1.00	1.00	1.00		1.00	1.00		1.00	1.00	
PT_3normal_sec	1.00	1.00	1.00		1.00	1.00		1.00	1.00	
TD_1normal_sec	1.00		1.00	1.00		1.00	1.00		1.00	1.00
TD_3normal_sec	1.00		1.00	1.00		1.00	1.00		1.00	1.00
PTD_1normal_sec	1.00	1.00	1.00	1.00	1.00	1.00	1.00	1.00	1.00	1.00
PTD_3normal_sec	1.00	1.00	1.00	1.00	1.00	1.00	1.00	1.00	1.00	1.00
PT_1inv_sec	1.00	1.00	1.00		1.00	1.00		1.00	1.00	
PT_3inv_sec	1.00	1.00	1.00		1.00	1.00		1.00	1.00	
TD_1inv_sec	1.00		1.00	1.00		1.00	1.00		1.00	1.00
TD_3inv_sec	1.00		1.00	1.00		1.00	1.00		1.00	1.00
PTD_1inv_sec	1.00	1.00	1.00	1.00	1.00	1.00	1.00	1.00	1.00	1.00
PTD_3inv_sec	1.00	1.00	1.00	1.00	1.00	1.00	1.00	1.00	1.00	1.00
PT_1diff_sec	1.00	1.00	1.00		1.00	1.00		1.00	1.00	
PT_3diff_sec	1.00	1.00	1.00		1.00	1.00		1.00	1.00	
TD_1diff_sec	1.00		1.00	1.00		1.00	1.00		1.00	1.00
TD_3diff_sec	1.00		1.00	1.00		1.00	1.00		1.00	1.00
PTD_1diff_secB	1.00	1.00	1.00	1.00	1.00	1.00	1.00	1.00	1.00	-5.42
PTD_3diff_secB	1.00	1.00	1.00	1.00	1.00	1.00	1.00	1.00	1.00	-15.83
PTD_1diff_secT	1.00	1.00	1.00	1.00	1.00	1.00	1.00	1.00	1.00	1.00
PTD_3diff_secT	1.00	1.00	1.00	1.00	1.00	1.00	1.00	1.00	1.00	1.00
PTD_1diff_secP	1.00	1.00	1.00	1.00	1.00	1.00	1.00	1.00	1.00	-3.19
PTD_3diff_secP	1.00	1.00	1.00	1.00	1.00	1.00	1.00	1.00	1.00	-7.73
PT_exp	1.00	1.00	1.00		1.00	1.00		1.00	1.00	0.00
TD_exp	1.00		1.00	1.00		1.00	1.00		1.00	1.00
PTD_exp	1.00	1.00	1.00	1.00	1.00	1.00	1.00	1.00	1.00	1.00

Table 3. Normalised maximum error (NME) associated with the comparison of GM and SM for all sets of parameters used for simulations, and discrepancy coefficient η reflecting the difference in evolution of compound concentrations simulated relative to C or Cl isotopologues when performing SM with all sets of parameters. No NME was calculated for *c*DCE Cl isotopic composition associated with TD when no secondary effect occurred since the Cl isotopic composition is then constant and equal to the initial TCE Cl isotopic composition.

	NME						η	
	PCE $\delta^{13}C$	TCE $\delta^{13}C$	*c*DCE $\delta^{13}C$	PCE $\delta^{37}Cl$	TCE $\delta^{37}Cl$	*c*DCE $\delta^{37}Cl$	PCE	TCE
Simulation type	%	%	%	%	%	%		
PT_1no_sec	0.1	0.0		0.1	0.0		1.001	
PT_2no_sec	0.1	0.0		0.1	0.0		0.999	
PT_3no_sec	0.1	0.0		0.0	0.0		0.998	
TD_1no_sec		0.2	0.0		0.2	X		1.001
TD_2no_sec		0.2	0.0		0.2	X		0.999
TD_3no_sec		0.1	0.0		0.0	X		0.998
PTD_1no_sec	0.0	0.4	0.8	0.1	0.0	0.0	1.001	
PTD_2no_sec	0.1	0.3	0.8	0.1	0.0	0.0	0.999	
PTD_3no_sec	0.1	0.0	0.2	0.0	0.0	0.0	0.998	
PT_1normal_sec	0.6	0.2		0.1	0.0		0.980	
PT_3normal_sec	0.3	0.1		0.0	0.0		0.988	
TD_1normal_sec		0.4	0.1		0.3	0.1		0.995
TD_3normal_sec		0.3	0.1		0.1	0.0		0.991
PTD_1normal_sec	0.5	0.2	0.3	0.1	0.0	0.0	0.980	
PTD_3normal_sec	0.3	0.2	0.2	0.0	0.0	0.0	0.988	
PT_1inv_sec	0.1	0.0		0.1	0.0		1.000	
PT_3inv_sec	0.2	0.1		0.0	0.0		1.008	
TD_1inv_sec		0.0	0.1		0.1	0.0		1.008
TD_3inv_sec		0.1	0.0		0.0	0.0		1.005
PTD_1inv_sec	0.0	0.9	1.7	0.0	0.0	0.0	1.000	
PTD_3inv_sec	0.2	0.4	0.7	0.0	0.0	0.0	1.008	
PT_1diff_sec	0.5	0.2		0.0	0.1		0.983	
PT_3diff_sec	0.2	0.1		0.1	0.1		0.991	
TD_1diff_sec		0.2	0.1		0.9	0.3		0.997
TD_3diff_sec		0.2	0.1		0.6	0.3		0.995
PTD_1diff_secB	0.4	0.4	1.3	0.0	0.0	56.7	0.983	
PTD_3diff_secB	0.2	0.1	0.1	0.1	0.1	93.8	0.991	
PTD_1diff_secT	0.5	0.4	1.3	0.0	0.0	0.1	0.979	
PTD_3diff_secT	0.3	0.2	0.1	0.0	0.1	0.1	0.988	
PTD_1diff_secP	0.4	0.4	1.3	0.0	0.0	46.9	0.983	
PTD_3diff_secP	0.2	0.2	0.1	0.1	0.0	69.8	0.991	
PT_exp	0.1	0.1		0.0	0.0		0.995	
TD_exp		0.6	0.2		0.34	0.07		0.989
PTD_exp	0.0	0.2	0.2	0.0	0.0	0.1	0.998	

2.6.4. Models responses

Graphs representing the chlorinated ethenes concentrations, C and Cl evolution in function of time as well as dual C-Cl isotope plots obtained for a selection of the 31 simulation sets are given in Table 4. All simulations responded as expected for the different isotopic effects sets (Figure 5, Table 4). For example, for one element, no enrichment was observed when all enrichments associated with this element were set to 0 ‰. When secondary effects were set to 0 for Cl, the initial Cl isotopic composition of TCE equalled that of PCE for PT (e.g. PT_no_sec, Table 4). On the contrary, when a normal secondary isotopic effect (i.e. ε_{ClSec} < 0 ‰) was set for Cl, the initial Cl isotopic composition of TCE was lighter than that of PCE for PT (e.g. PT_normal_sec, Table 4).

Table 4. Plots representing the evolution of C and Cl isotopic compositions with time for each type of simulated isotopic effect as well as corresponding C-Cl isotope slopes. PCE, TCE and *c*DCE are represented in blue, green and red, respectively. Plots are given for simulation with GM.

simulation type	$\delta^{13}C$	$\delta^{37}Cl$	dual C-Cl isotope slopes
PT_1no_sec	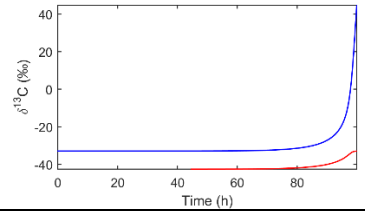	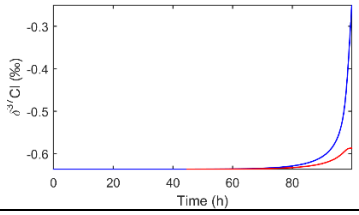	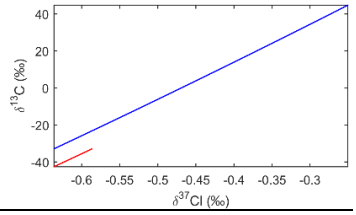
TD_1no_sec	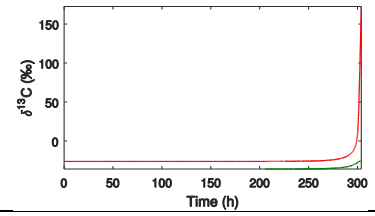	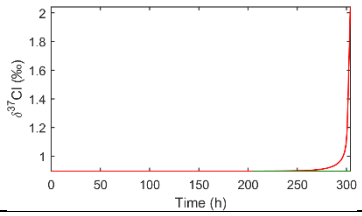	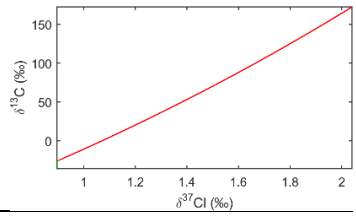
PTD_1no_sec	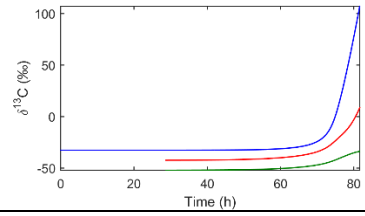	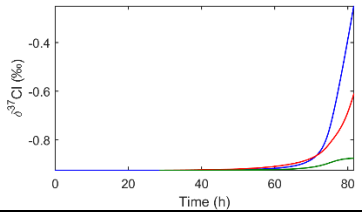	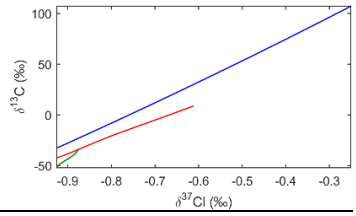
PT_1normal_sec	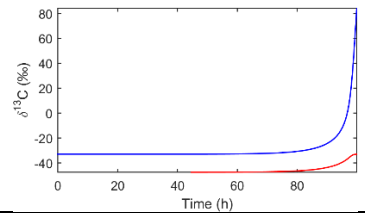	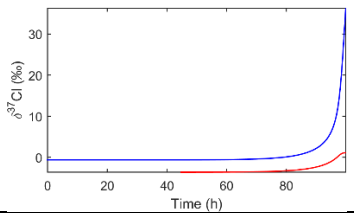	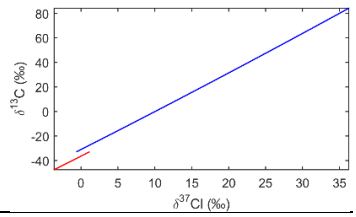
TD_1normal_sec	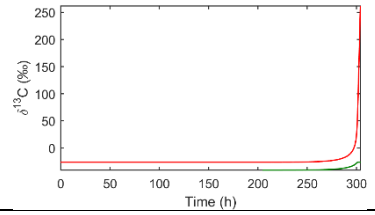	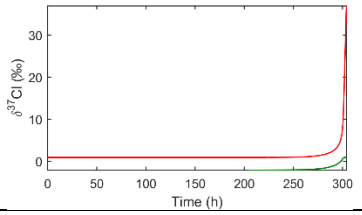	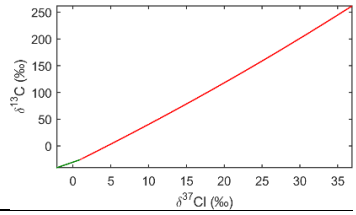

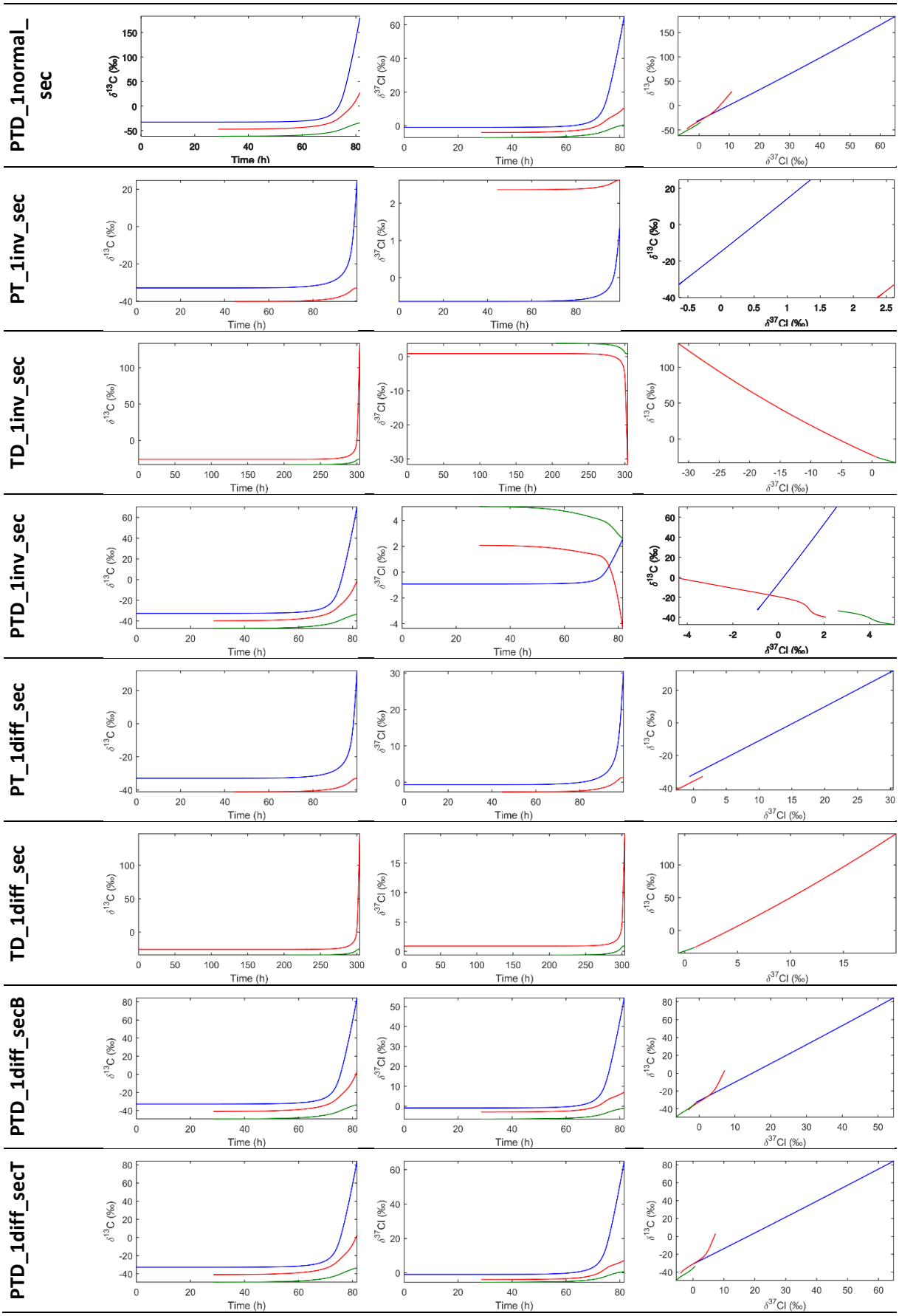
PTD_1normal_sec
PT_1inv_sec
TD_1inv_sec
PTD_1inv_sec
PT_1diff_sec
TD_1diff_sec
PTD_1diff_secB
PTD_1diff_secT
Time (h)
δ13C (‰)
δ37Cl (‰)

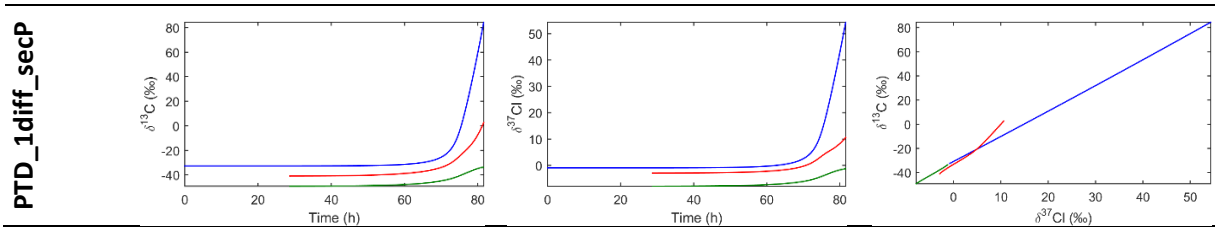

3. Experimental data simulation by model SM

3.1. Method

We showed when evaluating and comparing GM and SM that both models almost identically simulate chlorinated ethenes concentrations and the evolution of their relative C and Cl isotopic compositions along reductive dechlorination of PCE to *c*DCE within an experimentally plausible frame. More particularly, the goodness of fit between SM and GM is confirmed by NME < 1% and the applicability of SM is supported by η > 0.989 for the sets of parameters used to fit the experimental data. Simulations performed to assess to what extent the developed model can truly reproduce experimental data were hence carried out with SM. Results from chapter 2 and chapter 3 were simulated. Simulations were fit on one replicate of each set of experiments, i.e. for one replicate of reductive dechlorination of PCE to TCE (PT), PCE to *c*DCE (PTD), and TCE to *c*DCE (TD), respectively. Experimentally observed lag phases t_{lag} of 45 h, 29 h and 205 h for PT, PTD, and TD, respectively, were taken into account when simulating the experimental data. Simulations were performed for periods corresponding to the experimentally observed degradation time.

The kinetic parameters (μ_{MAX}, K_m) and t_{lag} were optimized first, followed by optimization of isotopic parameters (ε). The resulting kinetic parameters are in the same range as previously reported values *(Maymo-Gatell et al., 1997, Yu & Semprini, 2004)*. Isotopic parameters were optimized based on a range varying around experimentally determined C enrichment factor and Cl primary and secondary isotopic effects. The goodness of fit between simulated and experimental data was evaluated by NSE.

3.2. Results

Chlorinated ethenes concentration and isotopic composition plots of both simulated and experimental data are shown in Figure 5. Values of optimized model parameters as well as NSEs are also given in Figure 5. Concentrations simulated with Monod kinetics fit experimentally measured concentrations very faithfully (NSEs from 0.66 to 1.00). Isotopic compositions are also generally well simulated with NSEs > 0.91 in 67% of cases. More particularly, the unusual inverse secondary Cl isotopic effect observed for PT and PTD when assuming a one-step scenario could be simulated. This indicates that the simulated data generally show a very good fit with experimental data, which is visually confirmed by the plots (Figure 5). One clear outlier is the C isotopic composition of TCE associated with PT where a NSE of -0.14 was determined. Visually, a less good fit between simulated and experimental data is also observed in this case. This agrees with the large variety of observed dual C-Cl isotope slopes associated with TCE from PT between the experimental replicates which resulted in the impossibility to determine a unique dual C-Cl isotope slope associated with TCE from PT by combining data from all replicates (Figure A 6, Appendices).

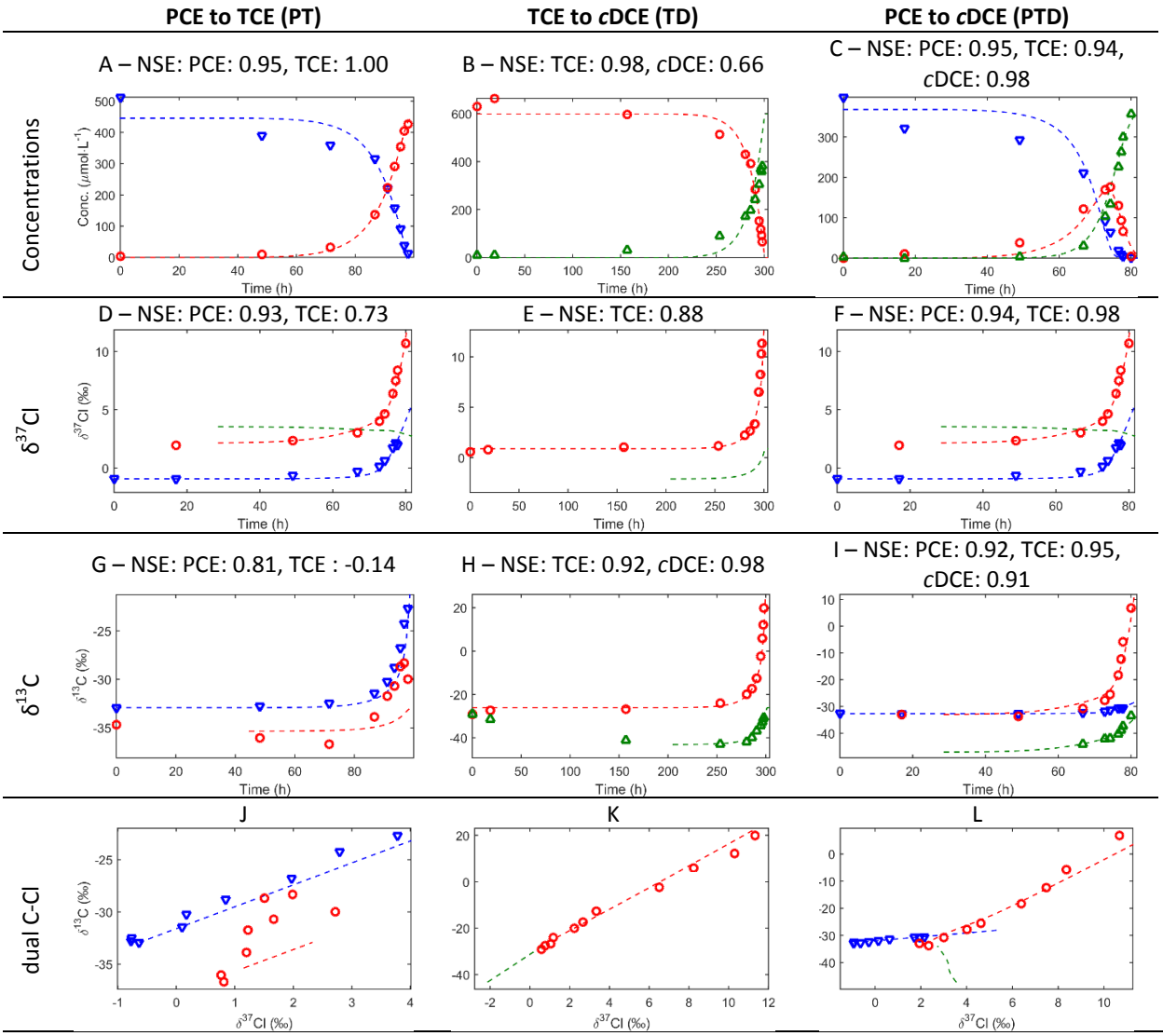

	PCE	TCE	PCE	TCE
μ_{MAX}	$3.36 \cdot 10^{-5}$	$1.88 \cdot 10^{-5}$	$3.83 \cdot 10^{-5}$	$2.3 \cdot 10^{-5}$
Y	0.9	0.9	0.9	0.9
K_m	22.0	10	58.8	70
t_{lag}	44.7	205.2	28.6	
eCp	-5.0	-20.0	-0.7	-29.1
eCs	0.0	-15.0	0.0	0.0
eClp	-10.0	-5.3	-11.1	-12.8
eCls	1.8	-3.0	3.1	1.4
ε_C	-2.5 (exp. : -3.6[a])	-17.6 (exp.: -18.9)	-0.4 (exp.: -0.7[a])	
ε_{Cl}	-1.2 (exp.: -1.2[a])	-3.8 (exp.: -4.3)	-0.5 (exp.: -0.9[a])	

Figure 5. Simulation results, experimental results (one replicate per experiment), and corresponding optimized parameters. NSE: Nash Sutcliff Coefficient. Blue, green and red lines correspond to simulated PCE, TCE, and cDCE, respectively. Red circles, blue triangles and green triangles correspond to experimental PCE, TCE and cDCE. µMAX is given in µmol·g of protein-1·s-1; Y is given in g of protein·(µmol of released chloride)-1; Km is given in µmol·L-1; isotopic effects e are given in ‰; tlag is given in h; P, T, D stand for PCE, TCE and cDCE; p and s stand for primary and secondary. εC and εCl are the overall C and Cl enrichment factors in ‰ determined by application of Rayleigh to the simulated data. Corresponding εC and εCl experimentally determined are given in brackets. a: Badin *et al.*, 2014 or Chapter 2.

4. Implications for environmental studies

C and Cl isotope behaviors of PCE, TCE and *c*DCE during sequential reductive dechlorination taking into account secondary isotope effects and Monod type kinetics was successfully simulated both when C and Cl isotopes were considered both simultaneously (GM) and separately (SM). Except for a specific case, NSEs > 0.995 and NMEs < 2 % were obtained when comparing GM and SM simulated data. This indicates that both models almost identically simulate chlorinated ethenes reductive dechlorination for a large set of isotopic effects combinations. The only exception applies for *c*DCE Cl isotopic composition when different Cl secondary isotopic effects are considered for PCE to TCE dechlorination step during PCE to *c*DCE degradation. Here only GM is able to represent reliable results. However such case was not yet experimentally documented. While GM represents the most accurate way to simulate the evolution of isotopic composition over time during degradation, the less complex and computationally demanding model SM may hence be applied for a majority of cases. Simulation of experimental data was performed with the simplified model SM for PCE dechlorination to TCE (PT) and *c*DCE (PTD) as well as for TCE dechlorination to *c*DCE (TD). All models faithfully reproduced the experimental data with NSE > 0.66 except for TCE C isotopic composition where NSE = -0.14, reflecting the inconsistency between experimental replicates. Such good fitting results are promising for further incorporation of isotope data in reactive transport models simulating processes occurring at the field scale, for example.

Finally, as highlighted by Meckenstock *et al*., 2015, there is a need for understanding processes affecting contaminant degradation at various scales (from conceptual model of aquifers to mass transfer through cell membranes and biochemical enzymatic reaction) in order to increase the accuracy of plume fate prediction where biodegradation occurs. These results offer the possibility to integrate information on processes occurring at the organism scale in models addressing contaminant degradation at the aquifer scale.

Acknowledgements: This research was completed within the framework of the Marie Curie Initial Training Network ADVOCATE - Advancing sustainable in situ remediation for contaminated land and groundwater, funded by the European Commission, Marie Curie Actions Project No. 265063. Christof Holliger (EPFL) is acknowledged for providing the bacterial consortia and Géraldine Buttet (EPFL) is thanked for her help with setting up microcosms.

Chapter 5

Plume characterisation after tetrachloroethene source remediation by in situ thermal treatment by means of isotopic and molecular biology tools

Alice Badin, Mette M. Broholm, Carsten S. Jacobsen, Jordi Palau, Philip Dennis, Daniel Hunkeler

To be submitted to the *Journal of Contaminant Hydrology*

Abstract: The efficiency of a tetrachloroethene (PCE) source thermal remediation by steam injection on a chlorinated ethenes plume in a sandy aquifer was investigated by means of carbon and chlorine isotopic analysis, *Dehalococcoides* sp. (*Dhc*) DNA and rRNA analysis, vinyl chloride (VC) reductive dehalogenase (*rdhA*) presence (DNA) and activity (mRNA), 454 16S rRNA gene targeted pyrotag sequencing, as well as the characterisation of redox and chlorinated ethenes concentrations. Data collected prior to the remediation event and eight years later were compared in order to evaluate the fate of chlorinated ethenes along the 2 km long plume displaying primarily *cis*-dichloroethene (*c*DCE) in the plume core and front.

A release in Non-Volatile Organic Carbon (NVOC) attributed to heating in the source zone was observed which likely enhanced microbial activity, thus leading to more reduced conditions allowing for PCE and trichloroethene (TCE) biotic reductive dechlorination. Based on the assumption that dual C-Cl isotope slopes reflect degradation pathways, the slopes associated with PCE and TCE in the first part of the plume down to 400 m indeed suggested the occurrence of PCE and TCE biotic reductive dechlorination. The shift in chlorinated ethenes molar fractions moreover showed that *c*DCE became the predominant compound after the remediation down to 400 m whereas PCE was predominant before the thermal treatment. The *Dhc* DNA and *Dhc* targeted rRNA analysis as well as the 454 pyrotag sequencing data additionally supported the presence of active microorganisms likely involved in complete dechlorination in this part of the plume, close to the source.

On the other hand, it was suggested based on the C-Cl dual isotope slope approach that *c*DCE was primarily abiotically degraded by pyrite or other reduced iron species in the core to downstream part of the plume (from 1000 to 1500 m downstream from the source). The existence of pyrite oxidation in this part was supported by the pyrotag sequencing data which suggested the presence of microorganisms involved in pyrite oxidation further allowing for abiotic reduction of chlorinated ethenes. In the middle of the plume, a *c*DCE C isotopic composition lighter than the estimated initial one for PCE documented the occurrence of further *c*DCE degradation despite the very low vinyl chloride (VC) concentrations. On the contrary, a *c*DCE C isotopic composition equal to that of the initially released PCE indicated the absence of or only little further *c*DCE degradation at the plume

front (2014). This conclusion was in agreement with the observed plume expansion documented by larger concentration contours in the second campaign compared to the first.

Finally, this study illustrates the valuable complementary application of compound-specific isotopic analysis combined with molecular biology tools to evaluate which biogeochemical processes are taking place in an aquifer contaminated with chlorinated ethenes.

1. Introduction

Management of sites contaminated with chlorinated ethenes is known to be challenging. Among the various developed remediation methods, thermal treatment by steam injection is particularly adapted for source treatment in subsurface sediments of relatively high permeability such as sandy aquifers *(von Schnakenburg, 2013)*. Such remediation strategy is known to release Non-Volatile Organic Carbon (NVOC) *(Friis et al., 2005)* which increase may trigger a chain of microbial-mediated redox processes. When natural attenuation has been observed prior to active source remediation, steam injection might thus influence the naturally occurring degradation.

Natural degradation of chlorinated ethenes might occur biotically due to the presence of adequate active microorganisms in specific redox conditions, as well as abiotically in the presence of reduced iron (Fe) minerals. Sequential biotic reductive dechlorination of the ubiquitous groundwater contaminant tetrachloroethene (PCE) consecutively yields trichloroethene (TCE), *cis*-dichloroethene (*c*DCE), vinyl chloride (VC) and eventually non-toxic ethene. Such process takes place in strictly anaerobic systems *(Wiedemeier et al., 1999, Bradley, 2000)* and is the most commonly encountered naturally occurring biotic degradation of chlorinated ethenes. According to laboratory and field observations, PCE could undergo reductive dechlorination in virtually any anaerobic conditions while TCE, *c*DCE and VC reductive dechlorination would generally occur in more reduced conditions such as iron-reducing for TCE and ideally sulphate-reducing to methanogenic for *c*DCE and VC *(Vogel et al., 1987, Chapelle, 1996, Bradley, 2000, Tiehm & Schmidt, 2011)*. The presence of molecular hydrogen (H_2) which is a key electron donor as well as the competition for it between microorganisms can also be determining *(Ballapragada et al., 1997)*. The occurrence of reductive dechlorination also depends on the presence and activity of specific dechlorinating microorganisms. Members from various bacterial genera such as S*ulfurospirillum*, *Dehalobacter*, *Desulfitobacterium*, *Desulfuromonas* or *Geobacter* have been reported to catalyse some steps of chlorinated ethene reductive dechlorination. However, while some enrichment cultures and consortia are able to dechlorinate down to ethene *(Flynn et al., 2000, Aulenta et al., 2002, Hoelen & Reinhard, 2004)*, to date, the only organisms which have been reported to catalyse complete reductive dechlorination to ethene are some species of the genus *Dehalococcoides* (*Dhc*) *(Löffler, 2013)* and genus *Dehalogenimonas* (*Dhg*) *(Yang et al., 2015)*. Only few microorganisms are able to dechlorinate further than *c*DCE and only when strongly reducing conditions are met. Therefore, the latter is often found to accumulate in the subsurface. Microbial oxidation might also take place, more particularly in the case of *c*DCE and VC *(Hartmans et al., 1985, Bradley & Chapelle, 1998, Bradley & Chapelle, 2000)*. Despite their presence in the subsurface, microorganisms may display a low activity, are sometimes inactive or even dormant *(Meckenstock et al., 2015)* which may additionally affect the achievement of reductive dechlorination. Abiotic reductive dechlorination can also take place naturally, provided that the adequate minerals and geochemical conditions occur. Iron sulphides such as mackinawite ($Fe^{II}S$) or pyrite ($Fe^{II}S_2$), iron oxides such as magnetite ($Fe^{II}O{\cdot}Fe^{III}{}_2O_3$), and iron hydroxides such as green rusts which are corrosion products of iron or steel ($[Fe_{6-x}{}^{II}Fe_x{}^{III}(OH)_{12})]^{X+}[(A)_{x/n}yH_2O]^{X-}$ where A is an anion, typically SO_4^{2-} or Cl^-) have been reported to catalyse abiotic reductive degradation yielding less chlorinated compounds and other non-toxic compounds such acetylene in various proportions *(Tobiszewski & Namieśnik, 2012)*. FeS_2 is known to reduce all chlorinated ethenes *(Lee & Batchelor, 2002)* while FeS was shown to reduce PCE and TCE but was non-reactive with *c*DCE *(Butler & Hayes, 1999, Jeong et al., 2011)*. Surface-bound Fe(II) is also known to catalyse abiotic degradation of reducible contaminants *(Elsner, 2002)*. Furthermore, the activity of various bacteria in the subsurface may change the local redox conditions. This might affect the redox potential of metals contained in

minerals which might in turn affect the likelihood of abiotic degradation to take place *(Tobiszewski & Namieśnik, 2012)*.

Various tools may be employed to explore the occurrence of such processes in the subsurface and thus evaluate the effect of remediation or site management.

In the past decades, compound specific isotopic analysis have been increasingly used to explore chlorinated ethenes degradation processes. It was among others demonstrated that the extent of biodegradation could be determined based on isotopic measurements *(Hunkeler et al., 2010)*. Additionally, it was suggested that dual C-Cl isotopic analysis may help differentiating degradation pathways, for example biotic from abiotic degradation *(Elsner et al., 2005, Abe et al., 2009, Audí-Miró et al., 2013)*. The range of laboratory determined dual C-Cl isotope slopes associated with various chlorinated ethenes degradation processes has increased in recent years thus enriching the database to which dual C-Cl isotope slopes measured in the field can be compared for process identification (Figure 1) *(Abe et al., 2009, Audí-Miró et al., 2013, Cretnik et al., 2013, Kuder et al., 2013, Wiegert et al., 2013, Badin et al., 2014, Cretnik et al., 2014, Renpenning et al., 2014* and chapter 3*)*. Moreover, the rapid advances in molecular biology opens new possibilities for the characterisation of microbial communities present in the subsurface (e.g. pyrotag sequencing) and the assessment of their activity based on mRNA analysis. Bacterial 16S rRNA gene pools characterization via amplicon pyrosequencing can be used to identify the present bacterial communities in high detail *(Novais & Thorstenson, 2011)*. It was among others demonstrated that pyrotag sequencing is a robust and reproducible method, adapted for a reliable microbial community exploration in natural systems *(Pilloni et al., 2012)*. Additionally, as *c*DCE and VC degradation usually represents the bottle neck of chlorinated ethenes natural attenuation, it is essential to screen for markers of their degradation. *Dhc* screening has been carried out in numerous studies since it is the only microorganisms reported to perform *c*DCE and VC dechlorination. Moreover the presence of genes encoding for VC reductive dehalogenases (*rdhA*) known to catalyse VC reduction to ethene as well as measuring their mRNA level constitutes a stronger line of evidence supporting complete reductive dechlorination. The *vcrA* and *bvcA* genes identified in *Dhc* are so far the only two functional genes described to encode VC *rdhA (Krajmalnik-Brown et al., 2004, Müller et al., 2004)*. Their presence in field samples from sites contaminated with chlorinated ethenes was successfully related to complete dechlorination *(Scheutz et al., 2008, van der Zaan et al., 2010, Damgaard et al., 2013)*. It was moreover shown based on field samples that *rdhA* genes directly involved in dechlorination should be targeted in addition to *Dhc* as different microbial species might harbour *vcrA* and *bvcA* genes due to horizontal gene transfer and are therefore also able to dechlorinate VC down to ethene *(van der Zaan et al., 2010)*. Targeting mRNA constitutes an essential additional analysis as it will additionally inform on the activity of the corresponding degrader *(Bælum et al., 2013)*.

We here apply such innovative methods to assess the impact of source remediation by steam injection on a chlorinated ethenes plume occurring in a complex biogeochemical system where iron minerals are present. More specifically, the aim was to evaluate if a plume detachment occurred due to steam injection as reported by a previous study *(Sleep & Ma, 1997)*, and if in addition natural degradation was stimulated by the thermal treatment.

A major advantage of this field site resides in the fact that the plume was formerly well characterised and studied *(Hunkeler et al., 2011)* which allows for comparison between before and after (7-8 years later) source remediation. An extensive campaign was carried out to evaluate the impact of steam injection where redox parameters, chlorinated ethenes concentrations and isotopic compositions thereof, 454 pyrotag sequencing, *Dhc* DNA and rRNA as well as *bvcA* and *vcrA* functional genes and

gene transcripts (mRNA) were analysed in samples taken from 20 wells at different screening depths along the plume flow line.

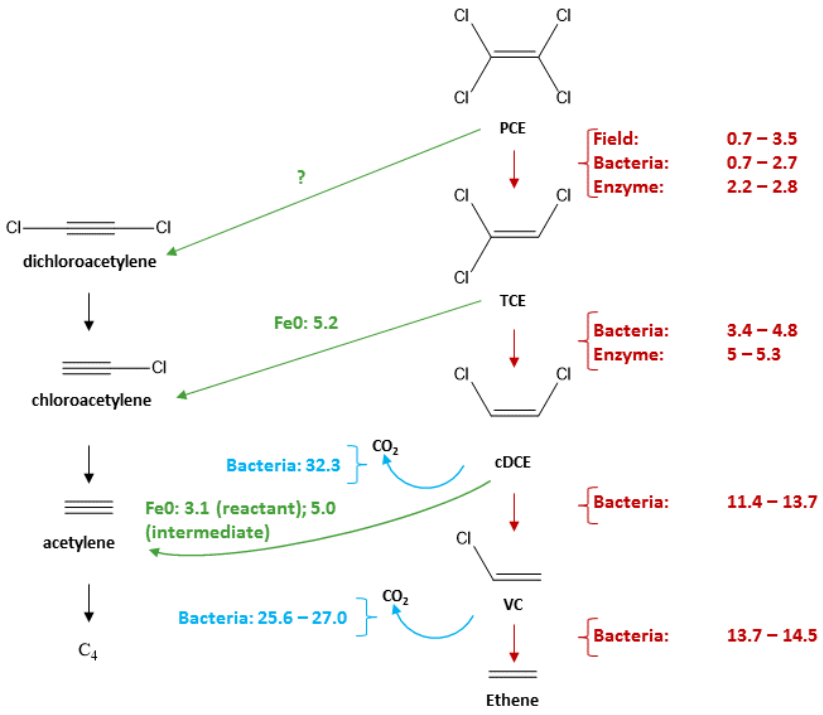

Figure 1. Literature values for dual C-Cl isotope slopes associated with various degradation pathways of chlorinated ethenes *(Abe et al., 2009, Audí-Miró et al., 2013, Cretnik et al., 2013, Kuder et al., 2013, Badin et al., 2014, Cretnik et al., 2014, Renpenning et al., 2014)*. Slopes are given for each of the substrates. Green arrows represent dihaloelimination, i.e. the main pathway for abiotic reduction typically occurring in presence of zero-valent Fe. Blue arrows represent aerobic oxidation of chlorinated ethenes. Red arrows correspond to hydrogenolysis occurring during reductive dechlorination mediated by bacteria via their specific corrinoid-containing reductive dehalogenase enzymes. Dual C-Cl isotope slopes associated with hydrogenolysis by these dehalogenases and corrinoids as well as by chemical models mimicking corrinoids (cobalamin, cobaloxime) were also recently reported *(Renpenning et al., 2014)*. However, due to the lack of correlations between these slopes and slopes associated with bacterial mediated dechlorination, these values are not reported here.

2. Materials and methods

2.1. Study site

The studied site previously described by Hunkeler *et al.*, 2011, is located in southern Jutland, Denmark, in the town of Rødekro. Briefly, the original PCE groundwater contamination comes from a dry-cleaning facility which operated between 1964 and 2001. A sandy aquifer > 50 m thick occasionally containing less permeable silt and clay lenses was characterized based on former site characterization campaigns. A chlorinated ethenes plume of ~2 km length following the groundwater flow (Figure 2), extending southwards from the site and turning towards southeast after 1 km was identified based on a massive monitoring well cover (55 multilevels). The difference in equipotential lines between 2006 and 2014 indicates that the gradient is less steep in 2014 than in 2006 (Figure 2). Low amounts of organic matter as well as high levels of iron are expected in this part of Jutland aquifers *(Postma, 1991)*. An average groundwater velocity of 0.24 m/day was previously estimated

(Hunkeler et al., 2011), however the latter might change depending on the location in the aquifer due to heterogeneities such as the claylense in the middle of the aquifer.

Thermal remediation by steam injection was applied to the source zone between October and December 2006. The entire plume was sampled in 2006 before remediation and some points much further out in the plume which were therefore not yet impacted by remediation were sampled in 2007. The data previously discussed by Hunkeler *et al.*, 2011, consist of data collected during these two sampling campaigns and are referred to as data from 2006, for simplification purposes. The main conclusions drawn from the previous campaign are that (i) PCE and TCE were likely being biotically degraded by reductive dechlorination in the first 400 m downstream of the source, (ii) *c*DCE was not affected by degradation (neither biotic nor abiotic) in the first 1050 m downgradient from the source but it was being degraded between 1050 and 1900 m downgradient, likely at least partially by biotic reductive dechlorination, and (iii) VC was being transformed further by undetermined process(es). The process responsible for *c*DCE degradation remained uncertain due to the lack in dual C-Cl studies associated with abiotic reductive dechlorination of *c*DCE to which the dual C-Cl slope observed in Rødekro could be compared.

Redox species concentrations and chlorinated ethenes concentrations were regularly measured between 2004 and 2014 as part of the monitoring process. The evolution of redox species between 2004 and 2014 is given in Figure 4 for sampling points from the centreline located close to the source (B16-1; 100 m), in the middle of the plume (B34-4; 1050 m) and at the front of the plume (B61-2; 1700 m).

Based on the assessed average groundwater velocity, it can be estimated that species might have been transported about 600 m downstream between the end of 2006 and the new campaign carried out in 2014. Such estimation should however be treated cautiously as heterogeneities might change the hydraulic conductivity of a few orders of magnitude in areas where different subsurface material such as gravel/coarse sand or silt/clay lenses is present. Furthermore, the progressive disappearance of the claylense with increasing distance and depth from the source leads to the diving of the plume deeper into the aquifer due to the resulting flow direction divergence.

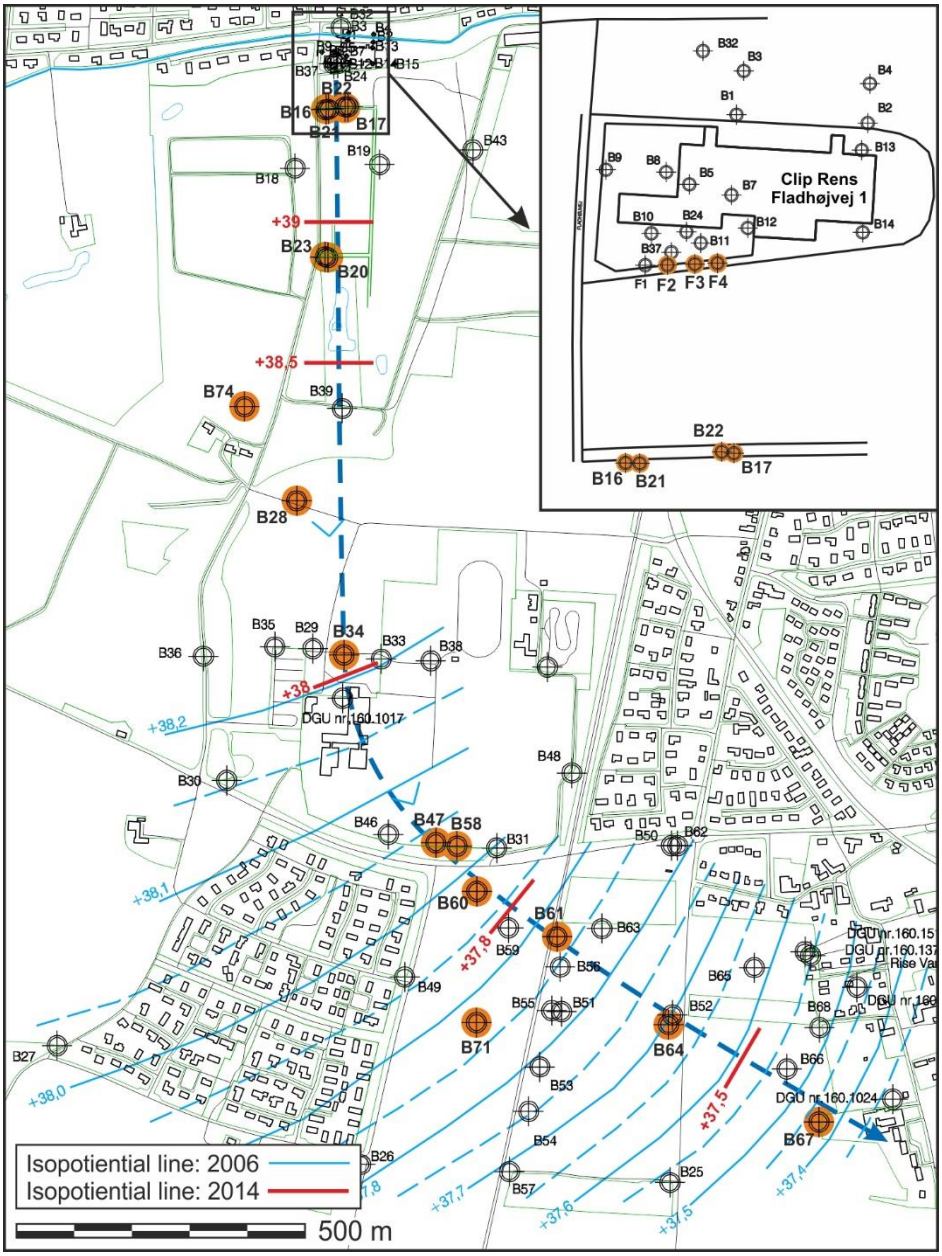

Figure 2. Groundwater equipotential lines from 2006 (blue) and 2014 (red), approximate plume flow line (blue dashed arrow) and monitoring wells (grey and orange targets). Wells sampled in 2014 appear in orange.

2.2. Groundwater sampling

Groundwater in about thirty screens from twenty different locations was sampled in May 2014 after purging 3 times the volume of wells and checking the stability of pH, temperature, oxygen (O_2) and conductivity. Samples for nitrate (NO_3^-) and sulphate (SO_4^{2-}) analysis were collected in hard plastic bottles; samples for non-volatile organic carbon (NVOC) were collected in glass bottles and spiked with H_3PO_4 upon arrival in the laboratory; samples for dissolved Fe were sampled in plastic bottles after filtration (sterile filter, 0.45 µm) and spiked with HNO_3 upon arrival in the laboratory; samples for chlorinated ethenes concentrations were collected in 40 mL glass vials closed without headspace with a Teflon-coated cap and analysed upon arrival in the laboratory. Samples for chlorinated ethenes isotope analysis were collected in 40 mL glass vials or 1 L Schott bottles (for isotope analysis

with low chlorinated ethenes concentrations) closed without headspace with a cap containing a Teflon-coated septum. HNO_3 was added previously to the containers in order to reach pH 2 when filled with the sample and to stop any microbial activity. Samples for methane, acetylene, ethene and ethane were collected in 6 mL Exetainer® glass vials (LabCo, UK) with 3 mL headspace which were previously evacuated and filled with 100 µL concentrated H_2SO_4. Caution was taken so that no air bubbles were injected together with groundwater samples. All aqueous samples were stored in ice boxes topped with ice packs until arrival at the laboratory where they were stored at 4 °C until analysis. Samples for 454 pyrotag next generation sequencing analysis were collected on Sterivex™ Filters (EMD Millapore, Billerica, MA, USA) after passing 300 to 400 mL of groundwater and shipped to Guelph (SIREM, commercial laboratory, Canada) with ice packs. Samples for *Dhc* DNA and rRNA, *bvcA* and *vcrA* functional genes (DNA) and genes transcripts (mRNA) analysis were collected as described previously in Baelum *et al.*, 2013, snap-shot frozen in liquid N_2, and kept at -80°C until analysis Copenhagen (GEUS, Denmark).

2.3. Analyses

Chemical analysis: NO_3^-, dissolved Fe, SO_4^{2-} and NVOC were measured by accredited methods by the accredited (DANAK, ISO 17025) laboratory ALS (ALS Denmark A/S, alsglobal.dk, alsglobal.com) in Denmark with quantification limits of 0.03 $mg \cdot L^{-1}$, 0.01 $mg \cdot L^{-1}$, 0.5 $mg \cdot L^{-1}$ and 0.1 $mg \cdot L^{-1}$ respectively. Chlorinated ethenes concentrations were analysed in ALS by Purge & Trap GC-MS with a detection limit of 0.02 $\mu g \cdot L^{-1}$ and standard deviations of 10%. Ethene, methane, ethane and acetylene were determined at the Technical University of Denmark (DTU, Kgs. Lyngby, Denmark) by headspace GC-FID with detection limits of 0.43 $\mu g \cdot L^{-1}$, 0.94 $\mu g \cdot L^{-1}$, 0.47 $\mu g \cdot L^{-1}$ and 0.38 $\mu g \cdot L^{-1}$, respectively.
A summary of the analytical methods for isotopic measurements is given in the Appendices (Appendix 1).
Isotopic analysis: C isotopic analysis were performed at the University of Neuchâtel (CHYN, Switzerland) by the system previously described for samples containing chlorinated ethenes concentrations exceeding 5 $\mu g \cdot L^{-1}$ *(Badin et al., 2014* or Chapter 2*)* except for the use of a QS-PLOT column instead of a DB-VRX to improve VC separation. Briefly, the compounds degassed by N_2 purging were retained on a Vocarb 3000 trap (VICI), transferred to a cryogenic trap (Tekmar Dohrmann) at -120 °C enabling compound concentration, and sent to the gas chromatograph (GC) column (QS-PLOT, 30 m, 0.32 mm, 10 µm) of an Agilent™ 7890a GC allowing for compound separation (35 °C for 6 min, ramp of 15 $°C \cdot min^{-1}$ until 130 °C kept for 0.1 min followed by a ramp of 20 $°C \cdot min^{-1}$ until 240 °C kept for 5 min). After combustion via an Isoprime GC5 combustion interface, the resulting CO_2 gas was sent to an Isoprime™ 100 isotope ratio mass spectrometer (IRMS) allowing for C isotope ratio measurement. Samples were measured in duplicate. Standard deviations σ of the in-house reference materials measured in the same sequences as samples from the field site were 0.6 ‰ (n=32), 0.3 ‰ (n=24), 0.5 ‰ (n=24), 1.0 ‰ (n=26) for PCE, TCE, *c*DCE, and VC, respectively. The standard uncertainty of duplicate measurements was determined according to ISO guidelines *(BIPM, 1993)* as $\sigma/\sqrt{2}$, i.e. 0.4 ‰, 0.2 ‰, 0.3 ‰, 0.7 ‰ for PCE, TCE, *c*DCE, and VC, respectively. Samples containing reference compounds with known isotope ratios (EA-IRMS measurement) were included in each sequence to verify the method accuracy except for VC which was not characterised by EA.
For the samples showing chlorinated ethenes concentrations below 5 $\mu g \cdot L^{-1}$, 1 L bottles were manually connected to a purge system consisting of a frit from a gas-washing bottle as described

formerly *(Hunkeler et al., 2012)* instead of passing 40 mL glass vials by autosampler. The bottles were purged for 30 min at a rate of 150 mL·min^{-1} which led to a removal of 90, 75, 50 and 100 % of the dissolved PCE, TCE, *c*DCE and VC, respectively, considering Henry coefficients at 20 °C of 0.533, 0.314, 0.14, 0.891 (gas/water) for PCE, TCE, *c*DCE and VC, respectively.

Cl isotopic analysis of PCE and TCE was performed as previously described with an Agilent 7890 GC coupled to an Agilent 5975C quadrupole mass selective detector (Santa Clara, CA, USA) *(Badin et al., 2014)*. Molecular ions were targeted and calculations were carried out according to the method developed by Aeppli *et al*., 2010. Calibration with two external standards ($\delta^{37}Cl_{EIL1}$ = +0.3 ‰ and $\delta^{37}Cl_{EIL2}$ = -2.5 ‰ for PCE and $\delta^{37}Cl_{EIL1}$ = +3.05 ‰ and $\delta^{37}Cl_{EIL2}$ = -2.70 ‰ for TCE) which were formerly characterized by the Holt method *(Holt et al., 1997)* at the University of Waterloo was completed for each sequence to obtain δ values on the SMOC scale. Cl isotopic analysis of *c*DCE was performed at the University of Waterloo according to the method developed by Shouakar-Stash *et al*., 2006 using a continuous flow (CF) IRMS.

Molecular biology analysis: DNA extraction for the 454 pyrotag analysis was carried out at SiREM (Guelph, ON, Canada) as follows: Sterivex™ filters were opened and the filter membrane with attached biomass was removed and placed into the Bead Solution of a PowerMag DNA Isolation Kit (MoBio, Carlsbad, CA, USA) and pulverized using a sterile pipet tip. Cell lyses were performed using a MiniBeadbeater-8 (Biospec Products Bartlesville, OK, USA) at 50% of the maximum setting for 30 s. DNA was purified using a KingFisher™Duo (ThermoFisher Waltham, MA, USA) and was eluted in 150 µL. DNA was quantified using a NanoDrop spectrophotometer (NanoDrop Inc. Wilmington, DE) and stored at -80 °C after extraction. 16S rRNA genes were amplified from DNA extracts with universal primers 926f (5'-AAA CTY AAA KGA ATT GAC GG-3') and 1392r (5'-ACG GGC GGT GTG TRC-3') for 454 pyrotag analysis. The reverse primer also contained a 10 nucleotide barcode and 454 FLX Titanium Lib-L 'B' adapter. PCR was performed under the following conditions: 94 °C for 3 min; 25 cycles of 94 °C for 30 s, 52 °C for 30 s, and 72 °C for 1 min; and finally 72 °C for 10 min. Amplicons were purified with GeneJET PCR Purification Kit (Life Technologies, Burlington, ON, Canada) and sequenced with Roche GS-FLX Titanium series kits and system (Roche, Branford, CT, USA) at Genome Quebec and McGill University Innovation Centre (Montreal, PQ, Canada). Finally, analysis of the reads was performed using QIIME v.1.8 *(Caporaso, 2010)*. Initially, raw reads were demultiplexed and filtered by quality (>Q20) and length (> 250 nt) using the pick_otus.py script with usearch61 *(Edgar et al., 2011)* option and representative sequences were selected using the pick_rep_set.py. The sequences were aligned to the core Greengenes Core reference alignment by PyNAST *(Caporaso, 2010)*. Putative chimeric sequences were removed using ChimeraSlayer *(Haas et al., 2011)*. Taxonomic assignment of the operational taxonomic units (OTU) was performed by assign_taxonomy.py script with the Ribosomal Database Project (RDP) method *(Wang et al., 2007, Martins et al., 2013)*. The similarity level based on which sequences were defined as belonging to a particular OTU was of 97 %.

In order to evaluate which microorganisms relevant to redox processes potentially occurring in the subsurface were present and to which extent, OTU reads per sample were transformed to cells·L^{-1} based on the total bacteria count (i.e. total DNA extracted from the samples). It was assumed that all the extracted DNA was prokaryotic, which leads to a slight overestimation, and that the average microbial genome contains 4·10^{-6} ng DNA·cell^{-1} *(Paul, 1996)*. Since chlorinated ethenes degradation as well as redox processes occurring in the subsurface were of interest, detected microorganisms were grouped in taxonomic categories such as genera of which some strains are known to perform complete reductive dechlorination, partial reductive dechlorination of PCE and/or TCE, oxidation of *c*DCE and or VC under aerobic conditions; bacteria reported to be found in iron- and sulphate-

reducing conditions as well as during pyrite oxidation. Bacteria counts were then summed in each group and divided by the sum of bacteria counts of all targeted groups in each sample to evaluate the proportion of each bacteria group within each sample, relative to the groups of interest. These data are summarised in Table A 14 and Table A 15.

Dhc DNA and rRNA, bvcA and vcrA functional genes (DNA) and genes transcripts (mRNA) analysis was performed at GEUS, Denmark, and carried out as described in Baelum *et al.*, 2013, with a detection limit of 10'000 copies·L^{-1}. The ratio between the measured amount of rRNA and DNA was used as a marker of the specific degrader's activity.

2.4. Calculations for isotopic data interpretation

2.4.1. C isotope balance

In order to evaluate isotopic data and more particularly to determine whether degradation released a significant amount of compounds which were not detected such as ethene during complete sequential reductive dechlorination, the C isotope balance was determined for each sampling point according to:

$$\delta^{13}C_{sum} = \frac{[\text{PCE}] \cdot \delta^{13}C_{\text{PCE}} + [\text{TCE}] \cdot \delta^{13}C_{\text{TCE}} + [\text{cDCE}] \cdot \delta^{13}C_{\text{cDCE}} + [\text{VC}] \cdot \delta^{13}C_{\text{VC}}}{[\text{PCE}] + [\text{TCE}] + [\text{cDCE}] + [\text{VC}]} \quad (1)$$

where [PCE], [TCE], [*c*DCE] and [VC] are the molar concentrations of PCE, TCE, *c*DCE and VC, respectively, and $\delta^{13}C_{\text{PCE}}$, $\delta^{13}C_{\text{TCE}}$, $\delta^{13}C_{c\text{DCE}}$, and $\delta^{13}C_{\text{VC}}$ their corresponding C isotopic composition. The uncertainty was determined by error propagation as described by Reddy *et al*., 2002.

2.4.2. Extent of degradation

In order to estimate the extent of degradation in certain parts of the plume, the following coefficient was calculated:

$$D = 1 - \exp\left(\frac{\Delta\delta^{13}C}{\varepsilon}\right) \quad (2)$$

where $\Delta\delta^{13}C$ corresponds to the difference between the initial and final C isotopic composition of the considered chlorinated ethene. Such calculation was performed only for compounds in sampling points where no precursor was present (e.g. for *c*DCE when no PCE or TCE was detected) to ensure that the isotopic composition was merely affected by the compound degradation and not by its production. In the case of PCE, such caution is unnecessary as it can only be degraded. Minimum and maximum enrichment factors reported in the literature were used as summarised in Table A16.

3. Results and discussion

In this section, results from chemical, isotopic and molecular biology analysis are given and discussed in view of understanding the effect of thermal remediation on the chlorinated ethenes plume.

3.1. Redox conditions

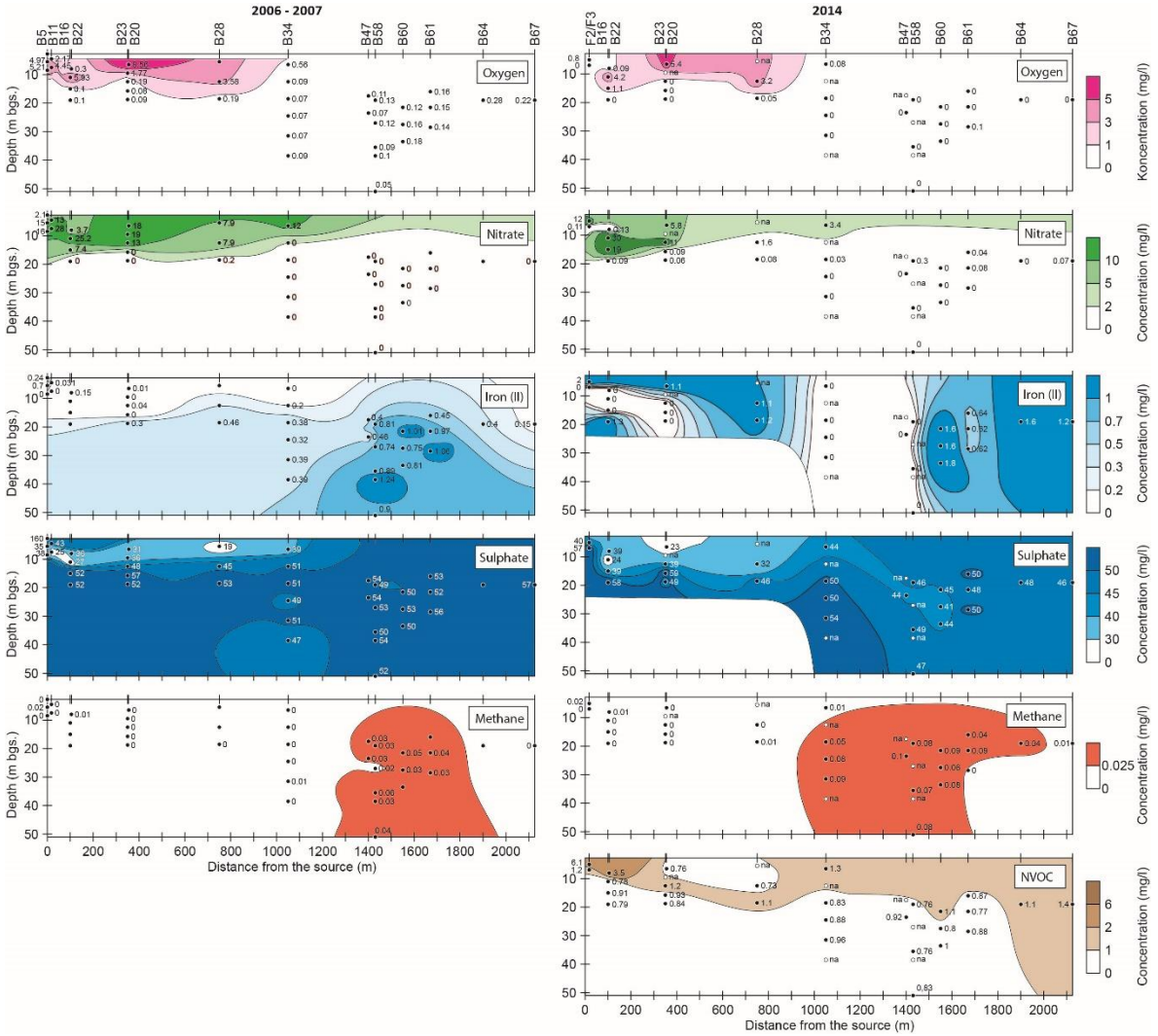

Figure 3. Redox sensitive species concentrations in 2006 *(Hunkeler et al., 2011)* and 2014 (this study)

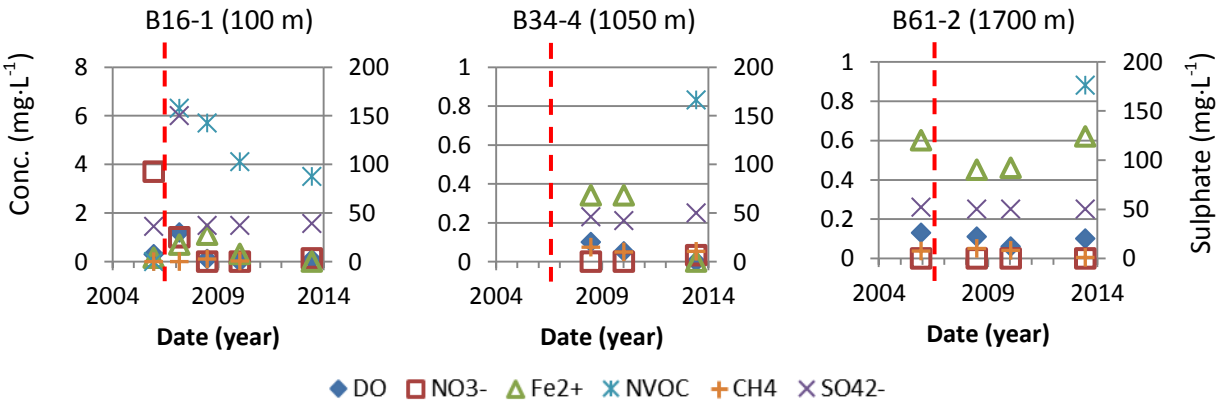

Figure 4. Evolution of redox species concentrations between 2004 and 2014 along the plume centre line at 100 m (well B16-1), 1050 m (B34-4), and 1700 m (B61-2) downgradient from the source. NVOC concentrations were measured from the time of source remediation in B16-1 and only in 2014 in B34-4 and B61-2. The red dashed line corresponds to the source remediation event. Note that the left graph has a different left y-axis than the other two graphs.

Concentrations of redox sensitive species measured in 2006 *(Hunkeler et al., 2011)* and 2014 are shown in Figure 3. In general, O_2 and/or NO_3^- concentrations larger than 1 mg·L^{-1} were detected in the shallow top part of the aquifer (down to 10 - 15 m depth) whereas very low concentrations (< 0.1 mg·L^{-1}) were found in deeper parts. Here, the presence of dissolved Fe and/or methane indicated the occurrence of reducing conditions. Concentrations of SO_4^{2-} ranged from 23 to 59 mg·L^{-1} and were above 40 mg·L^{-1}, i.e. in the higher part of the concentration range, below 15 m depth. Based on the sulfur isotopic composition of SO_4^{2-}, Hunkeler *et al.*, 2011 suggested that the disappearance of O_2 / NO_3^- and the increase of Fe(II) / SO_4^{2-}concentrations with depth could be associated with pyrite oxidation processes, which is supported by the presence of pyrite in sandy aquifers in Jutland *(Postma, 1991)*.

Contrary to 2006, very mixed conditions in terms of redox were generally observed in 2014 where different conditions are found within screens (e.g. O_2 and dissolved Fe in same well). This might be explained by a certain subsurface heterogeneity resulting in various redox zones overlaying each other within screen intervals ranging from 1 to 4 m. Such spatial change in redox conditions may result from the temporal change in redox conditions affecting geologically different layers at different speed. This temporal change was supported by the redox species evolution between 2004 and 2014 as depicted in Figure 4 and was especially apparent in the first 750 m after the source where both Fe(II) and O_2 were present. More particularly, the NO_3^- concentration abruptly dropped 100 m downgradient from the source where Fe(II) concentrations increased right after the remediation event (Figure 4) which may explain the shrunk NO_3^- zone and generally higher Fe(II) concentrations in 2014 compared to 2006 in the first 750 m of the plume (Figure 3). A striking change directly following thermal remediation was the appearance of NVOC in and downgradient of the source area which decreased over time (Figure 3 and B16-1 in Figure 4), presumably due to its transport and consumption. Although this part of Jutland aquifers generally contains very low levels of organic matter, high concentrations of NVOC were measured in the source area after the thermal remediation treatment, reaching values of 6.1 mg·L^{-1} (F3) and 3.1 mg·L^{-1} (B16, located 100 m downstream) in 2014. Such release of sediment-bound organic matter due to thermal treatment was previously reported near treated source areas *(Newmark, 1995, Friis et al., 2005)*. Friis *et al.* confirmed based on experiments performed with field material that up to 8 % of sediment-bound organic carbon could be released for temperature conditions usually achieved with thermal treatments *(Friis et al., 2005)*. Releasing organic matter is expected to affect redox conditions. This was indeed observed immediately downstream of the former source area (wells F2 and F3) where O_2 (< 1 mg·L^{-1}) and NO_3^- (up to 12.1 mg·L^{-1}) concentrations were much lower than those measured in 2006 in nearby wells (B5, in the source and B11, 100 m downstream), where concentrations of up to 5.2 mg·L^{-1} and 28.0 mg·L^{-1} for O_2 and NO_3^- were measured, respectively. The lower values measured in 2014 could be related to O_2 and NO_3^- consumption during oxidation of organic matter. The significant change in Fe(II) and SO_4^{2-} concentrations observed between 2006 and 2014 in the upper part of the aquifer from the source zone to 750 m downgradient could also be attributed to the oxidation of organic matter released from remediation and consequently leading to more reduced conditions as well as temporal lack of pyrite oxidation due to lack of oxygen. Indeed, higher Fe(II) concentrations (> 1 mg·L^{-1}) especially in the shallow part and in B28 as well as slightly lower SO_4^{2-} concentrations were observed in this part, indicating more reduced conditions. Such NVOC impact leading to more reduced conditions is in particularly reflected by B16-1 (Figure 4). High NVOC and SO_4^{2-} concentrations were indeed observed right after remediation in this sampling point where less concentrated NO_3^- and O_2 concentrations were concomitantly observed. The NVOC concentration

then gradually decreased (B16-1 in Figure 4). Another striking change between 2006 and 2014 was the lack of Fe(II) detection in 2014 between 1000 and 1500 m downstream from the source (wells B34, B47 and B58). In these wells, concentrations of methane increased whereas SO_4^{2-} concentrations showed up to 20 % decrease in 5 out of 8 sampling points, suggesting the occurrence of SO_4^{2-} reduction followed by the precipitation of metastable iron sulphide (FeS) or Fe(II) sorption on other minerals *(Elsner, 2002)*. This suggested that the NVOC release affected this part of the aquifer too as the flowline descends where the clay layer observed under the source area disappears. The occurrence of sulphate-reducing conditions in this part of the plume would be additionally favorable for chlorinated ethenes microbial reductive dechlorination, especially of *c*DCE and VC *(Vogel et al., 1987, Chapelle, 1996)*. At the fringe of the plume (i.e. > 1800 m from the source), concentrations of Fe(II) increased in 2014 compared to 2006 (> 1 $mg \cdot L^{-1}$) and methane was detected in B64, indicating stronger reducing conditions in 2014 than in 2006.

3.2. Chlorinated ethenes concentrations

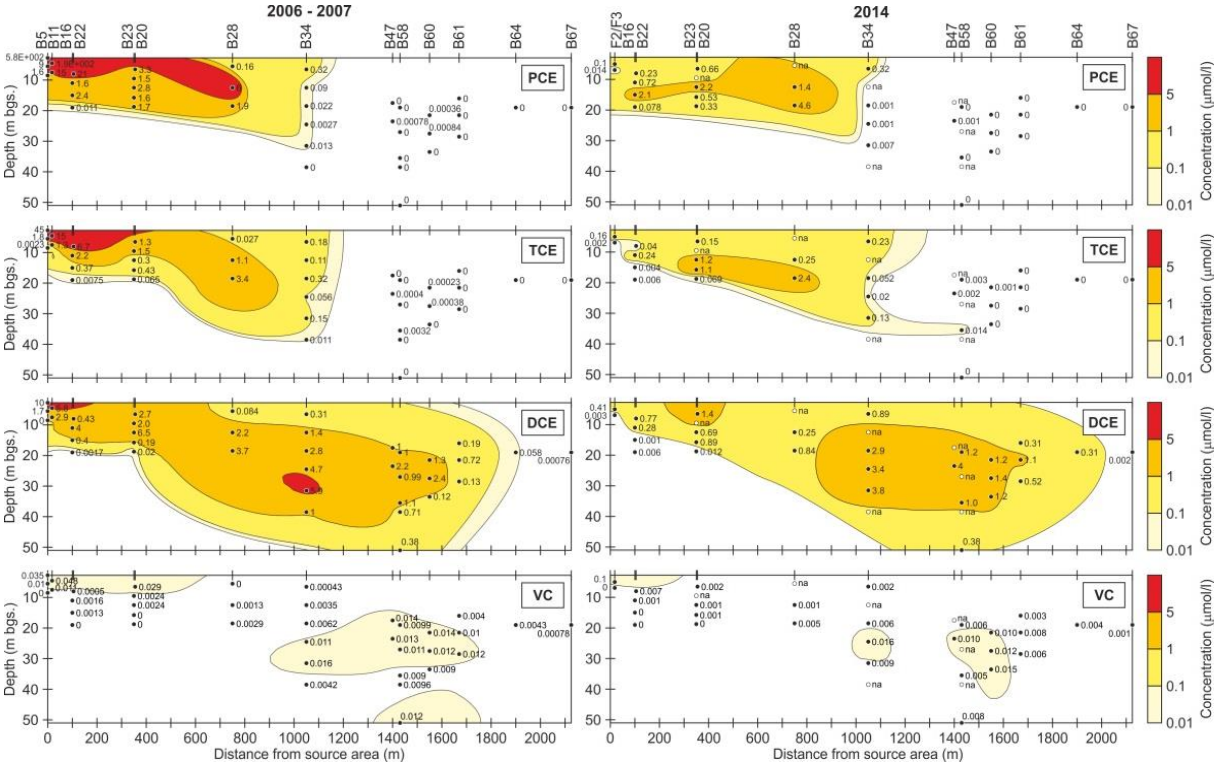

Figure 5. Chlorinated ethenes concentration in the subsurface in 2006 (*Hunkeler et al., 2011*) and 2014 (this study)

The distribution of individual chlorinated ethenes was evaluated in a vertical section along the plume centerline before (2006 *(Hunkeler et al., 2011)*), and eight years after (2014) performing the thermal source remediation (Figure 5). In the first 350 m from the source, the contaminant plume is confined in the upper part of the aquifer due to the presence of a clayey layer at 20 m depth. Further downgradient, the plume widens and dives towards deeper zones showing more reducing conditions, as discussed above. The remediation primarily resulted in a dramatic drop in chlorinated ethenes concentration immediately downgradient.

In 2014, a strong decrease in PCE, TCE and *c*DCE concentrations of more than 85 % was observed in wells immediately downstream (i.e. wells F2, F3 and F4, Figure 2) between 2006 and 2014. Much lower concentrations were also generally measured in wells situated within 750 m from the source in 2014 compared to 2006, with the exception of higher values obtained for TCE at the bottom of B23 (e.g. 1.1 µmol·L^{-1} in 2014 instead of 0.43 µmol·L^{-}1 in 2006). Further downgradient, lower concentrations were generally found for PCE and TCE which eventually disappear 1050 m (PCE) and 1450 m (TCE) downgradient. Similarly, *c*DCE concentrations decreased 1050 m downstream in 2014 compared to 2006. The most pronounced change in chlorinated ethene composition occured as the plume crosses the pyrite oxidation boundary which is depicted in Figure 10. However, an increase in *c*DCE concentrations at the plume front (> 1550 m) together with a plume front extending further downgradient in 2014 compared to 2006 indicated that *c*DCE accumulated in this area and is still expanding, as depicted by the difference in concentration contours in Figure 5. The highest mole fractions of VC (up to 40 % in B67) were determined in this part of the aquifer (Figure 6) although VC concentrations were lower in 2014 than in 2006. Contrary to 2006 where the highest concentration of chlorinated ethenes was detected in the source area, the high concentration core of the plume is now located around 750 m to 1450 m downstream.

From the source zone to 750 m downgradient, PCE was generally the predominant chlorinated ethene in the lower part of the plume in 2014, its concentration reaching more than 85 % of the total chlorinated ethenes concentration on a molar basis at the bottom of wells B22 and B23 (Figure 6). On the other hand, the mole fraction of *c*DCE dominated in the upper part of the plume within 350 m from the source where mole fractions reached up to 74 %. The change in chlorinated ethenes distribution between 2006 where PCE was the predominant chlorinated ethene in the first 750 m of the plume and 2014 suggested the occurrence of PCE/TCE biotic reductive dechlorination. Such occurrence was additionally supported by higher NVOC concentrations and stronger reducing conditions observed in 2014 compared to 2006 in this part of the plume. By contrast to the part of the plume immediately downgradient from the source where PCE dominated, *c*DCE was the predominant chlorinated ethene further downgradient (i.e. > 750 m).

During biotic reductive dechlorination, PCE can be transformed via sequential hydrogenolysis to ethene (i.e. PCE -> TCE -> *c*DCE -> VC -> ethene). Yet, VC and ethene were here either detected at trace levels (VC) or not detected (VC and ethene), suggesting that *c*DCE transformation was the rate limiting step if it is primarily degraded by biotic reductive dechlorination. Abiotic reductive dechlorination of PCE, TCE and *c*DCE by pyrite which bears Fe(II) could also contribute to their attenuation *(Lee & Batchelor, 2002)*. In this case, transformation of PCE, TCE and *c*DCE generally leads to formation of acetylene as the main intermediate via β-dichloroelimination. Although acetylene was not detected in the aquifer, the additional occurrence of abiotic reductive dechlorination could not be discarded as acetylene can be further transformed to readily biodegradable compounds such as acetaldehyde, acetate and ethanol in groundwater *(Liang et al., 2009)*. Finally, while FeS may catalyse PCE and TCE abiotic reductive dechlorination *(Butler & Hayes, 1999)*, it was shown that *c*DCE was not reactive with FeS *(Jeong et al., 2011)*. *c*DCE abiotic reductive dechlorination is thus not likely to take place in the presence of FeS but non-measurable surface-bound Fe(II) *(Elsner, 2002)* and other reduced iron minerals such as green rust *(Lee & Batchelor, 2002)* may on the contrary catalyse such reaction.

3.3. Chlorinated ethenes C and Cl isotopic composition

Chlorinated ethenes concentrations and isotopic compositions measured in 2014 are summarised in Table A 16 of the Appendices.

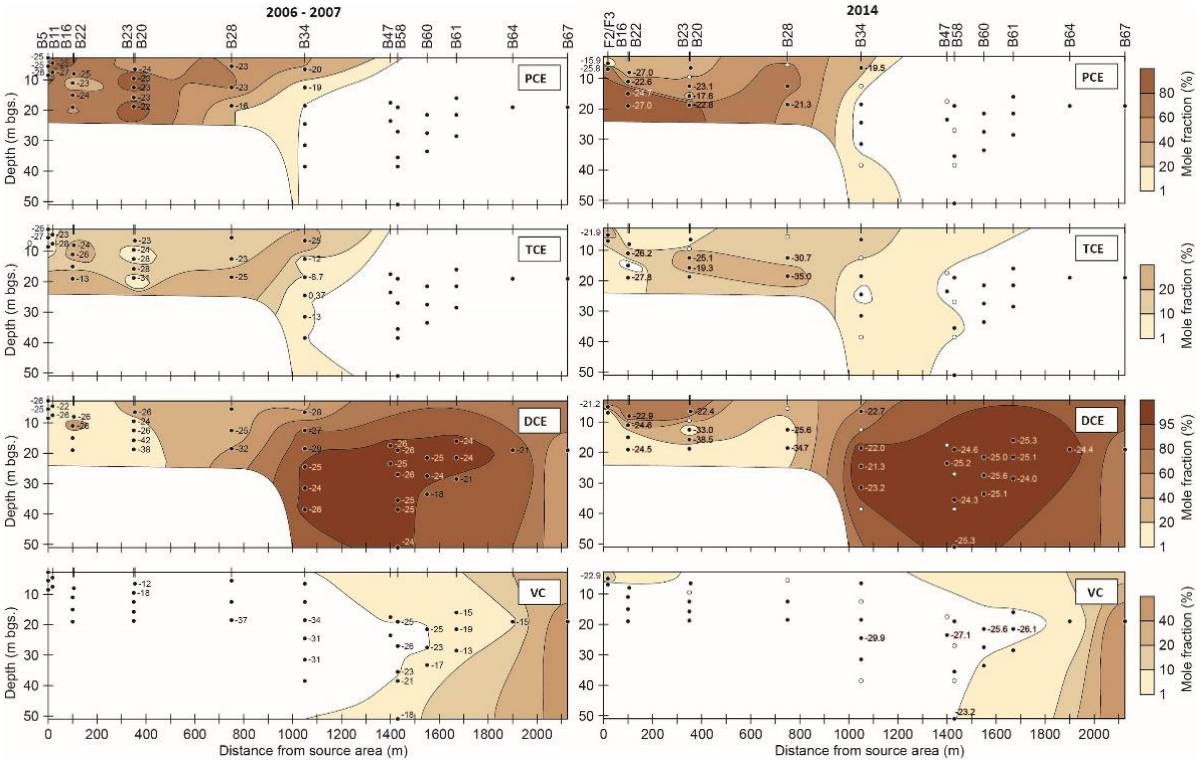

Figure 6. Mole fractions and C isotopic composition of chlorinated ethenes before (2006, *Hunkeler et al., 2011*) and after (2014, this study) source thermal treatment

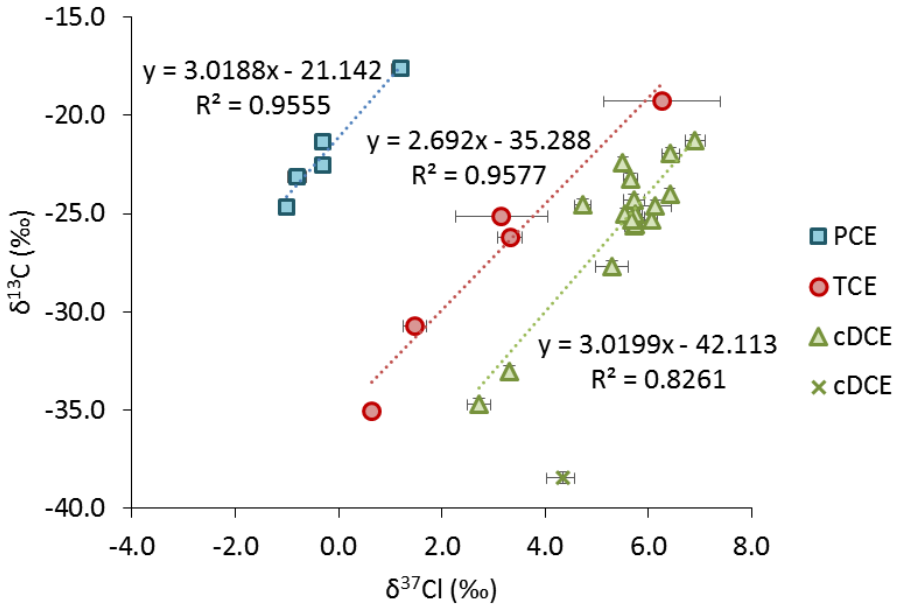

Figure 7. Dual C-Cl isotope slopes associated with PCE, TCE and *c*DCE. One C-Cl isotopic composition of *c*DCE which did not align with the others is represented separately as a cross.

The C isotopic ratio of released PCE was formerly estimated to be -25.0 ‰ *(Hunkeler et al., 2011)*. The Cl isotope measurements performed in 2014 showed a lowest $\delta^{37}Cl$ value of -1.0 ‰ for PCE at 100 and 750 m downgradient from the source, which is the closest measured value to the initial Cl isotope signature of released PCE. Without further data, the initial PCE isotopic signature is hence assumed to be $\delta^{13}C$ = -25.0 ‰ and $\delta^{37}Cl$ = -1.0 ‰.

In 2014, apart from two sampling points located 100 m downstream from the source, PCE C isotopic values were generally more enriched in ^{13}C than the initial isotopic signature, reaching up to -19.5 ‰ in B34-6 (Figure 6), which clearly indicated that PCE degradation was occurring in the plume. On the other hand, TCE C isotopic values exhibited a higher spatial variability. The sampling points in the source area up to 350 m downstream showed C isotopic compositions varying from -27.0 to -19.3 ‰ (Figure 6), which indicated the occurrence of TCE degradation. Conversely, 750 m downstream, values of -30.7 ‰ to -35.0 ‰ indicated that if TCE was being further degraded, this process was either slower than TCE production from PCE or only taking place to a limited extent. The Cl isotopic values of PCE and TCE were coherent with their respective C isotopic values: highest values reflecting an enrichment in ^{37}Cl were found where higher C isotopic values were detected (e.g. B23-2 for PCE and TCE, B22-3 for TCE, Table A 16). This additional line of evidence pointed towards the occurrence of degradation in these sampling points (between the source and 350 m downstream).

C isotopic ratios of *c*DCE varied from -38.5 ‰ (B23-2, 350 m downstream) to -21.3 ‰ (B34-3, 1050 m downstream). Isotopic values enriched in ^{13}C compared to the assumed initial PCE isotopic signature of -25.0 ‰ were found in the source zone up to 350 m downstream in the upper part of the aquifer, as well as 1050 m downstream. This suggested that *c*DCE is being degraded in these parts of the aquifer. Lower C isotopic values found in the deeper part of the aquifer 350 m to 750 m from the source area indicated that if *c*DCE was being degraded, this process was either slower than *c*DCE production from TCE or only taking place to a limited extent. Contrary to 2006 where C isotopic values of *c*DCE and VC reached up to -18 ‰ and -13 ‰ at the plume front (> 1400 m), respectively, such enriched values were not observed in the same part of the plume in 2014 where C isotopic values of *c*DCE and VC reached up to -24.0 ‰ and -23.2 ‰, respectively. This either suggests that *c*DCE, or VC when it is present, was not much further degraded or that the degradation process was not much fractionating and is thus different from the main degrading process taking place before the source remediation. Such lower values could also be attributed to the influx of the not much degraded *c*DCE present 1050 m downgradient from the source in 2006. The most ^{13}C enriched values for *c*DCE are found 1050 m downstream of the source as well as close to the source, indicating a stronger degradation activity (either biotic or abiotic) in these areas than in the rest of the aquifer. While single element isotopic analysis enabled identification of areas where degradation was taking place, it did not permit differentiation between various processes governing degradation.

Dual C-Cl isotope slopes may provide more insight into such processes *(Abe et al., 2009, Elsner, 2010, Cretnik et al., 2013, Kuder et al., 2013, Badin et al., 2014, Renpenning et al., 2014)*. For PCE, the dual C-Cl isotope slope of 3.0 ± 1.2 associated with data points located between the source area and 750 downgradient falled within the range reported for microbial reductive dechlorination in field studies (0.7 – 3.5) and in laboratory experiments (0.7 – 2.7) *(Badin et al., 2014)* (Figure 1 and Figure 7). Since no dual C-Cl slope for PCE abiotic reduction has been reported so far, no comparison was possible. These observations thus constitute at the moment an additional line of evidence supporting the likeliness of PCE undergoing biotic reductive dechlorination in the first 750 m of the plume.

The dual C-Cl isotope slope of 2.7 ± 1.0 observed for TCE for sampling points located between the source area and 1050 m downstream could not be compared to reported ranges of dual isotope

slopes associated with sole TCE degradation in a way as straightforward as for PCE since TCE is being here both produced and consumed. It was yet previously shown that the dual isotope slope associated with a both produced and degraded chlorinated ethene was controlled by its degradation when this step was rate-limiting, i.e. when an accumulation of this intermediate compound is observed *(Hunkeler et al., 2009)*. This was additionally supported by experimental data in chapter 3. TCE accounted for up to 30-40 % at 350 and 750 m downgradient from the source, suggesting that it was accumulating before getting further degraded to *c*DCE. It could thus be assumed that the dual isotope slope associated with TCE in this part of the plume was controlled by TCE degradation and may be compared with slopes associated with TCE biotic reductive dechlorination. When taking the uncertainty into account, the TCE dual C-Cl isotope slope observed in Rødekro was not significantly different from the range observed for TCE biotic reductive dechlorination (3.4 – 4.8 *(Cretnik et al., 2013, Kuder et al., 2013)*), but was significantly different from the slope obtained for TCE abiotic reduction (5.2 ± 0.3 *(Audí-Miró et al., 2013)*). These observations hence supported the occurrence of TCE biotic reductive dechlorination in this part of the plume.

The formerly reported dual C-Cl isotope slope of 2.1 (published $\varepsilon_{Cl}/\varepsilon_C$ = 0.48 ± 0.05, *(Hunkeler et al., 2011)*) associated with *c*DCE from data points located 1050 m downgradient of the source to the plume front was at the time compared with slopes associated with *c*DCE biotic reductive dechlorination (11.4 to 13.7, published $\varepsilon_{Cl}/\varepsilon_C$ = 0.088 ± 0.004 to 0.073 ± 0.006). It was thus concluded based on the dual isotope approach that *c*DCE was either reductively dechlorinated by other strains than those previously studied or that abiotic degradation occurred. Audi-Miro *et al*., 2013, recently reported a dual C-Cl isotopic slope of 3.1 ± 0.2 associated with *c*DCE abiotic reductive dechlorination. The slope value observed in Rødekro in 2006 was closer to the one observed for *c*DCE abiotic reductive dechlorination than to those associated with biotic reductive dechlorination. A slope of 1.5 ± 0.2 associated with *c*DCE degradation which occurred by simultaneous biotic and abiotic reductive dechlorination in the subsurface in presence of a permeable reactive barrier containing 3 % (v/v) zero-valent Fe was more recently reported *(Audí-Miró et al., 2015)*. Although Audí-Miró *et al*. concluded that abiotic reduction was not the predominant degrading process, it cannot be discarded that this slope is being influenced by the latter. *c*DCE was thus likely to be abiotically reduced by pyrite oxidation (and/or other reduced iron minerals) in the sediment in 2006 between 1050 m downgradient of the source and the plume front although acetylene (degradation product of abiotic dihaloelimination) was not detected. In 2014, except for one point (B23-3), C-Cl isotope data align with generally less enriched values closer to the source and more enriched values further downstream to generate a slope of 3.0 ± 0.7 (R^2 = 0.8) which is significantly similar to the slope of 3.1 ± 0.2 associated with *c*DCE abiotic degradation determined by Audí-Miró *et al*., 2013 (Figure 7). This supported the predominance of *c*DCE abiotic reduction in the core of the plume in 2014. On the other hand, the presence of VC still suggested the possibility that *c*DCE hydrogenolysis occured in parallel, though abiotic degradation may also produce a small fraction of VC. Sulphate-reducing conditions found from 1050 m downgradient were better if not optimal for *c*DCE reduction and supported the potentially parallel occurrence of *c*DCE hydrogenolysis *(Chapelle, 1996, Lee & Batchelor, 2002)*.

Apart from immediately downgradient of the source area where VC C isotopic composition was of -22.9 ‰ and at the deepest sampling point in B58, the C isotopic composition of VC did not get much more enriched than the assumed initial isotopic signature of PCE (-25.0 ‰). It is therefore unlikely that further hydrogenolysis of VC to ethene takes place despite more optimal/better redox conditions for VC reductive dechlorination (i.e. sulphate-reducing *(Chapelle, 1996)*). Finally, while

anaerobic oxidation was formerly suggested as a possible degradation pathway, the likeliness of such process to occur remains unclear. Gossett *et al.*, 2010 indeed previously suggested that what was in microcosms thought to be anaerobic oxidation might actually be aerobic oxidation with O_2 concentrations so low that O_2 is quickly consumed and not measured. The conditions were not aerobic in this part of the aquifer which discarded the possibility that aerobic oxidation takes place.
The highest C isotope balance $\delta^{13}C_{sum}$ value at the site (-21.3 ‰ in B34-3, Appendices, Table A 16) indicated a maximum enrichment in ^{13}C of 3.7 ‰. This therefore additionally supported the little transformation of chlorinated ethenes to ethene unless the degradation process showed little isotopic fractionation.
In order to determine the extent of degradation of PCE and *c*DCE in some sampling points, minimum and maximum enrichment factor values reported in the literature were chosen since no microcosm experiment was carried out based on which site specific enrichment factors could be determined. As the data supported PCE biotic reductive dechlorination and *c*DCE abiotic reduction, corresponding enrichment factors were chosen. The extent of degradation D was determined both with C and Cl isotope data. Results can be found in Table A 16 (Appendices). For PCE, the extent of degradation determined with C enrichment factors varied from 0 to 100 %. This is due to the very low enrichment factor of -0.4 ‰ reported by Cichoka *et al*., 2007 leading to a 100 % degradation for almost any enrichment in ^{13}C. As such value is extreme and in order to remain on the safe side by underestimating the extent of degradation, the average value of 19 % determined with the largest enrichment factor might be considered as minimum degraded proportion of PCE. This was in agreement with the average extent of degradation determined with largest and smallest Cl enrichment factors associated with PCE reductive dechlorination of 10 and 34 %, respectively. Finally, for *c*DCE abiotic reductive dechlorination, average extents of degradation of 7 and 19 % could be determined based on largest and smallest enrichment factors associated with this degradation process, respectively. This was in agreement with the observed stalling *c*DCE plume.

3.4. Input from molecular biology

454 pyrotag sequencing, *Dhc* DNA and rRNA as well as *bvcA* and *vcrA* functional genes and gene transcripts (mRNA) analysis were performed in view of acquiring complementary information to understand the processes affecting chlorinated ethenes in the aquifer after the source thermal remediation.
The total *Dhc* population analysis performed by qPCR shows a relatively large range across sampling wells from not detected (below detection limit, b.d.l.) to $1.73 \cdot 10^6$ gene copies$\cdot L^{-1}$ (Figure 8 and Table A 17, Appendices). Higher abundance were measured from the source area to 350 m downstream while lower abundance to non-detect were measured from 1050 m outwards except in B34-4 where intermediate quantities of $1.03 \cdot 10^5$ gene copies$\cdot L^{-1}$ were detected. Only a few sampling locations (i.e. F4-3, B16-1, B17-1, B23-1, B23-2, B23-3, and B34-4) indicated *Dhc* quantities in the range previously reported for other sites where biotic reductive dechlorination naturally occurred *(Damgaard et al., 2013)* (from 10^5 to 10^6 gene copies$\cdot L^{-1}$,Table A 17 of the Appendices) and are thus high enough to support a certain dechlorination potential. Yet, the detection of *Dhc* DNA is not sufficient to confirm the actual occurrence of dechlorination as DNA does not indicate bacterial activity. On the other hand, *Dhc* targeted rRNA was detected reaching up to $2.48 \cdot 10^5$ copies$\cdot L^{-1}$ in sampling points located between the source zone to 1050 m downstream (Table A 17 of the Appendices). Relatively higher proportions of 16S rRNA than corresponding DNA in wells B16-1 and B23-2 compared with other

wells indicated that *Dhc* in B16-1 and B23-2 were more metabolically active than *Dhc* in some other locations. The presence and apparent high activity of *Dhc* in B16-1 and B23-2 coincide with highly enriched C isotope ratios of -17.6 ‰ for PCE and -19.3 ‰ for TCE in B23-2 and -22.9 ‰ for *c*DCE in B16-1 (Figure 6, Figure 8, and Table A 17 of the Appendices).

Genes coding for the enzyme involved in the final transformation of VC to ethene (*vcrA* and *bvcA*) were neither present (DNA) nor expressed (mRNA) above the detection limit. This is consistent with the minor C isotopic enrichment observed for VC which supports an absence of VC degradation by reductive dechlorination at the site. Nevertheless, further VC reductive dechlorination cannot be ruled out as VC *rdhA* genes other than *vcrA* and *bvcA* may exist. It was indeed recently demonstrated that some members of the *Dehalogenimonas* (*Dhg*) genus respire VC and thus participate in VC dechlorination to ethene *(Yang, 2015)*.

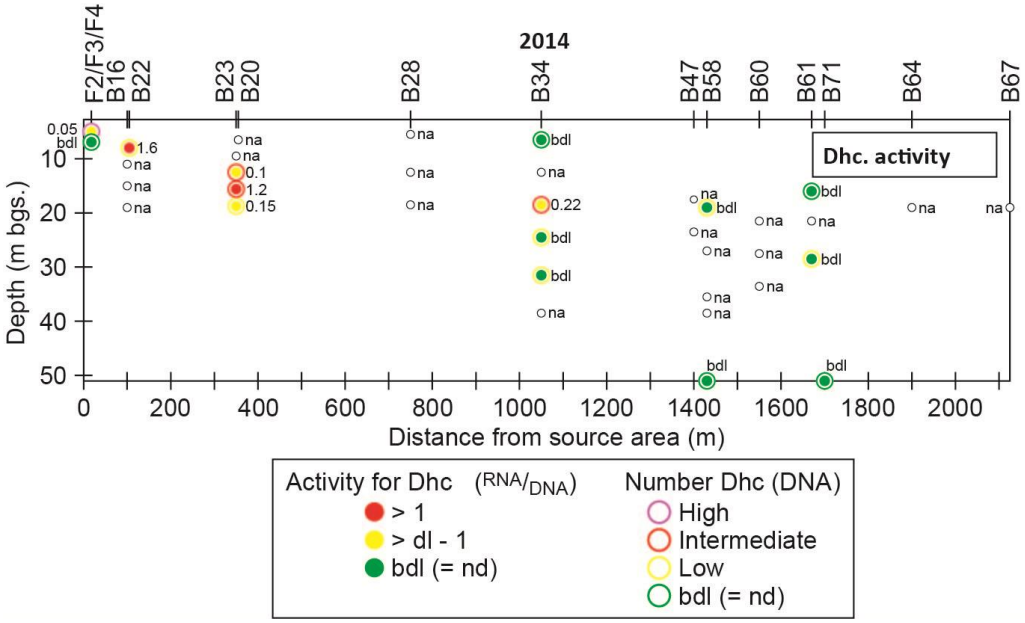

Figure 8. Dhc population size and activity in the subsurface.

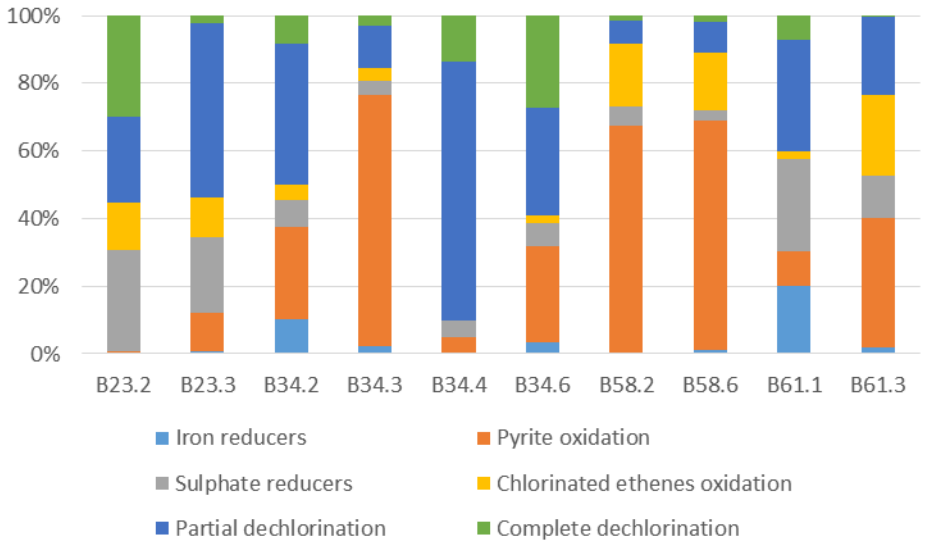

Figure 9. Relative proportion of microorganisms which have been identified to a 16s rRNA gene based phylogenetic group that has been shown to contain bacteria involved in iron-reducing, sulphate-reducing, partial dechlorination, pyrite oxidation, chlorinated ethenes biotic oxidation or complete dechlorination processes. Only these phylogenetic groups (Table A 14 and Table A 15) are included in the analysis.

The 454 pyrotag sequencing enabled the identification of the relative abundance of various bacteria in the sampled locations (Figure 9 and Table A 18). Generally, low relative abundance (ranging from 0 to 4 %) were found in all samples for bacteria likely involved in iron reduction among all the considered groups (i.e. bacteria involved in iron- and sulphate-reduction, pyrite oxidation, chlorinated ethenes oxidation, and partial and complete reductive dechlorination, Figure 9 and Table A 18, Appendices) which coincides with the relatively reducing conditions observed in most of the aquifer based on redox species concentrations. Bacteria reported to be found in presence of sulphate-reducing conditions as well as during pyrite oxidation were detected in high relative abundance (Figure 9 and Table A 18, Appendices) confirming redox data and indicating a high likelihood of pyrite oxidation and sulphate-reducing conditions. More specifically, bacteria reported to be found during pyrite oxidation were found in relative abundance higher than 20 % in B34-2, B34-3, B34-6, B58-2, B58-6 and B61-3, i.e. from 1050 m downstream of the source. This coincides with *c*DCE dual C-Cl isotope data that suggests a predominant abiotic *c*DCE reduction in these locations. Bacteria genera among which some members are known to catalyse complete reductive dechlorination of chlorinated ethenes (i.e. *Dhc (Löffler, 2013)* and *Dhg (Yang, 2015)*) were detected in the majority of sampling locations (Figure 9). In particular, relative abundance of bacteria potentially able to completely dechlorinate chlorinated ethenes are high in B23-2 (350 m downstream) and B34-6 (1050 m downstream). The counts of *Dhc* from pyrotag sequencing do not exactly coincide with the copy number of *Dhc* determined by targeted quantitative PCR after extracting DNA (Table A 17 and Table A 18, Appendices) which may be due to the fact that 454 pyrotag sequencing is considered as a semi-quantitative method and different amplification primers were used. Contrary to *Dhc*, *Dhg* was detected in all samples, and reads were particularly high in B23-2 ($1.7 \cdot 10^6$ cells·L^{-1}, Table A 17, Appendices), indicating the possibility that complete reductive dechlorination may have occurred in this location, 350 m from the source. Among the bacterial genera among which some members are known to reduce chlorinated ethenes only partially, several were detected in particular in B23-3,

B34-2, B34-4, B34-6 and B61-1 (Figure 9 and Table A 18, Appendices), indicating that bacteria potentially able to dechlorinate chlorinated ethenes were present throughout the entire plume.
Generally, the molecular biology data hence suggests that reductive dechlorination could potentially occur in any sampling location showing a higher likelihood in B16-1, F4-3 (which are located immediately downstream from the source), B23-2 and B34-4 (which are located 350 and 1050 m downstream from the source). Moreover, no specific marker enables to support complete dechlorination as neither *bvcA* nor *vcrA* genes were detected.
Pyrotag sequencing data also highlight the possibility that *c*DCE and/or VC may have been oxidized, especially downstream (from B58 to B61) where *Polaromonas* reads are the highest (Table A 18, Appendices). This is however rather plausible in the upper part of the aquifer where oxic conditions may occur contrary to the deeper part of the aquifer.

4. Summary of redox and chlorinated ethenes degradation processes occurring in the aquifer from 2006 to 2014

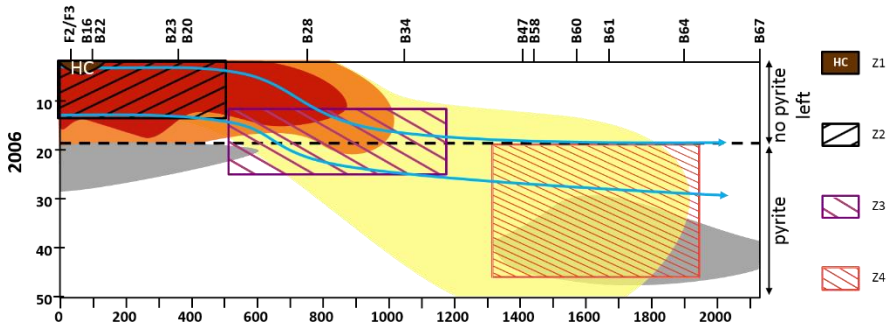

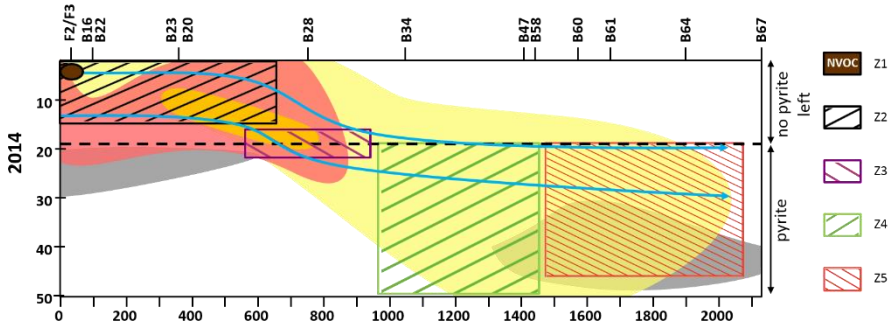

Redox conditions/processes	Processes affecting CE	Evidence for processes affecting CE
Z1: HC: reduces redox conditions	Biotic degradation: PCE → TCE	- Presence of TCE and *c*DCE
Z2: Aerobic to nitrate reducing conditions	- Transport - Little biotic degradation: PCE → TCE	- Presence of TCE and *c*DCE - $\delta^{13}C_{PCE} > \delta^{13}C_{source}$ - $\delta^{13}C_{TCE}$ and $\delta^{13}C_{cDE} < \delta^{13}C_{source}$
Z3: Oxygen and nitrate consumption due to pyrite oxidation leading to manganese-iron-reducing conditions O_2 / NO_3^- (FeS_2 → Fe(II) + SO_4^{2-})	Biotic degradation: PCE → TCE → *c*DCE	- Presence of TCE and *c*DCE; *c*DCE dominates - $\delta^{13}C_{PCE}$ and $\delta^{13}C_{TCE} > \delta^{13}C_{source}$ - $\delta^{13}C_{cDE} < \delta^{13}C_{source}$
Z4: Iron-reducing to methanogenic	- Biotic degradation: *c*DCE → VC (→ Ethene?)	- Presence of VC - $\delta^{13}C_{cDE}$ and $\delta^{13}C_{VC} > \delta^{13}C_{source}$ - Little methane present
	- Abiotic *c*DCE degradation by pyrite oxidation (and potentially other reduced iron species)	- Little VC, no ethene - Dual *c*DCE C-Cl slope - Homogeneous sulphate concentration

Redox conditions/processes	Processes affecting CE	Evidence for processes affecting CE
Z1: NVOC: reduces redox conditions	Biotic degradation: PCE → TCE → *c*DCE (→ VC)	- Presence of TCE, *c*DCE and VC; *c*DCE dominates - $\delta^{13}C_{PCE}$, $\delta^{13}C_{TCE}$ and $\delta^{13}C_{cDE} > \delta^{13}C_{source}$ - *Dhc* presence and activity - 454 pyrotag sequencing
Z2: Reduced redox due to NVOC release	Biotic degradation: PCE → TCE → *c*DCE and transport	- Presence of TCE and *c*DCE - $\delta^{13}C_{PCE}$, $\delta^{13}C_{TCE}$ and $\delta^{13}C_{cDE} > \delta^{13}C_{source}$ - $\delta^{13}C_{cDE} < \delta^{13}C_{source}$ - Dual PCE and TCE C-Cl slopes
Z3: Oxygen and nitrate consumption due to pyrite oxidation leading to iron-reducing conditions O_2 / NO_3^- (FeS_2 → Fe(II) + SO_4^{2-})	Biotic degradation: PCE → TCE → *c*DCE	- Presence of TCE and *c*DCE; *c*DCE dominates - $\delta^{13}C_{TCE}$ and $\delta^{13}C_{cDE} < \delta^{13}C_{source}$
Z4: - Sulphate reduction followed by precipitation of sulphide with iron (II) to yield metastable iron sulphide Fe(II) (SO_4^{2-} → S^{2-} → FeS) / iron (II) sorption on minerals - Sulphate-reducing	- Biotic degradation: *c*DCE → VC (→ Ethene?)	- $\delta^{13}C_{cDCE} > \delta^{13}C_{source}$ - Little VC - Decrease in sulphate - Little methane present
	- Abiotic degradation of *c*DCE by pyrite and/or surface-bound iron (II) (and potentially other reduced iron species)	- $\delta^{13}C_{cDCE} > \delta^{13}C_{source}$ - Not much VC, no ethene - Dual *c*DCE C-Cl slope - 454 pyrotag sequencing
Z5: Iron reducing	- Not much *c*DCE degradation - *c*DCE influx of produced but little degraded *c*DCE from 1000 m from 2006	- Not much VC - Little methane present - $\delta^{13}C_{cDCE} \approx \delta^{13}C_{source}$

Clay

PCE dominating

TCE mole fraction > 20%

PCE and TCE concentrations are however much lower in 2014 than in 2006 due to the source remediation

cDCE dominating

Pyrite oxidation

HC: hydrocarbons

Figure 10. Overview summarising redox conditions and processes as well as processes affecting chlorinated ethenes (CE) in the subsurface in 2006 and in 2014 .

Summaries describing redox and chlorinated ethenes degradation processes which are likely occurring in the subsurface in 2006 and 2014 as well as the consequences on chlorinated ethenes distribution in the plume are given in Figure 10. These drawings result from the combination of lines of evidence brought by the different methods applied in this study (i.e. redox conditions, contaminant concentration, isotope analysis and molecular biology).

4.1. First 750 m

Based on the performed investigations, it could be confirmed that PCE and TCE were very likely dechlorinated by biotic reductive dechlorination in the upper part of the plume, in the first 350 to 750 m downgradient from the source, either due to the former presence of hydrocarbons (2006) and natural influx of low background NVOC or to the release of NVOC during thermal remediation (2014). Redox conditions were generally more reduced in the source area in 2014 than in 2006 due to the NVOC release. *c*DCE is the dominant chlorinated ethene immediately downgradient of the source in 2014 as a result of PCE and TCE reductive dechlorination occurring in more reducing conditions. Biotic reductive dechlorination of *c*DCE also likely occurred but to a lesser extent and both *c*DCE and VC may be biotically oxidised in the upper part of the aquifer shortly downgradient of the source where aerobic conditions were present.

4.2. 750 to 900 m downgradient

As the plume moves forward, it dips and enters a more reducing zone starting from ~15 m depth which is created by pyrite oxidation consuming the influx of O_2 and NO_3^- from the water recharge (both in 2006 and 2014). Biotic reductive dechlorination of PCE and TCE takes place as conditions here become manganese/iron reducing, explaining the disappearance of these compounds between ~700 and ~900 m downgradient from the source, when the plume crosses the pyrite oxidation zone. Reductive dechlorination of *c*DCE does not appear to have occurred in this part of the plume in 2006 nor in 2014 as supported by $\delta^{13}C_{cDE} < \delta^{13}C_{source}$ and the presence of insufficient reducing conditions.

4.3. From 1000 m to 1500 m

The fate of *c*DCE in 2006 after 1000 m could be better evaluated based on studies performed since 2011 allowing a better dual C-Cl isotope slopes interpretation. It could be concluded that *c*DCE was likely predominantly abiotically reduced by pyrite in 2006 between 1000 m and the plume front although biotic degradation may have occurred as well (presence of VC and detection of *Dhc*). In 2014, the NVOC release leading to more reducing conditions seems to have impacted the subsurface to ~1500 m downgradient of the source area. Indeed, no Fe(II) and lower SO_4^{2-} concentrations are abruptly observed between ~1000 and ~1500 m in 2014, indicating that SO_4^{2-} reduction followed by FeS precipitation and/or Fe(II) sorption on minerals (and potential formation of green rust and other reduced iron species) likely occurred. Such drop in Fe(II) and SO_4^{2-} could also be partially attributed to the absence of pyrite oxidation resulting from O_2 and NO_3^- consumption in the upper part of the aquifer close to the source after the NVOC release. *c*DCE degradation is probably occurring in this part of the plume, as indicated by $\delta^{13}C_{cDE} > \delta^{13}C_{source}$ 1050 m downgradient from the source. Based on C-Cl isotope data and on the assumption that currently available dual isotope slopes represent the range of slopes associated with the corresponding degradation process, it was also suggested that *c*DCE was predominantly abiotically reduced in 2014. The low VC concentrations could additionally

document the occurrence of abiotic degradation to which the possible presence of non-measurable surface-bound Fe (II,) which is known to catalyse abiotic degradation of some compounds *(Elsner, 2002)*, could contribute. On the other hand, the observed redox conditions are more favourable for *c*DCE and VC biotic reductive dechlorination than before remediation explaining the occurrence of *Dhc* and *Dhc* activity around 1050 m downgradient in 2014.

4.4. From 1500 m to the plume front

Further downstream where the source remediation did not impact the plume (> 1500 m), *c*DCE does not seem to be degraded as indicated by the presence of little VC as well as $\delta^{13}C_{cDE} \approx \delta^{13}C_{source}$. Moreover, a plume front extending ~200 m further in 2014 compared to 2006 (concentration contours, Figure 5) together with the presence of *c*DCE in slightly higher concentrations in 2014 in the downstream part of the plume compared to 2006 suggests that *c*DCE is still expanding, even though slowly. This coincides with the observation of small extents of *c*DCE degradation based on isotope data ranging from 7 to 19 %. Such observed difference in *c*DCE concentration at the plume front between 2006 and 2014 might also be attributed to a slight lateral change in flow direction. An explanation to the lack of further degradation would be the absence of active degraders in 2014 as depicted in Figure 8. Finally, it could be concluded based on isotope and molecular biology data that the little VC produced in the downstream part is being little further degraded.

5. Assessment of source thermal remediation effect on redox conditions and the fate of chlorinated ethenes

Due to the contaminant source removal, the overall chlorinated ethenes concentrations in and downgradient of the source area dramatically decreased between 2006 and 2014. Although no plume detachment was observed, the source thermal remediation seems to have triggered a change in redox species concentrations, more particularly of iron. Indeed, an increase in NVOCs in the source zone, likely due to the release of organic matter during the treatment, would support microbial growth triggering in turn changes in redox conditions as a result of electron acceptors consumption such as O_2 and NO_3^-. A chain of redox reactions influenced by the additional presence of pyrite in the present aquifer eventually affected the degradation of chlorinated ethenes, allowing primarily for an increase in PCE and TCE biotic degradation to *c*DCE immediately downgradient of the source area, and further *c*DCE predominantly abiotic reduction in the plume centre. Such intricate situation where iron plays a role in redox reactions involving both bacterial and abiotic degradation of chlorinated contaminants was also previously reported, confirming the need for studies exploring the dynamics of biogeochemical systems in presence of iron *(Elsner, 2002, Broholm et al., 2014)*.

This study thus demonstrated the strength of complementary application of analytical and molecular biology tools to get more insight in processes occurring in the subsurface where a plume of chlorinated ethenes flows in a complex geochemical system.

Acknowledgements: The authors would like to acknowledge Niels Just and the Region of Southern Denmark for providing a sampling opportunity in the study site and additional funding as well as sharing information relative to the site, and Jesper Gregersen for his precious help in organising and performing field sampling. Orfan Shouakar-Stash and Mirna Stas are acknowledged for measuring Cl isotopic ratios of *c*DCE. Julien Maillard is acknowledged for critical reading of the manuscript. This research was completed within the framework of the Marie Curie Initial Training Network ADVOCATE - Advancing sustainable *in situ* remediation for contaminated land and groundwater, funded by the European Commission, Marie Curie Actions Project No. 265063.

Conclusions and outlook

The occurrence of chlorinated ethenes in groundwater is a recurrent issue encountered by many developed countries around the world. Owing to analytical development during the past decades, compound specific isotopic analysis (CSIA) has been increasingly employed during investigation of sites contaminated with organic compounds. Contrary to C, an automatized Cl isotopic analysis method for chlorinated ethenes enabling comparable laboratory and field sample analysis between different laboratories has only since recently been made available. This work hence aimed at exploring the application of C-Cl isotopic analysis opened by the new possibility to analyse Cl isotopic composition of chlorinated ethenes to evaluate the origin and fate thereof in groundwater.

1. Summary of findings and contribution

1.1. Source differentiation (Chapter 1)

For regulatory reasons, determining the contamination perpetrator is often of interest. The extent of applicability of C-Cl isotopic analysis of chlorinated ethenes for source delineation was hence first addressed. Despite the existence of a large variety of isotopic signatures for compounds produced by different manufacturers, it was shown that such variability was smaller between 10 out of an estimated 12'300 sites located in Switzerland for PCE (i.e. -26.0 to -23.7 ‰ for C and -0.5 to 0.6 ‰ for Cl in Switzerland and -37.4 to -23.2 ‰ for C and -4.4 to 1.2 ‰ for Cl in PCE from manufacturers). Although the amount of investigated sites was low compared to the total estimated amount of sites, the chosen sites represented the various industrial PCE utilisation purposes and were widespread throughout the country. It was thus concluded that CSIA may or may not, depending on cases, allow for contaminant source delineation by comparing isotopic signatures between suspected contaminant sources and downstream contamination. One should thus be aware of the possible failure when choosing such method to determine the origin of a contamination.

1.2. Tracking degradation processes (Chapter 2)

Once chlorinated ethenes have been detected in groundwater, it may be of interest to determine whether the latter are being naturally degraded or not, as this will influence the site management choice (e.g. application of monitored natural attenuation). In order to differentiate between biotic and abiotic degradation in the field based on dual C-Cl isotope analysis, more should be known about the isotopic characteristics associated with biotic degradation itself. Two significantly different dual C-Cl isotope slopes associated with PCE reductive dechlorination performed by two bacterial consortia SL2-PCEc and SL2-PCEb harbouring members of *Sulfurospirillum* spp. were determined. The only other dual C-Cl isotope slope associated with PCE reductive dechlorination reported at the time was in the same range as one of the experimentally determined slopes. Two dual C-Cl isotope slopes associated with PCE reductive dechlorination in two field sites where each slope corresponded to one experimentally determined slope were also determined. This further supported the existence of two unique slopes. These results imply that caution should be taken when applying dual C-Cl isotopic analysis to differentiate occurring degradation processes in the field as different slopes could be associated with biotic reductive dechlorination alone.

1.3. Exploring reaction mechanisms underlying PCE biotic reductive dechlorination (Chapters 2 and 3)

Chlorinated ethenes are known to undergo sequential biotic reductive dechlorination in strictly anoxic conditions (i.e. PCE → TCE → *c*DCE → VC → ethene). However, the exact reaction mechanism underlying each step of reductive dechlorination remains at the stage of hypothesis where three different reaction mechanisms have so far been proposed: i.e. first rate-limiting step consisting in (i) single electron transfer, (ii) addition followed by elimination, or (iii) nucleophilic substitution. The existence of two distinct slopes associated with PCE biotic reductive dechlorination was additionally interpreted as the occurrence of two different reaction mechanisms associated with PCE reductive dechlorination, under the assumption that dual C-Cl isotope slopes solely reflected reaction mechanisms. It was moreover demonstrated that phylogenetically close bacteria could yield different C-Cl isotope slopes. More specifically, the two experimentally determined C-Cl isotope slopes resulted from PCE reductive dechlorination catalysed by two different reductive dehalogenases (RdhA) having similar protein sequences. This hence further indicates that similarities in RdhA protein sequences do not necessarily imply similarities in reductive dechlorination mechanisms. Based on C and Cl isotopic data as well as AKIEs calculations where secondary isotopic effects were neglected, we furthermore suggested that one consortium (SL2-PCEc) more likely involved an electron-transfer or nucleophilic substitution as a first step of reaction mechanism than a nucleophilic addition. Comparing the corresponding $(\mathrm{AKIE(C)}-1)/(\mathrm{AKIE(Cl)}-1)$ to $(\mathrm{KIE(C)}-1)/(\mathrm{KIE(Cl)}-1)$ obtained for the Streitwieser limit suggested that either the primary Cl isotope effect was larger than the isotope effect given by the Streitwieser limit, or that a secondary Cl isotope effect occurred.
The likeliness that secondary Cl isotope effects occur during PCE reductive dechlorination was yet supported by the observed offset in initial Cl isotopic composition of degraded PCE and merely produced TCE during the performed laboratory experiments. Due to the lighter initial Cl isotopic composition of TCE than PCE, it was even suggested that inverse secondary isotopic effects occurred. Such behaviour was observed both in TCE merely produced and TCE as an accumulating intermediate (i.e. produced and degraded). Depending on the scenario (one-step or two-steps) involved during PCE to TCE reductive dechlorination, this offset may however only reflect the difference between primary and secondary isotopic effects rather than reflecting an inverse secondary effect. Nevertheless, attributing this offset to one or another scenario still remained challenging as information regarding all the biochemical steps affecting PCE during its reductive dechlorination is missing.

1.4. Modelling isotope trends (Chapter 4)

Incorporating isotope data in reactive transport models was formerly suggested to improve plume fate predictions and allow gaining further insight into processes occurring at a site. As our experimental data supported the evidence for so far neglected secondary Cl isotope effects, the latter were taken into account in a mathematical model developed to simulate the evolution of chlorinated ethenes C and Cl isotopic composition during sequential reductive dechlorination where Monod kinetics were additionally considered. The two developed models (i.e. one general (MG) considering C and Cl isotopocules simultaneously and one simplified (MS) considering C and Cl separately) almost identically simulated C and Cl isotopic compositions of PCE, TCE and *c*DCE during reductive dechlorination, with the exception of *c*DCE Cl isotopic composition when different Cl secondary isotopic effects were considered during PCE dechlorination to *c*DCE. In this case, MS was

not sufficient anymore to accurately reproduce the *c*DCE Cl isotopic composition as the different Cl secondary isotopic effects occurring during PCE dechlorination affected the distribution of Cl isotopes in TCE. As TCE was successively dechlorinated to *c*DCE, MS failed to reflect the true *c*DCE Cl isotopic composition as the unequal Cl isotopes distribution in TCE could not be taken into account, contrary to MG. The actual occurrence of such situation has however not yet been experimentally documented but the probability that significantly different secondary Cl isotopic effects are observed can expected to be low. Finally, both models accurately reproduced our previously collected experimental data which opens the possibility for further implementation of isotope data in reactive transport models.

1.5. Evaluation of reactive processes occurring in an aquifer (Chapter 5)

Finally, applying C and Cl isotopic analysis to groundwater samples in Rødekro demonstrated that CSIA is a valuable complementary tool to evaluate what biogeochemical processes are taking place in an aquifer contaminated with chlorinated ethenes. More specifically, it served to assess the effect of source remediation by steam injection based on two sampling campaigns carried out before and after remediation. Based on the assumption that dual C-Cl isotope slopes directly reflect degradation pathways, it was suggested that steam injection enhanced PCE and TCE biotic reductive dechlorination in the first part of the plume. This was in agreement with the occurrence of more reducing conditions resulting from the release of organic matter likely triggered by the thermal remediation. Further downgradient, the dual isotope slope approach suggested that *c*DCE was probably primarily abiotically reduced by pyrite in the downstream part of the plume before and after the remediation event. In the middle of the plume, a lighter *c*DCE C isotopic composition than the estimated initial PCE C isotopic composition documented the occurrence of further *c*DCE degradation in 2014 despite the very low VC concentrations. On the contrary, a *c*DCE C isotopic composition equal to that of the initially released PCE indicated the absence of further *c*DCE degradation at the front of the plume. Such conclusion was in agreement with the observed plume expansion documented by larger concentration contours in the second campaign than in the first. In the end, C and Cl isotopic analysis served as a tool to support the interpretation of redox data and chlorinated ethenes concentrations. So did molecular biology tools which documented the activity of *Dhc* in the first part and centre of the plume.

2. Limitations and further research needs

New discoveries raise new questions. We thus point out in this last section the limits encountered when exploring the use of C-Cl dual isotope analysis to determine the fate of chlorinated ethenes in groundwater and propose further research directions to address these gaps.

2.1. Improving our understanding of isotopic trends

2.1.1. Reaction mechanisms and other rate-limiting steps

The occurrence of two significantly different dual C-Cl isotope slopes associated with PCE microbial reductive dechlorination was attributed to the existence of two different reaction mechanisms underlying this reaction, under the assumption that dual C-Cl isotope slopes strictly reflect the chemical reaction. Such assumption was formerly suggested supposing that other rate-limiting steps occurring during substrate-enzyme interactions would equally affect both elements *(Elsner et al.,*

2005). It can however not be discarded that rate-limiting steps may affect C and Cl isotopic compositions differently consequently leading to the distinct dual isotope slopes observed. Additional experiments where dual C-Cl isotope slopes are studied during reductive dechlorination by other bacterial consortia, or even by chemical systems mimicking the undergoing chemical reaction during biotic reductive dechlorination, may enable to elucidate to what extent dual C-Cl isotope slope are actually representative of reaction mechanisms. Such studies were in fact performed in parallel to this work where dual C-Cl isotope slopes associated with PCE and TCE reductive dechlorination catalysed by purified enzymes and corrinoids were reported *(Renpenning et al., 2014)*. The larger observed variety of slopes associated with PCE reductive dechlorination performed by enzymes and corrinoids constitutes an additional argument which questions the assumption according to which dual isotope slopes strictly reflect the sole rate-limiting step of the chemical reaction. Further research is thus required to improve our understanding of the processes controlling dual C-Cl isotope slopes during chlorinated ethenes reductive dechlorination. Supplementary field and laboratory studies would for example help elucidating the behaviour of dual C-Cl isotope slopes based on representative and practical observations. Performing reductive dechlorination with purified enzymes and corrinoids extracted from bacteria used in this study would for example be of great value.

2.1.2. Secondary Cl isotopic effects

The evidence of secondary Cl isotopic effects highlighted by this work should also be further explored as their regular occurrence may change the way we treat isotopic data since secondary isotopic effects were so far neglected. Our developed model indeed documented how the Cl isotopic composition of produced compound varied depending on the existence and extent of secondary Cl isotopic effects. Verifying the extent to which secondary Cl isotopic effects may actually occur could be achieved by more systematically analysing both produced and degraded compound isotopic compositions. Depending on the degree of importance of secondary Cl isotopic effects, models used to simulate the evolution of chlorinated ethenes during reductive dechlorination will then have to take such effects into account or not. More particularly, the existence of different secondary Cl isotopic effects depending on the Cl atom position in a molecule should be investigated. Although the discrepancy was small, we indeed showed - based on our modelling approach - that *c*DCE Cl isotopic composition varied depending on whether different secondary Cl isotopic effects could be taken into account or not during the step of PCE transformation to TCE. This was due to the resulting unequal Cl isotope distribution in the asymmetric TCE and further indicates that the original Cl isotope distribution in asymmetric molecule affects the isotopic behaviour of a produced compound. To experimentally confirm this supposition, experiments with TCE in which the distribution of heavy and light Cl atoms in each position is known could be performed. A limitation resides in the measurement of these position-specific isotopic compositions which may be addressed by measuring all fragments detected by GCqMS whereby complex probability calculations would have to be carried out, or by pushing the analytical boundaries further in the field of NMR for example.

It was additionally recently demonstrated that primary and secondary Cl isotopic effects could be distributed between the two Cl atoms bound to the same C in the case of TCE as both Cl atoms could be cleaved followed by a selective interconversion of *trans*- to *cis*-DCE explaining the usually observed predominant formation of *cis*-DCE *(Cretnik et al., 2014)*. Incorporating the possible distribution of primary and secondary Cl isotopic effects between Cl atoms of TCE in our developed

model would allow an even more accurate simulation of the produced compound *c*DCE and thus generally of chlorinated ethenes isotopic composition during sequential reductive dechlorination.

2.1.3. Limits of the Rayleigh equation

Another gap was revealed when developing the model enabling the simulation of accurate chlorinated ethenes C and Cl isotopic compositions during reductive dechlorination by considering the evolution of isotopocules as independent species instead of isotopes. Although global C and Cl enrichment factors could be determined by applying the Rayleigh equation to simulated data, we observed a slightly non-linear relationship between $\ln(C_t/C_0)$ and $\ln((\delta^{13}C+1)/(\delta^{13}C_0+1))$. This non-linearity was more pronounced for lower remaining fractions (i.e. longer simulation times). Assuming the validity of the Rayleigh equation was suitable in the present work as the deviation was less than the analytical uncertainty for an experimentally plausible frame (i.e. simulation until 1% fraction remaining of degraded compound). Numerous studies in the field of contaminant hydrogeology also successfully applied the Rayleigh equation to isotopic data which additionally supports its validity in most environmental studies dedicated to organic contaminants. Finally, using an isotopocule approach implies that we can measure isotopomer concentrations which is at the moment not feasible. It might yet be of interest to explore the limits imposed by assuming that different isotopes, instead of different isotopocules, undergo different kinetics with regards to the evolution of the studied compounds isotopic composition to either validate or invalidate the Rayleigh approximation.

2.2. Improving the quantification of biodegradation by a modelling approach

Ultimately, when considering monitored natural attenuation as a management strategy of a site contaminated with chlorinated ethenes, one needs a reliable tool to quantify the extent of biodegradation occurring in the plume and further predict the plume fate. Although several studies applied CSIA to quantify the extent of biodegradation in situ *(Meckenstock et al., 2015)*, none set out to validate such quantification by comparing predicted contaminant fate with actually observed contaminant fate. An extended version of our developed model in which transport and other processes occurring in the subsurface (e.g. sorption) would be taken into account could be used for this purpose. Such model could be calibrated based on data collected from a site which should not have been remediated in order to prevent the effect of other processes on the plume as well as on the contaminants isotopic composition. In parallel, another classical reactive transport model which do not take isotopic data into account could be calibrated with the collected field data. A validation could then be performed where the plume fate prediction based on both models would be compared to actually obtained field data. Such study would enable to validate the robustness of this tool to evaluate a contaminants plume fate.

References

Abe, Y., R. Aravena, J. Zopfi, O. Shouakar-Stash, E. Cox, J. D. Roberts and D. Hunkeler: Carbon and Chlorine Isotope Fractionation during Aerobic Oxidation and Reductive Dechlorination of Vinyl Chloride and cis-1,2-Dichloroethene. Environmental Science & Technology 43 (1), 101-107 (2009)

ADEME: Atténuation naturelle des composés organo-chlorés aliphatiques dans les aquifères, guide méthodologique. (2007)

Aeppli, C., M. Berg, O. A. Cirpka, C. Holliger, R. P. Schwarzenbach and T. B. Hofstetter: Influence of Mass-Transfer Limitations on Carbon Isotope Fractionation during Microbial Dechlorination of Trichloroethene. Environmental Science & Technology 43 (23), 8813-8820 (2009)

Aeppli, C., H. Holmstrand, P. Andersson and O. Gustafsson: Direct Compound-Specific Stable Chlorine Isotope Analysis of Organic Compounds with Quadrupole GC/MS Using Standard Isotope Bracketing. Analytical Chemistry 82 (1), 420-426 (2010)

Amaral, H. I., C. Aeppli, R. Kipfer and M. Berg: Assessing the transformation of chlorinated ethenes in aquifers with limited potential for natural attenuation: Added values of compound-specific carbon isotope analysis and groundwater dating. Chemosphere 85 (5), 774-781 (2011)

Arnold, W. A. and A. L. Roberts: Pathways and Kinetics of Chlorinated Ethylene and Chlorinated Acetylene Reaction with Fe(0) Particles. Environmental Science & Technology 34 (9), 1794-1805 (2000)

Aronson, D., Howard, P., H. (1997). Anaerobic Biodegradation of Organic Chemicals in Groundwater: A Summary of Field and Laboratory Studies, Environmental Science Center.

Atteia, O., M. Franceschi and A. Dupuy: Validation of Reactive Model Assumptions with Isotope Data: Application to the Dover Case. Environmental Science & Technology 42 (9), 3289-3295 (2008)

Audí-Miró, C., S. Cretnik, N. Otero, J. Palau, O. Shouakar-Stash, A. Soler and M. Elsner: Cl and C isotope analysis to assess the effectiveness of chlorinated ethene degradation by zero-valent iron: Evidence from dual element and product isotope values. Applied Geochemistry (32), 175-183 (2013)

Audí-Miró, C., S. Cretnik, C. Torrentó, M. Rosell, O. Shouakar-Stash, N. Otero, J. Palau, M. Elsner and A. Soler: C, Cl and H compound-specific isotope analysis to assess natural versus Fe(0) barrier-induced degradation of chlorinated ethenes at a contaminated site. Journal of Hazardous Materials (299), 747-754, (2015)

Aulenta, F., M. Majone, P. Verbo and V. Tandoi: Complete dechlorination of tetrachloroethene to ethene in presence of methanogenesis and acetogenesis by an anaerobic sediment microcosm. Biodegradation 13 (6), 411-424 (2002)

Badin, A., G. Buttet, J. Maillard, C. Holliger and D. Hunkeler: Multiple Dual C–Cl Isotope Patterns Associated with Reductive Dechlorination of Tetrachloroethene. Environmental Science & Technology 48 (16), 9179-9186 (2014)

Bælum, J., J. C. Chambon, C. Scheutz, P. J. Binning, T. Laier, P. L. Bjerg and C. S. Jacobsen: A conceptual model linking functional gene expression and reductive dechlorination rates of chlorinated ethenes in clay rich groundwater sediment. Water Research 47 (7), 2467-2478 (2013)

Ballapragada, B. S., H. D. Stensel, J. A. Puhakka and J. F. Ferguson: Effect of Hydrogen on Reductive Dechlorination of Chlorinated Ethenes. Environmental Science & Technology 31 (6), 1728-1734 (1997)

Barth, J. A. C., G. Slater, C. Schüth, M. Bill, A. Downey, M. Larkin and R. M. Kalin: Carbon Isotope Fractionation during Aerobic Biodegradation of Trichloroethene by Burkholderia cepacia G4: a Tool To Map Degradation Mechanisms. Applied and Environmental Microbiology 68 (4), 1728-1734 (2002)

Beneteau, K. M., R. Aravena and S. K. Frape: Isotopic characterization of chlorinated solvents-laboratory and field results. Organic Geochemistry 30 (8A), 739-753 (1999)

Bernstein, A., O. Shouakar-Stash, K. Ebert, C. Laskov, D. Hunkeler, S. Jeannottat, K. Sakaguchi-Soeder, J. Laaks, M. A. Jochmann, S. Cretnik, J. Jager, S. B. Haderlein, T. C. Schmidt, R. Aravena and M. Elsner: Compound-Specific Chlorine Isotope Analysis: A Comparison of Gas Chromatography/Isotope Ratio Mass Spectrometry and Gas Chromatography/Quadrupole Mass Spectrometry Methods in an Interlaboratory Study. Analytical Chemistry 83 (20), 7624-7634 (2011)

Bhatt, P., M. S. Kumar, S. Mudliar and T. Chakrabarti: Biodegradation of Chlorinated Compounds—A Review. Critical Reviews in Environmental Science and Technology 37 (2), 165-198 (2006)

BIPM, I., IFCC, ISO, IUPAC, IUPAP, OIML (1993). Guide to the expression of uncertainty in measurement. Geneva, Switzerland, International Organization for Standardization.

Blessing, M., T. C. Schmidt, R. Dinkel and S. B. Haderlein: Delineation of Multiple Chlorinated Ethene Sources in an Industrialized Area - A Forensic Field Study Using Compound-Specific Isotope Analysis. Environmental Science & Technology 43 (8), 2701-2707 (2009)

Bloom, Y., R. Aravena, D. Hunkeler, E. Edwards and S. K. Frape: Carbon isotope fractionation during microbial dechlorination of trichloroethene, cis-1,2-dichloroethene, and vinyl chloride: Implications for assessment of natural attenuation. Environmental Science & Technology 34 (13), 2768-2772 (2000)

Bradley, P. M.: Microbial degradation of chloroethenes in groundwater systems. Hydrogeology Journal 8 (1), 104-111 (2000)

Bradley, P. M.: History and Ecology of Chloroethene Biodegradation: A Review. Bioremediation Journal 7 (2), 81-109 (2003)

Bradley, P. M. and F. H. Chapelle: Microbial Mineralization of VC and DCE Under Different Terminal Electron Accepting Conditions. Anaerobe 4 (2), 81-87 (1998)

Bradley, P. M. and F. H. Chapelle: Aerobic Microbial Mineralization of Dichloroethene as Sole Carbon Substrate. Environmental Science & Technology 34 (1), 221-223 (2000)

Bradley, P. M., F. H. Chapelle and D. R. Lovley: Humic Acids as Electron Acceptors for Anaerobic Microbial Oxidation of Vinyl Chloride and Dichloroethene. Applied and Environmental Microbiology 64 (8), 3102-3105 (1998)

Brand, W., Coplen, T., Vogl, J., Rosner, M., Prohaska, T.: Assessment of international reference materials for isotope-ratio analysis (IUPAC Technical Report). Pure and Applied Chemistry 86 (3), 425-467 (2014)

Broholm, M. M., D. Hunkeler, N. Tuxen, S. Jeannottat and C. Scheutz: Stable carbon isotope analysis to distinguish biotic and abiotic degradation of 1,1,1-trichloroethane in groundwater sediments. Chemosphere 108 (0), 265-273 (2014)

Butler, E. C. and K. F. Hayes: Kinetics of the transformation of trichloroethylene and tetrachloroethylene by iron sulfide. Environmental Science & Technology 33 (12), 2021-2027 (1999)

Butler, E. C. and K. F. Hayes: Factors Influencing Rates and Products in the Transformation of Trichloroethylene by Iron Sulfide and Iron Metal. Environmental Science & Technology 35 (19), 3884-3891 (2001)

Buttet, G. F., C. Holliger and J. Maillard: Functional Genotyping of Sulfurospirillum spp. in Mixed Cultures Allowed the Identification of a New Tetrachloroethene Reductive Dehalogenase. Applied and Environmental Microbiology 79 (22), 6941-6947 (2013)

Caporaso, J. G., Kuczynski, J., Stombaugh, J., Bittinger, K., Bushman, F.D., Costello, E.K., et al.: QIIME allows analysis of high-throughput community sequencing data. Nature Methods 7 (5), 335-336 (2010)

Chapelle, F. H.: Identifying redox conditions that favor the natural attenuation of chlorinated ethenes in contaminated ground-water systems. Symposium on natural attenuation of chlorinated organics in groundwater. U. EPA. Washington, DC, US EPA**:** 17-20.(1996)

Chapelle, F. H. and D. R. Lovley: Rates of Microbial Metabolism in Deep Coastal Plain Aquifers. Applied and Environmental Microbiology 56 (6), 1865-1874 (1990)

Chartrand, M. M. G., A. Waller, T. E. Mattes, M. Elsner, G. Lacrampe-Couloume, J. M. Gossett, E. A. Edwards and B. S. Lollar: Carbon isotopic fractionation during aerobic vinyl chloride degradation. Environmental Science & Technology 39 (4), 1064-1070 (2005)

Chen, Y.-t., J.-t. Li, L.-x. Chen, Z.-s. Hua, L.-n. Huang, J. Liu, B.-b. Xu, B. Liao and W.-s. Shu: Biogeochemical Processes Governing Natural Pyrite Oxidation and Release of Acid Metalliferous Drainage. Environmental Science & Technology 48 (10), 5537-5545 (2014)

Chu, K. H., S. Mahendra, D. L. Song, M. E. Conrad and L. Alvarez-Cohen: Stable carbon isotope fractionation during aerobic biodegradation of chlorinated ethenes. Environmental Science & Technology 38 (11), 3126-3130 (2004)

Cichocka, D., G. l. Imfeld, H.-H. Richnow and I. Nijenhuis: Variability in microbial carbon isotope fractionation of tetra- and trichloroethene upon reductive dechlorination. Chemosphere 71 (4), 639-648 (2008)

Cichocka, D., M. Siegert, G. Imfeld, J. Andert, K. Beck, G. Diekert, H.-H. Richnow and I. Nijenhuis: Factors controlling the carbon isotope fractionation of tetra- and trichloroethene during reductive dechlorination by Sulfurospirillum ssp. and Desulfitobacterium sp. strain PCE-S. FEMS Microbiology Ecology 62 (1), 98-107 (2007)

Cincinelli, A., F. Pieri, Y. Zhang, M. Seed and K. C. Jones: Compound Specific Isotope Analysis (CSIA) for chlorine and bromine: A review of techniques and applications to elucidate environmental sources and processes. Environmental Pollution 169 (0), 112-127 (2012)

Clark, I. D., . Fritz, P.: Environmental isotopes in hydrogeology. Environmental isotopes in hydrogeology, Lewis Publishers, Boca Raton, FL**:** 328.(1997)

Coleman, N. V., T. E. Mattes, J. M. Gossett and J. C. Spain: Biodegradation of cis-Dichloroethene as the Sole Carbon Source by a β-Proteobacterium. Applied and Environmental Microbiology 68 (6), 2726-2730 (2002)

Coplen, T. B.: Guidelines and recommended terms for expression of stable-isotope-ratio and gas-ratio measurement results. Rapid Communications in Mass Spectrometry 25 (17), 2538-2560 (2011)

Cretnik, S., A. Bernstein, O. Shouakar-Stash, F. Löffler and M. Elsner: Chlorine Isotope Effects from Isotope Ratio Mass Spectrometry Suggest Intramolecular C-Cl Bond Competition in Trichloroethene (TCE) Reductive Dehalogenation. Molecules 19 (5), 6450-6473 (2014)

Cretnik, S., K. A. Thoreson, A. Bernstein, K. Ebert, D. Buchner, C. Laskov, S. Haderlein, O. Shouakar-Stash, S. Kliegman, K. McNeill and M. Elsner: Reductive Dechlorination of TCE by Chemical Model Systems in Comparison to Dehalogenating Bacteria: Insights from Dual Element Isotope Analysis (13C/12C, 37Cl/35Cl). Environmental Science & Technology 47 (13), 6855-6863 (2013)

Damgaard, I., P. L. Bjerg, J. Bælum, C. Scheutz, D. Hunkeler, C. S. Jacobsen, N. Tuxen and M. M. Broholm: Identification of chlorinated solvents degradation zones in clay till by high resolution chemical, microbial and compound specific isotope analysis. Journal of Contaminant Hydrology 146, 37-50 (2013)

Damgaard, I., P. L. Bjerg, C. S. Jacobsen, A. Tsitonaki, H. Kerrn-Jespersen and M. M. Broholm: Performance of Full-Scale Enhanced Reductive Dechlorination in Clay Till. Groundwater Monitoring & Remediation 33 (1), 48-61 (2013)

Dayan, H., T. Abrajano, N. C. Sturchio and L. Winsor: Carbon isotopic fractionation during reductive dehalogenation of chlorinated ethenes by metallic iron. Organic Geochemistry 30 (8A), 755-763 (1999)

Doherty, R. E.: A history of the production and use of carbon tetrachloride, tetrachloroethylene, trichloroethylene and 1,1,1-trichloroethane in the United States: Part 2 - Trichloroethylene and 1,1,1-trichloroethane. Environmental Forensics 1 (2), 83-93 (2000)

Doherty, R. E.: The Manufacture, Use, and Supply of Chlorinated Solvents in the United States During World War II. Environmental Forensics 13 (1), 7-26 (2012)

Dong, Y., X. Liang, L. R. Krumholz, R. P. Philp and E. C. Butler: The Relative Contributions of Abiotic and Microbial Processes to the Transformation of Tetrachloroethylene and Trichloroethylene in Anaerobic Microcosms. Environmental Science & Technology 43 (3), 690-697 (2008)

Ducommun, P., X. Boutsiadou and D. Hunkeler: Direct-push multilevel sampling system for unconsolidated aquifers. Hydrogeology Journal 21 (8), 1901-1908 (2013)

EA: An illustrated handbook of DNAPL transport and fate in the subsurface. (2003)

Eberts, S. M., C. Braun and S. Jones: Compound-Specific Isotope Analysis: Questioning the Origins of a Trichloroethene Plume. Environmental Forensics 9 (1), 85-95 (2008)

Edgar, R. C., B. J. Haas, J. C. Clemente, C. Quince and R. Knight: UCHIME improves sensitivity and speed of chimera detection. Bioinformatics 27 (16), 2194-2200 (2011)

Eisenmann, H., Fischer, A.: Isotopenuntersuchungen in der Altlastenbewertung. Handbuch der Altlastensanierung und Flächenmanagement. V. Franzius, Altenbockum, M., Gerhold, T. München, Hüthig Jehle Rehm**:** 47.(2010)

Elsner, M.: Reductive dehalogenation of chlorinated hydrocarbons by surface-bound Fe(II). kinetic and mechanistic aspects. . PhD, Eidgenössische Technische Hochschule Zürich (2002).

Elsner, M.: Stable isotope fractionation to investigate natural transformation mechanisms of organic contaminants: principles, prospects and limitations. Journal of Environmental Monitoring 12 (11), 2005-2031 (2010)

Elsner, M., M. Chartrand, N. Vanstone, G. L. Couloume and B. S. Lollar: Identifying abiotic chlorinated ethene degradation: Characteristic isotope patterns in reaction products with nanoscale zero-valent iron. Environmental Science & Technology 42 (16), 5963-5970 (2008)

Elsner, M., G. L. Couloume and B. Sherwood Lollar: Freezing To Preserve Groundwater Samples and Improve Headspace Quantification Limits of Water-Soluble Organic Contaminants for Carbon Isotope Analysis. Analytical Chemistry 78 (21), 7528-7534 (2006)

Elsner, M. and D. Hunkeler: Evaluating chlorine isotope effects from isotope ratios and mass spectra of polychlorinated molecules. Analytical Chemistry 80 (12), 4731-4740 (2008)

Elsner, M., M. Jochmann, T. Hofstetter, D. Hunkeler, A. Bernstein, T. Schmidt and A. Schimmelmann: Current challenges in compound-specific stable isotope analysis of environmental organic contaminants. Analytical and Bioanalytical Chemistry 403 (9), 2471-2491 (2012)

Elsner, M., L. Zwank, D. Hunkeler and R. P. Schwarzenbach: A new concept linking observable stable isotope fractionation to transformation pathways of organic pollutants. Environmental Science & Technology 39 (18), 6896-6916 (2005)

Fletcher, K. E., I. Nijenhuis, H. H. Richnow and F. E. Löffler: Stable Carbon Isotope Enrichment Factors for cis-1,2-Dichloroethene and Vinyl Chloride Reductive Dechlorination by Dehalococcoides. Environmental Science & Technology 45 (7), 2951-2957 (2011)

Flynn, S. J., F. E. Löffler and J. M. Tiedje: Microbial Community Changes Associated with a Shift from Reductive Dechlorination of PCE to Reductive Dechlorination of cis-DCE and VC. Environmental Science & Technology 34 (6), 1056-1061 (2000)

FOEN: Guide des hydrocarbures chlorés, propriétés et comportement dans l'environnement. (2008 (revised 2009))

FOEN, A.: A network for groundwater protection, ChloroNet. (2015)

Friis, A. K., H. J. Albrechtsen, G. Heron and P. L. Bjerg: Redox Processes and Release of Organic Matter after Thermal Treatment of a TCE-Contaminated Aquifer. Environmental Science & Technology 39 (15), 5787-5795 (2005)

Glod, G., W. Angst, C. Holliger and R. P. Schwarzenbach: Corrinoid-Mediated Reduction of Tetrachloroethene, Trichloroethene, and Trichlorofluoroethene in Homogeneous Aqueous Solution: Reaction Kinetics and Reaction Mechanisms. Environmental Science & Technology 31 (1), 253-260 (1997)

Glod, G., U. Brodmann, W. Angst, C. Holliger and R. P. Schwarzenbach: Cobalamin-Mediated Reduction of cis- and trans-Dichloroethene, 1,1-Dichloroethene, and Vinyl Chloride in Homogeneous Aqueous Solution: Reaction Kinetics and Mechanistic Considerations. Environmental Science & Technology 31 (11), 3154-3160 (1997)

Godin, J.-P. and J. S. O. McCullagh: Review: Current applications and challenges for liquid chromatography coupled to isotope ratio mass spectrometry (LC/IRMS). Rapid Communications in Mass Spectrometry 25 (20), 3019-3028 (2011)

Gossett, J. M.: Sustained Aerobic Oxidation of Vinyl Chloride at Low Oxygen Concentrations. Environmental Science & Technology 44 (4), 1405-1411 (2010)

Gossett, J. M., Zinder, S.H.: Microbiological aspects relevant to natural attenuation of chlorinated ethenes. Symposium on natural attenuation of chlorinated organics in groundwater. U. EPA. Washington, DC, US EPA**:** 10-13.(1996)

Haas, B. J., D. Gevers, A. M. Earl, M. Feldgarden, D. V. Ward, G. Giannoukos, D. Ciulla, D. Tabbaa, S. K. Highlander, E. Sodergren, B. Methé, T. Z. DeSantis, T. H. M. Consortium, J. F. Petrosino, R. Knight and B. W. Birren: Chimeric 16S rRNA sequence formation and detection in Sanger and 454-pyrosequenced PCR amplicons. Genome Research 21 (3), 494-504 (2011)

Hartmans, S. and J. A. De Bont: Aerobic vinyl chloride metabolism in Mycobacterium aurum L1. Applied and Environmental Microbiology 58 (4), 1220-1226 (1992)

Hartmans, S., J. A. M. de Bont, J. Tramper and K. C. A. M. Luyben: Bacterial degradation of vinyl chloride. Biotechnology Letters 7 (6), 383-388 (1985)

Hirschorn, S. K., M. J. Dinglasan, M. Elsner, S. A. Mancini, G. Lacrampe-Couloume, E. A. Edwards and B. S. Lollar: Pathway dependent isotopic fractionation during aerobic biodegradation of 1,2-dichloroethane. Environmental Science & Technology 38 (18), 4775-4781 (2004)

Hitzfeld, K. L., M. Gehre and H.-H. Richnow: A novel online approach to the determination of isotopic ratios for organically bound chlorine, bromine and sulphur. Rapid Communications in Mass Spectrometry 25 (20), 3114-3122 (2011)

Hoelen, T. P. and M. Reinhard: Complete Biological Dehalogenation of Chlorinated Ethylenes in Sulfate Containing Groundwater. Biodegradation 15 (6), 395-403 (2004)

Höhener, P. and O. Atteia: Multidimensional analytical models for isotope ratios in groundwater pollutant plumes of organic contaminants undergoing different biodegradation kinetics. Advances in Water Resources 33 (7), 740-751 (2010)

Holt, B. D., N. C. Sturchio, T. A. Abrajano and L. J. Heraty: Conversion of chlorinated volatile organic compounds to carbon dioxide and methyl chloride for isotopic analysis of carbon and chlorine. Analytical Chemistry 69 (14), 2727-2733 (1997)

Hug, L. A., F. Maphosa, D. Leys, F. E. Löffler, H. Smidt, E. A. Edwards and L. Adrian: Overview of organohalide-respiring bacteria and a proposal for a classification system for reductive dehalogenases. Philosophical Transactions of the Royal Society B: Biological Sciences 368 (1616) (2013)

Huling, S. G., Pivetz, B.E.: In-situ chemical oxidation. EPA/600/R-06/072. U. EPA. Cincinnati, US EPA.(2006)

Hunkeler, D., Y. Abe, M. M. Broholm, S. Jeannottat, C. Westergaard, C. S. Jacobsen, R. Aravena and P. L. Bjerg: Assessing chlorinated ethene degradation in a large scale contaminant plume by dual carbon-chlorine isotope analysis and quantitative PCR. Journal of Contaminant Hydrology 119 (1-4), 69-79 (2011)

Hunkeler, D., Y. Abe, M. M. Broholm, S. Jeannottat, C. Westergaard, C. S. Jacobsen, R. Aravena and P. L. Bjerg: Assessing chlorinated ethene degradation in a large scale contaminant plume by dual carbon–chlorine isotope analysis and quantitative PCR. Journal of Contaminant Hydrology 119 (1–4), 69-79 (2011)

Hunkeler, D., R. Aravena and B. J. Butler: Monitoring microbial dechlorination of tetrachloroethene (PCE) in groundwater using compound-specific stable carbon isotope ratios: Microcosm and field studies. Environmental Science & Technology 33 (16), 2733-2738 (1999)

Hunkeler, D., R. Aravena and E. Cox: Carbon isotopes as a tool to evaluate the origin and fate of vinyl chloride: Laboratory experiments and modeling of isotope evolution. Environmental Science & Technology 36 (15), 3378-3384 (2002)

Hunkeler, D., R. Aravena, B. L. Parker, J. A. Cherry and X. Diao: Monitoring Oxidation of Chlorinated Ethenes by Permanganate in Groundwater Using Stable Isotopes: Laboratory and Field Studies. Environmental Science & Technology 37 (4), 798-804 (2003)

Hunkeler, D., R. Aravena, O. Shouakar-Stash, N. Weisbrod, A. Nasser, L. Netzer and D. Ronen: Carbon and Chlorine Isotope Ratios of Chlorinated Ethenes Migrating through a Thick Unsaturated Zone of a Sandy Aquifer. Environmental Science & Technology 45 (19), 8247-8253 (2011)

Hunkeler, D., N. Chollet, X. Pittet, R. Aravena, J. A. Cherry and B. L. Parker: Effect of source variability and transport processes on carbon isotope ratios of TCE and PCE in two sandy aquifers. Journal of Contaminant Hydrology 74 (1–4), 265-282 (2004)

Hunkeler, D., N. Chollet, X. Pittet, R. Aravena, J. A. Cherry and B. L. Parker: Effect of source variability and transport processes on carbon isotope ratios of TCE and PCE in two sandy aquifers. Journal of Contaminant Hydrology 74 (1-4), 265-282 (2004)

Hunkeler, D., M. Elsner, C. M. Aelion, P. Hohener, D. Hunkeler and R. Aravena: Environmental Isotopes in Biodegradation and Bioremediation (2010).

Hunkeler, D., T. Laier, F. Breider and O. S. Jacobsen: Demonstrating a Natural Origin of Chloroform in Groundwater Using Stable Carbon Isotopes. Environmental Science & Technology 46 (11), 6096-6101 (2012)

Hunkeler, D., R. U. Meckenstock, B. Sherwood-Lollar, T. Schmidt and J. T. Wilson: A Guide for Assessing Biodegradation and Source Identification of Organic Groundwater Contaminant using Compound Specific Isotope Analysis (CSIA) (2008).

Hunkeler, D., Meckenstock, R.U., Lollar Sherwood, B., Schmidt, T.C., Wilson, J.T. (2008). A Guide for Assessing Biodegradation and Source Identification of Organic Groundwater Contaminants Using Compound Specific Isotope Analysis (CSIA), Environmental Protection Agency. EPA/600/R-08/148.

Hunkeler, D., B. M. Van Breukelen and M. Elsner: Modeling Chlorine Isotope Trends during Sequential Transformation of Chlorinated Ethenes. Environmental Science & Technology 43 (17), 6750-6756 (2009)

Hwang, H.-T., S.-W. Jeen, E. A. Sudicky and W. A. Illman: Determination of rate constants and branching ratios for TCE degradation by zero-valent iron using a chain decay multispecies model. Journal of Contaminant Hydrology(0)

Imfeld, G., I. Nijenhuis, M. Nikolausz, S. Zeiger, H. Paschke, J. Drangmeister, J. Grossmann, H. H. Richnow and S. Weber: Assessment of in situ degradation of chlorinated ethenes and bacterial community structure in a complex contaminated groundwater system. Water Research 42 (4–5), 871-882 (2008)

ITRC, I. S. C. O. T. (2005). Technical and regulatory guidance for In Situ Chemical Oxidation of contaminated soil and groundwater. ITRC. USA. 2nd Ed. ISCO-2.

ITRC, P. R. B. W. G. (1999). Regulatory guidance for permeable reactive barriers designed to remediate chlorinated solvents. ITRC. USA.

Jablonski, P. E. and J. G. Ferry: Reductive dechlorination of trichloroethylene by the CO-reduced CO dehydrogenase enzyme complex from Methanosarcina thermophila. FEMS Microbiology Letters 96 (1), 55-59 (1992)

Jeannottat, S. and D. Hunkeler: Chlorine and Carbon Isotopes Fractionation during Volatilization and Diffusive Transport of Trichloroethene in the Unsaturated Zone. Environmental Science & Technology 46 (6), 3169-3176 (2012)

Jeannottat, S. and D. Hunkeler: Can Soil Gas VOCs be Related to Groundwater Plumes Based on Their Isotope Signature? Environmental Science & Technology 47 (21), 12115-12122 (2013)

Jendrzejewski, N., H. G. M. Eggenkamp and M. L. Coleman: Sequential determination of chlorine and carbon isotopic composition in single microliter samples of chlorinated solvent. Analytical Chemistry 69 (20), 4259-4266 (1997)

Jendrzejewski, N., H. G. M. Eggenkamp and M. L. Coleman: Characterisation of chlorinated hydrocarbons from chlorine and carbon isotopic compositions: scope of application to environmental problems. Applied Geochemistry 16 (9-10), 1021-1031 (2001)

Jeong, H. Y., K. Anantharaman, Y.-S. Han and K. F. Hayes: Abiotic Reductive Dechlorination of cis-Dichloroethylene by Fe Species Formed during Iron- or Sulfate-Reduction. Environmental Science & Technology 45 (12), 5186-5194 (2011)

Jin, B., S. B. Haderlein and M. Rolle: Integrated Carbon and Chlorine Isotope Modeling: Applications to Chlorinated Aliphatic Hydrocarbons Dechlorination. Environmental Science & Technology 47 (3), 1443-1451 (2013)

Jin, B. A., C. Laskov, M. Rolle and S. B. Haderlein: Chlorine Isotope Analysis of Organic Contaminants Using GC-qMS: Method Optimization and Comparison of Different Evaluation Schemes. Environmental Science & Technology 45 (12), 5279-5286 (2011)

Jochmann, M. A., M. Blessing, S. B. Haderlein and T. C. Schmidt: A new approach to determine method detection limits for compound-specific isotope analysis of volatile organic compounds. Rapid Communications in Mass Spectrometry 20 (24), 3639-3648 (2006)

Kaown, D., O. Shouakar-Stash, J. Yang, Y. Hyun and K.-K. Lee: Identification of Multiple Sources of Groundwater Contamination by Dual Isotopes. Groundwater 52 (6), 875-885 (2014)

Kilchmann, S., Reinhardt, M., Schürch, M., Traber, D (2009). Résultats de l'observatoire national des eaux souterraines (NAQUA) - Etat et évolution de 2004 à 2006. Berne, Office fédéral de l'environnement.

Kliegman, S. and K. McNeill: Dechlorination of chloroethylenes by cob(i)alamin and cobalamin model complexes. Dalton Transactions(32), 4191-4201 (2008)

Komárek, M., V. Ettler, V. Chrastný and M. Mihaljevič: Lead isotopes in environmental sciences: A review. Environment International 34 (4), 562-577 (2008)

Kompala, D. S., D. Ramkrishna and G. T. Tsao: Cybernetic modeling of microbial growth on multiple substrates. Biotechnology and Bioengineering 26 (11), 1272-1281 (1984)

Krajmalnik-Brown, R., T. Hölscher, I. N. Thomson, F. M. Saunders, K. M. Ritalahti and F. E. Löffler: Genetic Identification of a Putative Vinyl Chloride Reductase in Dehalococcoides sp. Strain BAV1. Applied and Environmental Microbiology 70 (10), 6347-6351 (2004)

Krause, P., D. P. Boyle and F. Bäse: Comparison of different efficiency criteria for hydrological model assessment. Adv. Geosci. 5, 89-97 (2005)

Kuder, T. and P. Philp: Demonstration of Compound-Specific Isotope Analysis of Hydrogen Isotope Ratios in Chlorinated Ethenes. Environmental Science & Technology 47 (3), 1461-1467 (2013)

Kuder, T., B. M. van Breukelen, M. Vanderford and P. Philp: 3D-CSIA: Carbon, Chlorine, and Hydrogen Isotope Fractionation in Transformation of TCE to Ethene by a Dehalococcoides Culture. Environmental Science & Technology 47 (17), 9668-9677 (2013)

Labeeuw, V. (2013). In situ chemical reduction using zero valent iron injection - a technique for the remediation of source zones. CityChlor.

Lee, P. K. H., M. E. Conrad and L. Alvarez-Cohen: Stable carbon isotope fractionation of chloroethenes by dehalorespiring isolates. Environmental Science & Technology 41 (12), 4277-4285 (2007)

Lee, W. and B. Batchelor: Abiotic Reductive Dechlorination of Chlorinated Ethylenes by Iron-Bearing Soil Minerals. 1. Pyrite and Magnetite. Environmental Science & Technology 36 (23), 5147-5154 (2002)

Lee, W. and B. Batchelor: Abiotic Reductive Dechlorination of Chlorinated Ethylenes by Iron-Bearing Soil Minerals. 2. Green Rust. Environmental Science & Technology 36 (24), 5348-5354 (2002)

Liang, X., Y. Dong, T. Kuder, L. R. Krumholz, R. P. Philp and E. C. Butler: Distinguishing Abiotic and Biotic Transformation of Tetrachloroethylene and Trichloroethylene by Stable Carbon Isotope Fractionation. Environmental Science & Technology 41 (20), 7094-7100 (2007)

Liang, X., R. Paul Philp and E. C. Butler: Kinetic and isotope analyses of tetrachloroethylene and trichloroethylene degradation by model Fe(II)-bearing minerals. Chemosphere 75 (1), 63-69 (2009)

Liedekerke, M., Prokop, G., Rabl-Berger, S., Kibblewhite, M., Louwagie, G.: Progress in the management of contaminated sites in Europe. (2014)

Liu, Y., Y. Gan, A. Zhou, C. Liu, X. Li and T. Yu: Carbon and chlorine isotope fractionation during Fenton-like degradation of trichloroethene. Chemosphere 107, 94-100 (2014)

Löffler, F. E., Ritalahti, K.M., Zinder, S.H.: *Dehalococcoides* and reductive dechlorination of chlorinated solvents. SERDP ESTCP Environmental Remediation Technology. H. F. Stroo, Leeson, A., Ward, C.H. New York, NY, Springer. Bioaugmentation for Groundwater Remediation**:** 39-88.(2013)

Lojkasek-Lima, P., R. Aravena, B. L. Parker and J. A. Cherry: Fingerprinting TCE in a Bedrock Aquifer Using Compound-Specific Isotope Analysis. Ground water 50 (5), 754-764 (2012)

Lojkasek-Lima, P., R. Aravena, O. Shouakar-Stash, S. K. Frape, M. Marchesi, S. Fiorenza and J. Vogan: Ground Water Monit. Rem. 32, 53 (2012)

Lollar, B. S., G. F. Slater, J. Ahad, B. Sleep, J. Spivack, M. Brennan and P. MacKenzie: Contrasting carbon isotope fractionation during biodegradation of trichloroethylene and toluene: Implications for intrinsic bioremediation. Organic Geochemistry 30 (8A), 813-820 (1999)

Luijten, M. L. G. C., J. de Weert, H. Smidt, H. T. S. Boschker, W. M. de Vos, G. Schraa and A. J. M. Stams: Description of Sulfurospirillum halorespirans sp. nov., an anaerobic, tetrachloroethene-respiring bacterium, and transfer of Dehalospirillum multivorans to the genus Sulfurospirillum as Sulfurospirillum multivorans comb. nov. International Journal of Systematic and Evolutionary Microbiology 53 (3), 787-793 (2003)

Madsen, E. L.: Determining in situ biodegradation. Environmental Science & Technology 25 (10), 1662-1673 (1991)

Marchesi, M., R. Aravena, K. S. Sra, N. R. Thomson, N. Otero, A. Soler and S. Mancini: Carbon isotope fractionation of chlorinated ethenes during oxidation by Fe2+ activated persulfate. Science of The Total Environment 433 (0), 318-322 (2012)

Martins, P., D. F. R. Cleary, A. C. C. Pires, A. M. Rodrigues, V. Quintino, R. Calado and N. C. M. Gomes: Molecular Analysis of Bacterial Communities and Detection of Potential Pathogens in a Recirculating Aquaculture System for *Scophthalmus maximus* and *Solea senegalensis*. PLoS ONE 8 (11), e80847 (2013)

Marzorati, M., F. de Ferra, H. Van Raemdonck, S. Borin, E. Allifranchini, G. Carpani, L. Serbolisca, W. Verstraete, N. Boon and D. Daffonchio: A Novel Reductive Dehalogenase, Identified in a Contaminated Groundwater Enrichment Culture and in Desulfitobacterium dichloroeliminans Strain DCA1, Is Linked to Dehalogenation of 1,2-Dichloroethane. Applied and Environmental Microbiology 73 (9), 2990-2999 (2007)

Maymo-Gatell, X., Y.-t. Chien, J. M. Gossett and S. H. Zinder: Isolation of a Bacterium That Reductively Dechlorinates Tetrachloroethene to Ethene. Science 276 (5318), 1568-1571 (1997)

McHugh, T., T. Kuder, S. Fiorenza, K. Gorder, E. Dettenmaier and P. Philp: Application of CSIA to Distinguish Between Vapor Intrusion and Indoor Sources of VOCs. Environmental Science & Technology 45 (14), 5952-5958 (2011)

Meckenstock, R. U., M. Elsner, C. Griebler, T. Lueders, C. Stumpp, W. Dejonghe, L. L. Bastiaens, D. Springael, E. Smolders, N. Boon, S. N. Agathos, S. R. Sorensen, J. Aamand, H. J. Albrechtsen, P. L. Bjerg, S. Schmidt, W. E. Huang and B. M. Van Breukelen: Biodegradation: Updating the concepts of control for microbial clean-up in contaminated aquifers. Environmental Science & Technology (2015)

Meckenstock, R. U., B. Morasch, C. Griebler and H. H. Richnow: Stable isotope fractionation analysis as a tool to monitor biodegradation in contaminated acquifers. Journal of Contaminant Hydrology 75 (3-4), 215-255 (2004)

MEDD: Biodégradation des solvants chlorés en conditions naturelles, mécanismes et caractérisation, synthèse bibliographique. (2004)

Middeldorp, P. J. M., M. L. G. C. Luijten, B. A. v. d. Pas, M. H. A. v. Eekert, S. W. M. Kengen, G. Schraa and A. J. M. Stams: Anaerobic Microbial Reductive Dehalogenation of Chlorinated Ethenes. Bioremediation Journal 3 (3), 151-169 (1999)

Moran, M. J., J. S. Zogorski and P. J. Squillace: Chlorinated Solvents in Groundwater of the United States. Environmental Science & Technology 41 (1), 74-81 (2007)

Müller, J. A., B. M. Rosner, G. von Abendroth, G. Meshulam-Simon, P. L. McCarty and A. M. Spormann: Molecular Identification of the Catabolic Vinyl Chloride Reductase from Dehalococcoides sp. Strain VS and Its Environmental Distribution. Applied and Environmental Microbiology 70 (8), 4880-4888 (2004)

Neumann, A., G. Wohlfarth and G. Diekert: Tetrachloroethene Dehalogenase from Dehalospirillum multivorans: Cloning, Sequencing of the Encoding Genes, and Expression of the pceA Gene in Escherichia coli. Journal of Bacteriology 180 (16), 4140-4145 (1998)

Newmark, R. L., Aines, R.D. (1995). Summary of the LLNL gasoline spill demonstration - dynamic underground stripping project. U. S. D. o. Energy, Lawrence Livermore National Laboratory.

Nijenhuis, I., J. Andert, K. Beck, M. Kastner, G. Diekert and H. H. Richnow: Stable isotope fractionation of tetrachloroethene during reductive dechlorination by Sulfurospirillum multivorans and Desulfitobacterium sp strain PCE-S and abiotic reactions with cyanocobalamin. Applied and Environmental Microbiology 71 (7), 3413-3419 (2005)

Nijenhuis, I., M. Schmidt, E. Pellegatti, E. Paramatti, H. H. Richnow and A. Gargini: A stable isotope approach for source apportionment of chlorinated ethene plumes at a complex multi-contamination events urban site. Journal of Contaminant Hydrology 153 (0), 92-105 (2013)

Nonaka, H., G. Keresztes, Y. Shinoda, Y. Ikenaga, M. Abe, K. Naito, K. Inatomi, K. Furukawa, M. Inui and H. Yukawa: Complete Genome Sequence of the Dehalorespiring Bacterium Desulfitobacterium hafniense Y51 and Comparison with Dehalococcoides ethenogenes 195. Journal of Bacteriology 188 (6), 2262-2274 (2006)

Novais, R. C. and Y. R. Thorstenson: The evolution of Pyrosequencing® for microbiology: From genes to genomes. Journal of Microbiological Methods 86 (1), 1-7 (2011)

Numata, M., N. Nakamura, H. Koshikawa and Y. Terashima: Chlorine isotope fractionation during reductive dechlorination of chlorinated ethenes by anaerobic bacteria. Environmental Science & Technology 36 (20), 4389-4394 (2002)

O'Sullivan, G. and R. M. Kalin: Investigation of the Range of Carbon and Hydrogen Isotopes Within a Global Set of Gasolines. Environmental Forensics 9 (2-3), 166-176 (2008)

Oldenhuis, R., R. L. Vink, D. B. Janssen and B. Witholt: Degradation of chlorinated aliphatic hydrocarbons by Methylosinus trichosporium OB3b expressing soluble methane monooxygenase. Applied and Environmental Microbiology 55 (11), 2819-2826 (1989)

OSEC: Ordonnance du Département Fédéral de l'Intérieur sur les substances étrangères et les composants dans les denrées alimentaires (OSEC). 817.021.23 (1995)

OSites (1998). Ordonnance sur l'assainissement des sites pollués (OSites). 814.680. L. c. f. suisse. Bern, Le conseil fédéral suisse.

Palau, J., M. Marchesi, J. C. C. Chambon, R. Aravena, À. Canals, P. J. Binning, P. L. Bjerg, N. Otero and A. Soler: Multi-isotope (carbon and chlorine) analysis for fingerprinting and site characterization at a fractured bedrock aquifer contaminated by chlorinated ethenes. Science of The Total Environment 475 (0), 61-70 (2014)

Pankow, J. F. and J. A. Cherry: Dense chlorinated solvents and other DNAPLs in groundwater: history, behavior, and remediation, Waterloo Press (1996).

Patterson, B. M., R. Aravena, G. B. Davis, A. J. Furness, T. P. Bastow and D. Bouchard: Multiple lines of evidence to demonstrate vinyl chloride aerobic biodegradation in the vadose zone, and factors controlling rates. Journal of Contaminant Hydrology 153, 69-77 (2013)

Paul, E. A. a. C., F.E.: Soil microbiology and biochemistry. San Diego, CA, USA (1996).

Pilloni, G., M. S. Granitsiotis, M. Engel and T. Lueders: Testing the Limits of 454 Pyrotag Sequencing: Reproducibility, Quantitative Assessment and Comparison to T-RFLP Fingerprinting of Aquifer Microbes. PLoS ONE 7 (7), e40467 (2012)

Postma, D., Boesen, C., Kristiansen, H., Larsen, F.: Nitrate Reduction in an Unconfined Sandy Aquifer: Water Chemistry, Reduction Processes, and Geochemical Modeling. Water Resources Research 27 (8), 1944-7973 (1991)

Poulson, S. R. and H. Naraoka: Carbon Isotope Fractionation during Permanganate Oxidation of Chlorinated Ethylenes (cDCE, TCE, PCE). Environmental Science & Technology 36 (15), 3270-3274 (2002)

R.P, P.: Application of stable isotopes and radioisotopes in environmental forensics. Introduction to Environmental Forensics. R. D. M. E. B.L. Murphy. China**:** 99-136.(2002)

Reddy, C., N. Drenzek, T. Eglinton, L. Heraty, N. Sturchio and V. Shiner: Stable chlorine intramolecular kinetic isotope effects from the abiotic dehydrochlorination of DDT. Environmental Science and Pollution Research 9 (3), 183-186 (2002)

Reese, B., A. Witmer, S. Moller, J. Morse and H. Mills: Molecular assays advance understanding of sulfate reduction despite cryptic cycles. Biogeochemistry 118 (1-3), 307-319 (2014)

Renpenning, J., S. Keller, S. Cretnik, O. Shouakar-Stash, M. Elsner, T. Schubert and I. Nijenhuis: Combined C and Cl Isotope Effects Indicate Differences between Corrinoids and Enzyme (Sulfurospirillum multivorans PceA) in Reductive Dehalogenation of Tetrachloroethene, But Not Trichloroethene. Environmental Science & Technology 48 (20), 11837-11845 (2014)

Richardson, R. E.: Genomic insights into organohalide respiration. Current Opinion in Biotechnology 24 (3), 498-505 (2013)

Rügner, H., M. Finkel, A. Kaschl and M. Bittens: Application of monitored natural attenuation in contaminated land management—A review and recommended approach for Europe. Environmental Science & Policy 9 (6), 568-576 (2006)

Rupakula, A., T. Kruse, S. Boeren, C. Holliger, H. Smidt and J. Maillard: The restricted metabolism of the obligate organohalide respiring bacterium Dehalobacter restrictus: lessons from tiered functional genomics. Philosophical Transactions of the Royal Society B: Biological Sciences 368 (1616), 20120325 (2013)

Sakaguchi-Söder, K., J. Jager, H. Grund, F. Matthäus and C. Schüth: Monitoring and evaluation of dechlorination processes using compound-specific chlorine isotope analysis. Rapid Communications in Mass Spectrometry 21 (18), 3077-3084 (2007)

Scheutz, C., N. d. Durant, P. Dennis, M. H. Hansen, T. Jørgensen, R. Jakobsen, E. e. Cox and P. L. Bjerg: Concurrent Ethene Generation and Growth of Dehalococcoides Containing Vinyl Chloride Reductive Dehalogenase Genes During an Enhanced Reductive Dechlorination Field Demonstration. Environmental Science & Technology 42 (24), 9302-9309 (2008)

Schmidt, T. C., L. Zwank, M. Elsner, M. Berg, R. U. Meckenstock and S. B. Haderlein: Compound-specific stable isotope analysis of organic contaminants in natural environments: a critical review of the state of the art, prospects, and future challenges. Anal Bioanal Chem 378 (2), 283-300 (2004)

Schmitz, R. P. H., J. Wolf, A. Habel, A. Neumann, K. Ploss, A. Svatos, W. Boland and G. Diekertt: Evidence for a radical mechanism of the dechlorination of chlorinated propenes mediated by the

tetrachloroethene reductive dehalogenase of Sulfurospirillum multivorans. Environmental Science & Technology 41 (21), 7370-7375 (2007)

Seshadri, R., L. Adrian, D. E. Fouts, J. A. Eisen, A. M. Phillippy, B. A. Methe, N. L. Ward, W. C. Nelson, R. T. Deboy, H. M. Khouri, J. F. Kolonay, R. J. Dodson, S. C. Daugherty, L. M. Brinkac, S. A. Sullivan, R. Madupu, K. E. Nelson, K. H. Kang, M. Impraim, K. Tran, J. M. Robinson, H. A. Forberger, C. M. Fraser, S. H. Zinder and J. F. Heidelberg: Genome Sequence of the PCE-Dechlorinating Bacterium Dehalococcoides ethenogenes. Science 307 (5706), 105-108 (2005)

Seyedabbasi, M. A., C. J. Newell, D. T. Adamson and T. C. Sale: Relative contribution of DNAPL dissolution and matrix diffusion to the long-term persistence of chlorinated solvent source zones. Journal of Contaminant Hydrology 134–135, 69-81 (2012)

Shani, N.: Assessing the Bacterial Ecology of Organohalide Respiration for the Design of Bioremediation Strategies Book (2012)

Shani, N., P. Rossi and C. Holliger: Correlations between Environmental Variables and Bacterial Community Structures Suggest Fe(III) and Vinyl Chloride Reduction As Antagonistic Terminal Electron-Accepting Processes. Environmental Science & Technology 47 (13), 6836-6845 (2013)

Shouakar-Stash, O., R. J. Drimmie, M. Zhang and S. K. Frape: Compound-specific chlorine isotope ratios of TCE, PCE and DCE isomers by direct injection using CF-IRMS. Applied Geochemistry 21 (5), 766-781 (2006)

Shouakar-Stash, O., S. K. Frape and R. J. Drimmie: Stable hydrogen, carbon and chlorine isotope measurements of selected chlorinated organic solvents. Journal of Contaminant Hydrology 60 (3-4), 211-228 (2003)

Slater, G. F., J. M. E. Ahad, B. Sherwood Lollar, R. Allen-King and B. Sleep: Carbon Isotope Effects Resulting from Equilibrium Sorption of Dissolved VOCs. Analytical Chemistry 72 (22), 5669-5672 (2000)

Slater, G. F., H. S. Dempster, B. S. Lollar and J. Ahad: Headspace analysis: A new application for isotopic characterization of dissolved organic contaminants. Environmental Science & Technology 33 (1), 190-194 (1999)

Sleep, B. E. and Y. Ma: Thermal variation of organic fluid properties and impact on thermal remediation feasibility. Journal of Soil Contamination 6 (3), 281-306 (1997)

Smits, T. H. M., Assal, A., Hunkeler, D., Holliger, C.: Anaerobic degradation of vinyl chloride in aquifer microcosms. Journal of Environmental Quality 40, 915-922 (2011)

Stroo, H. F., Ward, C.H.: In situ remediation of chlorinated solvent plumes, Springer (2010).

Su, C. and R. W. Puls: Kinetics of Trichloroethene Reduction by Zerovalent Iron and Tin: Pretreatment Effect, Apparent Activation Energy, and Intermediate Products. Environmental Science & Technology 33 (1), 163-168 (1999)

Suarez, M. P. and H. S. Rifai: Biodegradation Rates for Fuel Hydrocarbons and Chlorinated Solvents in Groundwater. Bioremediation Journal 3 (4), 337-362 (1999)

Sung, Y., K. E. Fletcher, K. M. Ritalahti, R. P. Apkarian, N. Ramos-HernÃ¡ndez, R. A. Sanford, N. M. Mesbah and F. E. Löffler: Geobacter lovleyi sp. nov. Strain SZ, a Novel Metal-Reducing and Tetrachloroethene-Dechlorinating Bacterium. Applied and Environmental Microbiology 72 (4), 2775-2782 (2006)

Sung, Y., K. M. Ritalahti, R. A. Sanford, J. W. Urbance, S. J. Flynn, J. M. Tiedje and F. E. Löffler: Characterization of Two Tetrachloroethene-Reducing, Acetate-Oxidizing Anaerobic Bacteria and Their Description as Desulfuromonas michiganensis sp. nov. Applied and Environmental Microbiology 69 (5), 2964-2974 (2003)

Suyama, A., M. Yamashita, S. Yoshino and K. Furukawa: Molecular Characterization of the PceA Reductive Dehalogenase of Desulfitobacterium sp. Strain Y51. Journal of Bacteriology 184 (13), 3419-3425 (2002)

Świderek, K. and P. Paneth: Extending Limits of Chlorine Kinetic Isotope Effects. The Journal of Organic Chemistry 77 (11), 5120-5124 (2012)

Terzenbach, D. P. and M. Blaut: Transformation of tetrachloroethylene to trichloroethylene by homoacetogenic bacteria (1994).

Thullner, M., F. Centler, H.-H. Richnow and A. Fischer: Quantification of organic pollutant degradation in contaminated aquifers using compound specific stable isotope analysis – Review of recent developments. Organic Geochemistry 42 (12), 1440-1460 (2012)

Thullner, M., A. Fischer, H.-H. Richnow and L. Wick: Influence of mass transfer on stable isotope fractionation. Applied Microbiology and Biotechnology 97 (2), 441-452 (2013)

Tiehm, A. and K. R. Schmidt: Sequential anaerobic/aerobic biodegradation of chloroethenes—aspects of field application. Current Opinion in Biotechnology 22 (3), 415-421 (2011)

Tiehm, A., K. R. Schmidt, B. Pfeifer, M. Heidinger and S. Ertl: Growth kinetics and stable carbon isotope fractionation during aerobic degradation of cis-1,2-dichloroethene and vinyl chloride. Water Research 42 (10-11), 2431-2438 (2008)

Tobiszewski, M. and J. Namieśnik: Abiotic degradation of chlorinated ethanes and ethenes in water. Environmental Science and Pollution Research International 19 (6), 1994-2006 (2012)

USEPA (1993). DNAPL site evaluation. E. r. laboratory, U.S. Environmental Protection Agency.

Van Breukelen, B. M.: Extending the Rayleigh Equation to Allow Competing Isotope Fractionating Pathways to Improve Quantification of Biodegradation. Environmental Science & Technology 41 (11), 4004-4010 (2007)

Van Breukelen, B. M., D. Hunkeler and F. Volkering: Quantification of Sequential Chlorinated Ethene Degradation by Use of a Reactive Transport Model Incorporating Isotope Fractionation. Environmental Science & Technology 39 (11), 4189-4197 (2005)

Van Breukelen, B. M. and M. Rolle: Transverse Hydrodynamic Dispersion Effects on Isotope Signals in Groundwater Chlorinated Solvents' Plumes. Environmental Science & Technology 46 (14), 7700-7708 (2012)

van der Zaan, B., F. Hannes, N. Hoekstra, H. Rijnaarts, W. M. de Vos, H. Smidt and J. Gerritse: Correlation of Dehalococcoides 16S rRNA and Chloroethene-Reductive Dehalogenase Genes with Geochemical Conditions in Chloroethene-Contaminated Groundwater. Applied and Environmental Microbiology 76 (3), 843-850 (2010)

VanStone, N. A., R. M. Focht, S. A. Mabury and B. S. Lollar: Effect of Iron Type on Kinetics and Carbon Isotopic Enrichment of Chlorinated Ethylenes During Abiotic Reduction on Fe(0). Ground Water 42 (2), 268-276 (2004)

vanWarmerdam, E. M., Frape, S. K., Aravena, R., Drimmie, R. J., Flatt, H., Cherry, J. A.: Stable chlorine and carbon isotope measurements of selected chlorinated organic solvents. Applied Geochemistry 10 (5), 547-552 (1995)

Vogel, T. M., C. S. Criddle and P. L. McCarty: ES Critical Reviews: Transformations of halogenated aliphatic compounds. Environmental Science & Technology 21 (8), 722-736 (1987)

von Schnakenburg, P. (2013). In situ thermal remediation of contaminated sites - A technique for the remediation of source zones. CityChlor.

Wagner, D., L. Hug, J. Hatt, M. Spitzmiller, E. Padilla-Crespo, K. Ritalahti, E. Edwards, K. Konstantinidis and F. Löffler: Genomic determinants of organohalide-respiration in Geobacter lovleyi, an unusual member of the Geobacteraceae. BMC Genomics 13 (1), 1-17 (2012)

Wang, Q., G. M. Garrity, J. M. Tiedje and J. R. Cole: Naïve Bayesian Classifier for Rapid Assignment of rRNA Sequences into the New Bacterial Taxonomy. Applied and Environmental Microbiology 73 (16), 5261-5267 (2007)

Wanner, P. and D. Hunkeler: Carbon and chlorine isotopologue fractionation of chlorinated hydrocarbons during diffusion in water and low permeability sediments. Geochimica et Cosmochimica Acta 157 (0), 198-212 (2015)

Wiedemeier, T. H., C. J. Newell, H. S. Rifai and J. T. Wilson: Natural attenuation of fuels and chlorinated solvents (1999).

Wiegert, C., C. Aeppli, T. Knowles, H. Holmstrand, R. Evershed, R. D. Pancost, J. Macháčková and Ö. Gustafsson: Dual Carbon–Chlorine Stable Isotope Investigation of Sources and Fate of Chlorinated Ethenes in Contaminated Groundwater. Environmental Science & Technology 46 (20), 10918-10925 (2012)

Wiegert, C., M. Mandalakis, T. Knowles, P. Polymenakou, C. Aeppli, J. Machackova, H. Holmstrand, R. P. Evershed, R. Pancost and O. Gustafsson: Carbon and Chlorine Isotope Fractionation During Microbial Degradation of Tetra- and Trichloroethene. Environmental Science & Technology 47 (12), 6449-6456 (2013)

Yang, Y., Löffler, F. E. (2015). Reductive dechlorination of vinyl chloride in the absence of dehalococcoides mccartyi. Third international symposium on bioremediation and sustainable remediation technologies. Battelle. Miami, Florida.

Yu, S. and L. Semprini: Kinetics and modeling of reductive dechlorination at high PCE and TCE concentrations. Biotechnology and Bioengineering 88 (4), 451-464 (2004)

Appendices

Appendix 1 – Summary of analytical methods

1. C isotopic composition ($\delta^{13}C$)

In this work, C isotope ratios were determined using an Agilent™ 7890a gas chromatograph (GC) coupled to an Isoprime™ 100 isotope ratio mass spectrometer (IRMS) via an Isoprime GC5 combustion interface and a purge-and-trap (P&T) system (Stratum, Teledyne Tekmar).

1.1. Concentrations > 5 µg·L^{-1}

For samples showing individual chlorinated ethenes concentrations > 5 µg·L^{-1} and containing no VC (i.e. all chapters except samples from Rødekro), aqueous samples containing PCE, TCE or *c*DCE were first analysed by GCqMS to determine their concentrations, and then diluted before analysis in 40 mL glas vials with a PTFE-lined screw cap to reach final chlorinated ethenes concentration of 30 µg·L^{-1} (i.e. total 10 nmol C analysed). 25 mL of the diluted samples were purged with N_2 gas (40 mL·min^{-1}) and the degassed compounds were retained on a Vocarb 3000 trap (VICI). After the purging step (10 min, 40 mL·min^{-1}), the compounds were transferred into a cryogenic trap (Tekmar Dohrmann) connected to the GC column (DB-VRX, 60 m, 0.25 mm, 1.4 µm). This step was followed by a rapid temperature increase (from -100 °C to 180 °C, using a ramp of 15 °C·s^{-1}) which released the concentrated compounds to the column. Helium was used as a gas carrier (1.2 mL·min^{-1}). The GC oven temperature was first hold at 40 °C during 6 min, then followed a ramp of 10 °C·min^{-1} until 130 °C hold for 0.1 min followed by a ramp of 20 °C·min^{-1} until 220 °C hold for 1 min. Samples were measured in duplicate unless not enough material was available and the average accounts for the final isotopic composition.

1.2. Case of VC

For samples containing VC (i.e. samples from Rødekro only), a QS-PLOT (30 m, 0.32 mm, 10 µm) column which enabled a better VC separation than the DB-VRX was used. The cryogenic trap (Tekmar Dohrmann) temperature was lowered to -120 °C to allow for a better compound concentration. The GC compound separation was performed via the following temperature program: 35 °C hold for 6 min followed by a ramp of 15 °C·min^{-1} until 130 °C kept for 0.1 min followed by a ramp of 20 °C·min^{-1} until 240 °C kept for 5 min.

1.3. Concentrations < 5 µg·L^{-1}

For samples showing individual chlorinated ethenes concentrations > 5 µg·L^{-1}, 1 L bottles were manually connected to a purge system consisting of a frit from a gas-washing bottle as described formerly *(Hunkeler et al., 2012)* instead of passing 40 mL glass vials by autosampler. The bottles were purged for 30 min at a rate of 150 mL·min^{-1} which led to a removal of 90, 75, 50 and 100 % of the dissolved PCE, TCE, *c*DCE and VC, respectively, considering Henry coefficients at 20 °C of 0.533, 0.314, 0.14, 0.891 (gas/water) for PCE, TCE, *c*DCE and VC, respectively.

1.4. Standard uncertainty

Samples were measured in duplicate. Standard deviations σ of the in-house reference materials measured in the same sequences as samples from each study were determined for PCE, TCE, *c*DCE, and VC. The standard uncertainty of duplicate measurements was then determined according to ISO

guidelines *(BIPM, 1993)* as σ/√2 (Table A 1). Samples containing reference compounds with known isotope ratios (EA-IRMS measurement) were included in each sequence to verify the method accuracy except for VC which was not characterised by EA.

Table A 1. Standard uncertainties of duplicate measurements (σ/√2) given in ‰ associated with C isotopic ratios determined for each study

Study	PCE	TCE	*c*DCE	VC
Source variability (Chapter 1)	0.1, n=15	-	-	-
Experiments (Chapters 2, 3, 4)	0.2, n=47	0.6, n=37	0.2, n=18	-
Rødekro (Chapter 5)	0.4, n=32	0.2, n=24	0.3, n=24	0.7, n=26

2. Cl isotopic composition ($\delta^{37}Cl$)

In this work, Cl isotopic ratios were measured using a GCqMS system.

2.1. Choice of the method

Three methods have been so far proposed to determine Cl isotopic ratios by means of such instrumentation: (1) the multiple ion method which considers the two most abundant ions in each ion group *(Sakaguchi-Söder et al., 2007)*, (2) the molecular ion method which considers only the two most abundant molecular ions differing by one chlorine isotope *(Aeppli et al., 2010)*, and (3) the complete ion method which considers all ions of the mass spectra that contain chlorine atoms *(Jin et al., 2011)*. Elsner and Hunkeler validated from a theoretic viewpoint that isotope ratios should be derivable from ratios of any pair of two-mass apart isotopologues, whether molecular or fragment ions are used *(Elsner & Hunkeler, 2008)*. From a practical viewpoint, Jin *et al.* showed that the complete ion method was suited only for analytes with two or less chlorine atoms. Indeed, a lower precision was obtained for PCE and TCE as preserving a sufficient dwell time and a reasonable scan rate seems to conflict with targeting a high number of ions in the SIM mode *(Jin et al., 2011)*. Finally, to allow for simpler data treatment, the method proposed by Aeppli *et al.* was applied.
Isotope ratios were thus calculated as follows

$$R_{Cl}^{PCE} = \frac{1}{4} \times \frac{A^{166}}{A^{164}}$$

$$R_{Cl}^{TCE} = \frac{1}{3} \times \frac{A^{132}}{A^{130}}$$

where A^{166}, A^{164}, A^{132} and A^{130} are the areas under the peaks of the isotopologues of m/z 166, 164, 132 and 130, respectively.

2.2. Instrumental setup

The instrumental setup consisted of an Agilent 7890 GC coupled to an Agilent 5975C quadrupole mass selective detector (Santa Clara, CA, USA). In order to ensure a high accuracy, a calibration with two external standards ($\delta^{37}Cl_{EIL1}$ = +0.3 ‰ and $\delta^{37}Cl_{EIL2}$ = -2.5 ‰ for PCE and $\delta^{37}Cl_{EIL1}$ = +3.05 ‰ and

$\delta^{37}Cl_{EIL2}$ = -2.70 ‰ for TCE) which were formerly characterized by the Holt method *(Holt et al., 1997)* at the University of Waterloo was completed for each sequence to obtain δ values on the SMOC scale. A working PCE standard was measured after every ten sample to check the measurement stability. To reach a high precision and in order to be largely above the quantification limit of 30 $\mu g \cdot L^{-1}$, samples were diluted to a constant concentration of 100 $\mu g \cdot L^{-1}$ and analysed ten times by 1000 µL headspace injections using a CombiPal Autosampler (CTC Analytics, Zwingen, Switzerland). Vials were agitated at 750 rpm and incubated at 60 °C during 3 min before headspace injection. A split ratio of 20:1 was applied with a split flow of 24 $mL \cdot min^{-1}$. A DB-5 column (30 m, 0.25 mm, 0.25 µm, Agilent) with a constant helium flow of 1.2 $mL \cdot min^{-1}$ was used to perform chromatographic separation with a temperature program of 40 °C hold for 2 min, followed by a ramp of 15 $°C \cdot min^{-1}$ until 85 °C hold for 0.1 min, followed by a ramp of 30 $°C \cdot min^{-1}$ until 150 °C hold for 1 min. Mass to charge ratios (m/z) of 166 and 164, 132 and 130 were targeted in SIM mode for PCE and TCE, respectively. The Cl isotopic ratio in delta notation corresponds to the mean value of the ten injections, and the uncertainty thereof is given by the standard deviation of the injections divided by the square root of the number of injections (i.e. the standard error of the mean).

Appendix 2 – Supporting information to the introduction

1. Toxicology and limit values of the most frequently observed chlorinated solvents in groundwater

Table A 2. Toxicology and limit values of the most frequently observed chlorinated solvents in groundwater, after Guide des hydrocarbures chlorés, INERIS index, OSites *(OSites, 1998, FOEN, 2008 (revised 2009))*. In Switzerland, in groundwater intended for drinking, chlorinated ethenes concentrations in groundwater originating from the site immediately downstream should be below half of the concentration limit near polluted sites

Compound	Toxicology	Concentration limit near polluted sites = concentration limit in drinking water in CH	Occupational exposure limit value in CH
PCE	Probable carcinogenic, affects nervous system	40 $\mu g \cdot L^{-1}$	345 $mg \cdot m^{-3}_{air}$ (51 ppm) *USA: 25 ppm*[2]
TCE	Suspected carcinogenic, affects fertility, nervous, respiratory, cardiac, and digestive systems; irritates eyes and skin	70 $\mu g \cdot L^{-1}$	260 $mg \cdot m^{-3}_{air}$ (47 ppm) *USA: 10 ppm*[1]
***c*DCE**	Little data	50 $\mu g \cdot L^{-1}$	790 $mg \cdot m^{-3}_{air}$ (201 ppm)
VC	Carcinogenic (EU, IARC, US-EPA); affects nervous, respiratory, cardiac, and digestive systems	0.1 $\mu g \cdot L^{-1}$	5.2 $mg \cdot m^{-3}_{air}$ (2 ppm)
1,1,1-TCA		2000 $\mu g \cdot L^{-1}$	1080 $mg \cdot m^{-3}_{air}$ (200 ppm)

[2] Average exposure value on the basis of 8h per day, 40h per week

2. Chlorinated ethenes and 1,1,1-TCA physic and chemical properties

Table A 3. Summary of chlorinated ethenes and 1,1,1-TCA physic and chemical properties, after Guide des hydrocarbures chlorés and INRS toxicology records

Compound	Tetrachloro-ethylene	Trichloroethylene	1,2-Dichloro-ethylene	1,1-Dichloro-ethylene	Vinyl Chloride	1,1,1-Trichloroethane
Abbreviation	PCE	TCE	*cis*-DCE / *trans*-DCE	1,1-DCE	VC	1,1,1-TCA
Formula	C_2Cl_4	C_2HCl_3	$C_2H_2Cl_2$	$C_2H_2Cl_2$	C_2H_3Cl	$C_2H_3Cl_3$
Global characteristics at ambiant conditions	Colourless liquid, soft odour	Colourless liquid, soft odour, detectable from 50 to 100 ppm concentration in the air	Colourless, sweet-smelling liquid	Colourless liquid, sharp odour	Gas	Colourless, sweet-smelling liquid
Molecular mass ($g \cdot mol^{-1}$)	165.85	131.4	96.94	96.94	62.5	133.4
Solubility ($mg \cdot L^{-1}$)	150 (25 °C)	1’090 (25 °C)	Cis: 5’090 (25 °C) Trans: 6’260 (25 °C)	2'490 (25 °C)	2’800 (25° C)	950 (20 °C)
Density ($kg \cdot l^{-1}$, 20 °C)	1.62	1.46	Cis: 1.29 Trans: 1.26	1.22	0.91	1.32
Boiling point (1 atm)	121.2 °C	87 °C	Cis: 60.2 °C Trans: 48.2 °C		-13.7 °C	74 °C
Vapour density	5.8	4.5	3.4		2.15	4.6
Vapour pressure (kPa, 20 °C)	1.9	8.6	Cis: 24 Trans: 35	79.4 (25°C)	340	13.3
Henry’s constant at 25 °C	0.730	0.490	Cis: 0.219 Trans: 0.257	1.25	1.10	0.663
Partition coefficient K_{oc} ($L \cdot kg^{-1}$)	374	185	Cis: 38 Trans: 48	47	5	119

3. Degradation pathways of most encountered chlorinated solvents

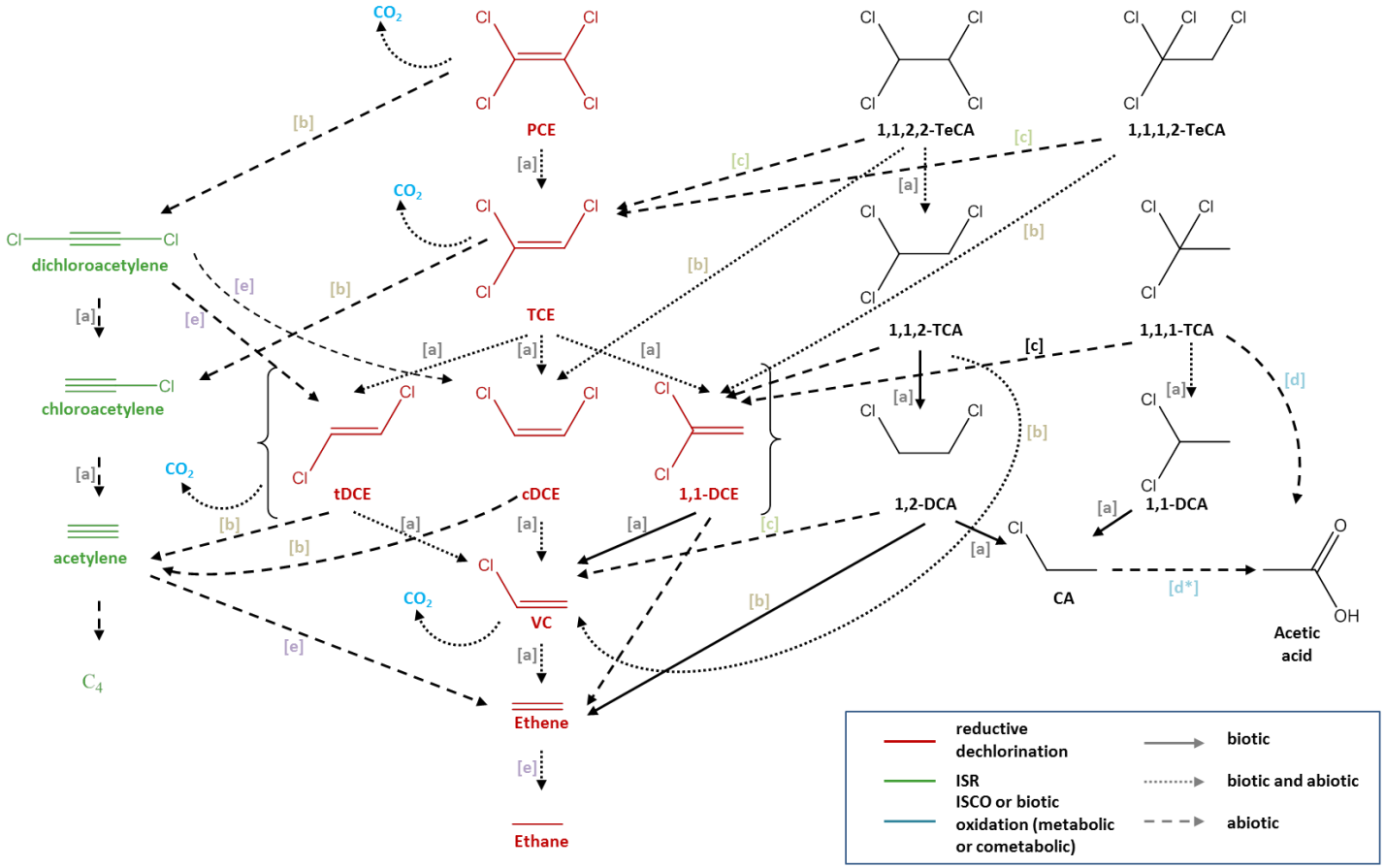

Figure A 1. Degradation pathways of chlorinated solvents commonly encountered in groundwater. Anaerboic biodegradation only is presented except for chlorinated ethenes on which the emphasis is given. Abiotic degradation pathways correspond to those catalysed by iron bearing minerals, zero valent iron, or other metals. Reactions proceed via [a] hydrogenolysis, [b] dihaloelimination, [c] dehydrohalogenation, [d] hydrolysis, [d*] hydrolysis to ethanol followed by fermentation, [e] hydrogenation and [f] α-elimination. Modified from Arnold *et al.* and Palau *et al.* [1] (in prep).

Appendix 3 – Supporting information to Chapter 1

1. Bruto data from C-Cl PCE isotopic signatures

Table A 4. PCE C-Cl isotopic composition for each sampling point of each site. For the site averages, the uncertainty is given by the standard uncertainty between wells of a site or the analytical uncertainty in case the latter is larger than the standard uncertainty between wells.

Site	Sampling point	Chlorinated ethenes concentration			$\delta^{37}Cl$	$\delta^{13}C$	Redox parameters				
		PCE ($\mu g \cdot l^{-1}$)	TCE ($\mu g \cdot l^{-1}$)	*c*DCE ($\mu g \cdot l^{-1}$)	PCE (‰)	PCE (‰)	DO ($mg \cdot l^{-1}$)	electrical conductivity ($\mu S \cdot cm^{-1}$)	pH	Mn^{2+} ($mg \cdot l^{-1}$)	Fe^{2+} ($mg \cdot l^{-1}$)
SA	**Site average**				**0.0 ± 0.1**	**-25.1 ± 0.5**					
SA	W1	5900	<25	<25	0.0 ± 0.1	-25.3 ± 0.1	2.3	770	7.6	0.019	
SA	W2	1000	<5	<5	0.0 ± 0.1	-25.5 ± 0.1	1.0	802	7.5	0.041	0.00
SA	W3	5400	24	<10	0.1 ± 0.1	-24.6 ± 0.1	0.5	1212	7.3	0.705	0.04
SB	**Site average**				**-0.5 ± 0.2**	**-24.4 ± 0.4**					
SB	W1	170	<5	<5	-0.6 ± 0.1	-24.4 ± 0.1	7.1	311	8		
SB	W2	100	<5	<5	-0.7 ± 0.1	-24.9 ± 0.1	6.9	286	8.0		
SB	W3	110	<5	<5	-0.5 ± 0.1	-24.6 ± 0.1	5.3	273	8.0		
SB	W4	1110	<5	<5	-0.1 ± 0.2	-24.0 ± 0.1	3.7	313	7.8		
SB	W5	6400	<5	<5	-0.3 ± 0.1	-24.2 ± 0.1	4.2	257	8.1		
SC	**Site average**				**0.0 ± 0.1**	**-23.7 ± 0.1**					
SC	W1	1700	<5	<5	-0.1 ± 0.1	-23.7 ± 0.1	7.5	840	7.4		
SC	W2	890	<5	<5	0.1 ± 0.1	-23.7 ± 0.1	5.5	759	7.5		

Site	Sampling point	Chlorinated ethenes concentration			$\delta^{37}Cl$	$\delta^{13}C$	Redox parameters				
		PCE	TCE	cDCE	PCE	PCE	DO	electrical conductivity	pH	Mn^{2+}	Fe^{2+}
		($\mu g \cdot l^{-1}$)	($\mu g \cdot l^{-1}$)	($\mu g \cdot l^{-1}$)	(‰)	(‰)	($mg \cdot l^{-1}$)	($\mu S \cdot cm^{-1}$)		($mg \cdot l^{-1}$)	($mg \cdot l^{-1}$)
SD	**Site average**				**0.6 ± 0.2**	**-26.0 ± 0.6**					
SD	W1	140	<5	<5	0.6 ± 0.2	-26.2 ± 0.1	5.7	496	7.1		
SD	W2	210	<5	<5	0.4 ± 0.1	-25.6 ± 0.1	4.6	504	7.1		
SD	W3	80	<5	<5	0.7 ± 0.2	-26.8 ± 0.1	6.2	498	7.1		
SD	W4	190	<5	<5	0.8 ± 0.1	-25.6 ± 0.1	4.8	529	7.2		
SE	**Site average**				**0.4 ± 0.3**	**-24.9 ± 0.6**					
SE	W1	520	<5	<5	0.7 ± 0.1	-24.7 ± 0.1	8.1	555	7.2		
SE	W2	450	<5	<5	0.2 ± 0.2	-24.2 ± 0.1	5.3	641	7.1		
SE	W3	380	<5	6	0.1 ± 0.2	-25.3 ± 0.1	7.4	503	7.3		
SE	W4	570	<5	<5	0.7 ± 0.2	-25.6 ± 0.1	10.7	384	7.7		
SF	**Site average**				**0.0 ± 0.2**	**-25.7 ± 0.3**					
SF	W1	630	<5	<5	0.0 ± 0.1	-25.4 ± 0.1	0.3	598	7.3	0.082	0.00
SF	W2	650	<5	<5	0.0 ± 0.2	-26.0 ± 0.1	0.2	584	7.3	0.043	0.00
SG	**Site average**				**0.1 ± 0.3**	**-24.7 ± 0.5**					
SG	W1	132000	<625	<625	0.2 ± 0.1	-25.1 ± 0.1	4.0	979	7.5		
SG	W2	890	10	<5	-0.3 ± 0.1	-24.9 ± 0.1	5.2	654	7.4		
SG	W3	17500	616	<83	0.3 ± 0.1	-24.1 ± 0.1	7.0	775	7.3		
SH	**Site average**				**0.1 ± 0.4**	**-25.8 ± 0.1**					
SH	W1	600	<5	<5	-0.1 ± 0.1	-25.8 ± 0.1	10.1	596	7.3		
SH	W2	70	<5	<5	0.4 ± 0.2	-25.7 ± 0.1	8.8	754	7.2		

Site	Sampling point	Chlorinated ethenes concentration			$\delta^{37}Cl$	$\delta^{13}C$	Redox parameters				
		PCE	TCE	cDCE	PCE	PCE	DO	electrical conductivity	pH	Mn^{2+}	Fe^{2+}
		($\mu g \cdot l^{-1}$)	($\mu g \cdot l^{-1}$)	($\mu g \cdot l^{-1}$)	(‰)	(‰)	($mg \cdot l^{-1}$)	($\mu S \cdot cm^{-1}$)		($mg \cdot l^{-1}$)	($mg \cdot l^{-1}$)
SI	**Site average**				**0.0 ± 0.2**	**-25.5 ± 0.5**					
SI	W1	164000	<300	<850	-0.1 ± 0.1	-25.6 ± 0.1	5.4	695	7.4		
SI	W2	73000	<150	<360	0.1 ± 0.1	-25.3 ± 0.1	4.6	872	7.3		
SI	W3	37000	<70	<200	-0.2 ± 0.1	-26.1 ± 0.1	2.5	812	7.4		
SI	W4	268000	<700	<1300	0.1 ± 0.1	-24.9 ± 0.1	4.3	768	7.4		
SJ	**Site average**				**0.0 ± 0.3**	**-24.1 ± 0.2**					
SJ	W1	40	<5	<5	0.3 ± 0.2	-23.9 ± 0.1	6.7	748	7.4		
SJ	W2	20	<5	<5	-0.2 ± 0.2	-24.3 ± 0.1	7.5	767	7.4		

Appendix 4 – Supporting information to Chapter 2

1. Concentration and isotope data at field sites

Table A 5. PCE molar percentage, chlorinated ethenes concentration, carbon and chlorine isotope ratios in sites X and Y as well as sampled depth and well distance from the source.

Site	Well	Sampled depth	Distance from source	PCE			TCE	DCE	VC
				Conc.	$\delta^{37}Cl$	$\delta^{13}C$	Conc.	Conc.	Conc.
		m	m	$\mu g \cdot L^{-1}$	‰	‰	$\mu g \cdot L^{-1}$	$\mu g \cdot L^{-1}$	$\mu g \cdot L^{-1}$
X	X1	11.5	150	192	0.1 ± 0.1	-23.2 ± 0.3	0.4	0.3	n.d.
X	X3	8	30	1500	-0.7 ± 0.1	-23.7 ± 0.3	3.3	3.4	n.d.
X	X4	7	350	147	0.4 ± 0.1	-23.0 ± 0.3	1.7	2.4	n.d.
X	X2	8	200	317	0.1 ± 0.2	-23.4 ± 0.3	3	10.4	1.5
X	X5	7	700	83	0.3 ± 0.1	-23.0 ± 0.3	5.7	44	5.5
Y	ML15-3	4	13	106	0.0 ± 0.1	-23.4 ± 0.3	0	3	n.d.
Y	P13	5	30	146	-0.1 ± 0.2	-23.4 ± 0.3	0.5	6	n.d.
Y	ML14-4	4	13	88	0.2 ± 0.1	-21.9 ± 0.3	5	39	n.d.
Y	ML13-2	7	13	166	0.4 ± 0.1	-21.7 ± 0.3	35	318	61
Y	ML13-3	6	13	321	0.6 ± 0.1	-21.2 ± 0.3	97	769	150

2. PCE peak resolution relative to the Cl isotope analysis

A chromatogram of one of the GCqMS measurements performed to determine the Cl isotopic ratio of PCE in a field sample is presented in Figure A 2.

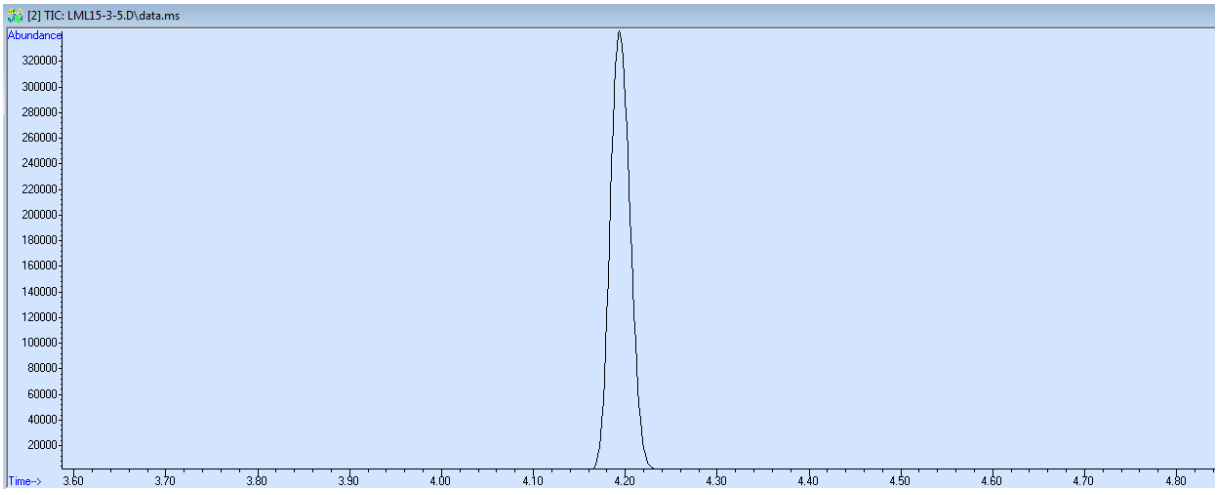

Figure A 2. Chromatogram of one of the GCqMS measurements performed to determine the Cl isotopic ratio of PCE in ML15-3

Appendix 5 – Supporting information to Chapter 3

1. Data for all replicates

Table A 6. Summary of C and Cl enrichment factors, primary and secondary Cl isotopic effects denoted as εCl prim and εCl sec, respectively, dual C-Cl slopes, C isotope balance and mass balance associated with reductive dechlorination of PCE to TCE (SL2-PCEc), PCE to *c*DCE (SL2-PCEb), and TCE to *c*DCE (SL2-PCEb).

Experiment	ε_C (‰)	ε_{Cl} (‰)	ε_{Cl} (‰) prim	ε_{Cl} (‰) sec	ε_{Cl} (‰) diff	dual C-Cl PCE	dual C-Cl TCE	C isotope balance	Mass balance
PCE to TCE	**-3.6 ± 0.2**	**-1.2 ± 0.1**	**-9.2 ± 0.9**	**1.4 ± 0.2**	**-10.6 ± 1**	**2.7 ± 0.3 (R^2 = 0.94, n=23)**			
PCE to TCE A	-3.9 ± 0.1	-1.1 ± 0.2	-8.2 ± 0.4	1.3 ± 0.2	-9.6 ± 0.4		2.7 ± 0.8 (R^2 = 0.89, n=9)	-32.9 to -31.0	60%
PCE to TCE B	-3.7 ± 0.4	-1.5 ± 0.3	-10.1 ± 0.6	1.4 ± 0.3	-11.5 ± 0.6		3.8 ± 3.2 (R^2 = 0.59, n=8)	-32.9 to -29.8	90%
PCE to TCE C	-3.3 ± 0.7	-1.2 ± 0.2	-9.8 ± 0.4	1.6 ± 0.2	-11.5 ± 0.4		2.1 ± 1.1 (R^2 = 0.81, n=9)	-33.4 to -33.5	90%
PCE to TCE D	-3.4 ± 0.3	-1.2 ± 0.1	-8.7 ± 0.4	1.3 ± 0.3	-10 ± 0.4		3.4 ± 1.3 (R^2 = 0.74, n=11)	-33.2 to -32.6	90%
PCE to *c*DCE	**-0.7 ± 0.1**	**-0.9 ± 0.1**	**-12.8 ± 2.1**	**3.1 ± 0.6**	**-15.9 ± 2.8**	**0.7 ± 0.2 (R^2 = 0.74, n=29)**	**3.7 ± 0.4 (R^2 = 0.93, n=30)**		
PCE to *c*DCE A	-0.6 ± 0.2	-0.9 ± 0.1	-10.4 ± 0.3	2.3 ± 0.2	-12.8 ± 0.3			-33.1 to -33.0	85%
PCE to *c*DCE B	-0.7 ± 0.2	-0.8 ± 0.2	-13.3 ± 0.5	3.3 ± 0.3	-16.6 ± 0.5			-33.2 to -32.6	85%
PCE to *c*DCE C	-0.7 ± 0.2	-0.9 ± 0.1	-12 ± 0.3	2.9 ± 0.2	-14.9 ± 0.3			-32.4 to -32.9	80%
PCE to *c*DCE D	-0.8 ± 0.1	-1 ± 0.1	-15.4 ± 0.3	3.8 ± 0.2	-19.2 ± 0.3			-32.7 to -32.9	95%
TCE to *c*DCE	**-18.9 ± 1.3**	**-4.3 ± 0.4**					**4.3 ± 0.2 (R^2 = 0.99, n=29)**		
TCE to *c*DCE A	-20.6 ± 1.2	-4.7 ± 0.4						-29.2 to -23.6	70%
TCE to *c*DCE B	-17.7 ± 2.3	-3.8 ± 0.5						-27.7 to -23.3	65%
TCE to *c*DCE C	-18.1 ± 1.1	-4.2 ± 1						-27.8 to -23.3	60%

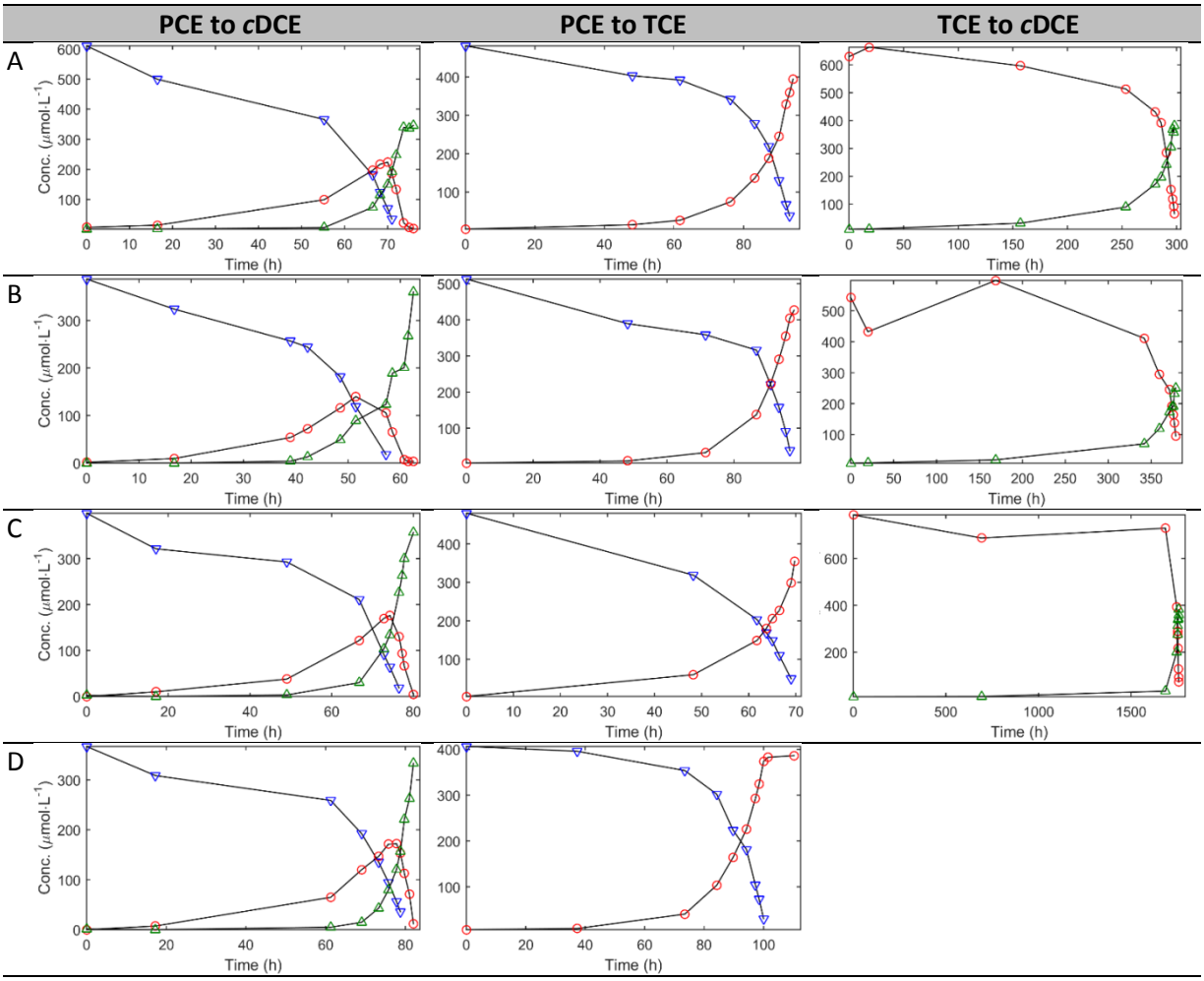

Figure A 3. Evolution of PCE (blue triangles), TCE (red circles) and *c*DCE (green triangles) concentrations during reductive dechlorination performed by SL2-PCEb (PCE to *c*DCE and TCE to cDCE) and SL2-PCEc (PCE to TCE) for all replicates

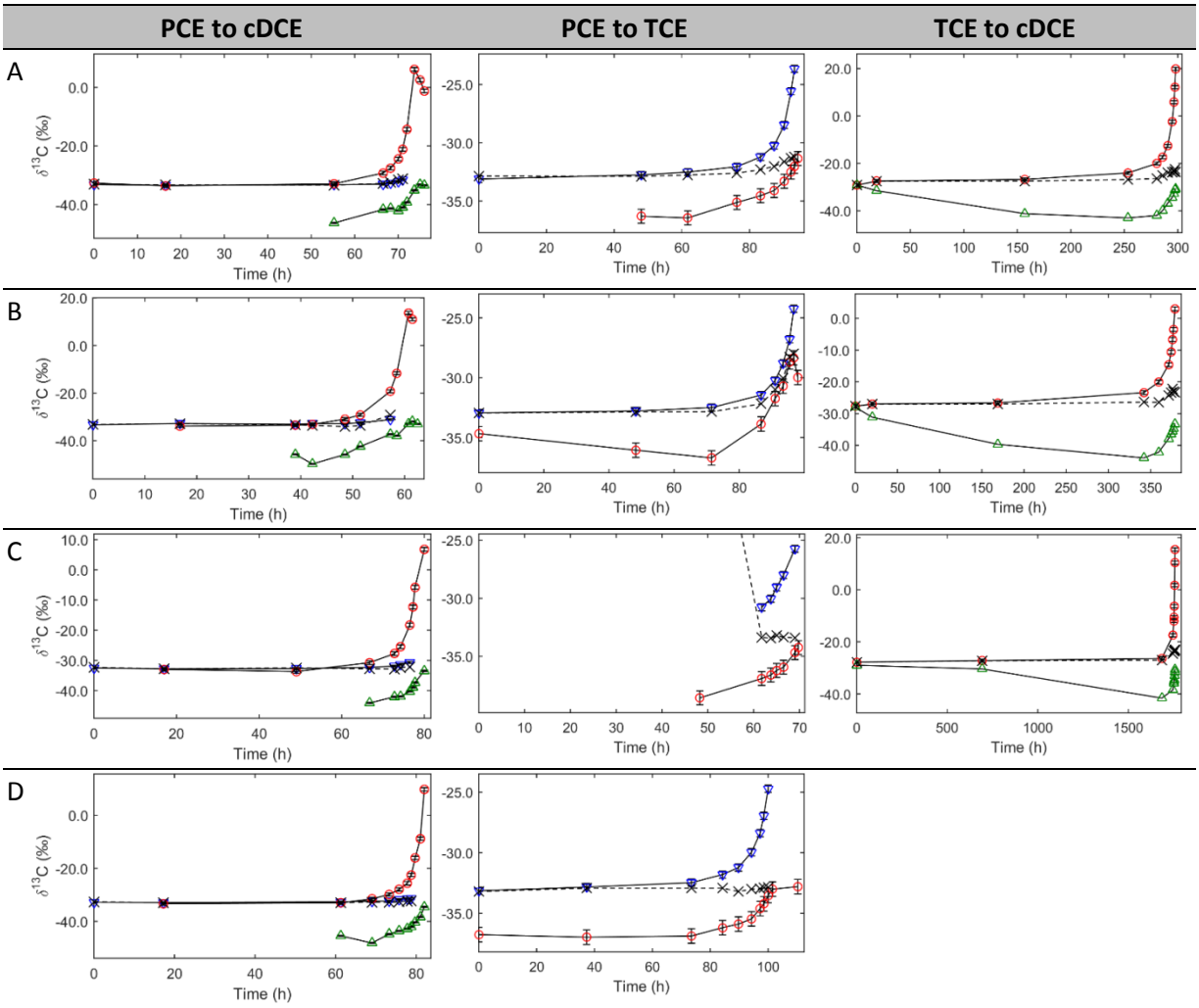

Figure A 4. Evolution of PCE (blue triangles), TCE (red circles) and *c*DCE (green triangles) C isotopic composition during reductive dechlorination performed by SL2-PCEb (PCE to *c*DCE and TCE to cDCE) and SL2-PCEc (PCE to TCE) for all replicates

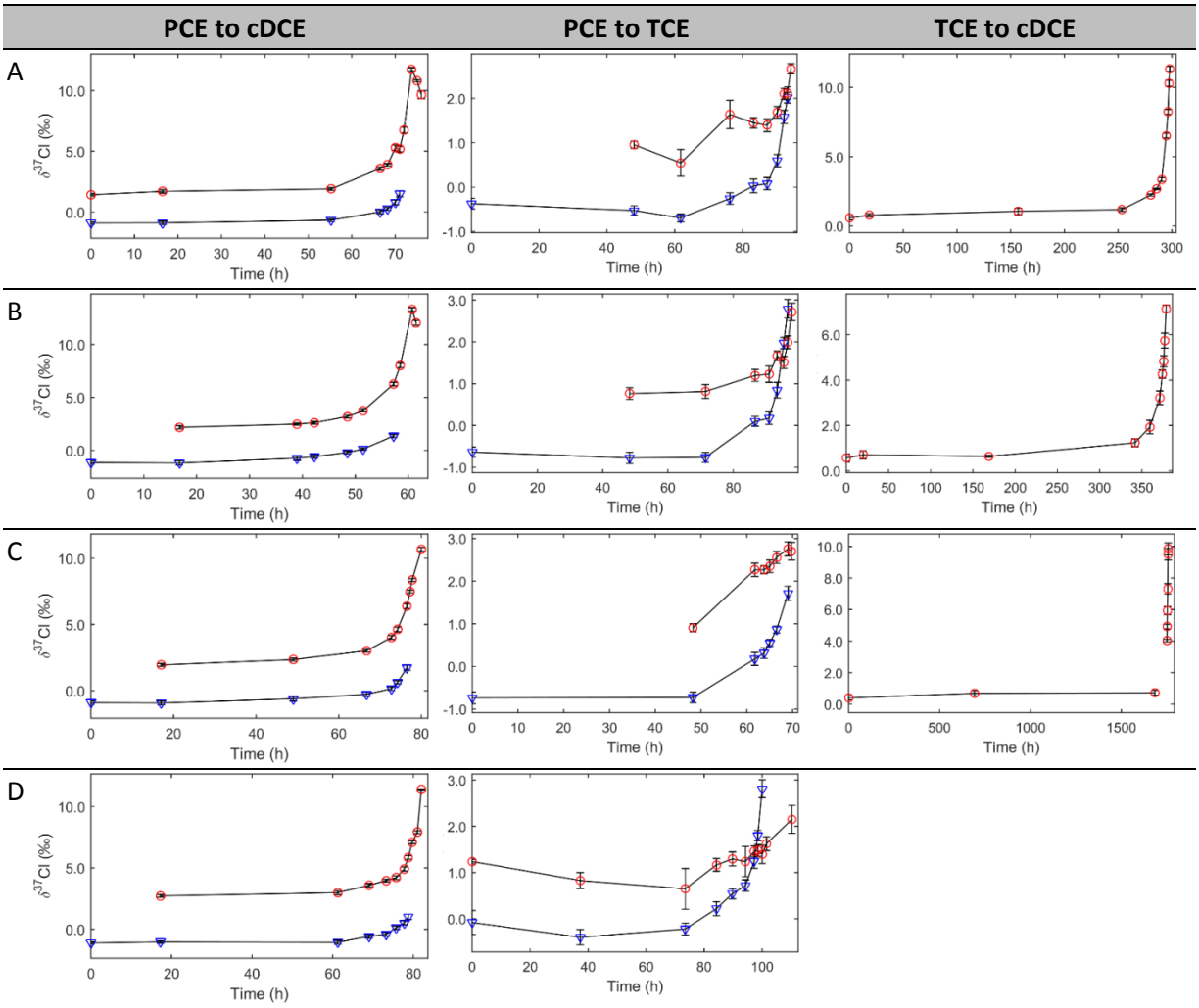

Figure A 5. Evolution of PCE (blue triangles), TCE (red circles) and *c*DCE (green triangles) Cl isotopic composition during reductive dechlorination performed by SL2-PCEb (PCE to *c*DCE and TCE to cDCE) and SL2-PCEc (PCE to TCE) for all replicates

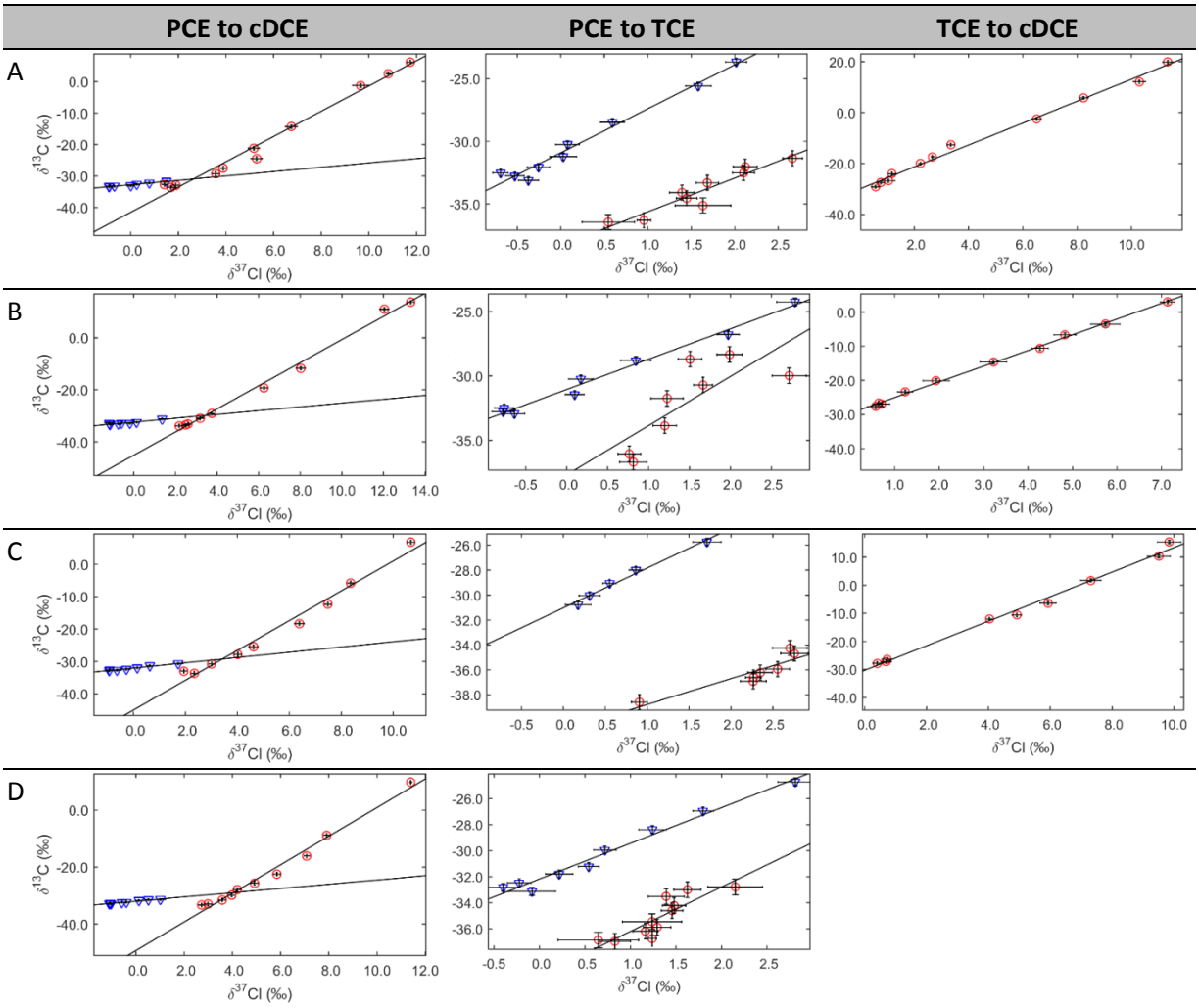

Figure A 6. Evolution of PCE (blue triangles), TCE (red circles) and *c*DCE (green triangles) C-Cl dual isotope slopes associated with reductive dechlorination performed by SL2-PCEb (PCE to *c*DCE and TCE to cDCE) and SL2-PCEc (PCE to TCE) for all replicates

Appendix 6 – Supporting information to Chapter 4

1. Optimised parameters used for the simulations

Table A 7. Summary of optimised parameters when fitting simulations to experimental data

Parameter	Parameter	Unit	PT	TD	PTD	Description
MATLAB notation	**COMSOL notation**					
X0	**X0**	**mg of protein.L^{-1}**	1	1	1	initial biomass concentration
t0_delay	**-**	**h**	45	-	29	Lag phase delay
PCE_C0	**CP0**	**µmol.L^{-1}**	445	-	368	initial PCE concentration
PCE_delta13C	**d13CP0**	**‰**	-32.9	-	-32.7	initial d13C PCE
PCE_delta37Cl	**d37ClP0**	**‰**	-0.6	-	-0.9	initial d37Cl PCE
TCE_C0	**CT0**	**µmol.L^{-1}**	-	598	0	initial TCE concentration
TCE_delta13C	**d13CT0**	**‰**	-	-26.1		initial d13C TCE
TCE_delta37Cl	**d37ClT0**	**‰**	-	0.9		initial d37Cl TCE
CDCE_C0		**µmol.L^{-1}**	-	-	0	initial *c*DCE concentration
CDCE_delta13C		**‰**	-	-		initial d13C cDCE
CDCE_delta37Cl		**‰**	-	-		initial d37Cl cDCE
PCE2TCE_muMax	**uMAXP**	**µmol.mg of protein^{-1}.s^{-1}**	3.36E-05	-	3.83E-05	maximum growth rate for PCE
PCE2TCE_Yi	**YP**	**mg of protein.µmol of released chloride^{-1}**	0.9	-	0.9	biomass yield for PCE
PCE2TCE_Km	**KmP**	**µmol.L^{-1}**	22.0	-	58.8	half saturation constant for PCE
PCE2TCE_Epsilon_Ca	**ePCp**	**‰**	-5.0	-	-0.7	C primary effect for PCE
PCE2TCE_Epsilon_Cb	**ePCs**	**‰**	0.0	-	0.0	C secondary effect for PCE
PCE2TCE_Epsilon_Cla1	**ePClp**	**‰**	-10.0	-	-11.1	Cl primary effect /Epsilon_Clα1 for PCE
PCE2TCE_Epsilon_Cla2	**ePCls**	**‰**	1.8	-	3.1	Cl secondary effect /Epsilon_Clα2 for PCE
PCE2TCE_Epsilon_Clb1	**-**	**‰**	1.8	-	3.1	Cl secondary effect /Epsilon_Clβ1 for PCE

PCE2TCE_Epsilon_Clb2	**-**	**‰**	1.8	-	3.1	Cl secondary effect /Epsilon_Clβ2 for PCE
TCE2CDCE_muMax	**uMAXT**	**µmol.mg of protein^{-1}.s^{-1}**		1.88E-05	2.30E-05	maximum growth rate for TCE
TCE2CDCE_Yi	**YT**	**mg of protein.µmol of released chloride^{-1}**		0.9	0.9	biomass yield for TCE
TCE2CDCE_Km	**KmT**	**µmol.L^{-1}**		10.00	69.9	half saturation constant for TCE
TCE2CDCE_Epsilon_Ca	**eTCp**	**‰**		-30.0	-29.1	C primary effect for TCE
TCE2CDCE_Epsilon_Cb	**ePCs**	**‰**		-5.0	0.0	C secondary effect for TCE
TCE2CDCE_Epsilon_Cla1	**eTClp**	**‰**		-5.3	-12.8	Cl primary effect /Epsilon_Clα1 for TCE
TCE2CDCE_Epsilon_Cla2	**eTCls**	**‰**		-3.0	1.4	Cl secondary effect /Epsilon_Clα2 for TCE
TCE2CDCE_Epsilon_Clb1	**-**	**‰**		-3.0	1.4	Cl secondary effect /Epsilon_Clβ1 for TCE
TCE2CDCE_Epsilon_Clb2	**-**	**‰**		-3.0	1.4	Cl secondary effect/Epsilon_Clβ2 for TCE

2. COMSOL differential equations

Table A 8. COMSOL differential equations for PT, C

LLP	LLPt+(uMAXP*X/(YP*(KmP+CP)))*LLP	LLP0	0
LHP	LHPt+(uMAXP*X/(YP*(KmP+CP)))*LHP*(1/(KIEPCs*2)+1/(KIEPCp*2))	LHP0	0
HHP	HHPt+(uMAXP*X/(YP*(KmP+CP)))*HHP*(1/(KIEPCs*KIEPCp))	HHP0	0
LLT	LLTt-(uMAXP*X/(YP*(KmP+CP)))*LLP	0	0
LHT	LHTt-(uMAXP*X/(YP*(KmP+CP)))*LHP*(1/(KIEPCs*4)+1/(KIEPCp*4))	0	0
HLT	HLTt-(uMAXP*X/(YP*(KmP+CP)))*LHP*(1/(KIEPCs*4)+1/(KIEPCp*4))	0	0
HHT	HHTt-(uMAXP*X/(YP*(KmP+CP)))*HHP*(1/(KIEPCs*KIEPCp))	0	0

Table A 9. COMSOL differential equations for PT, Cl

LLLL	LLLLt+(uMAXP*X/(YP*(KmP+CP)))*LLLL	LLLL0	0
LLLH	LLLHt+(uMAXP*X/(YP*(KmP+CP)))*LLLH*((1/KIEPCls)*3/4+((1/KIEPClp)*1/4))	LLLH0	0
LLHH	LLHHt+(uMAXP*X/(YP*(KmP+CP)))*LLHH*(((1/KIEPCls)^2)*1/2+((1/KIEPClp)*(1/KIEPCls)*1/2))	LLHH0	0
LHHH	LHHHt+(uMAXP*X/(YP*(KmP+CP)))*LHHH*(((1/KIEPCls)^3)*1/4+((1/KIEPClp)*((1/KIEPCls)^2)*3/4))	LHHH0	0
HHHH	HHHHt+(uMAXP*X/(YP*(KmP+CP)))*HHHH*(((1/KIEPClp)*((1/KIEPCls)^3)))	HHHH0	0
LLL	LLLt-uMAXP*X/(YP*(KmP+CP))*(LLLL+LLLH*(1/KIEPClp)*1/4)	0	0
LLH	LLHt-uMAXP*X/(YP*(KmP+CP))*(LLLH*(1/KIEPCls)*1/4+LLHH*(1/(KIEPClp*KIEPCls)*1/6))	0	0
LHL	LHLt-uMAXP*X/(YP*(KmP+CP))*(LLLH*(1/KIEPCls)*1/4+LLHH*(1/(KIEPClp*KIEPCls)*1/6))	0	0
HLL	HLLt-uMAXP*X/(YP*(KmP+CP))*(LLLH*(1/KIEPCls)*1/4+LLHH*(1/(KIEPClp*KIEPCls)*1/6))	0	0
LHH	LHHt-uMAXP*X/(YP*(KmP+CP))*(LLHH*(1/KIEPCls^2)*1/6+LHHH*(1/KIEPClp)*(1/KIEPCls)^2*1/4)	0	0
HLH	HLHt-uMAXP*X/(YP*(KmP+CP))*(LLHH*(1/KIEPCls^2)*1/6+LHHH*(1/KIEPClp)*(1/KIEPCls)^2*1/4)	0	0
HHL	HHLt-uMAXP*X/(YP*(KmP+CP))*(LLHH*(1/KIEPCls^2)*1/6+LHHH*(1/KIEPClp)*(1/KIEPCls)^2*1/4)	0	0
HHH	HHHt-uMAXP*X/(YP*(KmP+CP))*(LHHH*(1/KIEPCls^3)*1/4+HHHH*(1/KIEPClp)*(1/KIEPCls)^3)	0	0
X	Xt-uMAXP*X*CP/(KmP+CP)	X0	0

Table A 10. COMSOL differential equations for TD, C

LLT	LLTt+(uMAXT*X/(YT*(KmT+CT)))*LLT	LLT0	0
LHT	LHTt+(uMAXT*X/(YT*(KmT+CT)))*LHT*((1/KIETCp))	LHT0	0
HLT	HLTt+(uMAXT*X/(YT*(KmT+CT)))*HLT*((1/KIETCs))	LHT0	0
HHT	HHTt+(uMAXT*X/(YT*(KmT+CT)))*HHT*(1/(KIETCs*KIETCp))	HHT0	0
LLD	LLDt-(uMAXT*X/(YT*(KmT+CT)))*LLT	0	0
LHD	LHDt-(uMAXT*X/(YT*(KmT+CT)))*(LHT*(1/KIETCp)+HLT*(1/KIETCs))	0	0
HHD	HHDt-(uMAXT*X/(YT*(KmT+CT)))*HHT*(1/(KIETCs*KIETCp))	0	0

Table A 11. COMSOL differential equations for TD, Cl

LLL	LLLt+(uMAXT*X/(YT*(KmT+CT)))*LLL	LLL0	0
LLH	LLHt+(uMAXT*X/(YT*(KmT+CT))*LLH*(1/KIETClp))	LLH0	0
LHL	LHLt+(uMAXT*X/(YT*(KmT+CT)))*LHL*((1/KIETCls))	LHL0	0
HLL	HLLt+(uMAXT*X/(YT*(KmT+CT)))*HLL*((1/KIETCls))	HLL0	0
LHH	LHHt+(uMAXT*X/(YT*(KmT+CT)))*LHH*((1/(KIETClp*KIETCls)))	LHH0	0
HLH	HLHt+(uMAXT*X/(YT*(KmT+CT)))*HLH*(1/(KIETClp*KIETCls))	HLH0	0
HHL	HHLt+(uMAXT*X/(YT*(KmT+CT)))*HHL*(((1/KIETCls)^2))	HHL0	0
HHH	HHHt+(uMAXT*X/(YT*(KmT+CT)))*HHH*(1/(KIETClp*(KIETCls)^2))	HHH0	0
X	Xt-uMAXT*X*CT/(KmT+CT)	X0	0
LL	LLt-uMAXT*X/(YT*(KmT+CT))*(LLL+LLH*((1/KIETClp)))	0	0
LH	LHt-uMAXT*X/(YT*(KmT+CT))*((LHL+HLL)*(1/KIETCls)+(LHH+HLH)*(1/(KIETClp*KIETCls)))	0	0
HH	HHt-uMAXT*X/(YT*(KmT+CT))*(HHL*(1/KIETCls^2)+HHH*(1/(KIETClp*(KIETCls^2))))	0	0

Table A 12. COMSOL differential equations for PTD, C

LLP	LLPt+(uMAXP*X/(YP*(KmP+CP)))*LLP	LLP0	0
LHP	LHPt+(uMAXP*X/(YP*(KmP+CP)))*LHP*(1/(KIEPCs*2)+1/(KIEPCp*2))	LHP0	0
HHP	HHPt+(uMAXP*X/(YP*(KmP+CP)))*HHP*(1/(KIEPCs*KIEPCp))	HHP0	0
LLT	LLTt-(uMAXP*X/(YP*(KmP+CP)))*LLP+(uMAXT*X/(YT*(KmT+CT)))*LLT	0	0
LHT	LHTt-(uMAXP*X/(YP*(KmP+CP)))*LHP*(1/(KIEPCs*4)+1/(KIEPCp*4))+(uMAXT*X/(YT*(KmT+CT)))*LHT*((1/KIETCp))	0	0
HLT	HLTt-(uMAXP*X/(YP*(KmP+CP)))*LHP*(1/(KIEPCs*4)+1/(KIEPCp*4))+(uMAXT*X/(YT*(KmT+CT)))*HLT*((1/KIETCs))	0	0
HHT	HHTt-(uMAXP*X/(YP*(KmP+CP)))*HHP*(1/(KIEPCs*KIEPCp))+(uMAXT*X/(YT*(KmT+CT)))*HHT*(1/(KIETCs*KIETCp))	0	0
LLD	LLDt-(uMAXT*X/(YT*(KmT+CT)))*LLT	0	0
LHD	LHDt-(uMAXT*X/(YT*(KmT+CT)))*(LHT*(1/(KIETCp))+HLT*(1/(KIETCs)))	0	0
HHD	HHDt-(uMAXT*X/(YT*(KmT+CT)))*HHT*(1/(KIETCs*KIETCp))	0	0

Table A 13. COMSOL differential equations for PTD, Cl

LLLL	LLLLt+(uMAXP*X/(YP*(KmP+CP)))*LLLL	LLLL0	0
LLLH	LLLHt+(uMAXP*X/(YP*(KmP+CP)))*LLLH*((1/KIEPCls)*3/4+((1/KIEPClp)*1/4))	LLLH0	0
LLHH	LLHHt+(uMAXP*X/(YP*(KmP+CP)))*LLHH*(((1/KIEPCls)^2)*1/2+((1/KIEPClp)*(1/KIEPCls)*1/2))	LLHH0	0
LHHH	LHHHt+(uMAXP*X/(YP*(KmP+CP)))*LHHH*(((1/KIEPCls)^3)*1/4+((1/KIEPClp)*((1/KIEPCls)^2)*3/4))	LHHH0	0
HHHH	HHHHt+(uMAXP*X/(YP*(KmP+CP)))*HHHH*(((1/KIEPClp)*((1/KIEPCls)^3)))	HHHH0	0
LLL	LLLt-uMAXP*X/(YP*(KmP+CP))*(LLLL+LLLH*(1/KIEPClp)*1/4)+(uMAXT*X/(YT*(KmT+CT)))*LLL	0	0
LLH	LLHt-uMAXP*X/(YP*(KmP+CP))*(LLLH*(1/KIEPCls)*1/4+LLHH*(1/(KIEPClp*KIEPCls)*1/6))+(uMAXT*X/(YT*(KmT+CT)))*LLH*(1/KIETClp)	0	0
LHL	LHLt-uMAXP*X/(YP*(KmP+CP))*(LLLH*(1/KIEPCls)*1/4+LLHH*(1/(KIEPClp*KIEPCls)*1/6))+(uMAXT*X/(YT*(KmT+CT)))*LHL*(1/KIETCls)	0	0
HLL	HLLt-uMAXP*X/(YP*(KmP+CP))*(LLLH*(1/KIEPCls)*1/4+LLHH*(1/(KIEPClp*KIEPCls)*1/6))+(uMAXT*X/(YT*(KmT+CT)))*HLL*(1/KIETCls)	0	0
LHH	LHHt-uMAXP*X/(YP*(KmP+CP))*(LLHH*(1/KIEPCls^2)*1/6+LHHH*(1/KIEPClp)*(1/KIEPCls)^2*1/4)+uMAXT*X/(YT*(KmT+CT))*LHH*(1/(KIETClp*KIETCls))	0	0
HLH	HLHt-uMAXP*X/(YP*(KmP+CP))*(LLHH*(1/KIEPCls^2)*1/6+LHHH*(1/KIEPClp)*(1/KIEPCls)^2*1/4)+uMAXT*X/(YT*(KmT+CT))*HLH*(1/(KIETClp*KIETCls))	0	0
HHL	HHLt-uMAXP*X/(YP*(KmP+CP))*(LLHH*(1/KIEPCls^2)*1/6+LHHH*(1/KIEPClp)*(1/KIEPCls)^2*1/4)+uMAXT*X/(YT*(KmT+CT))*HHL*(1/(KIETCls)^2)	0	0
HHH	HHHt-uMAXP*X/(YP*(KmP+CP))*(LHHH*(1/KIEPCls^3)*1/4+HHHH*(1/KIEPClp)*(1/KIEPCls)^3)+uMAXT*X/(YT*(KmT+CT))*HHH*(1/(KIETClp*(KIETCls)^2))	0	0
X	Xt-uMAXP*X*CP/(KmP+CP)-uMAXT*X*CT/(KmT+CT)	X0	0
LL	LLt-uMAXT*X/(YT*(KmT+CT))*(LLL+LLH*(1/KIETClp))	0	0
LH	LHt-uMAXT*X/(YT*(KmT+CT))*((LHL+HLL)*(1/(KIETCls))+(LHH+HLH)*(1/(KIETClp*KIETCls)))	0	0
HH	HHt-uMAXT*X/(YT*(KmT+CT))*((HHL*(1/KIETCls)^2)+HHH*(1/(KIETClp*(KIETCls^2))))	0	0

Appendix 7 – Supporting information to Chapter 5

1. List of microorganisms used to evaluate molecular biology data

Table A 14. Microorganisms reported to be found in iron- and sulphate-reducing conditions as well as during pyrite oxidation. *(Chen et al., 2014, Reese et al., 2014)*

Redox	Abiotic process	Microorganism	Classification
iron-reducing		*Geobacteraceae*	family
iron-reducing		*Shewanellaceae*	family
iron-reducing		*Campylobacteraceae*	family
iron-reducing		*Pelobacteraceae*	family
iron-reducing		*Ferrimonadaceae*	family
iron-reducing		*Acidiphilium cryptum*	
iron-reducing		*Ferribacterium*	species
iron-reducing		*Bacillus*	genus
sulphate-reducing		*Desulfobacteraceae*	family
sulphate-reducing		*Desulfobulbaceae*	family
sulphate-reducing		*Desulfoarculaceae*	family
sulphate-reducing		*Desulfohalobioaceae*	family
sulphate-reducing		*Desulfomicrobiaceae*	family
sulphate-reducing		*Desulfovibrionaceae*	family
sulphate-reducing		*Desulfurellaceae*	family
sulphate-reducing		*Desulfuromonadaceae*	family
sulphate-reducing		*Myxococcales*	order
		Myxococcaceae	family
sulphate-reducing		*Syntrophobacteraceae*	family
	pyrite oxidation	*Acidithiobacillus ferrooxidans*	species
	pyrite oxidation	*Leptospirillum ferrooxidans*	species
	pyrite oxidation	*Ferroplasma*	genus
	pyrite oxidation	*Acidiphilum*	genus
	pyrite oxidation	*Acidithiobacillus thiooxidans*	species
	pyrite oxidation	*Acidithiobacillus caldus*	species
	pyrite oxidation	*Euryarchaeota*	phylum
	pyrite oxidation	*Sphingomonas*	genus
	pyrite oxidation	*Sulfobacillus*	genus

Table A 15. Microorganisms among which some strains are known to perform partial (most cases) or complete reductive dechlorination under anaerobic conditions, or oxidation of *c*DCE and/or VC under aerobic conditions *(Hartmans et al., 1985, Oldenhuis et al., 1989, Wackett et al., 1989, Coleman et al., 2002, Coleman et al., 2002, Hug et al., 2013, Richardson, 2013)*. In the case of reductive dechlorination, specific bacteria known to contain a reductive dehalogenase homologous (*rdhA*) gene are reported as in *(Hug et al., 2013)*. When several strains or species of one genus were reported to contain a *rdhA* gene, OTUs at the genus level were included in the treatment. When only one strain of a genus was reported to contain a *rdhA* gene, OTUs at the corresponding specie level were taken into account in the treatment. The *Dehalococcoidetes* class which includes the genera *Dehalococcoides*, *Dehalogenimonas* and *Dehalobium*, among which some members are known to respire chlorinated compounds, was also considered.

Degradation pathway	**Microorganism**
cometabolic oxidation	*Methylosinus* *Methylosinus trichosporium OB3b*
(cometabolic) oxidation	*Mycobacterium* *Mycobacterium vaccae* JOB5 *Mycobacterium aurum L1*
oxidation	*Polaromonas*-like
oxidation	*Nocardioides*-like
Reductive dechlorination	*Geobacter lovleyi* SZ
Reductive dechlorination	*Sulfurospirillum* *Sulfurospirillum halorespirans* PCE-M2 *Sulfurospirillum multivorans*
Reductive dechlorination	*Acidobacterium capsulatum*
Reductive dechlorination	*Ruegeria* *Ruegeria pomeroyi* DSS-3 *Ruegeria sp.* TM1040
Reductive dechlorination	*Photobacterium profundum* 3TCK
Reductive dechlorination	*Jannaschia* sp. CCS1
Reductive dechlorination	*Ahrensia* sp. R2A130
Reductive dechlorination	*Shewanella sediminis* HAW-EB3
Reductive dechlorination	*Vibrio* sp. RC586
Reductive dechlorination	*Anaeromyxobacter* *Anaeromyxobacter* sp. K *Anaeromyxobacter dehalogenans* 2CP-1 *Anaeromyxobacter dehalogenans* 2CP-C
Reductive dechlorination	delta proteobacterium NaphS2
Reductive dechlorination	*Dehalococcoidetes*
Reductive dechlorination	*Dehalococcoides* *Dehalococcoides mccartyi* CBDB1 *Dehalococcoides mccartyi* GT *Dehalococcoides mccartyi* FL2 *Dehalococcoides mccartyi* KB-1 consortium *Dehalococcoides mccartyi* BAV1 *Dehalococcoides mccartyi* 195 *Dehalococcoides mccartyi* MB *Dehalococcoides mccartyi* - WL consortium

	Dehalococcoides mccartyi VS
Reductive dechlorination	Dehalogenimonas *Dehalogenimonas lykanthroporepellens* BL-DC-9
Reductive dechlorination	*Dethiobacter alkaliphilus* AHT 1
Reductive dechlorination	*Clostridium* *Clostridium difficile 630* *Clostridium difficile* R20291
Reductive dechlorination	*Desulfitobacterium* *Desulfitobacterium hafniense* PCP-1 *Desulfitobacterium sp.* PCE-S *Desulfitobacterium hafniense* Y51 *Desulfitobacterium hafniense* TCE1 *Desulfitobacterium hafniense* DCB-2 *Desulfitobacterium chlororespirans* *Desulfitobacterium dehalogenans* *Desulfitobacterium* sp. KBC1 *Desulfitobacterium* sp. Viet-1 *Desulfitobacterium* dichloroeliminans LMG P-21439 *Desulfitobacterium* sp. CR1
Reductive dechlorination	*Dehalobacter* *Dehalobacter restrictus* PER-K23 *Dehalobacter* - WL consortium *Dehalobacter* CF *Dehalobacter* - MS consortium
Reductive dechlorination	*Heliobacterium modesticaldum* Ice1
Reductive dechlorination	*Thermotogales* bacterium mesG1.Ag.4.2
Reductive dechlorination	*Ferroglobus placidus* DSM 10642

2. Field data relative to chlorinated ethenes

Table A 16. Summary of chlorinated ethenes concentrations isotopic composition data from 2014. Highlighted lines correspond to points along the plume centerline. The extent of degradation D was calculated based on enrichment factors found in the literature, i.e. εC = -0.4 to -16.7 for PCE biotic reductive dechlorination, εC = -6.9 to -20.5 for *c*DCE abiotic reduction by iron-bearing minerals, and εCl = -0.9 to -5 for PCE biotic reductive dechlorination.

distance from source	depth	sampling point	PCE	PCE	PCE	TCE	TCE	TCE	cDCE	cDCE	cDCE	VC	VC	isotope balance	error isotope balance	Extent of degradation D					
			[]	$\delta^{13}C$	$\delta^{37}Cl$	[]	$\delta^{13}C$	$\delta^{37}Cl$	[]	$\delta^{13}C$	$\delta^{37}Cl$	[]	$\delta^{13}C$	$\delta^{13}C$	$\delta^{13}C$	PCE - ε_C (‰)		PCE - ε_{Cl} (‰)		cDCE - ε_C (‰)	
m	m		µg·L^{-1}	‰	‰	µg·L^{-1}	‰	‰	µg·L^{-1}	‰	‰	µg·L^{-1}	‰	‰	‰	-16.7	-0.4	-5	-0.9	-20.5	-6.9
18	-7	F2-2	2.4	**-25.8**		0.28			0.25			0		-25.8	0.9						
18	-5	F3-3	17	**-15.9**		21	**-21.9**		40	**-22.1**		6.5	**-22.9**	-21.4	0.6	42%	100%				
105	-8	B16-1	38	**-27**		5.3			75	**-22.9**		0.46		-23.8	0.6						
355	-6.5	B20-1	110		**-0.8**	20		**4.5**	140	**-22.4**	**5.5**	0.12						4%	20%		
100	-19	B22-1	13	**-27**		0.73	**-27.8**		0.56	**-24.5**		0		-26.9	0.6						
100	-15	B22-2	350	**-24.7**	**-1**	0.47			0.13			0		-24.7	0.6	2%	54%	0%	0%		
100	-11	B22-3	120	**-22.6**	**-0.3**	32	**-26.2**	**3.3**	27	**-24.6**	**4.7**	0.085		-23.7	0.6	14%	100%	13%	54%		
350	-18.75	B23-1	54	**-22.8**		9.1			1.2			0		-22.8	0.8	12%	100%				
350	-15.75	B23-2	87	**-17.6**	**1.2**	140	**-19.3**	**6.3**	86	**-38.5**	**4.3**	0.045		-25.9	0.9	36%	100%	36%	91%		
350	-12.5	B23-3	360	**-23.1**	**-0.8**	160	**-25.1**	**3.2**	67	**-33**	**3.3**	0.072		-25.4	0.7	11%	99%	4%	20%		
750	-18.5	B28-1	770	**-21.3**	**-0.3**	310	**-35**	**0.6**	81	**-34.7**	**2.7**	0.33		-26.9	0.8	20%	100%	13%	54%		
750	-12.5	B28-2	240		**-1**	33	**-30.7**	**1.5**	24	**-25.6**	**5.7**	0.073						0%	0%		
1050	-31.5	B34-2	1.1			17			370	**-23.2**	**5.7**	0.58		-23.2	0.6					8%	23%
1050	-24.5	B34-3	0.18			2.6			330	**-21.3**	**6.9**	0.97	**-29.9**	-21.3	0.6					17%	42%
1050	-18.5	B34-4	0.23			6.8			280	**-22**	**6.4**	0.4		-22	0.6					14%	36%
1050	-6.5	B34-6	53	**-19.5**		38		**5.5**	86	**-27.7**	**5.3**	0.12									
1400	-23.5	B47-1	0.085			0.28			230	**-25.2**	**5.7**	0.6	**-27.1**	-25.2	0.6						
1430	-51	B58-2	0.061			0			75	**-25.3**	**6.1**	0.48	**-23.2**	-25.3	0.6						
1430	-35.5	B58-4	0.062			1.9			99	**-24.3**	**5.7**	0.34		-24.3	0.6					3%	10%
1430	-19	B58-6	0.076			0.37			120	**-24.6**	**6.1**	0.37		-24.6	0.6					2%	5%
1550	-33.5	B60-1	0			0			120	**-25.1**		0.92		-25.1	0.6						
1550	-27.5	B60-2	0			0			140	**-25.6**	**5.7**	0.74		-25.6	0.6						
1550	-21.5	B60-3	0			0.15			120	**-25**	**5.6**	0.64	**-25.6**	-25.1	0.6						
1670	-28.5	B61-1	0.041			0			50	**-24**	**6.4**	0.39		-24	0.6					5%	13%
1670	-21.5	B61-2	0			0			110	**-25.1**	**5.8**	0.53	**-26.1**	-25.1	0.5						
1670	-16	B61-3	0.049			0			30	**-25.3**	**5.7**	0.17		-25.3	0.6						
1900	-19	B64-1	0			0			30	**-24.4**		0.25		-24.4	0.6					3%	8%

3. Molecular biology results

Table A 17. Detection by qPCR of *Dhc* DNA, rRNA and activity as well as vcrA and bvcA DNA and mRNA expressed as gene copies·L^{-1}.b.d.l.: below detection limit.

	Dhc DNA	Dhc RNA	Dhc RNA/DNA	vcrA, bvcA DNA	vcrA, bvcA RNA
F2-2	b.d.l.	b.d.l.	b.d.l.	b.d.l.	b.d.l.
F4-3	1.73E+06	8.82E+04	0.05	b.d.l.	b.d.l.
B16-1	1.59E+05	2.48E+05	1.56	b.d.l.	b.d.l.
B17-1	2.26E+05	b.d.l.	b.d.l.	b.d.l.	b.d.l.
B23-1	1.31E+05	1.96E+04	0.15	b.d.l.	b.d.l.
B23-2	1.09E+05	1.32E+05	1.21	b.d.l.	b.d.l.
B23-3	3.39E+05	3.40E+04	0.10	b.d.l.	b.d.l.
B34-2	b.d.l.	b.d.l.	b.d.l.	b.d.l.	b.d.l.
B34-3	b.d.l.	b.d.l.	b.d.l.	b.d.l.	b.d.l.
B34-4	1.03E+05	2.24E+04	0.22	b.d.l.	b.d.l.
B34-6	b.d.l.	b.d.l.	b.d.l.	b.d.l.	b.d.l.
B58-2	b.d.l.	b.d.l.	b.d.l.	b.d.l.	b.d.l.
B58-6	b.d.l.	b.d.l.	b.d.l.	b.d.l.	b.d.l.
B61-1	b.d.l.	b.d.l.	b.d.l.	b.d.l.	b.d.l.
B61-3	b.d.l.	b.d.l.	b.d.l.	b.d.l.	b.d.l.

Table A 18. Bacteria identified by pyrotag sequencing which were reported to be found in iron- and sulphate-reducing conditions as well as during pyrite oxidation, chlorinated ethenes oxidation, partial and complete dechlorination. Results are given in cells·L^{-1} (c·L^{-1}) and in % cells from all the groups given in Table A 14 and Table A 15 identified by pyrotag sequencing in one sample. n.d.: not detected.

Microorganism group / Microorganism	Classification	B23-2		B23-3		B34-2		B34-3		B34-4		B34-6		B58-2		B58-6		B61-1		B61-3	
		c·L^{-1}	%	c·L^{-1}	%	c·L^{-1}	%	c·L^{-1}	%	c·L^{-1}	%	c·L^{-1}	%	c·L^{-1}	%	c·L^{-1}	%	c·L^{-1}	%	c·L^{-1}	%
Iron reducers		**n.d.**	**0**	**$6.1 \cdot 10^4$**	**1**	**$1.1 \cdot 10^6$**	**10**	**$3.2 \cdot 10^5$**	**2**	**$1.5 \cdot 10^4$**	**1**	**$5.8 \cdot 10^4$**	**3**	**$3.3 \cdot 10^4$**	**1**	**$9.2 \cdot 10^4$**	**1**	**$1.4 \cdot 10^5$**	**20**	**$3.5 \cdot 10^4$**	**2**
Geobacteraceae without *Geobacter lovleyi*	family	n.d.	0	n.d.	0	$9.7 \cdot 10^5$	9	$2.7 \cdot 10^5$	2	$1.5 \cdot 10^4$	1	$5.8 \cdot 10^4$	3	$3.3 \cdot 10^4$	1	$9.2 \cdot 10^4$	1	$1.3 \cdot 10^5$	18	$1.8 \cdot 10^4$	1
Shewanellaceae	family	n.d.	0	n.d.	0	n.d.	0	n.d.	0	n.d.	0	n.d.	0	n.d.	0	n.d.	0	n.d.	0	$1.8 \cdot 10^4$	1
Bacillus	genus	n.d.	0	$6.1 \cdot 10^4$	1	$1.4 \cdot 10^5$	1	$5.3 \cdot 10^4$	0	n.d.	0	n.d.	0	n.d.	0	n.d.	0	$1.1 \cdot 10^4$	2	n.d.	0
Pyrite oxidation		**$3.9 \cdot 10^4$**	**1**	**$7.9 \cdot 10^5$**	**11**	**$3.0 \cdot 10^6$**	**27**	**$1.1 \cdot 10^7$**	**74**	**$1.2 \cdot 10^5$**	**4**	**$4.8 \cdot 10^5$**	**28**	**$4.1 \cdot 10^6$**	**67**	**$6.5 \cdot 10^6$**	**68**	**$7.2 \cdot 10^4$**	**10**	**$7.6 \cdot 10^5$**	**39**
Euryarchaeota	phylum	$3.9 \cdot 10^4$	1	0	0	$1.4 \cdot 10^5$	1	$9.3 \cdot 10^4$	1	0	0	$3.8 \cdot 10^4$	2	$1.3 \cdot 10^5$	2	$1.3 \cdot 10^4$	0	$5.5 \cdot 10^4$	8	$5.9 \cdot 10^3$	0
Sphingomonas	genus	n.d.	0	$7.9 \cdot 10^5$	11	$2.9 \cdot 10^6$	26	$1.1 \cdot 10^7$	73	$1.2 \cdot 10^5$	4	$4.4 \cdot 10^5$	26	$4.0 \cdot 10^6$	65	$6.5 \cdot 10^6$	68	$1.7 \cdot 10^4$	2	$7.6 \cdot 10^5$	38
Sulphate reducers		**$1.7 \cdot 10^6$**	**30**	**$1.5 \cdot 10^6$**	**22**	**$8.6 \cdot 10^5$**	**8**	**$6.1 \cdot 10^5$**	**4**	**$1.3 \cdot 10^5$**	**5**	**$1.2 \cdot 10^5$**	**7**	**$3.3 \cdot 10^5$**	**5**	**$2.9 \cdot 10^5$**	**3**	**$1.9 \cdot 10^5$**	**27**	**$2.4 \cdot 10^5$**	**12**
Desulfobacteraceae	family	$1.3 \cdot 10^4$	0	$1.0 \cdot 10^4$	0	$1.1 \cdot 10^5$	1	$2.1 \cdot 10^5$	1	n.d.	0	$3.8 \cdot 10^4$	2	$1.0 \cdot 10^5$	2	$5.3 \cdot 10^4$	1	$1.7 \cdot 10^4$	2	$1.1 \cdot 10^5$	6
Desulfobulbaceae	family	$1.3 \cdot 10^4$	0	n.d.	0	$8.8 \cdot 10^4$	1	$1.2 \cdot 10^5$	1	$1.5 \cdot 10^4$	1	n.d.	0	$6.7 \cdot 10^4$	1	$1.3 \cdot 10^4$	0	$5.5 \cdot 10^3$	1	$1.2 \cdot 10^4$	1
Desulfovibrionaceae	family	n.d.	0	n.d.	0	$7.1 \cdot 10^4$	1	n.d.	0	n.d.	0	n.d.	0	n.d.	0	$2.6 \cdot 10^4$	0	$5.5 \cdot 10^3$	1	n.d.	0
Desulfuromonadaceae	family	n.d.	0	n.d.	0	n.d.	0	$1.3 \cdot 10^4$	0	n.d.	0	n.d.	0	n.d.	0	n.d.	0	n.d.	0	n.d.	0
Myxococcales	order	$3.8 \cdot 10^5$	7	$7.6 \cdot 10^5$	11	$1.6 \cdot 10^5$	1	$1.7 \cdot 10^5$	1	$3.0 \cdot 10^4$	1	$3.8 \cdot 10^4$	2	$1.0 \cdot 10^5$	2	$7.9 \cdot 10^4$	1	$6.1 \cdot 10^4$	9	$5.9 \cdot 10^4$	3
Myxococcaceae among *Myxococcales*	family	n.d.	0	$1.0 \cdot 10^4$	0	n.d.	0	n.d.	0	n.d.	0	n.d.	0	n.d.	0	n.d.	0	n.d.	0	n.d.	0
Syntrophobacteraceae	family	$1.3 \cdot 10^6$	23	$7.7 \cdot 10^5$	11	$4.4 \cdot 10^5$	4	$9.3 \cdot 10^4$	1	$9.0 \cdot 10^4$	3	$3.9 \cdot 10^4$	2	$6.7 \cdot 10^4$	1	$1.2 \cdot 10^5$	1	$9.9 \cdot 10^4$	14	$5.9 \cdot 10^4$	3
Chlorinated ethenes oxidation		**$7.9 \cdot 10^5$**	**14**	**$8.0 \cdot 10^5$**	**12**	**$5.3 \cdot 10^5$**	**5**	**$5.7 \cdot 10^5$**	**4**	**n.d.**	**0**	**$3.9 \cdot 10^4$**	**2**	**$1.1 \cdot 10^6$**	**19**	**$1.7 \cdot 10^6$**	**17**	**$1.7 \cdot 10^4$**	**2**	**$4.7 \cdot 10^5$**	**24**
Mycobacterium	genus	$2.6 \cdot 10^4$	0	$1.3 \cdot 10^5$	2	$3.5 \cdot 10^4$	0	n.d.	0	n.d.	0	n.d.	0	n.d.	0	n.d.	0	n.d.	0	n.d.	0
Nocardioides	genus	$2.6 \cdot 10^4$	0	$4.4 \cdot 10^5$	6	$3.5 \cdot 10^4$	0	n.d.	0	n.d.	0	$3.9 \cdot 10^4$	2	$1.7 \cdot 10^4$	0	n.d.	0	n.d.	0	$1.2 \cdot 10^4$	1
Polaromonas	genus	$7.4 \cdot 10^5$	13	$2.0 \cdot 10^5$	3	$3.9 \cdot 10^5$	4	$5.7 \cdot 10^5$	4	n.d.	0	n.d.	0	$1.1 \cdot 10^6$	18	$1.7 \cdot 10^6$	17	$1.7 \cdot 10^4$	2	$4.6 \cdot 10^5$	23
Methylosinus	genus	n.d.	0	$2.0 \cdot 10^4$	0	$7.1 \cdot 10^4$	1	n.d.	0	n.d.	0	n.d.	0	n.d.	0	n.d.	0	n.d.	0	n.d.	0
Partial dechlorination		**$1.5 \cdot 10^6$**	**25**	**$3.6 \cdot 10^6$**	**52**	**$4.6 \cdot 10^6$**	**42**	**$1.8 \cdot 10^6$**	**12**	**$2.1 \cdot 10^6$**	**77**	**$5.4 \cdot 10^5$**	**32**	**$4.3 \cdot 10^5$**	**7**	**$8.6 \cdot 10^5$**	**9**	**$2.3 \cdot 10^5$**	**33**	**$4.6 \cdot 10^5$**	**23**

Geobacter lovleyi	specie	n.d.	0	n.d.	0	$1.8 \cdot 10^4$	0	$4.0 \cdot 10^4$	0	n.d.	0	n.d.	0	n.d.	0	$2.2 \cdot 10^4$	3	n.d.	0
Dehalococcoidetes without *Dhc* and *Dhg*	class	$1.3 \cdot 10^6$	23	$3.6 \cdot 10^6$	52	$3.8 \cdot 10^6$	35	$1.4 \cdot 10^6$	9	$2.1 \cdot 10^6$	77	$5.4 \cdot 10^5$	32	$4.3 \cdot 10^5$	7	$8.1 \cdot 10^5$	8	$1.3 \cdot 10^5$	18	$4.6 \cdot 10^5$	23
Clostridium	genus	n.d.	0	n.d.	0	$4.6 \cdot 10^5$	4	$6.7 \cdot 10^4$	0	n.d.	0	n.d.	0	n.d.	0	$5.3 \cdot 10^4$	1	$1.7 \cdot 10^4$	2	n.d.	0
Dehalobacter syntrophobotulus	genus	$1.3 \cdot 10^5$	2	n.d.	0	$2.6 \cdot 10^5$	2	$3.2 \cdot 10^4$	2	n.d.	0	n.d.	0	n.d.	0	n.d.	0	$6.1 \cdot 10^4$	9	n.d.	0
Complete dechlorination		**$1.7 \cdot 10^6$**	**30**	**$1.6 \cdot 10^5$**	**2**	**$9.0 \cdot 10^5$**	**8**	**$4.2 \cdot 10^5$**	**3**	**$3.7 \cdot 10^5$**	**14**	**$4.6 \cdot 10^5$**	**27**	**$8.3 \cdot 10^4$**	**1**	**$1.7 \cdot 10^5$**	**2**	**$5.0 \cdot 10^4$**	**7**	**$5.9 \cdot 10^3$**	**0**
Dehalococcoides (*Dhc*)	genus	$5.2 \cdot 10^4$	1	n.d.	0	$7.1 \cdot 10^4$	1	$9.3 \cdot 10^4$	1	n.d.	0	n.d.	0	n.d.	0	$1.1 \cdot 10^5$	1	$4.4 \cdot 10^4$	6	n.d.	0
Dehalogenimonas (*Dhg*)	genus	$1.7 \cdot 10^6$	29	$1.6 \cdot 10^5$	2	$8.3 \cdot 10^5$	8	$3.3 \cdot 10^5$	2	$3.7 \cdot 10^5$	14	$4.6 \cdot 10^5$	27	$8.3 \cdot 10^4$	1	$6.6 \cdot 10^4$	1	$5.5 \cdot 10^3$	1	$5.9 \cdot 10^3$	0
Total from all groups		**$5.7 \cdot 10^6$**		**$6.9 \cdot 10^6$**		**$1.1 \cdot 10^7$**		**$1.4 \cdot 10^7$**		**$2.8 \cdot 10^6$**		**$1.7 \cdot 10^6$**		**$6.1 \cdot 10^6$**		**$9.5 \cdot 10^6$**		**$6.9 \cdot 10^5$**		**$2.0 \cdot 10^6$**	